# NOVEL COLLOIDAL METHODS FOR FABRICATION OF COMPOSITE COATINGS

# NOVEL COLLOIDAL METHODS FOR FABRICATION OF

# COMPOSITE COATINGS

By Xinqian Liu, B. Eng, M.Eng

A Thesis Submitted to the School of Graduate Studies in Partial Fulfillment of

the Requirements for the Degree Doctor of Philosophy

McMaster University

Title: Novel Colloidal Methods for Fabrication of Composite

Coatings


Author: Xinqian Liu,

M.Eng (University of Science and Technology Beijing, China),

B.Eng (University of Jinan, China)


SUPERVISORS:

Prof. Igor Zhitomirsky and Prof. Stephen C. Veldhuis


NUMBER OF PAGES: 231

## LAY ABSTRACT

Polymer and composite coatings have been utilized for a wide range of applications due to their barrier properties, scratch and abrasion resistance, chemical resistance, and biocompatibility. Various techniques have been developed to fabricate polymer and composite coatings, such as electrophoretic deposition (EPD) and the dip coating method.

However, limitations remain. EPD unitizes an electrical field to drive charged particles in a suspension toward conductive substrates to achieve film deposition. This process requires a stable suspension with charged particles, therefore, the electroneutral polymers present difficulties in their EPD. In addition, dissolving high molecular weight polymers at high concentrations in a non-toxic solvent is currently challenging, which is vital to utilize dip coating technique.

The objective of this work was to develop advanced charging dispersants for EPD of electroneutral polymers and non-toxic solvents for dip coating of high molecular weight polymers. New biomimetic and versatile approaches have been developed for EPD of different electrically neutral polymers, chemically inert materials, and their composite coatings. A non-toxic co-solvent was proposed to dissolve high molecular weight polymer at high concentration for dip coating of the polymer and its composite

coatings containing flame retardant materials. The results presented in this work showed

the formation of high-quality films with multifunctionality and paved new strategies for

further developments.

# ABSTRACT

Polymer coatings are thin films of polymer deposited on different substrates for various applications. Such surface coatings can serve a functional purpose (adhesives, photographic films), protective purpose (anticorrosion), or decorative purpose (paint). Additionally, their composite coatings containing ceramic, or metal particles are often used to enhance durability, functionality, or aesthetics. Electrophoretic deposition (EPD) and dip coating are two promising methods for the fabrication of polymer and composite coatings due to the ease of fabrication, low cost, and high-volume production.

EPD involves the electrophoresis of charged particles and their deposition on the electrode surface, which requires the colloidal particles to be charged in a stable suspension as a precursor solution for deposition. Many polymers cannot be deposited by EPD directly because of their charge neutrality and poor dispersion. Therefore, it is critical to develop efficient charging dispersants to modify electrically neutral polymers for their EPD. The approach was inspired by the strong solubilization power of bile acids in the human body. Two types of bile salts, cholic acid sodium salt and sodium chenodeoxycholate, and three types of biosurfactants, carbenoxolone sodium salt, glycyrrhizic acid, and 18β-glycyrrhetinic acid, which share similar structures with bile salts, were discovered for charging, dispersion, and EPD of different materials. The

electrically neutral polymers (PTFE and PVDF), chemically inert materials (diamond, nanodiamond, graphene, carbon dots, carbon nanotubes and Zr-doped hydrotalcite (MHT)), and their composites can be well dispersed in suspension and deposited using these bio-surfactants as dispersants. It was found that the unique chemical structures of these biomolecules play vital roles in the surface modification and EPD of different materials. Moreover, the deposited polymer (PVDF, PTFE) and composite (PTFE-MHT) coatings can provide outstanding corrosion protection for stainless steel. The biomimetic and versatile strategy opens a way for the deposition of other electrically neutral materials through EPD. These findings also provide a promising strategy for selecting new dispersants for EPD.

The deposition of high molecular weight ($M_W$) polymers such as poly(ethyl methacrylate) (PEMA) at high concentrations in non-toxic solvents continues to be a challenge for dip coating. In this work, we firstly proposed using water-isopropanol as a co-solvent to dissolve high $M_W$ PEMA at high concentrations. It was found that water molecules can solvate carbonyl groups of PEMA and facilitate their dissolution. This method avoided the usage of toxic solvents and a long-time heating procedure for their removal. Moreover, it allows the fabrication of high-quality PEMA and composite coatings containing different flame retardant materials (FRMs), including double hydroxide $LiAl_2(OH)_7.2H_2O$ (LiAlDH), huntite, halloysite and hydrotalcite, through the

dip coating method. A novel solid state synthesis method was proposed to fabricate

LiAlDH, which is promising for the fabrication of other advanced DHs. Such composite

coatings combined advanced properties of PEMA and functional properties of FRMs,

such as corrosion inhibition and FR properties.

# ACKNOWLEDGEMENTS

First, I would like to thank my supervisor, Professor Igor Zhitomirsky, whose expertise was invaluable in formulating the research questions and methodology. Thank you for your kind guidance, constant support, great encouragement and patience throughout my Ph.D. study. To be honest, it is my great honor to be one of your students.

I would also like to thank my co-supervisor Prof. Veldhuis and committee member Prof. Grandfield, for their valuable discussion and suggestions. They made me realize what I have not known but need to know in my research. I would express my gratitude to Prof. Bassim for becoming my examiner for my comprehensive II exam and giving me valuable suggestions. I would also thank Prof. Kish for his great suggestions for my presentations in the two seminars.

It was my pleasure to be part of Prof. Igor Zhitomirsky's group. I enjoyed the time we helped each other in the group. I would like to thank Ryan Poon, Mohamed Nawwar, Ri Chen, Amanda Clifford, Xuelin Li, Kaelan Rorabeck, Zhengzheng Wang, Wenyu Liang and Qinfu Zhao for their help with my research and daily life.

Last but most importantly, I would like to thank my parents for their endless love and encouragement. Thanks to my husband and groupmate Qinfu Zhao for his continuous help and support for my research and life. To my daughter Annabel, you have made me

stronger, better and more fulfilled than I could have ever imagined. I love you to the

moon and back.

# Declaration of academic achievements

This dissertation was used to fulfil the requirements of the degree Doctor of Philosophy. The primary research project was conducted from September 2018 to April 2022. The results of this dissertation were published in peer-reviewed journals, and I am the first author on six of these papers, which were listed below:

1. **Xinqian Liu**, Qinfu Zhao, Stephen C. Veldhuis, Igor Zhitomirsky, "Cholic acid is a versatile coating-forming dispersant for electrophoretic deposition of diamond, graphene, carbon dots and polytetrafluoroethylene", *Surface & Coatings Technology*, 384 (2020): 125304.

2. **Xinqian Liu**, Amanda Clifford, Qinfu Zhao, Igor Zhitomirsky, "Biomimetic strategies in colloidal-electrochemical deposition of functional materials and composites using chenodeoxycholic acid", *Colloids and Surfaces A: Physicochemical and Engineering Aspects*, 603 (2020): 125189.

3. **Xinqian Liu**, Stephen C. Veldhuis, Ritch Mathews, and Igor Zhitomirsky, "Dip coating of poly(ethyl methacrylate) and composites from solutions in isopropanol-water co-solvent", *Colloids and Surfaces A: Physicochemical and Engineering Aspects*, 631 (2021): 127703.

4. **Xinqian Liu**, Stephen C. Veldhuis, Ritch Mathews, and Igor Zhitomirsky, "Carbenoxolone as a multifunctional vehicle for electrodeposition of materials", *Applied Sciences*, 11.19 (2021): 9110.

5. **Xinqian Liu**, Qinfu Zhao, Igor Zhitomirsky, "Versatile natural dispersants for electrophoretic deposition of materials", *Materials Letters*, 313 (2022): 131828.

6. **Xinqian Liu**, Stephen C. Veldhuis, Ritch Mathews, and Igor Zhitomirsky, "Poly(ethyl methacrylate) composite coatings with halogen-free inorganic flame-retardant additives", *Journal of Composites Science*, 6 (2022): 104.

7. Qinfu Zhao, **Xinqian Liu**, Stephen C. Veldhuis, Igor Zhitomirsky, "Sodium deoxycholate as a versatile dispersing and coating-forming agent: A new facet of electrophoretic deposition technology", *Colloids and Surfaces A: Physicochemical and Engineering Aspects*, 588 (2020): 124382.

8. Qinfu Zhao, **Xinqian Liu**, Igor Zhitomirsky, "Electrophoretic deposition of materials using lithocholic acid as a dispersant", *Materials Letters*, 275 (2020):128129.

# Table of Contents

# List of Figures and Tables

# List of Abbreviations and Symbols

| | |
|---|---|
| $1/\kappa$ | Debye Length |
| AC | Alternating Current |
| ATR | Attenuated Total Reflection |
| BS | Bile acid salts |
| CA | Caffeic Acid |
| CBXNa$_2$ | Carbenoxolone Sodium Salt |
| CDCH | Chenodeoxycholic Acid |
| CDCNa | Sodium Chenodeoxycholate |
| CDs | Carbon Dots |
| ChANa | Sodium Cholate |
| CNT | Carbon Nanotube |
| CV | Cyclic Voltammetry |
| DH | Double Hydroxides |
| DHB | 3,4-dihydroxybenzoic acid |
| DHC | 3,4-dihydroxyhydrocinnamic acid |
| DHP | 3,4-dihydroxyphenylacetic acid |

| | |
|---|---|
| DOPA | L-3,4-dihydroxyphenylalanine |
| EIS | Electrochemical Impedance Spectroscopy |
| EPD | Electrophoretic Deposition |
| FR | Fire Retardant |
| FRM | Flame Retardant Materials |
| FTIR | Fourier Transform Infrared Spectroscopy |
| GRTA | 18$\beta$-Glycyrrhetinic acid |
| GRZA | Glycyrrhizic Acid |
| IBP | Ibuprofen |
| LiAlDH | Double Hydroxide $LiAl_2(OH)_7.2H_2O$ |
| MHT | Zr-doped hydrotalcite |
| $M_w$ | Molecular Weight |
| ND | Nanodiamond |
| PAA | Poly(acrylic acid) |
| PB | Poisson-Boltzmann |
| PBMA | Polybuthylmethacrylate |
| PE | Phosphate Ester |
| PEEK | Polyetheretherketone |

| PEMA | Poly(ethyl methacrylate) |
| PMMA | Poly(methacrylic acid) |
| PPy | Polypyrrole |
| PTFE | Poly(tetrafluoroethylene) |
| PVDF | Polyvinylidene Fluoride |
| Py | Pyrrole |
| QCM | Quartz Crystal Microbalance |
| Rs | Volume Ratio |
| SCE | Saturated Calomel Electrode |
| SD | Submicrometre Diamond |
| SEM | Scanning Electron Microscope |
| TGA | Thermogravimetric Analysis |
| $V_A$ | Van der Waal's attraction |
| $V_R$ | Electrostatic Repulsion |
| $V_T$ | Total interaction energy |
| XRD | X-ray Diffraction |

# Chapter 1   Introduction

## 1.1  Overall context

Polymer and composite coatings are currently under development for different applications. Various polymers such as polytetrafluoroethylene (PTFE), polyvinylidene fluoride (PVDF), and poly(ethyl methacrylate) (PEMA) have been used as a coating in various technologies. [1] Polymer and composite coatings are used in a wide variety of applications, including aerospace and automotive parts for corrosion protection, food processing, biomedical and pharmaceutical appliances, and energy storage devices. [2, 3] Various techniques have been successfully employed for polymer coating fabrication. These include spin coating, dip coating, electrophoretic deposition (EPD), solution casting, and spray coating. [1] Considering the complexity, expense, and possibility of mass production, both dip coating and EPD are promising selections for the production of polymer coatings.

EPD has generated significant interest in fabricating coatings and thin films for biomedical, electronic, energy storage, and photovoltaic applications. [4-7] EPD technique involves electrophoresis of charged particles and their deposition on the electrode surface. [8-11] Therefore, charged particles and stable suspension are critical prerequisites for EPD. Many investigations were conducted to develop surface engineering strategies to charge particles, develop deposition mechanisms, and optimize the deposition conditions. [12-15] However, the

EPD of chemically inert and electrically neutral polymers such as PTFE and PVDF remains a challenge. PTFE is a fluoropolymer, the demand for which in domestic, industrial, and defense fields is consistently increasing due to its promising physical and chemical properties. PTFE is highly flexible, chemically stable, thermally stable, and electricity resistant polymer. [16] EPD technique of PTFE coatings has been reported in only four papers. [17-20] In these cases, toxic solvent [17] and hazard dispersants [18, 19] were employed for the EPD process, which limited its biomedical applications. De Riccardis et al. proposed polyvinylpyrrolidone (PVP) as a steric dispersant for EPD of PTFE. [20] However, the charge would be insufficient for achieving high-quality films through EPD. PVDF is a promising functional polymer that has been applied to biomedical implants, energy storage devices, multiferroic devices and other fields [21] due to its valuable properties, such as excellent mechanical strength, strong chemical resistance, piezoelectric and ferroelectric properties. [22-25] Two papers achieved the EPD of pure PVDF in various organic solvents and a mixture of 1-butanone-water without charging additives. [26, 27] Another paper proposed that PVDF films can be deposited in a mixture of N-methyl-2-pyrrolidinone-ethanol through EPD without charging agents. [28] However, charged dispersants are critically important for controlled EPD. Therefore, despite the progress achieved in the EPD of PTFE and PVDF, challenges remain. Problems still faced include the need to avoid using toxic solvents and hazardous dispersants, develop efficient and versatile charging dispersants, and better explain the mechanism of dispersion and deposition.

Dip coating techniques involve immersing a substrate into a tank containing coating material, sample withdrawal, and then drainage, which has been widely applied in both industry and laboratory fields. [29] However, polymers with low molecular weights ($M_W$) show weak film-forming and binding properties. The solubility of polymers decreases as $M_W$ increases, while it is difficult to achieve good substrate coverage using dilute polymer solutions. [30, 31] Consequently, if the high $M_W$ polymers cannot be dissolved at a high concentration, they cannot be deposited into a high-quality coating through the dip coating method. Poly(ethyl methacrylate) (PEMA) faces this problem. PEMA exhibits advanced properties, including mechanical strength, biocompatibility, chemical stability, and thermal stability. [32, 33] It has attracted significant interest for its use in bone and cartilage repair[33], polymer electrolytes and membranes for energy generation and storage devices[34, 35], and coatings for corrosion protection[36]. However, PEMA has difficulty dissolving at high concentrations in a nontoxic solvent. Various techniques have been proposed to fabricate PEMA coatings, including casting, spin coating, and electrospinning. [37-45] However, acetone, chloroform, and benzene are commonly used as solvents [37-43] and deposition process is usually followed by a long-time heating procedure for solvent removal. [39-42, 44, 45]. Therefore, it is of paramount importance to develop a nontoxic solvent to dissolve PEMA at high concentrations for dip coating.

In this work, one of the primary objectives was to develop new dispersing, charging, and film-forming agents for EPD of electrically neutral polymers. Based on biomimetic inspiration

from the strong solubilization ability of bile acids in the human digest system, two bile salt molecules and three steroid-like bio-surfactants were investigated to assist in the EPD of PTFE, PVDF, and other chemically inert particles, such as diamond, nanodiamond, graphene, carbon dots, carbon nanotubes and Zr-doped hydrotalcite (MHT), as well as their composites. All these materials were successfully deposited, which indicated that these bio-surfactants were versatile agents for surface modification of the materials and their EPD. These versatile agents can also help to achieve the fabrication of their composite coatings, such as PTFE-diamond, PVDF-diamond and PTFE-MHT. More than that, potentiodynamic and impedance spectroscopy studies indicated that PTFE and PVDF films could provide corrosion protection to steel. A conceptually new strategy was proposed to further enhance the protective properties of PTFE coatings through the incorporation of MHT in the PTFE matrix based on the memory properties of MHT. These findings hinted at a promising strategy for selecting new dispersants for EPD. It can be expected that the study of other steroid-like biomolecules will lead to further improvement in the development of surface modification techniques and EPD for different materials. It also opens a way for the deposition of other chemically inert and electrically neutral materials through EPD.

The other primary objective was to explore a non-toxic solvent for dissolving high $M_W$ polymers at high concentrations for dip coating. In this work, I firstly dissolved PEMA at a concentration of up to 50g $L^{-1}$ using mixed water-isopropanol as a co-solvent. The usage of non-toxic solvent doesn't limit its use in certain applications and saves fabrication time.

Moreover, this solvent allows for the fabrication of PEMA and composite coatings containing different flame retardant materials (FRMs), including double hydroxide $LiAl_2(OH)_7.2H_2O$ (LiAlDH), huntite, halloysite and hydrotalcite. I proposed a novel solid state synthesis method to fabricate LiAlDH, which is simple, waste-free and facilitates the control of stoichiometry. This waste-free method is promising for the fabrication of other advanced DHs. The composite coatings combined the corrosion-resistant properties of PEMA and the fire-resistant properties of FRMs. This investigation has provided a new direction for future research into the colloidal processing of polymers using non-toxic solvents and the fabrication of organic-inorganic composites using different colloidal techniques.

## 1.2  Thesis Overview

The following is a summary of the remaining chapters contained in this thesis:

Chapter 2 contains a thorough review of the fundamental colloidal science, dispersion of colloidal suspension, and problem statement and description of main gaps in the existing research. Different types of advanced dispersing agents are also reviewed. Finally, there is an overview of EPD and dip coating methods as coating fabrication techniques, which involves the challenges of these two methods.

Chapter 3 presents the primary objectives of this work.

Chapter 4 describes a biomimetic approach for EPD of advanced materials such as PTFE, diamond, graphene, pyrrole, carbon dots, and their composites utilizing sodium cholate

(ChANa) as a charging dispersant and coating-forming agent. SEM and FTIR were used to characterize the morphology, thickness, and composition of the as-deposited films. Also, it was discovered that these materials could be deposited as high-quality films through EPD because of the strong adsorption of amphiphilic ChANa on the material surfaces and the negative charge from its carboxylic group. Coating adhesion measurements showed good adhesion of the annealed PTFE films. Potentiodynamic and impedance spectroscopy studies indicate that the PTFE films provide corrosion protection of steel. It can be expected that bile salt mediated EPD will allow the deposition of other functional materials of different types.

Chapter 5 presents the application of another bile salt, sodium chenodeoxycholate (CDCNa) for the EPD of different materials, including PTFE, diamond, nanodiamond, ibuprofen, carbon nanotubes (CNTs), Zr-doped hydrotalcite (MHT), and their composites. SEM and FTIR characterized the film's morphology and functional groups. The CVs indicated the film formation of CDCH. XRD was used for the characterization of the resulting diamond and nanodiamond films. It was demonstrated that CDCH films can be deposited, and CDCNa allowed for EPD of carbon materials such as diamond, nanodiamond, CNTs, and PTFE and MHT. The incorporation of MHT in the PTFE matrix further improved the protective properties of PTFE coatings based on the memory properties of MHT, which was demonstrated by the Tafel and EIS tests. The protection mechanism involves in situ MHT reconstruction, thereby limiting water diffusion in various coatings' pores.

Chapter 6 builds upon the work presented in Chapters 4 and 5 and describes how to utilize a steroid-like biomolecule, carbenoxolone sodium salt ($CBXNa_2$), to disperse and charge different materials for EPD. The successfully deposited materials include PTFE, diamond, nanodiamond, graphene, carbon dots, and PTFE-diamond composite. We performed comprehensive characterization of the resulting coatings, including SEM, XRD, FTIR, potentiodynamic, and impedance spectroscopy. Coating characterization revealed that the materials were well deposited as high-quality films, and the resulting PTFE films can be applied to protect metals from corrosion. In addition, it indicated that $CBXNa_2$ is also a promising surface modification agent for future application in the EPD of different functional materials, compared with the two bile salt molecules discussed in Chapters 4 and 5.

Chapter 7 describes the application of glycyrrhizic acid (GRZA) and its principal metabolite 18β-Glycyrrhetinic acid (GRTA) for EPD of PVDF, PTFE, diamond, and their composites. Both molecules were selected based on the similar structure to bile acid molecules. We used SEM, deposit mass measurement, potentiodynamic, and impedance spectroscopy for film characterization. In this technique, both molecules were strongly adsorbed on the surfaces of the chemically inert materials. Furthermore, GRZA led to the higher deposition of PVDF, whereas GRTA resulted in higher mass loading of PTFE, which revealed the importance of the structure of bio-surfactants for the deposition of different materials. The obtained films can be used as protective coatings for metals.

Chapter 8 reports the exploration of the dip-coating method for the fabrication of PEMA and composite coatings containing double hydroxide $LiAl_2(OH)_7.2H_2O$ (LiAlDH) utilizing the mixture of water–isopropanol as a co-solvent. PEMA solutions with concentrations as high as 50 g $L^{-1}$ can be obtained. A waste-free solid-state synthesis method was used for preparing LiAlDH. The synthesis time can be reduced with higher temperatures to produce the LiAlDH on a large scale. We used SEM, XRD, potentiodynamic studies, electrochemical impedance spectroscopy, thermogravimetric analysis (TGA), and FTIR to characterize the films thoroughly. The characterization revealed that good-quality PEMA and composite coatings could be obtained and provide corrosion protection of stainless steel. LiAlDH shows advanced properties as a flame retardant additive for polymer coatings. These results confirmed that this dip-coating method shows great promise for use in colloidal processing of other polymers and composites using nontoxic solvents.

Chapter 9 continues the work described in Chapter 8. The use of a water–isopropanol co-solvent and the dip-coating technique allows the fabrication of PEMA-FRM composite coatings. The co-deposited FRM materials include huntite, halloysite, and hydrotalcite, avoiding the usage of conventional toxic halogenated FRMs. We used FTIR, XRD, SEM, and TGA to analyze the microstructure and composition of PEMA-FRM coatings. PEMA-FRM coatings provide corrosion protection of stainless steel, which was revealed by the electrochemical tests. The composite coating can be deposited as laminates with different

layers using a dip-coating method, which facilitates the fabrication of composite coatings with

enhanced properties.

Chapter 10 outlines this study's significant findings and contributions to the field, as well

as future studies.

## 1.3  References

[1]  A. Kausar, Polymer coating technology for high performance applications: Fundamentals and advances, Journal of Macromolecular Science, Part A 55(5) (2018) 440-448.

[2] H. Farzad, F. Najafi, M. Bengisu, E. Yilmaz, B.S. Hadavand, Synthesis and characterization of aliphatic tri-functional oligomeric urethane methacrylate used for UV-curable aluminum pigmented coatings, Journal of Macromolecular Science, Part A 50(5) (2013) 504-512.

[3]  B. Wang, G. Wilkes, Novel hybrid inorganic-organic abrasion-resistant coatings prepared by a sol-gel process, Journal of Macromolecular Science, Part A 31(2) (1994) 249-260.

[4]  I. Corni, M.P. Ryan, A.R. Boccaccini, Electrophoretic deposition: From traditional ceramics to nanotechnology, Journal of the European Ceramic Society 28(7) (2008) 1353-1367.

[5]  K. Ishii, C. Matsunaga, K. Kobayashi, A.J. Stevenson, C. Tardivat, T. Uchikoshi, Fabrication of BSCF-based mixed oxide ionic-electronic conducting multi-layered membrane by sequential electrophoretic deposition process, Journal of the European Ceramic Society 41(4) (2021) 2709-2715.

[6] S.B.A. Boraei, J. Nourmohammadi, F.S. Mahdavi, J. Yus, A. Ferrandez-Montero, A.J. Sanchez-Herencia, Z. Gonzalez, B. Ferrari, Effect of SrR delivery in the biomarkers of bone regeneration during the in vitro degradation of HNT/GN coatings prepared by EPD, Colloids and Surfaces B: Biointerfaces 190 (2020) 110944.

[7] I. Zhitomirsky, L. Gal-Or, Formation of hollow fibers by electrophoretic deposition, Materials Letters 38(1) (1999) 10-17.

[8] L. Yang, X. Pang, G. Fox-Rabinovich, S. Veldhuis, I. Zhitomirsky, Electrophoretic deposition of polymer and composite films, Surface engineering 28(8) (2012) 585-589.

[9] Y. Sun, M. Ata, I. Zhitomirsky, Electrophoretic deposition of linear polyethylenimine and composite films, Surface engineering 29(7) (2013) 495-499.

[10] Z. Jabbari, B. Nassernejad, N. Fallah, M. Javanbakht, N. Afsham, Fabrication of novel binderless anode via electrophoretic deposition for HT-PEMFC, Surface Engineering 35(12) (2019) 1013-1020.

[11] S.M. Emarati, M. Mozammel, Fabrication of superhydrophobic titanium dioxide coating on AISI 316L stainless steel by electrophoretic deposition and using trimethoxy (propyl) silane modification, Surface Engineering 35(5) (2019) 456-465.

[12] A. Rousta, D. Dorranian, M. Elahi, Electrophoretic deposition of cobalt oxide nanoparticles on aluminium substrate, Surface Engineering 36(9) (2020) 919-928.

[13] A. Saadati, H. Hesarikia, M.R. Nourani, R.A. Taheri, Electrophoretic deposition of hydroxyapatite coating on biodegradable Mg–4Zn–4Sn–0.6 Ca–0.5 Mn alloy, Surface Engineering 36(9) (2020) 908-918.

[14] M. Gorji, S. Sanjabi, C. Edtmaier, Combination of electrophoretic and electroless depositions to fabricate Ni/TiC cladding, Surface Engineering 36(9) (2020) 929-935.

[15] P. Tiwari, N.D. Ferson, J.S. Andrew, Elucidating the role of electrophoretic mobility for increasing yield in the electrophoretic deposition of nanomaterials, Journal of colloid and interface science 570 (2020) 109-115.

[16] E. Dhanumalayan, G.M. Joshi, Performance properties and applications of polytetrafluoroethylene (PTFE)—a review, Advanced Composites Hybrid Materials 1(2) (2018) 247-268.

[17] J.-i. Hamagami, T. Nakajima, K. Kanamura, T. Umegaki, Electrophoretic fabrication and photocatalytic performance of TiO {sub 2}/Fluorocarbon polymer composite films, Key Engineering Materials 216 (2002).

[18] J.H. Jang, K. Machida, Y. Kim, K. Naoi, Electrophoretic deposition (EPD) of hydrous ruthenium oxides with PTFE and their supercapacitor performances, Electrochimica acta 52(4) (2006) 1733-1741.

[19] D. Zhang, G. Dong, Y. Chen, Q. Zeng, Electrophoretic deposition of PTFE particles on porous anodic aluminum oxide film and its tribological properties, Applied Surface Science 290 (2014) 466-474.

[20] M.F. De Riccardis, V. Martina, D. Carbone, Study of polymer particles suspensions for electrophoretic deposition, The Journal of Physical Chemistry B 117(6) (2013) 1592-1599.

[21] Q. Zhao, S. Veldhuis, R. Mathews, I. Zhitomirsky, Influence of chemical structure of bile acid dispersants on electrophoretic deposition of poly (vinylidene fluoride) and composites, Colloids Surfaces A: Physicochemical Engineering Aspects 627 (2021) 127181.

[22] C. Ribeiro, C.M. Costa, D.M. Correia, J. Nunes-Pereira, J. Oliveira, P. Martins, R. Goncalves, V.F. Cardoso, S. Lanceros-Mendez, Electroactive poly (vinylidene fluoride)-based structures for advanced applications, Nature protocols 13(4) (2018) 681.

[23] B. Ji-Hun, C. Seung-Hwan, PVDF-based ferroelectric polymers and dielectric elastomers for sensor and actuator applications: a review, Functional Composites and Structures 1(1) (2019) 012003 (19 pp.).

[24] J. Inderherbergh, Polyvinylidene fluoride (PVDF) appearance, general properties and processing, Ferroelectrics 115(4) (1991) 295-302.

[25] J. Zhong, W. Li, J. Qian, C. Fu, H. Chu, J. Xu, X. Ran, W. Nie, Modulation of the interfacial architecture enhancing the efficiency and energy density of ferroelectric nanocomposites via the irradiation method, Journal of Colloid and Interface Science 586 (2021) 30-38.

[26] K.T. Lau, M.S.M. Suan, M. Zaimi, J. Abd Razak, M. Azam, N. Mohamad, Microstructure And Phase Of Poly (Vinyliden Fluoride) Films By Electrophoretic Deposition: Effect Of Polymer Dispersion's Stirring Conditions, Journal of Advanced Manufacturing Technology (JAMT) 10(2) (2016) 57-66.

[27] K.T. Lau, M.H.R. Ab Razak, S.L. Kok, M. Zaimi, M.W. Abd Rashid, N. Mohamad, M.A. Azam, Electrophoretic deposition and heat treatment of steel-supported PVDF-graphite composite film, Applied Mechanics and Materials, Trans Tech Publ, 2015, pp. 412-416.

[28] J. Yin, T. Fukui, K. Murata, M. Matsuda, M. Miyake, T. Hirabayashi, S. Yamamuro, Fabrication of protective KB/PVdF composite films on stainless steel substrates for PEFCs through electrophoretic deposition, Journal of the Ceramic Society of Japan 116(1350) (2008) 201-204.

[29] F. Grillon, D. Fayeulle, M. Jeandin, Quantitative image analysis of electrophoretic coatings, Journal of materials science letters 11(5) (1992) 272-275.

[30] R. Hoogenboom, C.R. Becer, C. Guerrero-Sanchez, S. Hoeppener, U.S. Schubert, Solubility and thermoresponsiveness of PMMA in alcohol-water solvent mixtures, Australian journal of chemistry 63(8) (2010) 1173-1178.

[31] B.A. Miller-Chou, J.L. Koenig, A review of polymer dissolution, Progress in Polymer Science 28(8) (2003) 1223-1270.

[32] S. Ramesh, O. Uma, R. Shanti, L.J. Yi, K. Ramesh, Preparation and characterization of poly (ethyl methacrylate) based polymer electrolytes doped with 1-butyl-3-methylimidazolium trifluoromethanesulfonate, Measurement 48 (2014) 263-273.

[33] G. Hutcheon, C. Messiou, R. Wyre, M. Davies, S. Downes, Water absorption and surface properties of novel poly (ethylmethacrylate) polymer systems for use in bone and cartilage repair, Biomaterials 22(7) (2001) 667-676.

[34] K.S. Ngai, S. Ramesh, K. Ramesh, J.C. Juan, A review of polymer electrolytes: fundamental, approaches and applications, Ionics 22(8) (2016) 1259-1279.

[35] C.M. Mathew, B. Karthika, M. Ulaganathan, S. Rajendran, Electrochemical analysis on poly (ethyl methacrylate)-based electrolyte membranes, Bulletin of Materials Science 38(1) (2015) 151-156.

[36] R. Armstrong, J. Wright, Impedance studies of poly ethylmethacrylate coatings formed upon tin-free steel, Corrosion science 33(10) (1992) 1529-1539.

[37] Y. Kamiya, K. Mizoguchi, Y. Naito, A dielectric relaxation study of plasticization of poly (ethyl methacrylate) by carbon dioxide, Journal of Polymer Science Part B: Polymer Physics 28(11) (1990) 1955-1964.

[38] G. Gery, H. Masuhara, Laser-induced molecular mixing of electron donor and acceptor in poly (ethyl methacrylate), Chemical Communications (7) (1998) 811-812.

[39] M. Sanopoulou, D. Stamatialis, Study of the transition from Fickian to Case II sorption kinetics in the system poly (ethyl methacrylate)–liquid methyl alcohol, Polymer 42(4) (2001) 1429-1439.

[40] C. Chen, M.L. Clarke, J. Wang, Z. Chen, Comparison of surface structures of poly (ethyl methacrylate) and poly (ethyl acrylate) in different chemical environments, Physical Chemistry Chemical Physics 7(11) (2005) 2357-2363.

[41] S. Rajendran, M.R. Prabhu, M.U. Rani, Ionic conduction in poly (vinyl chloride)/poly (ethyl methacrylate)-based polymer blend electrolytes complexed with different lithium salts, Journal of power sources 180(2) (2008) 880-883.

[42] A. Tiwari, A. Gupta, R. Bajpai, J. Keller, Structural and mechanical studies of in-situ generated poly (vinylidene fluoride) particle comprising poly (ethylmethacrylate) and poly (methylmethacrylate) ternary films, Polymer-Plastics Technology Engineering 49(6) (2010) 573-580.

[43] J.A. Gómez-Tejedor, N. Van Overberghe, P. Rico, J.L.G. Ribelles, Assessment of the parameters influencing the fiber characteristics of electrospun poly (ethyl methacrylate) membranes, European Polymer Journal 47(2) (2011) 119-129.

[44] E. Abdelrazek, Influence of FeCl3 filler on the structure and physical properties of polyethyl-methacrylate films, Physica B: Condensed Matter 400(1-2) (2007) 26-32.

[45] J. Chiou, D. Paul, Gas sorption and permeation in poly (ethyl methacrylate), Journal of membrane science 45(1-2) (1989) 167-189.

# Chapter 2   Literature Review

## 2.1  Fundamental aspects of colloidal processing

### 2.1.1  The DLVO theory

The classic DLVO theory established by Derjaguin, Landau, Verwey and Overbeek is the basis for interpretation of the interaction between colloidal particles and their behavior. [1, 2] According to this theory, the Coulombic double-layer repulsion and van der Waals' attraction contribute to the total pair interaction between colloidal particles. Therefore, the total interaction energy ($V_T$) of two separated, equivalently charged particles can be calculated using [3]

$$V_T = V_A + V_R \tag{1}$$

where the $V_A$ is the attractive energy due to the London-van der Waals' interaction between two spherical colloidal particles:

$$V_A = -\frac{A}{6}\left(\frac{2}{S^2-4} + \frac{2}{S^2} + \ln\frac{S^2-4}{S^2}\right) \tag{2}$$

where A is the Hamaker constant, and $s$ can be defined as:

$$s = 2 + H/a \tag{3}$$

where H is the separation distance between the two particles, and a is the radius of the spherical particles.

13

When the distance H is far less than the radius of particles, the Eq.(2) can be simplified:

$$V_A = -A \frac{a}{12H} \tag{4}$$

The repulsion energy between two charged spheres, $V_R$, can be represented by:

$$V_R = 2\pi\varepsilon\varepsilon_0 a\psi^2 \ln[1 + e^{-\kappa H}] \tag{5}$$

where $\varepsilon$ represents the dielectric constant of the liquid, $\varepsilon_0$ represents the dielectric permittivity of vacuum, $\psi$ represents the surface potential, $1/\kappa$ represents the Debye length which characterizes the thickness of the double layer:

$$\kappa = \left( \frac{e_0^2 \sum n_i z_i^2}{\varepsilon\varepsilon_0 \kappa T} \right)^{1/2} \tag{6}$$

where T is the absolute temperature, and $n_i$ and $z_i$ are the concentration and valence of ions, respectively, $e_0$ is the charge of a single electron, and $\kappa$ is the Boltzmann constant.

Fig. 2-1A describes the relationship between the interaction force profiles between particles and the interparticle separation. The Van der Waals forces governed the profiles at large and small distances, whereas the double layer contribution dictated the forces at the intermediate distances. Fig.2-1B indicates that the total interaction energy showed a maximum which is called energy barrier that prevents particles from flocculation. This peak in the total energy curve occurs when the repulsion force between the double layers is significantly higher than the van der Waals' attraction.
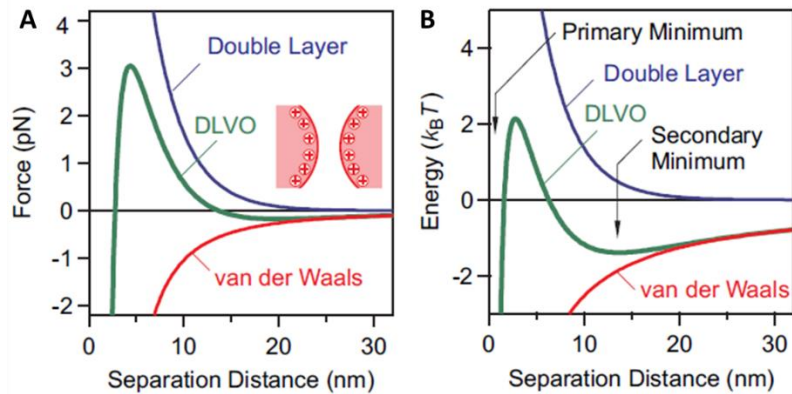
Fig. 2-1 The force profiles (A) and the potential energy profiles (B) as functions of the separation distance between two particles, according to the DLVO theory, used with permission. [4]

As indicated in the equations above, the DLVO theory considers the effect of concentration and valence of electrolyte ions, which allows for accurately predicting the stability of a colloidal suspension. The thickness of electrical double layers (characterized by the Debye length $1/\kappa$) is susceptible to the electrolyte concentration. [3] The DLVO theory reveals a threshold of electrolyte concentration for particles aggregation. This threshold decreases as the valence of the electrolyte ions of a charge opposite to that of the particles increases. [3] The double layer force dominates the interaction between particles at low electrolyte concentrations or high surface charge densities. In contrast, the attractive van der Waals' force dictates the interaction at high electrolyte concentrations or small surface charge densities. The energy profile exhibited a maximum at intermediate concentrations or charge densities, and the maximum value occurs at a separation distance close to the Debye length. [3, 4] The energy profile peak decreases with the increase of the electrolyte concentration. Coagulation occurs when the energy barrier disappears. [3]

## 2.1.2 Other interparticle forces

The accuracy of the DLVO theory has been discussed in the previous literature. [5-12] However, there remain limitations to analysing the interactions of two particles. For example, the DLVO theory is only applicable to highly diluted systems. It is based on the Poisson-Boltzmann (PB) approximation, though the PB approximation neglects the attractive ion correlation forces in the ion cloud. Therefore, this theory can only be used to study the interaction between isolated particles. The volume exclusion effect [7, 11] can result in an attractive force between the particles. This attractive contribution could lead the particles to aggregate and flocculate. [10]

In addition, the DLVO theory cannot explain the effect of the bonding or adsorption of polymers on the particle surface because it can introduce both attractive and repulsive forces. [13-19] After adding a polymer into the system, either stable suspension or aggregation of particles occurs [13, 19]. As shown in Fig.2-2, long-chain polymers anchored onto the particle surface provide steric hindrance and induce the repulsion force between particles, referred to as steric stabilization. This will be discussed in detail in sections 2.2.2 and 2.2.3. The adsorption of polyelectrolytes allows dispersion by electrostatic and steric repulsion. The single polymer chain can adsorb on two or more particle surfaces at low polymer concentration, resulting in "bridging flocculation", as seen in Fig. 2-2. [13, 19] Non-adsorbing polymers can also lead to depletion flocculation or depletion stabilization of particles in the colloidal system (see Fig.2-

2). [19-21] According to previous literature [14, 16, 21], the interactions between the particles

and polyelectrolytes consist of electrostatic, hydrophobic, and dipole-dipole attractions.
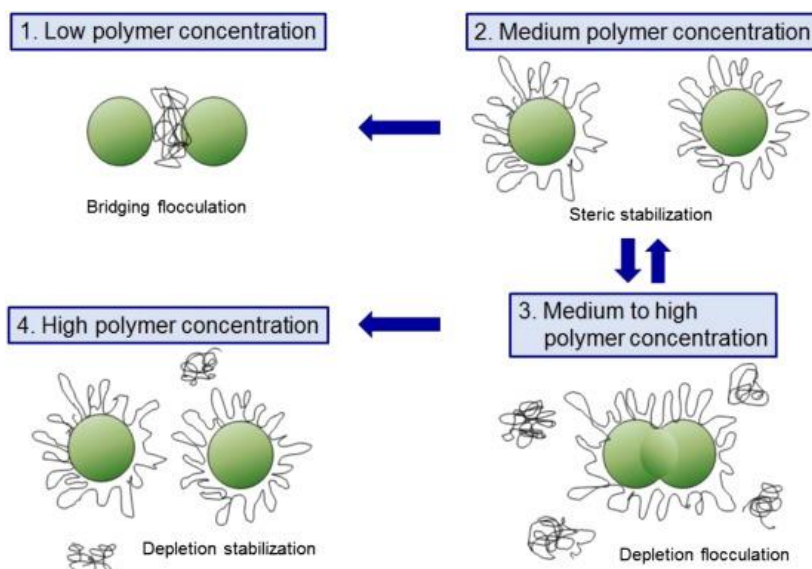


Fig. 2-2 A fairly simplified representation on the possible effects of polymer addition on the stability of colloidal system, used with permission. [21]

Therefore, DLVO theory provides a method to control the stabilization of the colloidal

system through varying the parameters, such as electrolyte concentration and surface charge.

However, from the above discussion of the cases when the DLVO theory has limitations,

adding dispersing agents is also a promising method to stabilize the colloidal system.

## 2.2  Suspension stability and particle charging

To stabilize the suspension, there is a need to create a repulsion force which is strong

enough to overcome the attractive force between the particles. The most commonly used

methods are electrostatic stabilization, steric stabilization and electrosteric stabilization.

## 2.2.1 Electrostatic stability

Electrostatic stabilization occurs when electrostatic charges on the particles generate repulsion between them. The repulsion is a result of the interaction of the electrical double layers of charge produced around each particle. To introduce electrostatic stability, we discuss how particles acquire an electrostatic charge in both aqueous and non-aqueous solution.

### 2.2.1.1 Electrostatic stability in aqueous media

In an aqueous liquid, there are different processes by which particles dispersed can obtain a charge on the surface. They are (1) preferential adsorption of ions, (2) dissociation of surface groups, (3) isomorphic substitution, and (4) adsorption of polyelectrolytes. For oxide particles, it is common to see the preferential adsorption of ions in liquid, while the process of isomorphic substitution is often seen in clays. The dissociation of common surface groups, including sulfate, carboxyl and sulfonate groups, has been discussed in [22].

There are two portions of charges in the electrostatically stabilized suspension: the charge on the particle surface and the opposite and equal countercharge. Here, the positive ions are assumed to be preferentially adsorbed on the particle surface. If there is no thermal motion, an equal number of counterions will neutralize the positive ions on the particle surface. However, the thermal motion exists so that a dense double layer can not form. On the contrary, the counterions move in the media rather than being firmly anchored on the object's surface. They are loosely packed and make up the diffuse layer (Fig. 2-3).
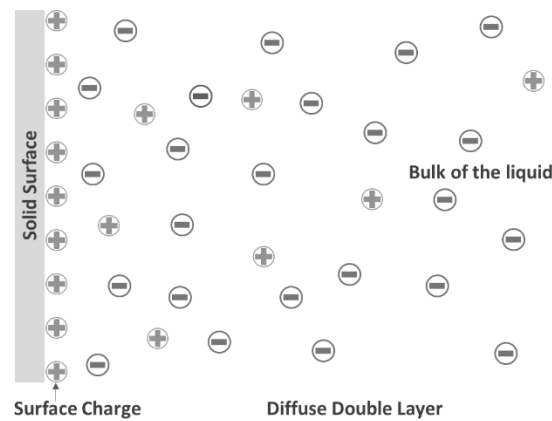
Fig. 2-3 The schematic diagram of the electrical double layer associated with a positively charged surface in a liquid. [20]

The concentration of ions changes rapidly with a longer distance from the surface, and the electrical potential drops accordingly in Fig.2-4. The potential decreased to $1/e$ of the potential at the particle surface at the distance of $1/\kappa$, and beyond this, the change of potential is tiny along with the increase of the distance. [20] Therefore, the $1/\kappa$ which is usually called Debye length can be considered the double layer thickness. It is common to use $1/\kappa$ for analysis of the electrical double layer. The size of the double layer relies on many experimental parameters according to Eq(6) in section 2.1.1. The adjustment of parameters can control the strength of the double layer repulsion and thus the suspension stability. [20]
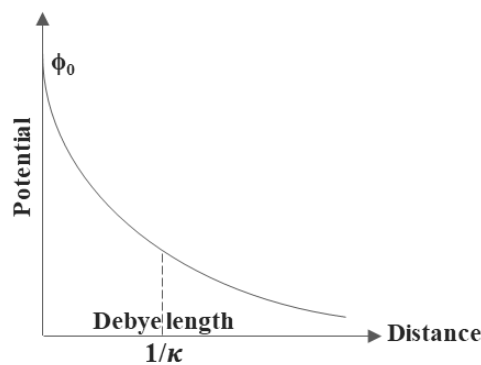


Fig. 2-4 The electrical potential as a function of distance from the surface. [20]

19

The diffuse double layers will begin to overlap when two particles make contact in the solution. As a result, a repulsion between these two particles occurs due to the interaction between the double layers. Then, a stable suspension will be developed if the repulsion is sufficiently enough to resist the attractive van der Waals' force.

## 2.2.1.2 Electrostatic stability in non-aqueous media

Theoretically, the magnitude of electrostatic stabilization in non-aqueous liquid is highly sensitive to the dielectric constant $\varepsilon$ of the media which influences stability in particular through the dissociation degree of the stabilizing electrolyte. There are also a certain number of ions in the solvents offering enough repulsion force except the presence of charge on the particles.

For non-aqueous media, their dielectric constant is relatively low, electrolytes in those liquids cannot dissociate entirely, and often the ionic strengths are far less than $10^{-6}$ M. There is only a small number of charges that exist in the non-aqueous media. Therefore, unless the particle concentration is extremely low, the charged and dispersed particles in such non-aqueous liquid are surrounded by the extended ionic layers and sit on the double layers of each other. [23-26]

Similar with electrostatic repulsion in aqueous media, there is also the interaction of double layers of the particles in non-aqueous media. The dielectric constant is a critical parameter in this case because it has a dual effect on the interaction: (1) it affects the

dissociation of electrolytes indirectly, and (2) it can measure the screening of charges by the solvent directly. It is often considered that the electrostatic repulsion in the liquid with low dielectric constant is too small to achieve the stability of suspension. [27]

In order to prevent the colloidal particles to coagulate irreversibly, three requirements must be met. (1) The particles need to be sufficiently charged. (2) The number of ions should be moderate. The presence of enough ions allows the potential decay around the particles steep, but if the number of ions exceeds demand, the double layer will be compressed thoroughly. (3) A position needs to be confirmed at which the electrostatic repulsion overcomes the attractive van der Waals' force.

In a media with a low dielectric constant, the van der Waals' attraction between particles can be evaluated according to the Liftshitz theory. There are several factors influencing the evaluation, such as the difference in refractive indices and/or dielectric permittivities of the dispersed inorganic solids and liquids at different frequencies. [28] Compared with water, the van der Waals' attraction between particles in the media with a low dielectric constant is relatively small. As a result, it requires a lower energy barrier to achieve repulsive pair interaction in the non-aqueous media with a low dielectric constant.

## 2.2.2 Steric stability

Steric stabilization represents colloidal stabilization which is achieved by the interaction between uncharged polymer chains adsorbed onto the surface of particles, as shown in Fig.2-5. [29]
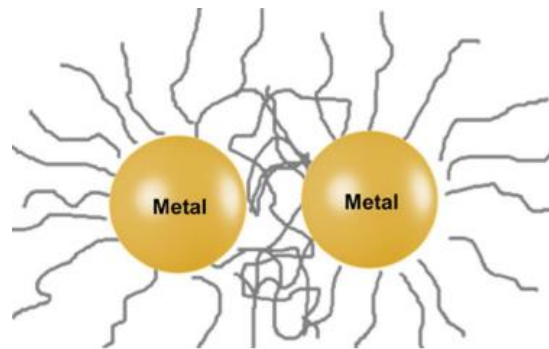


Fig. 2-5 Schematic representation of steric stabilization of metal colloid particles, used with permission. [29]

Different from the electrostatic stabilization accomplished by the interaction between the charged particles, steric stabilization is contributed by the interactions between the polymer chains, which is determined by the configurational entropy of the chains. Steric stabilization is commonly associated with the particles in an organic solvent, but it is still effective in aqueous media. Steric stabilization is presently applied to a wide range of products in industry, including paints, inks, coatings and pharmaceuticals. In ceramics processing, it is commonly employed to produce stable suspensions in the consolidation of ceramic powders by casting processes like slip casting and tape casting. To achieve effective steric stabilization, there are two requirements that need to be met: (1) the polymer chains must be well adsorbed onto the surface

of particles so that the risk of desorption can be minimized; (2) the adsorbed layer must be

thick enough to provide sufficient repulsion force when the particles approach each other. [20]

## 2.2.3 Electrosteric stabilization

Electrosteric stabilization combines electrostatic and steric repulsion (Fig.2-6). The

existence of adsorbed polymers and a considerable double layer repulsion is required.
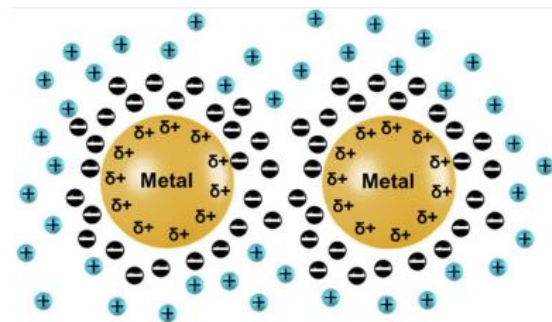


Fig. 2-6 Schematic representation of electrosteric stabilization of metal colloid particles, used
with permission. [29]

Electrosteric stabilization is generally associated with suspensions in aqueous media.

However, some investigations revealed that it also could be achieved in some non-aqueous

liquids. [30] In aqueous media, a common method of electrosteric stabilization is to use the

polyelectrolytes which contain at least one ionizable group (e.g., carboxylic or sulfonic acid

group) that can dissociate to form charged polymers.

Both the solvent properties and the particle surface have huge effects on the dissociation

and adsorption of polymers. Fig.2-7 displays the structure of two commonly used polymers for

electrosteric stabilization: poly(methacrylic acid) (PMAA) and poly(acrylic acid) (PAA). The

dissociation reaction is described by the following equation:

$$A- COOH + H_2O \rightleftharpoons A - COO^- + H_3O^+ \qquad (7)$$
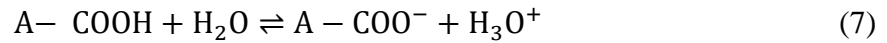
where A represents the main structure of PMAA or PAA without the chain of carboxylic group.

The dissociated and non-dissociated fraction of the functional groups depends on the pH and

the ionic concentration of the solution. [20]
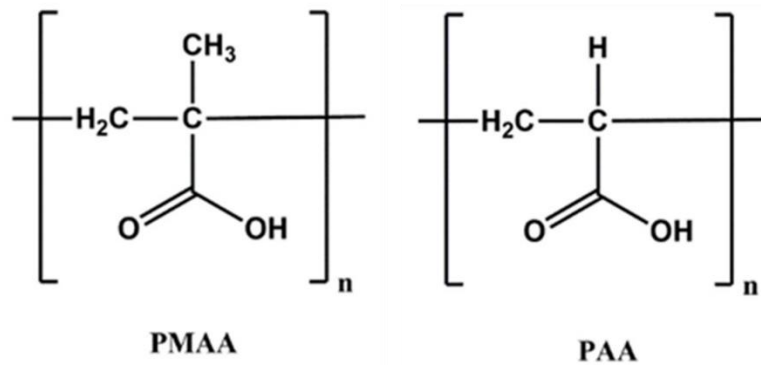


Fig. 2-7 Schematic diagram showing the polymer segments of poly(methacrylic acid) (PMAA) and poly(acrylic acid) (PAA) , used with permission.[30]

The polymers for electrosteric stabilization can be homopolymers such as poly(acrylic

acid), block copolymers, or graft copolymers. In the industry, polyelectrolytes are commonly

applied in the manufacture of highly concentrated ceramic suspensions (more than 50 vol%

particles) which are followed by the consolidation and burning to produce dense particles.

## 2.3 Advanced dispersing agents for colloidal processing

Dispersing agents are the materials that are used to form stable colloidal suspension

through electrostatic, steric or electrosteric stabilization methods. Particularly, the usage of

dispersing agents plays an essential role in the development of electrodeposition. The investigation of advanced additives that can charge and disperse functional particles in colloidal suspension has gained great interest in recent years.[31] To be an effective dispersing and charging agent for electrodeposition, there are two requirements that need to be met: first, a dispersant must be well adsorbed on the particle surface. Second, it must impart a charge to the particles, which could provide electrostatic repulsion between particles and help to achieve the deposition under the electric field.

## 2.3.1 Catechol-based dispersants for metal oxide particles

A new direction for research on the advanced dispersing agents which could be strongly anchored onto the particle surface arose from the study on the mechanism of the mussel adhesion to diverse surfaces. [32, 33] Previous studies indicated that the strong mussel adhesion involves protein macromolecules, containing catecholic amino acid, L-3,4-dihydroxyphenylalanine (DOPA). The key benefit of the catechol chemistry is its application to a vast variety of substrates and excellent binding strength under wet conditions.[34] The adhesion mechanism of mussels is ascribed to the complexation of metal atoms on the material surfaces by OH group of the catechol ligands (Fig. 2-8).
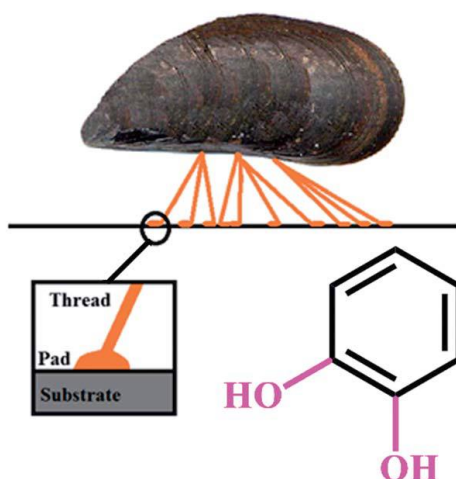
Fig. 2-8 Schematic of mussel adsorption and chemical structure of catechol, used with permission. [31]

Here, the structures and adsorption mechanisms of the catechol-based molecules are described (Fig. 2-9). A catechol is an unsaturated six-carbon ring (phenolic group) with two OH groups bonded to adjacent carbon atoms. DOPA belongs to the catechol family. The chemical structure of DOPA includes a catechol ligand, and additional carboxylic and amino groups (Fig. 2-9). This molecule shows zwitterionic properties and has bidentate interfacial interactions on different surfaces involving metal ions. Although the application of DOPA as charging agents for EPD still presents difficulties because of the zwitterionic properties, the analysis of DOPA adsorption has led to the research of other catechol-based molecules.

Fig. 2-9 Structure of molecules from catechol family, used with permission. [31]

Dopamine structure (Fig.2-9) has two OH groups of the catechol ligand, the adsorption of which is based on the chelating mechanism. The amino group can be protonated in inorganic acids. Consequently, dopamine shows cationic properties in acid. The self-polymerization of dopamine can be observed in basic solutions, which was used for the fabrication of polydopamine coatings. The polydopamine has strong adhesion to various substrates, such as Pt, stainless steel, $TiO_2$ and other materials.[31] Dopamine can be used as charging and dispersing agent for EPD of ceramic particles which can also be combined with the EPD of cationic polyelectrolytes for fabrication of organic-inorganic composites. [35]

Caffeic acid (CA) can act as efficient green corrosion inhibitor for stainless steel. CA has similar chemical structure with DOPA (Fig. 2-9). CA has anionic properties which are associated with the dissociation of the carboxylic group. The strong adsorption of CA can be seen on inorganic surfaces including stainless steel,[36] $TiO_2$, [37] and $MnO_2$ [38] in various liquids. Phenolic and carboxylic (Fig. 2-10) bonding sites are involved in the adsorption of CA.[38] Bidentate chelating bonding (Fig. 2-10a) and bidentate bridging bonding (Fig. 2-10b)

mechanisms [39, 40] were proposed. [36-38] The adsorption can involve inner sphere (Fig. 2-10b) or outer sphere bonding (Fig. 2-10b), depending on the nature of the adsorbent materials.

It was found that CA can be used as a co-dispersant for anodic deposition of composite films.
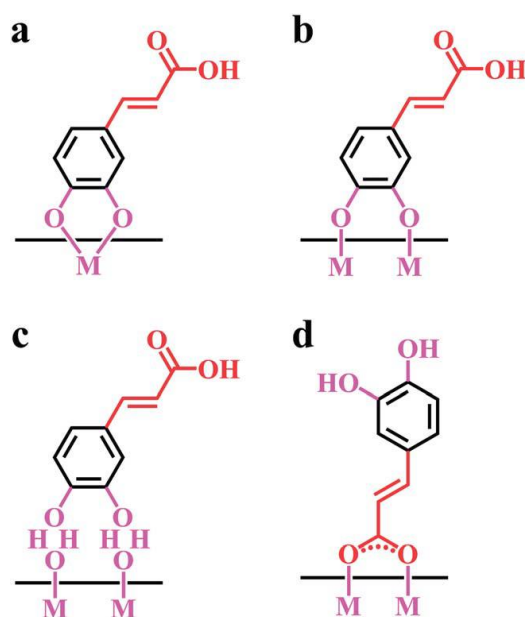


Fig. 2-10 Suggested adsorption mechanisms of caffeic acid: (a) bidentate chelating bonding, (b) bidentate bridging bonding (inner sphere), (c) bidentate bridging bonding (outer sphere) of catechol group, (d) adsorption, involving a carboxylic group, used with permission. [31]

Fig.2-9 displays the chemical structures of 3,4-dihydroxybenzoic acid (DHB), 3,4-dihydroxyphenylacetic acid (DHP) and 3,4-dihydroxyhydrocinnamic acid (DHC), which belong to the catechol family. The carboxylic groups contribute to the anionic properties of these molecules. They also show strong adsorption on metal salts. It was found in recent studies that these three molecules are promising charging and dispersing agents for electrophoretic deposition (EPD) of different oxide materials from suspensions in ethanol. Particularly, the investigations revealed strong adsorption of DHB and DHP on $TiO_2$ nanoparticles. [41, 42].

Investigations also showed that other molecules, such as gallic acid with a similar structure can

be used for EPD of materials.[43]

## 2.3.2 Phosphate ester as an electrosteric stabilizer

Previous studies [44, 45] demonstrated that phosphate ester (PE) can impart a significant

positive charge to the surface of $BaTiO_3$ particles. PE is considered as a great electrostatic

stabilizer since it can charge the particles positively in organic solvents by donating a proton

to the surface. Moreover, PE contains a mixture of long-chain phosphate esters of ethoxylated

alcohols (see in Fig. 2-11) so that it can also act as a steric dispersant through anchoring the

long-chain polymer to the particle surface.

**Monoester**                                    **Diester**

$$
\begin{array}{cc}
\text{OH} & \text{OR} \\
| & | \\
\text{RO} - \text{P} - \text{OH} \qquad & \text{RO} - \text{P} - \text{OH} \\
\| & \| \\
\text{O} & \text{O}
\end{array}
$$

$$R = [-(CH_2\text{-}CH_2\text{-}O)_n\text{-}R']$$
$$R' = \text{alkyl or alkylaryl radical}$$
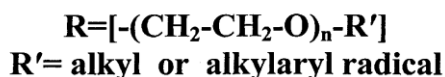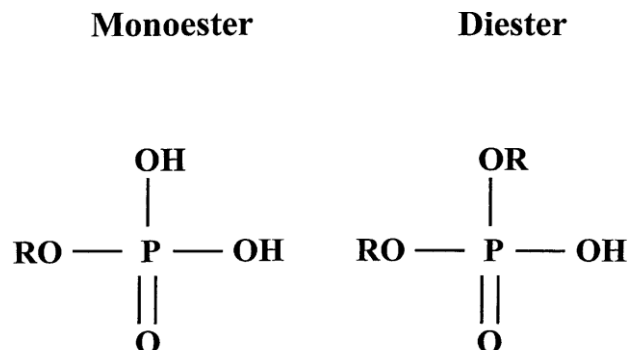
Fig. 2-11 Schematic structure representation of phosphate esters, used with permission. [3]

PE can be applied for cathodic EPD as positively charging and dispersing agents. [46] As

it is shown in Fig.2-12a, there was sedimentation in the suspension of $MnO_2$ in pure ethanol

one day after ultrasonic treatment. The particles were high agglomerated, and the deposited

coatings were non-uniform from such an unstable suspension. In contrast, $MnO_2$ particles in

the suspension containing PE as a dispersant were well dispersed even seven days after

ultrasonic treatment (Fig.2-12b) and deposited as relatively uniform coatings. The deposits

increased with increasing PE concentration, showed a maximum and then decreased at higher

PE concentrations. This indicated that the PE contributed to the charging and dispersion of the

ceramic particles. [46]
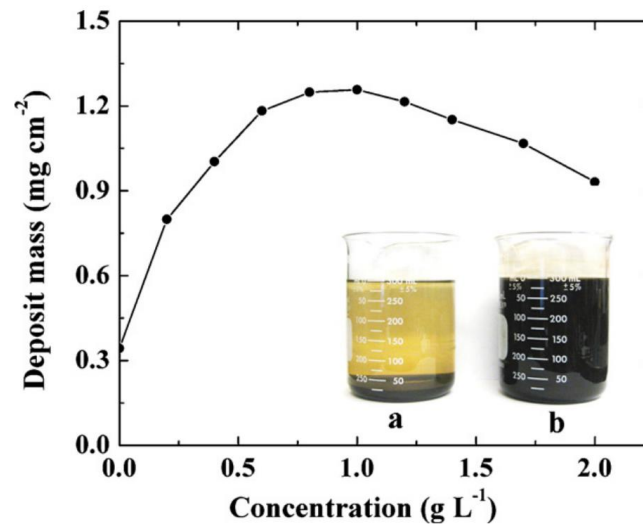


Fig. 2-12 Deposit mass for films on stainless steel substrates versus PE concentration in the 45 g $L^{-1}$ manganese dioxide suspensions at a deposition voltage of 20 V and deposition time of 1 min. Insert shows suspensions (a) without PE, 1 day after ultrasonic treatment and (b) containing 1 g $L^{-1}$ PE, 7 days after ultrasonic treatment, used with permission. [46]

## 2.4  Colloidal processing techniques

Colloidal processing techniques allow the consolidation from colloidal suspensions to

dense and homogeneous green bodies. It is desirable to form bodies directly from the slurry

state. [47] During the previous two decades, a growing number of colloidal processing

techniques have been developed. The physical or chemical processes, experimental techniques

and devices may vary, but well dispersed suspension with high solids loading is necessary in

all cases.

Several colloidal processing techniques for fabrication of ceramic components with

different shape and complexity and microstructural control are described in Table.2-1. [47, 48]

Their major characteristics are summarized below. Among these processing techniques, EPD

and dip coating methods are promising for application in different fields.

Table 2-1 Representative colloidal techniques classified by consolidation mechanism, used
with permission. [47, 48]

| Route | Mechanism | Processing technique | Features |
|---|---|---|---|
| Fluid removal | Filtration | Slip casting | Complex, 3D, thin walled |
| | | Pressure filtration | Simple, 3D |
| | | Osmotic consolidation | Simple, 3D |
| | Evaporation | Dip coating | |
| | | Spin coating | |
| | | Spray coating | |
| | | Tape casting | |
| | | Electrophoresis | |
| Particle flow | Particle flow due to applied gravitational force | Centrifugal consolidation | Complex, 3D |
| | Particle flow due to electric field | Electrophoretic deposition | Simple, 2D or 3D |
| Gelation | Thermal gelation | Thermogelation | Complex, 3D |
| | | protein casting | Complex, 3D; porous |
| | Chemical gelation | Injection moulding | Complex, 3D |
| | | Gelcasting | |

## 2.4.1 Dip coating

Among the techniques described above, dip coating is a very simple, low-cost, and

reproducible technique. The illustration of dip coating process is displayed in Fig. 2-13. [49]

During the dip coating process, the first step is to immerse the substrate into a solution

containing coating component particles. Next, it is withdrawal at constant speed into a water-

vapor-containing atmosphere. After that, a uniform liquid coating is produced on the surface

of substrate. The volatile solvents can be removed, and some possible chemical reactions will

occur, which leads to film formation, after drying at ambient temperature. [49] After that, the

coating usually needs hardening or chemical transformation by heat treatment. [49]
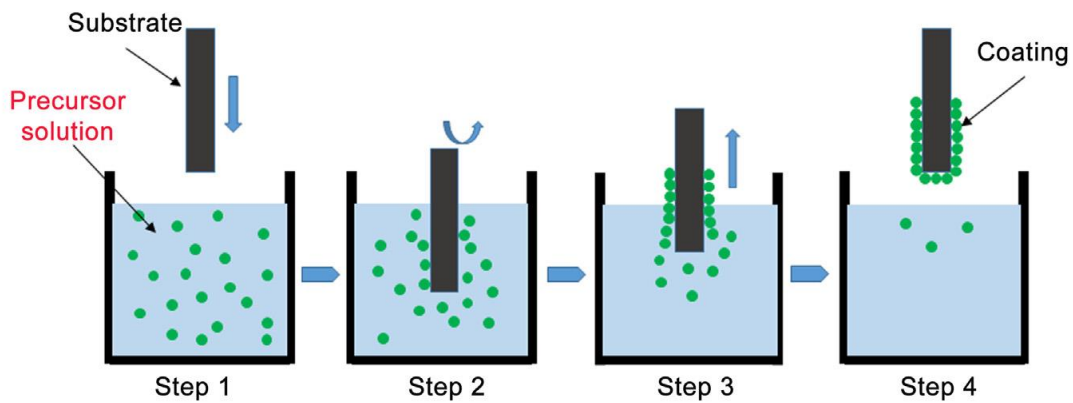


Fig. 2-13 Graphical representation of dip coating technique, used with permission.[49]

In the dip coating method, the quality and performance of the deposited coatings are

dictated by the liquid properties. Consequently, the careful selection of solvents and solutes is

essential. First, solvent volatility is an important factor that needs to be considered. Moderate

volatility allows the liquid film to level out sufficiently, and it can also keep the drying time as

short as possible. Second, the surface tension should be low enough so that the substrate can

be completely wetted, and the liquid can flow homogeneously. Based on the criteria, short-

chain aliphatic alcohols, such as ethanol, isopropanol, and n-propanol, are commonly selected

as solvents for dip coating.[50] Beyond that, a combination of various solvents is often used to

tailor the deposition performance. [50, 51] The selection of solute is much more complex. First,

the solute must be able to dissolve at an appropriate concentration. For example, using dilute

polymer solutions, good substrate coverage is difficult to achieve. Second, the solute is less

likely to crystallize or precipitate and tends to form an amorphous gel film by hydrolysis when the solvent is evaporating. [50] More than that, polymers with high $M_W$ are preferred due to their strong film-forming and binding properties.

The coating thickness can be predicted using the Landau-Levich equation (8) [52]

$$h = 0.94(\eta U)^{\frac{2}{3}}/\gamma_{LV}^{\frac{1}{6}}(\rho g)^{1/2} \qquad (8)$$

where h represents the thickness of the coating, $\eta$ is the viscosity of a liquid, U is the withdrawal speed, $\gamma_{LV}$ is the surface tension of liquid-vapour, $\rho$ is sol-specific gravity, and g represents gravity. According to this equation, higher viscosity and withdrawal speed lead to thicker films, while the following drying and sintering processes would cause the reduction of coating thickness. According to Hijon [53] and Mohseni [54], the concentration of the suspension is also an important factor influencing the thickness and uniformity of the as-deposited thin coating. The lower the concentration, the thinner the film is formed and the stronger the adhesion between coating and substrate is. Therefore, the thickness of deposited films can be controlled by the withdrawal speed and the concentration of the coating liquid in a given system. Films with a thickness of up to 1nm can be produced in a colloidal system, and the coating of an organic-inorganic composite can achieve a thickness of several microns because of the lower shrinkage and the higher flexibility of the network. [50] Multiple depositions in the dip coating process can also obtain thick films. Moreover, this method can build up laminate containing different coating materials.

Therefore, when fabricating a polymer coating, a high $M_W$ polymer with high solubility as the solute and a mixture of different solvents as the solvent are desired for a good quality film. Additionally, the multiple deposition method opens a gate to fabricating laminates with different functional layers containing different materials.

## 2.4.2 Electrophoretic deposition

The electrophoretic deposition (EPD) technique is a promising colloidal processing methods which has attracted significant attention recently due to its wide range of innovative applications in fabrication of functional ceramic coatings. It has many advantages, such as short formation time, nearly no limits for substrate shape and requires only a simple apparatus. The EPD method is particularly adaptable as it can be adjusted quickly for a given application. [55] Particularly, EPD enables easy control of the thickness and morphology of the as-deposited coatings through adjustment of the deposition time and electric field.

In EPD process, the dispersed and charged particles in a liquid, are deposited onto a conductive substrate with opposite charge under a DC electric field. EPD is classified into two types depending on which electrode the coating forms on: cathodic EPD and anodic EPD. In cathodic EPD, the particles are positively charged, and the deposition occurs on the negative electrode. The process of negatively charged particles depositing on an anode is named anodic EPD. Any of these two types of EPD can be achieved through proper tuning of charge on the particle surfaces. Fig.2-14 shows schematics for the two EPD processes. [55]
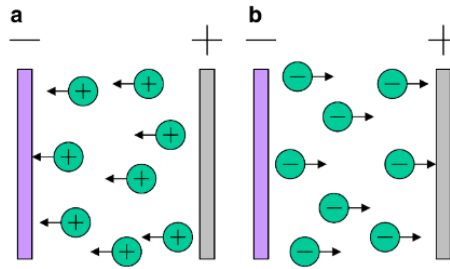
Fig. 2-14 Schematic illustration of electrophoretic deposition process. (a) Cathodic EPD and (b) anodic EPD, used with permission. [55]

## 2.4.2.1 Mechanism of EPD process

To date, there is no clear mechanism for EPD although it has been applied into different fields. [56]

Hamaker and Verwey [57, 58] first proposed the mechanism of EPD. They indicated that stable suspension is the precondition of efficient EPD, and the film formation is similar with gravity sediment while the main role of the electric field is to deliver the particles to the surface of the electrode for accumulation.

Grillon et al. [59] indicated that the charged particles would neutralize and then become static when they contact the electrode or the already deposited films. According to this theory, it will form a porous coating because the local electric fields interfere with continuous layer fabrication. However, the theory could not explain some cases, such as when continuous 2-D films were formed from a colloidal system [60-64].

Koelmans [65] proposed that the increase of electrolyte concentration near the electrode will cause the reduction of the repulsion between particles. This in turn reduces the zeta

potential and leads to flocculation of particles. This mechanism is feasible, for example, when there is generation of OH ions in the electrode reactions in aqueous suspensions, but it is invalid when there is no increase of electrolyte concentration near the electrode. The explanation for this invalidation was from Sarkar and Nicholson. [66]

Sarkar and Nicholson [66] proposed an electrical double layer distortion and thinning mechanism. They suggested that the double layer will be distorted to be thinner ahead and wider behind the particles when the particles are moving toward the electrode, and then the coagulation of particles will be promoted. However, De and Nicholson found this mechanism to be wrong after further research. [67] They developed a mechanism based on a local pH increase near the electrode surface.

## 2.4.2.2 Polymer binders in EPD

In ceramic processing, polymer binders are commonly used additives. They are multifunctional in EPD: (1) they can help to obtain adherent films and avoid cracks in deposits. (2) the adsorbed binders can act as steric stabilizer in the suspensions and lower the viscosity of the suspension. In EPD processing, since the binders are adsorbed on the charged particle surface, they can be delivered onto the electrode surface as well which means the binders will be incorporated into the deposited films. It is vitally important to control the adsorption of polymers on the charged particles for EPD. The fraction of adsorption depends on the concentration of polymer and the interactions between polymer and particle, polymer and

solvent, particle and solvent, and particle and dispersant. It's essential to dissolve high

concentration of polymers in suspension by using good solvents. However, when the solubility

of polymer is low in the suspension, it can be adsorbed on the particle surfaces. Their adsorption

can cause bridging flocculation in a poor solvent. On the contrary, good solvents help reach

steric stabilization because the polymer moieties which extend out from the particle surface

can be well solvated in a good solvent. Therefore, using the copolymers of a block or graft type

could be beneficial to EPD. Indeed, soluble polymers help to anchor copolymer molecules to

the particle surface, and thus the chains of soluble polymers offer steric stabilization. [55]

## 2.4.2.3 Solvents in EPD

The suspension for EPD is a complicated system, and each component makes a significant

impact on the deposition efficiency. There are two main types of solvent for EPD: water and

organic liquids (see in Table. 2-1). [3]

Table 2-2 Solvents used for EPD, used with permission. [3]

| Solvent | Method of deposition | Deposited material |
|---|---|---|
| Water | ELD | $Al_2O_3-Cr_2O_3$ [46], ZnO [47] |
|  | EPD | $Al_2O_3$ [48] |
| Dimethylformamide[a] | ELD | $Y_2O_3$ [49], $TiO_2$ [50] |
| Methyl alcohol−water | ELD | $TiO_2$ [8], $RuO_2-TiO_2$ [51] |
| Ethyl alcohol−water | ELD | $CeO_2$ [52], $SnO_2$ [5] |
|  | EPD | $CaSiO_3$ [53] |
| Isopropyl alcohol | EPD | Hydroxyapatite [54,55] |
| Isopropyl alcohol[a] | ELD | $YBa_2Cu_3O_{7-x}$ [56] |
| Ethyl alcohol−acetylacetone | EPD | MgO, $Al_2O_3$ [57] |
| Glacial acetic acid | EPD | PZT [58] |
| Ethyl alcohol | EPD | $Al_2O_3$, $ZrO_2$ [59] |
| Dichloromethane | EPD | β-alumina [60] |
| Acetone | EPD | YSZ [61] |
| Acetylacetone | EPD | YSZ [61] |
| Cyclohexanone | EPD | YSZ [61] |
| Methyl ethyl ketone | EPD | $Al_2O_3$ [62] |
| Toluene−ethyl alcohol | EPD | $Al_2O_3$ [62] |

There are many significant benefits of using an aqueous system for EPD. For example, the deposition potential is relatively low. The usage of an organic solvent can be avoided. [58] Faster kinetics, important health, environmental, and cost benefits can also be obtained when using an aqueous system in EPD. However, the aqueous-based suspension leads to a series of issues in the film-forming process. [68] The major issues are related to the electrochemical reaction at the electrodes while the current is passing through. This reaction will have a huge impact on process efficiency and coating quality. The electrolysis of water occurs at low voltages, and gas evolution cannot be avoided at the electrode when the field strengths is sufficient high. Subsequently, the bubbles will be retained in the as-deposited films unless certain procedures are adopted. [55] Additionally, the adsorption of water in deposited films may cause shrinkage and cracking during the drying procedure. [3]

In general, organic solvents are superior to water for EPD. The lower dielectric constant of organic solvents restricts particle charge due to its lower dissociation ability, so much higher field strengths need to be used. Because of the usage of higher electric field, the problems of electrolytic gas evolution are greatly reduced. Furthermore, the organic solvents are favoured because of their higher density, good chemical stability and low conductivity. [68] Using solvents that have high oxidation–reduction potentials including benzene and ketones can prevent the electrolysis of water and gas evolution in aqueous media. However, there are only a few free ions in these solvents, the charge on particle surface in benzene or ketones will be inadequate for EPD due to their low dielectric constant. [68] As a result, hundreds of volts need

to be applied. [55] The major issue along with the usage of organics is the requirement of higher voltages, cost, toxicity and flammability.

Using methyl alcohol-water and ethyl alcohol-water mixture as solvents was desirable to reduce cracking and porosity in the deposits fabricated in aqueous media. [69, 70] The total dielectric constant of solvent could be lowered by adding alcohols to the water. The deposition rate showed a significant improvement by this method. [71] Combining organic solvent and water is an efficient way to avoid some problems from their single use, however, the ratio needs to be carefully controlled.

## 2.4.2.4 Factors influencing EPD

In EPD process, there are two sets of important parameters: (1) the parameters associated with suspension, and (2) the parameters related to the process, such as the physical parameters (deposition voltages, deposition time, etc.) [72]

Ishihara et al. [73] and Chen and Liu [74] proposed the equation below for the weight (*w*) of charged particles deposited per unit area of electrode at the early stage, neglecting the charge provided by the free ions

$$w = \frac{2}{3} C \cdot \varepsilon_0 \cdot \varepsilon_r \cdot \xi \cdot \left(\frac{1}{\eta}\right) \cdot \left(\frac{E}{L}\right) \cdot t \tag{8}$$

where C is the particle concentration, $\varepsilon_0$ and $\varepsilon_r$ represents permittivity of vacuum and solvent, respectively, $\xi$ and E are the zeta potential of the particles and deposition potential, $\eta$ is solvent viscosity, L is the distance between the electrodes, and t is the deposition time. [73, 74]

This equation is named the Hamaker equation. It indicates that the deposition yield in EPD depends on the suspension and deposition parameters. If the suspension and the equipment for EPD are fixed, $\varepsilon_0$, $\varepsilon_r$, $\eta$ and L would be constant. Therefore, the mass loading (w) is a function of C, E and t. It means that the thickness of as-deposited films can be easily controlled by the suspension concentration, deposition voltage and time in the EPD process.

Additionally, the suspension system for EPD is complex, and each component has a huge impact on the deposition efficiency. Therefore, it is essential to build a stable suspension for EPD. Suspension stabilization can be achieved through electrostatic, steric, or electrosteric stabilization method, which requires the help of an efficient dispersant. [3] Moreover, EPD can only perform when the particles are electrically charged. [3] Consequently, adding an agent that has the function of both dispersing and charging into the suspension is ideal for performing EPD on electrically neutral particles.

## 2.5  References

[1] B. Derjaguin, L. Landau, Acta Physicochim. URSS,  (1941).

[2]  E.J.W. Verwey, J.T.G. Overbeek, K. Van Nes, Theory of the stability of lyophobic colloids: the interaction of sol particles having an electric double layer, Elsevier Publishing Company1948.

[3] I. Zhitomirsky, Cathodic electrodeposition of ceramic and organoceramic materials. Fundamental aspects, Advances in colloid interface science 97(1-3) (2002) 279-317.

[4] G. Trefalt, M. Borkovec, Overview of DLVO theory,  (2014).

[5] X. Chu, A. Nikolov, D. Wasan, Thin liquid film structure and stability: The role of depletion and surface-induced structural forces, The Journal of chemical physics 103(15) (1995) 6653-6661.

[6] I. Sogami, N. Ise, On the electrostatic interaction in macroionic solutions, The Journal of chemical physics 81(12) (1984) 6320-6332.

[7] R. Kjellander, S. Marcelja, R. Pashley, J. Quirk, Double-layer ion correlation forces restrict calcium-clay swelling, The Journal of Physical Chemistry 92(23) (1988) 6489-6492.

[8] J. Valleau, R. Ivkov, G. Torrie, Colloid stability: the forces between charged surfaces in an electrolyte, The Journal of chemical physics 95(1) (1991) 520-532.

[9] R. Kjellander, T. A, kesson, B. Jönsson, S. Marcelja, J. Chem. Phys 97 (1992) 1424.

[10] J.Y. Walz, A. Sharma, Effect of long range interactions on the depletion force between colloidal particles, Journal of colloid interface science 168(2) (1994) 485-496.

[11] X. Chu, D.T. Wasan, Attractive interaction between similarly charged colloidal particles, Journal of colloid interface science 184(1) (1996) 268-278.

[12] A. Delville, RJ-M. Pellenq, JM Caillol, J. Chem. Phys 106 (1997) 7275.

[13] J. Ennis, L. Sjöström, T. Åkesson, B. Jönsson, Surface interactions in the presence of polyelectrolytes. A simple theory, Langmuir 16(18) (2000) 7116-7125.

[14] T. Okubo, M. Suda, Absorption of polyelectrolytes on colloidal surfaces as studied by electrophoretic and dynamic light-scattering techniques, Journal of colloid  interface science 213(2) (1999) 565-571.

[15] L. Sjöström, T. Åkesson, The stability of charged colloids-Attractive double layer forces due to asymmetric charge distribution, Journal of colloid interface science 181(2) (1996) 645-653.

[16] N.G. Hoogeveen, M.A.C. Stuart, G.J. Fleer, Polyelectrolyte adsorption on oxides: II. Reversibility and exchange, Journal of colloid interface science 182(1) (1996) 146-157.

[17] N.G. Hoogeveen, M.A.C. Stuart, G.J. Fleer, Polyelectrolyte adsorption on oxides: I. Kinetics and adsorbed amounts, Journal of colloid interface science 182(1) (1996) 133-145.

[18] C. Stuart, MA; Fleer, GJ; Lyklema, J.; Norde, W.; Scheutjens, JMHM, Adv. Colloid Interface Sci 34 (1991) 477.

[19] E. Dickinson, L. Eriksson, Particle flocculation by adsorbing polymers, Advances in Colloid Interface Science 34 (1991) 1-29.

[20] M.N. Rahaman, Ceramic processing, CRC press2017.

[21] T. Kuroiwa, I. Kobayashi, A.M. Chuah, M. Nakajima, S. Ichikawa, Formulation and stabilization of nano-/microdispersion systems using naturally occurring edible polyelectrolytes by electrostatic deposition and complexation, Advances in Colloid 226 (2015) 86-100.

[22] T.W. Healy, L.R.J.A.i.C. White, I. Science, Ionizable surface group models of aqueous interfaces, 9(4) (1978) 303-345.

[23] H. Koelmans, J.T.G. Overbeek, Stability and electrophoretic deposition of suspensions in non-aqueous media, Discussions of the Faraday society 18 (1954) 52-63.

[24] A. Kitahara, S. Karasawa, H. Yamada, The effect of water on electrokinetic potential and stability of suspensions in nonpolar media, Journal of Colloid Interface Science 25(4) (1967) 490-495.

[25] J. Lyklema, Principles of the stability of lyophobic colloidal dispersions in non-aqueous media, Advances in Colloid Interface Science 2(2) (1968) 67-114.

[26] C. Chen, S. Levine, The double-layer interaction of two charged colloidal spherical particles of a concentrated dispersion in a medium of low dielectric constant: I. Force calculations, Journal of Colloid Interface Science 43(3) (1973) 599-615.

[27] G. Feat, S. Levine, The double-layer interaction of two charged colloidal spherical particles of a concentrated dispersion in a medium of low dielectric constant: III. Approximation of perfectly conducting particles, Journal of Colloid Interface Science 54(1) (1976) 34-44.

[28] D.B. Hough, L.R. White, The calculation of Hamaker constants from Liftshitz theory with applications to wetting phenomena, Advances in Colloid Interface Science 14(1) (1980) 3-41.

[29] D.H. Napper, Polymeric stabilization of colloidal dispersions, Academic Press1983.

[30] F.M. Fowkes, Advances in Ceramics 21 (1987) 412.

[31] M. Ata, Y. Liu, I. Zhitomirsky, A review of new methods of surface chemical modification, dispersion and electrophoretic deposition of metal oxide particles, Rsc Advances 4(43) (2014) 22716-22732.

[32] B.P. Lee, P.B. Messersmith, J.N. Israelachvili, J.H. Waite, Mussel-inspired adhesives and coatings, Annual review of materials research 41 (2011) 99-132.

[33] H. Lee, S.M. Dellatore, W.M. Miller, P.B. Messersmith, Mussel-inspired surface chemistry for multifunctional coatings, science 318(5849) (2007) 426-430.

[34] L. Petrone, Molecular surface chemistry in marine bioadhesion, Advances in colloid interface science 195 (2013) 1-18.

[35] K. Wu, P. Imin, A. Adronov, I. Zhitomirsky, Electrophoretic deposition of poly [3-(3-N, N-diethylaminopropoxy) thiophene] and composite films, Materials Chemistry Physics 125(1-2) (2011) 210-218.

[36] F.S. de Souza, A. Spinelli, Caffeic acid as a green corrosion inhibitor for mild steel, Corrosion science 51(3) (2009) 642-649.

[37] Y. Sun, I. Zhitomirsky, Electrophoretic deposition of titanium dioxide using organic acids as charging additives, Materials Letters 73 (2012) 190-193.

[38] Y. Wang, I. Zhitomirsky, Bio-inspired catechol chemistry for electrophoretic nanotechnology of oxide films, Journal of colloid interface science 380(1) (2012) 8-15.

[39] Q. Ye, F. Zhou, W. Liu, Bioinspired catecholic chemistry for surface modification, Chemical Society Reviews 40(7) (2011) 4244-4258.

[40] Q. Chen, Y. Jia, S. Liu, G. Mogilevsky, A. Kleinhammes, Y. Wu, Molecules immobilization in titania nanotubes: a solid-state NMR and computational chemistry study, The Journal of Physical Chemistry C 112(44) (2008) 17331-17335.

[41] I.A. Jankovic, Z.V. Saponjic, M.I. Comor, J.M. Nedeljkovic, Surface modification of colloidal TiO2 nanoparticles with bidentate benzene derivatives, The Journal of Physical Chemistry C 113(29) (2009) 12645-12652.

[42] J. Peyre, V. Humblot, C. Méthivier, J.-M. Berjeaud, C.-M. Pradier, Co-grafting of amino–poly (ethylene glycol) and magainin I on a TiO2 surface: tests of antifouling and antibacterial activities, The Journal of Physical Chemistry B 116(47) (2012) 13839-13847.

[43] K. Wu, Y. Wang, I. Zhitomirsky, Electrophoretic deposition of TiO2 and composite TiO2–MnO2 films using benzoic acid and phenolic molecules as charging additives, Journal of colloid interface science 352(2) (2010) 371-378.

[44] E. Streicher, T. Chartier, P. Boch, Influence of organic components on properties of tape-cast aluminum nitride substrates, Ceramics international 16(4) (1990) 247-252.

[45] U. Paik, V.A. Hackley, S.-C. Choi, Y.-G. Jung, The effect of electrostatic repulsive forces on the stability of BaTiO3 particles suspended in non-aqueous media, Colloids Surfaces A: Physicochemical Engineering Aspects 135(1-3) (1998) 77-88.

[46] J. Li, I. Zhitomirsky, Cathodic electrophoretic deposition of manganese dioxide films, Colloids Surfaces A: Physicochemical Engineering Aspects 348(1-3) (2009) 248-253.

[47] J.A. Lewis, Colloidal processing of ceramics, Journal of the American Ceramic Society 83(10) (2000) 2341-2359.

[48] R. Moreno, Colloidal processing of ceramics and composites, Advances in applied ceramics 111(5-6) (2012) 246-253.

[49] I.A. Neacşu, A.I. Nicoară, O.R. Vasile, B.Ş. Vasile, Inorganic micro-and nanostructured implants for tissue engineering, Nanobiomaterials in Hard Tissue Engineering, Elsevier2016, pp. 271-295.

[50] M.A. Aegerter, M. Mennig, Sol-gel technologies for glass producers and users, Springer Science & Business Media2013.

[51] P. Löbmann, Soluble powders as precursors for TiO2 thin films, Journal of sol-gel science technology 33(3) (2005) 275-282.

[52] B. Levich, L. Landau, Dragging of a liquid by a moving plate, Acta Physicochim. URSS 17 (1942) 42.

[53] N. Hijon, M.V. Cabañas, J. Pena, M. Vallet-Regí, Dip coated silicon-substituted hydroxyapatite films, Acta biomaterialia 2(5) (2006) 567-574.

[54] E. Mohseni, E. Zalnezhad, A.R. Bushroa, Comparative investigation on the adhesion of hydroxyapatite coating on Ti–6Al–4V implant: A review paper, International Journal of Adhesion Adhesives 48 (2014) 238-257.

[55] L. Besra, M. Liu, A review on fundamentals and applications of electrophoretic deposition (EPD), Progress in materials science 52(1) (2007) 1-61.

[56] O.O. Van der Biest, L. Vandeperre, Electrophoretic deposition of materials, Annual Review of Materials Science 29(1) (1999) 327-352.

[57] H. Hamaker, Formation of a deposit by electrophoresis, Transactions of the Faraday Society 35 (1940) 279-287.

[58] H. Hamaker, E. Verwey, Part II.—(C) Colloid stability. The role of the forces between the particles in electrodeposition and other phenomena, Transactions of the Faraday Society 35 (1940) 180-185.

[59] F. Grillon, D. Fayeulle, M. Jeandin, Quantitative image analysis of electrophoretic coatings, Journal of materials science letters 11(5) (1992) 272-275.

[60] Y. Solomentsev, M. Böhmer, J.L. Anderson, Particle clustering and pattern formation during electrophoretic deposition: a hydrodynamic model, Langmuir 13(23) (1997) 6058-6068.

[61] M. Trau, D. Saville, I.A. Aksay, Assembly of colloidal crystals at electrode interfaces, Langmuir 13(24) (1997) 6375-6381.

[62] M. Böhmer, In situ observation of 2-dimensional clustering during electrophoretic deposition, Langmuir 12(24) (1996) 5747-5750.

[63] M. Trau, D. Saville, I.A. Aksay, Field-induced layering of colloidal crystals, Science 272(5262) (1996) 706-709.

[64] K. Moritz, E. Mueller, Electrophoretic infiltration of woven carbon fibre mats with SiC powder suspensions, Key Engineering Materials 206 (2002).

[65] H. Koelmans, Suspensions in non aqueous media, publisher unknown1955.

[66] P. Sarkar, P.S.J.J.o.t.A.C.S. Nicholson, Electrophoretic deposition (EPD): mechanisms, kinetics, and application to ceramics, Journal of the American Ceramic Society 79(8) (1996) 1987-2002.

[67] D. De, P.S. Nicholson, Role of ionic depletion in deposition during electrophoretic deposition, Journal of the American Ceramic Society 82(11) (1999) 3031-3036.

[68] R. Moreno, B. Ferrari, Effect of the slurry properties on the homogeneity of alumina deposits obtained by aqueous electrophoretic deposition, Materials Research Bulletin 35(6) (2000) 887-897.

[69] N.B. Dahotre, T. Sudarshan, Intermetallic and ceramic coatings, CRC Press1999.

[70] I. Zhitomirsky, Cathodic electrosynthesis of titanium and ruthenium oxides, Materials Letters 33(5-6) (1998) 305-310.

[71] I. Zhitomirsky, Cathodic electrosynthesis of titania films and powders, Nanostructured materials 8(4) (1997) 521-528.

[72] M.J. Shane, J.B. Talbot, R.D. Schreiber, C.L. Ross, E. Sluzky, K. Hesse, Electrophoretic deposition of phosphors: I. Conductivity and zeta potential measurements, Journal of colloid interface science 165(2) (1994) 325-333.

[73] T. Ishihara, K. Shimose, T. Kudo, H. Nishiguchi, T. Akbay, Y. Takita, Preparation of Yttria-Stabilized Zirconia Thin Films on Strontium-Doped LaMnO3 Cathode Substrates via Electrophoretic Deposition for Solid Oxide Fuel Cells, Journal of the American Ceramic Society 83(8) (2000) 1921-1927.

[74] F. Chen, M. Liu, Preparation of yttria-stabilized zirconia (YSZ) films on La0. 85Sr0. 15MnO3 (LSM) and LSM–YSZ substrates using an electrophoretic deposition (EPD) process, Journal of the European Ceramic Society 21(2) (2001) 127-134.

# Chapter 3   Objectives

The objective of this investigation was the development of novel colloidal strategies for the fabrication of polymer and composite coatings with advanced functionality.

This was achieved by:

- Development of advanced dispersing, charging and film-forming agents for deposition of different polymers, including PTFE and PVDF, and various functional materials as well as their composite through EPD.

- Design of non-toxic co-solvent for dissolving high Mw PEMA at high concentration for dip coating method.

- Fabrication of organic-inorganic composite coatings with multifunctionality through EPD and dip coating methods.

- Exploration of properties and applications of as-deposited coatings.

# Chapter 4   Cholic acid is a versatile film-forming dispersant for electrophoretic deposition of diamond, graphene, carbon dots and polytetrafluoroethylene

X.Liu, Q.Zhao, S. Veldhuis and I.Zhitomirsky

# Abstract

Sodium cholate (ChANa) is used for the first time as an advanced charged dispersant and coating-forming molecular agent for electrophoretic deposition (EPD) of different advanced materials, such as diamonds, carbon dots, graphene and polytetrafluoroethylene (PTFE). The amphiphilic structure of ChANa facilitates its adsorption on the materials and allows their good dispersion. The coating formation mechanism is based on gel-forming properties as well as pH-dependent solubility and pH-dependent charge of ChANa. A conceptually novel strategy is proposed for the deposition of PTFE films and composites. PTFE films prepared by EPD show strong adhesion to stainless steel substrates. Potentiodynamic and impedance spectroscopy studies indicate that PTFE films provide corrosion protection of steel. The potentiodynamic studies of the coated stainless steel substrates show significant reduction of corrosion current, whereas impedance spectroscopy show increasing impedance. The film thickness is varied in the range of 1–30 μm by variation of deposition time in the range of 0.5–5 min and deposition voltage in the range of 7–50 V. Building on the strong dispersion power and electrochemical properties of ChANa we demonstrate the feasibility of composite film fabrication by a combined electrodeposition method, which involves electropolymerization of polypyrrole and EPD of diamonds. This investigation opens new and unexplored routes in the electrochemical deposition of advanced materials using ChANa as a co-dispersing and coating-forming agent.

## 4.1 Introduction

Bile acid salts (BS) are efficient natural surfactants. They enable dispersion of various biomolecules, such as lipids, proteins, cholesterol, vitamins, fatty acids and monoglycerides. [1] The strong dispersion power of BS is related to their electric charge and unique amphiphilic structure. [1-3] Studies of biomolecules solubilization by BS have driven the development of new colloidal techniques in materials processing and biotechnology.

A new biomimetic approach has been designed for the carbon nanotube (CNT) dispersion by commercial BS. [4-8] Previous research has shown excellent colloidal stability of CNT, dispersed using different BS, such as synthetic sodium cholate and sodium salt of taurocholic acid. [6] BS allowed for superior dispersion of carbon nanotubes, as compared to other surfactants. [9]

Cholic acid sodium salt (ChANa) is one of the primary BS, synthesized in the liver. ChANa exhibits a unique set of valuable properties for a large range of possible applications in colloidal manufacturing of materials. [10] Cholate anions showed adsorption on carbon nanotubes, graphene and carbon nanoparticles [11-14] and facilitated their dispersion. The outstanding characteristics of cholate anions include strong adsorption on inorganic materials [15], gel-forming properties [16, 17] and ability to form inclusion crystals with various molecules for their reversible insertion and release [18]. Metal ion complexing properties of ChANa were used for the synthesis of hydroxyapatite [19] and spinel ferrite compounds [20].

Various BS, such as ChANa, have been used in technologies for drug delivery. [21] Many promising drug molecules fail in applications due of their limited water solubility. The analysis [22-26] of interactions of water-insoluble drugs with BS showed that various drug molecules can be solubilized in water using BS. Moreover, BS inhibit crystallization of drug molecules. [27] ChANa and other BS are under investigation for the development of advanced strategies for delivery of various drugs. [1, 27-29] It was found [30] that ChANa can be used for the co-delivery of therapeutic and imaging agents.

Recent results from our laboratory [7] indicate that thin films of cholic acid (ChAH) can be deposited using electrophoretic deposition (EPD). The mechanism involved the dissociation of ChANa and formation of cholate anions (ChA−). The anodic pH reduction due to the reaction

$$2H_2O \rightarrow O_2 + 4H^+ + 4e^- \tag{1}$$

and electrophoretic transport of ChA− toward the anode led to the deposition of thin films of water insoluble ChAH in the anodic reaction:

$$ChA^- + H^+ \rightarrow ChAH \tag{2}$$

ChANa has been used as a coating-forming anionic dispersant for anodic EPD of CNT. [7] Moreover, water-insoluble drugs were dissolved in water in the presence of ChANa and co-deposited with ChAH. [31] Previous results indicate that ChANa can potentially be utilized as a charged dispersant for EPD of other functional materials.

The goal of this paper was the feasibility study of ChANa application for EPD of various functional materials. For the first time we demonstrate that diamond, graphene, carbon dots (CDs) and polytetrafluoroethylene (PTFE) can be deposited by EPD using ChANa as a versatile coating-forming dispersant. The use of ChANa opens the way for the co-deposition of different functional molecules and materials by co-EPD or new techniques, which combine EPD with other electrodeposition or electrosynthesis methods. We discuss advantages of the proposed approach for the electrodeposition of polymer composites and demonstrate the feasibility of composite film electrodeposition by combining EPD of diamond with electropolymerization of polypyrrole.

## 4.2  Experimental Procedures

### 4.2.1  Materials

ChANa, diamond (particle size<1 μm), pyrrole (Py), graphene nanoplatelets (surface area 750 m$^2$ g$^{-1}$, particle size<2 μm), polytetrafluoroethylene (PTFE, particle size<1 μm), Tiron (Aldrich) were used. CDs were prepared by the method described in Ref. [32].

### 4.2.2  Coating deposition

EPD was performed using aqueous ChANa solutions, containing diamonds, graphene, CDs and PTFE. The concentrations of ChANa was 0.5–2 g L$^{-1}$. The concentrations of diamond, graphene, CDs and PTFE were 1–5, 0.5–1, 0.5–0.6 and 1–5 g L$^{-1}$, respectively. The obtained

suspensions were ultrasonicated for 10 min before the deposition. The optimized anodic electropolymerization of polypyrrole (PPy) was performed from 0.1 M Py solutions, containing 0.01 M Tiron. Diamond particles, dispersed using ChANa were added to the electropolymerization solution for the deposition of composites. The concentrations of the diamond particles and ChANa in the Electropolymerization solutions were 1 g $L^{-1}$ and 0.5 g $L^{-1}$, respectively.

The electrodeposition cell included an anodic substrate (304 type stainless steel, $20 \times 30 \times 0.1$ mm) and a Pt cathode ($20 \times 30 \times 0.1$ mm). The electrode separation was 1.5 cm. The deposition voltage was 7–50 V. The obtained coatings were dried in air for 24 h. The concentrations of suspensions and deposition voltages were optimized. The experimental data for different coatings were presented at optimized conditions, described in figure captions. The suspensions prepared without dispersant showed sedimentation during 1–2 min. after ultrasonication. The suspensions, containing diamond and ChANa were stable for 2 days. The suspensions of other materials, dispersed using ChANa, were stable for>7 days.

## 4.2.3 Characterization

Electrochemical studies were performed in aqueous 3% NaCl using a PARSTAT 2273 potentiostat and a 3-electrode electrochemical cell with coated or uncoated stainless steel as a working electrode, SCE (saturated calomel electrode reference) and Pt counter-electrode. Potentiodynamic studies were performed at 1 mV $s^{-1}$ and the obtained data was presented in

Tafel plots. Impedance spectroscopy data was acquired at an AC voltage of 5 mV in the frequency range of 10mHz−10 kHz and presented in Bode plots. A JEOL scanning electron microscope (SEM) JSM-7000F was used for investigations. A Bruker Vertex 70 spectrometer was used for the Fourier Transform Infrared Spectroscopy (FTIR) studies. The coating adhesion strength was measured using ASTM D3359-09 standard.

## 4.3  Results and discussion
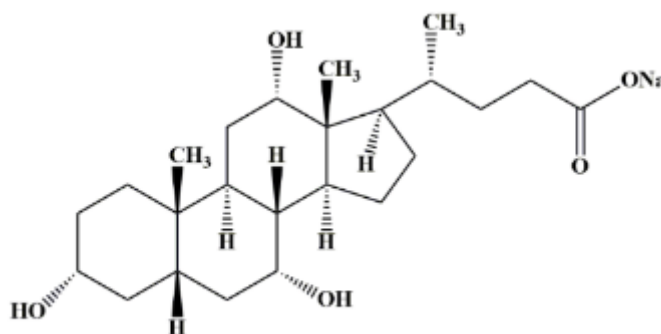


Fig. 4-1 Chemical structure of ChANa.

Fig. 4-1 presents a structure of ChANa used for EPD. The amphiphilic structure of ChANa contains a hydrophobic (convex) side and a hydrophilic (concave) side. [6] The steroid core of the chemical structure includes 4 fused rings, containing five or six carbon atoms. The negative charge of the dissociated ChANa results from $COO^-$ ligand. The hydrophobic side of the molecule facilitates its adsorption on hydrophobic surfaces, whereas the hydrophilic side, containing OH and $COO^-$ groups promotes the dissolution of the molecule in water. The experimental results described below showed that ChANa is a versatile dispersant and coating-

forming agent for materials deposition by EPD. We investigated EPD of diamond, graphene, CDs and PTFE using ChANa.

The colloidal stability of particles is critical for their deposition by EPD. [33-36] It is known that suspensions of diamonds in water, ethanol and isopropanol are very unstable. [37] Another difficulty is related to charging of diamond particles and control of particle charge. In our investigation, the diamond films were deposited from stable suspensions on anodic substrates by EPD using ChANa as a dispersant and coating-forming agent. Fig. 4-2(A–D) presents microstructures of films, obtained at different experimental conditions. The low magnification images (Fig. 4-2(A,C) and Supplementary information, Fig. 4-12 and Fig. 4-13) indicated that crack-free films were formed. The deposition method allowed for the fabrication of relatively thick films with thickness about 30 μm (Supplementary information, Fig. 4-14). The higher magnification images (Fig. 4-2(B,D)) showed porosity of the films, which resulted from the diamond particle packing. The film, formed from 2 g L$^{-1}$ ChANa solutions, containing 4 g L$^{-1}$ diamond, mainly consisted of diamond particles (Fig. 4-2(A,B)). The variation in bath composition resulted in microstructural changes. The analysis of images for the films deposited using 1 g L$^{-1}$ ChANa solutions with 1 g L$^{-1}$ diamond Fig. 4-2(C,D) indicated that many diamond particles were covered by ChAH. Moreover, ChAH was also formed in the spaces between the diamond particles. Therefore, the reduced film porosity Fig. 4-2(C,D) resulted from the enhanced deposition of ChAH.

The diamond film formation by EPD indicated that $ChA^-$ adsorbed on the diamond particles and negatively charged particles were dispersed in the suspension. The adsorption of anionic $ChA^-$ species on diamond allowed for the anaphoresis of the particles to the substrate surface. The charge neutralization in the reaction (2) facilitated film formation. Moreover, the electrophoresis of non-adsorbed $ChA^-$ resulted in the independent deposition of ChAH, as it was described in the previous investigation. [7] The EPD process is influenced by mass transport and deposit formation mechanism. The EPD rate (W) is described [38] by:

$$W=M\mu U/\delta \tag{3}$$

where M is the concentration of molecules or particles or molecules, $\mu$ is electrophoretic mobility, $\delta$ – is the distance between the electrodes, U – is the voltage drop in the solution. According to Ref. [38]

$$U = U_a\text{-}U_d, \tag{4}$$

where $U_a$ is the voltage applied to the cell and $U_d$ is the drop of voltage across the deposited material.

The deposition rate W (Eq. (3)) is a linear function of concentration M of particles or molecules in the solution. Therefore, it is not surprising that the increase in mass ratio of ChANa/diamond in the solution led (Fig. 4-2) to higher ChAH content in the film.
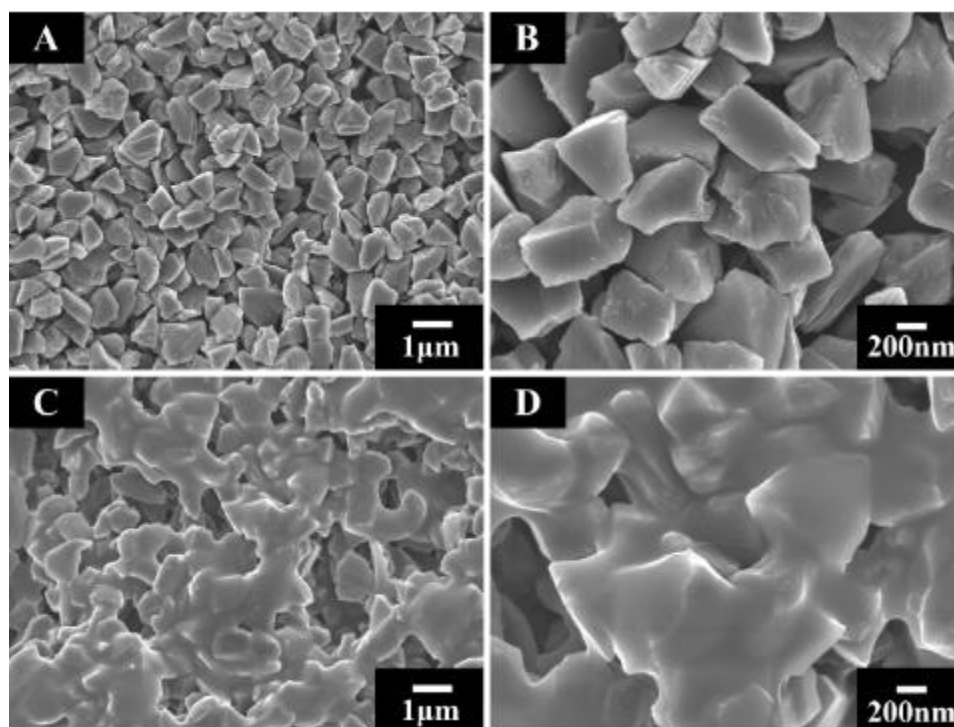
Fig. 4-2 SEM images of films, formed from (A,B) 2 g $L^{-1}$ ChANa solutions, containing 4 g $L^{-1}$ diamond and (C,D) 1 g $L^{-1}$ ChANa solutions, containing 1 g $L^{-1}$ diamond at a cell voltage of 15 V.

The comparison of the method developed in this investigation with literature on EPD of diamond indicated that EPD of diamond using ChANa as a dispersant offers many advantages such as strong $ChA^-$ adsorption on particle surface, good control of particle charge, suspension stability and possibility of co-deposition of the diamond particles with other materials. In previous investigations, anodic electrophoretic seeding techniques [39, 40] were based on the natural charge [41] of diamonds in different solvents. Treatment of diamonds in acids allowed the formation of surface $COO^-$ groups, which facilitated anaphoretic deposition. [42] Continuous films were obtained [43] by cathodic EPD of diamonds in isopropanol using $I_2$–$H_2O$–acetone additive for particle charging. It was found [43] that chemical reaction of $I_2$ and acetone, catalyzed by $H_2O$, resulted in the generation of $H^+$, which adsorbed on the diamond

particles making them positively charged. Later, this approach has been used for EPD of

nanodiamond [36] and composites of diamonds and inorganic materials [44, 45]. Diamond

charging has also been achieved by adsorption of $Al^{3+}$ [43] or $Mg^{2+}$ [46] ions. Various

difficulties have been identified in literature related to EPD of diamonds which were attributed

to poor adsorption of dispersants and charging agents on the chemically inert diamond surfaces,

poor suspension stability and lack of co-dispersants for co-EPD of diamond with other

materials for the manufacturing of composites. The use of $I_2$–acetone for EPD generates

problems of electrode corrosion and poor EPD bath compatibility with other materials, such as

polymers. In contrast, the EPD of diamond using ChANa is promising for the deposition of

composites of polymers with diamonds. As a step in this direction, we combined the EPD of

diamonds with electropolymerization of polypyrrole (PPy). Previous investigations [47]

demonstrated that adherent and uniform PPy films can be deposited on steel using Tiron as a

dopant. The addition of diamonds, dispersed using ChANa, to the electropolymerization baths

allowed the fabrication of composite films (Fig. 4-3, Supplementary information, Fig. 4-15 and

Fig. 4-16). Diamond particles were observed on the film surface (Fig. 4-3(A)). However, many

diamond particles were coated by PPy (Fig. 4-3(B)). The co-deposition of relatively large

diamond particles with PPy resulted in the increased roughness of the film surface, as compared

to smooth PPy films deposited using Tiron as a dopant. [47] It is suggested that anodic EPD of

diamond can be combined with electropolymerization of other polymers for the deposition of

new composites. It is expected that polymerbased composite films can also be formed by co-

EPD of diamond with different anionic polymers [33, 38, 48], containing $COO^-$ groups.
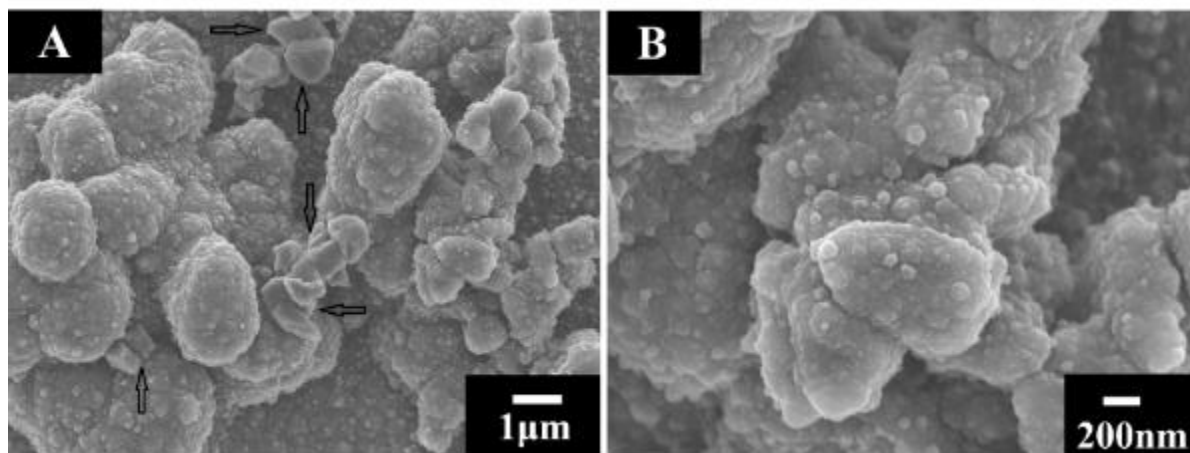


Fig. 4-3 SEM images for PPy-diamond films, formed from 0.1 Py solution, containing 0.01 M Tiron, 1 g $L^{-1}$ diamond and 0.5 g $L^{-1}$ ChANa at a cell voltage of 7 V, arrows show uncoated diamond particles.

We found that ChANa can be used as a dispersant for EPD of electrically neutral PTFE

polymer.
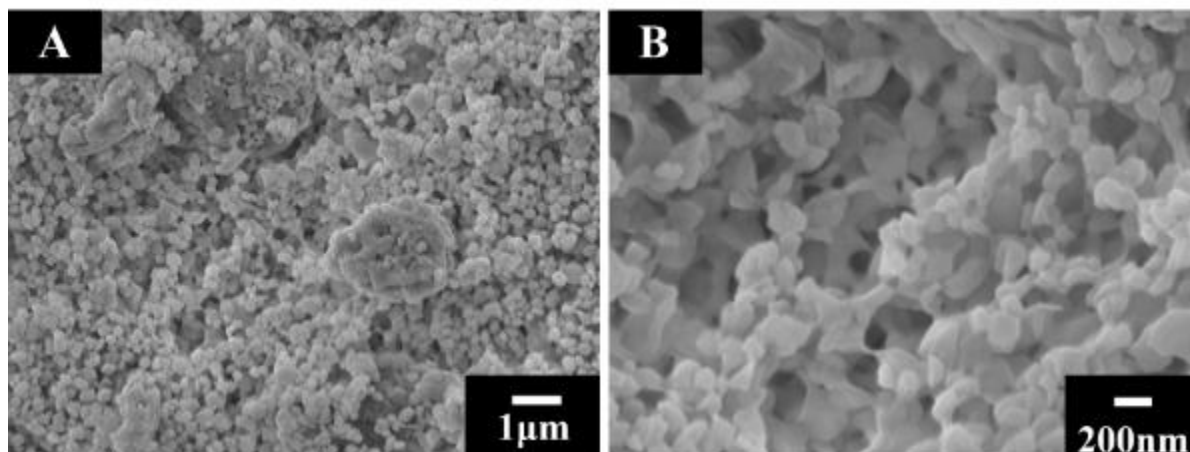


Fig. 4-4 SEM images of a film, formed from 1 g $L^{-1}$ ChANa solution, containing 5 g $L^{-1}$ PTFE at a cell voltage of 50 V.
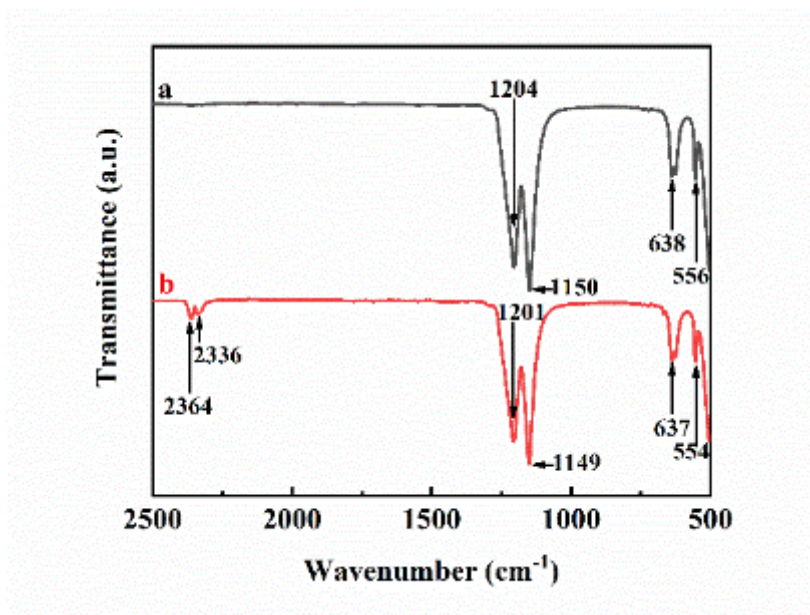
Fig. 4-5 FTIR data for (a) as-received PTFE and (b) deposit, formed from 1 g $L^{-1}$ ChANa solutions, containing 5 g $L^{-1}$ PTFE at a cell voltage of 50 V.

The use of ChANa facilitated the fabrication of stable PTFE suspensions. PTFE was successfully deposited by EPD from such suspensions. The SEM studies at low magnification (Fig. 4-4(A), Supplementary information, Fig. 4-17) showed the formation of a relatively dense crack-free film, containing submicrometre PTFE particles. The higher magnification SEM studies (Fig. 4-4(B)) revealed microporosity, which was mainly attributed to particle packing and $O_2$ evolution during the anodic deposition. The EPD method allowed for the deposition of relatively thick coatings with thickness about 30 μm (Supplementary information, Fig. 4-18). The deposition of PTFE was confirmed (Fig. 4-5) by the results of FTIR studies. The FTIR spectrum of PTFE showed strong absorption peaks at 1150 and 1204 $cm^{-1}$. The peak at 1204 $cm^{-1}$ was due to symmetric $CF_2$ vibration. [49, 50] The asymmetric $CF_2$ vibrations and C-C vibrations [49, 50] contributed to the absorption at 1150 $cm^{-1}$. Similar peaks were found in the

spectrum of the deposit in addition to the relatively weak absorptions related to ChAH. The

annealing of the films at 350 °C led to the melting of the PTFE particles and reduced porosity.

The SEM images (Fig. 4-6(A) Supplementary information, Fig. 4-19) at a low magnification

showed the formation of a crack-free PTFE film. However, the SEM investigations (Fig. 4-

6(B)) at a higher magnification revealed nano pores with a typical diameter < 5 nm. Therefore,

further optimization of the EPD bath composition, deposition conditions and annealing

conditions is necessary for the elimination of the nanopores. The SEM analysis of the cross

section of the sintered films indicated that films adhered well to the substrate (Supplementary

information, Fig. 4-20). The adhesion strength of the sintered PTFE film, measured according

to ASTM D3359–09 standard, corresponded to 5B classification.
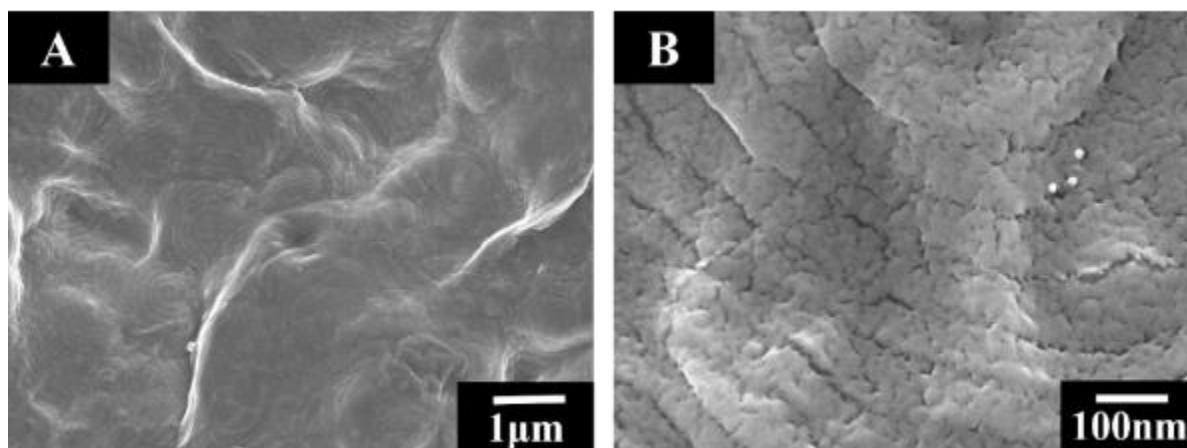


Fig. 4-6 SEM images of a film, formed from 1 g L$^{-1}$ ChANa solution, containing 5 g L$^{-1}$ PTFE at a cell voltage of 50 V and annealed at 350 °C.
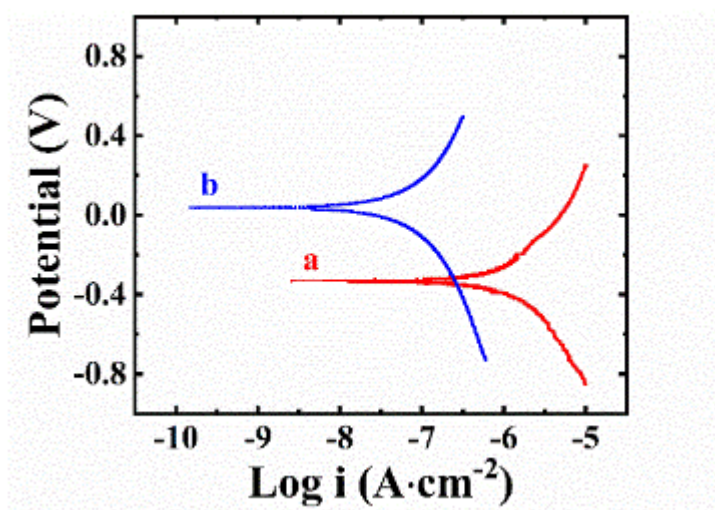
Fig. 4-7 Tafel dependences for steel: (a) uncoated and (b) coated from 1 g L$^{-1}$ ChANa solutions, containing 5 g L$^{-1}$ PTFE at a cell voltage of 50 V for 5 min and annealed at 350 °C.

Electrochemical testing showed that obtained coatings provide protection of steel from corrosion. The comparison of the Tafel dependences for coated and uncoated steel indicated that the coated sample showed reduction of anodic current and increase in corrosion potential (Fig. 4-7). The corrosion current density decreased from 2.59 mA cm$^{-2}$ for uncoated to 0.39 mA cm$^{-2}$ for coated steel. The analysis of the EIS data (Fig. 4-8) in the Bode plot for the same samples revealed significantly higher impedance of the coated samples, compared to the uncoated sample. The difference is especially evident at frequencies 10 Hz-10 kHz. Therefore, the PTFE coating acted as a barrier, limiting the electrolyte access to the electrode surface. Based on these results, the EPD of PTFE coatings show promise for protection of steel from corrosion. However, further investigations, currently under way, are required for the microstructure optimization and prevention of formation of defects, such as nanopores.
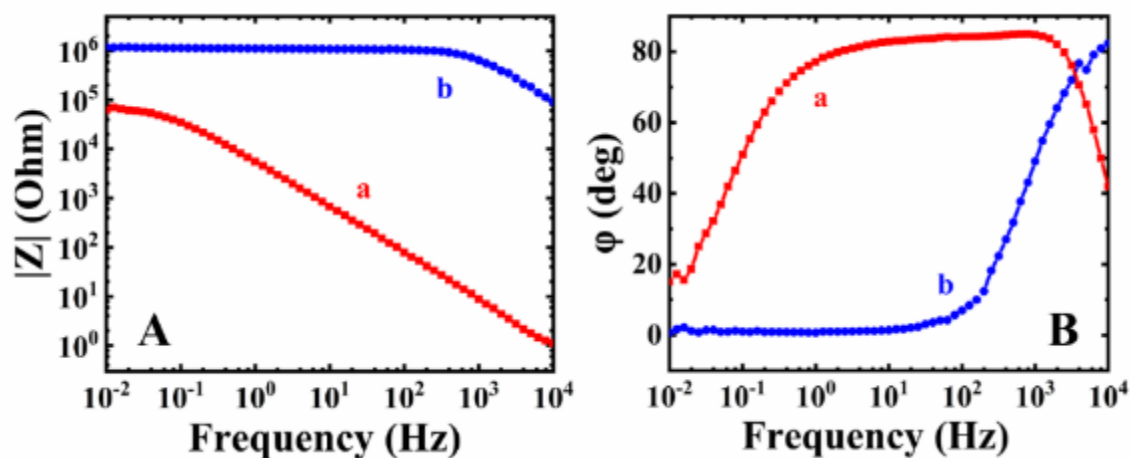
Fig. 4-8 Bode plots of impedance data for stainless steel: (a) uncoated and (b) coated from 1 g L$^{-1}$ ChANa solutions, containing 5 g L$^{-1}$ PTFE at a cell voltage of 50 V during 5 min and annealed at 350 °C.

ChANa offers advantages for EPD of neutral polymers, compared to other dispersants. EPD of neutral polymers was achieved using different dispersants, such as head-tail surfactants and polyelectrolytes. For example, head-tail surfactants [51] were used for EPD of polyetheretherketone (PEEK). The film formation by EPD requires the use of stable suspensions. The particles must be well-dispersed and charged in the bulk of the suspensions. However, the mutual repulsion of the particles must be avoided at the electrode surface in order to achieve particle coagulation and film formation. From this point of view the use of head-tail surfactants with pH-independent charge and pH-independent solubility is detrimental for coating formation. In contrast, ChA$^{-}$ species are discharged at the electrode surface to form electrically neutral water-insoluble ChAH, which exhibit gel-forming and film-forming properties. Therefore, in contrast to head-tail surfactants, ChANa promotes coating formation. Another strategy is based on the use of polyelectrolytes as charging additives. [52] However, polyelectrolytes usually promote bridging flocculation of particles.

The feasibility of EPD of PTFE and diamonds using ChANa indicates that ChANa can be used as a co-dispersant for their co-deposition and formation of composites. Moreover, PTFE film formation by EPD opens a novel and unexplored strategy for the deposition of composites containing particles of different materials in the PTFE matrix. PTFE films and composites are used for electrical insulation, corrosion protection, electronic, and biomedical applications. As pointed out above, EPD of multicomponent composites requires the use of universal co-dispersants for co-deposition of different materials. Of particular interest is the use of ChANa for the EPD of graphene and CDs and their co-deposition with other materials. It is important to note that graphene and CDs are important materials for applications in drug delivery. [53-55] The graphene-carbon nanotube composites and CDs have generated significant interest for energy storage devices. [32, 55, 56]Therefore, the use of ChANa for co-deposition of graphene and CDs with drugs and carbon nanotubes can facilitate the fabrication of novel composites for controlled drug delivery and energy storage.

We found that graphene and CDs can be successfully deposited by EPD using ChANa. Fig. 4-9 presents SEM data for the study of the graphene films. The SEM image taken at a lower magnification shows a porous microstructure (Fig. 4-9(A), Supplementary information, Fig. 4-21, containing graphene particles. The high magnification image (Fig. 4-9(B)) showed that ChAH was co-deposited, formed necks between the particles and acted as a binder for the relatively large graphene particles.
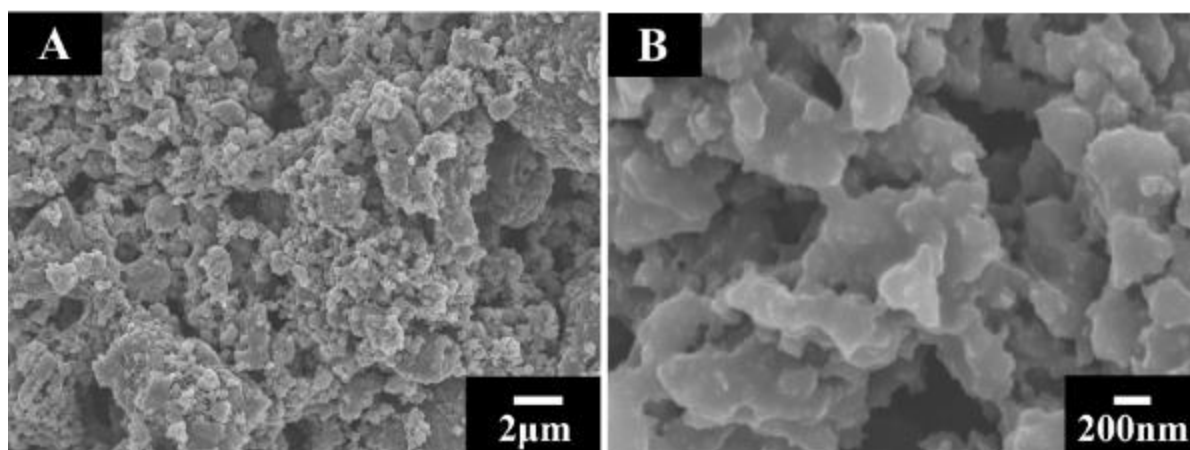
Fig. 4-9 SEM images of films, formed from 1 g $L^{-1}$ ChANa solutions, containing 0.5 g $L^{-1}$ graphene at a cell voltage of 50 V.
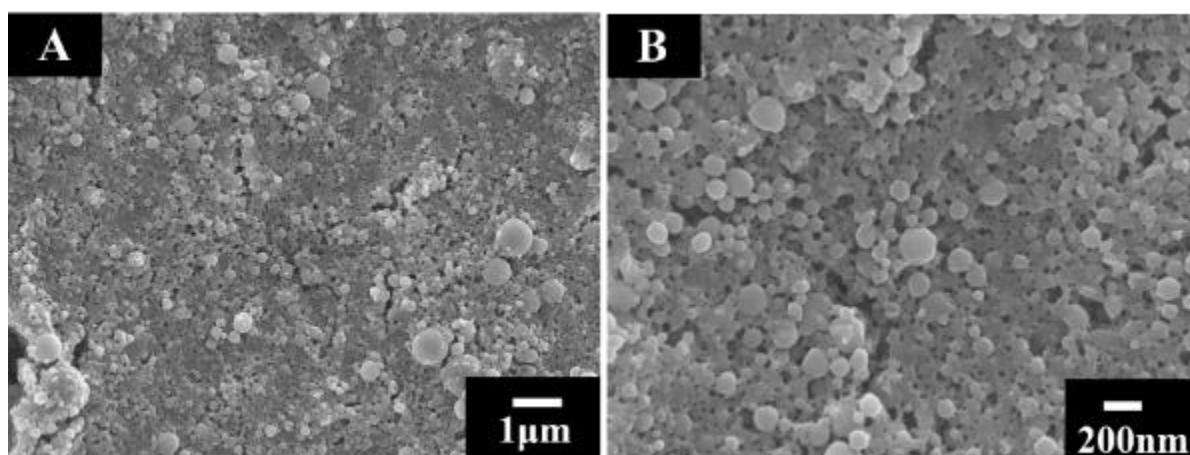


Fig. 4-10 SEM images of films, prepared from solutions, containing 0.5 g $L^{-1}$ CDs and 0.5 g $L^{-1}$ ChANa at a cell voltage of 15 V.

Smooth films, containing CDs and ChAH were obtained by EPD (Fig. 4-10). However, relatively large spherical particles with diameters of 0.1–0.6 μm were observed on the film surface. Such spherical particles were also observed in the images of pure ChAH film. [7] The films exhibited porosity on the nanometric scale. The co-deposition of CDs and ChAH was confirmed by the FTIR studies of the films. Fig. 4-11 shows FTIR spectra of as-received ChANa., deposited ChAH, as-prepared CDs and co-deposited CDs and ChAH. The bands at

2929 and 2860 cm$^{-1}$ for as-received ChANa were assigned to stretching C-H vibrations.

Similar bands were observed in the spectra of deposited ChAH, as-prepared CDs and co-

deposited CDs and ChAH. Fig. 4-11(a) shows strong absorptions at 1561 and 1403 cm$^{-1}$, which

were attributed to stretching asymmetric and symmetric COO– vibrations, respectively. [20]

The band at 1042 cm$^{-1}$ was attributed to C-O stretching. [7] The spectrum of the pure ChAH

revealed absorption at 1703 and 1379 cm$^{-1}$, assigned to stretching vibrations of protonated

COOH groups [7] and C-OH bending [57], respectively (Fig. 4-11(b)). Such absorptions were

also found for composite ChAH-CDs film (Fig. 4-11(d)). The spectrum of assynthesized CDs

(Fig. 4-11(c)) contained absorptions at 2362 and 2324 cm$^{-1}$ assigned to C-H vibrations. [58]

The absorptions at 1668 and 1454 cm$^{-1}$ were related to C-C/C=C stretching. [57] Similar bands

were found for a composite ChAH-CDs film (Fig. 4-11(d)).
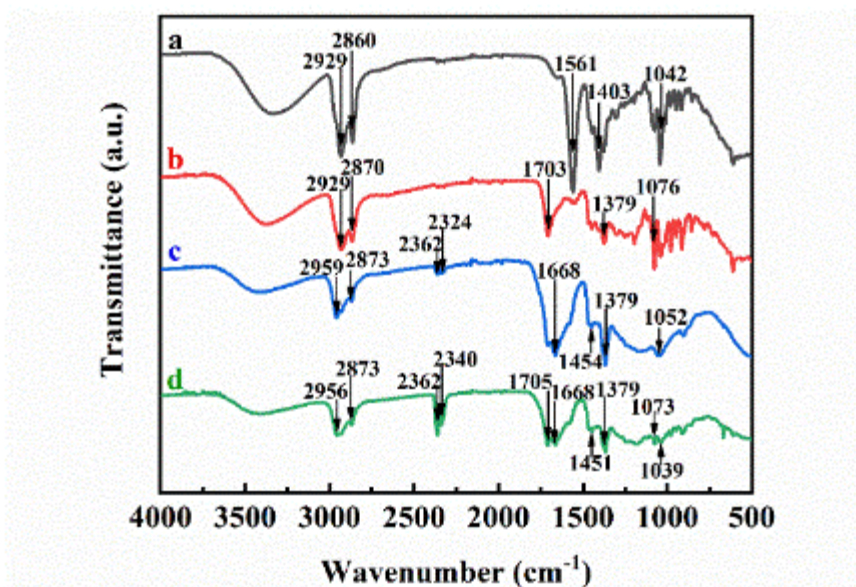


Fig. 4-11 FTIR data for (a) as received ChANa, (b) deposit, formed from 0.5 g L$^{-1}$ ChANa solution, (c) as-synthesized CDs, (d) deposit, prepared from a solution, containing 0.5 g L$^{-1}$ CD and 0.5 g L$^{-1}$ ChANa.

## 4.4  Conclusions

A biomimetic method has been designed for the electrostatic dispersion and EPD of different materials, such as diamonds, CDs, graphene and PTFE. ChANa adsorbed on the materials of different types and facilitated their efficient dispersion and charging. The gel-forming properties, pH-dependent solubility and charge of ChANa allowed for the use of this natural organic molecule as a coating-forming agent. The coating formation process was electrochemically controlled. ChANa can be utilized as a versatile co-dispersant for co-EPD of composite coatings.

The compatibility of ChANa-mediated EPD with other electrochemical processes allowed the fabrication of composites by combined electrochemical methods. EPD of diamonds was combined with PPy electropolymerization for the deposition of diamond-PPy composites. Annealed PTFE coatings showed strong adhesion to the stainless steel substrates. The results of the potentiodynamic and impedance spectroscopy studies showed that annealed PTFE films provide corrosion protection of stainless steel. It is expected that ChANa-mediated EPD will allow the deposition of other functional materials of different types.

## 4.5  Supplementary information
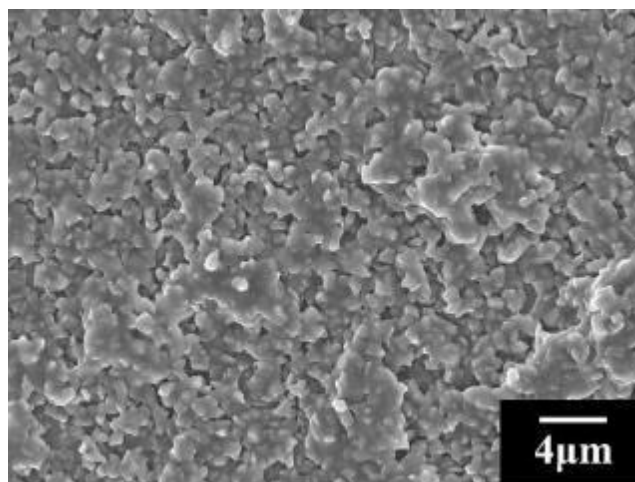


Fig. 4-12 Low magnification SEM image of a film, formed from 2 g L$^{-1}$ ChANa solutions, containing 4 g L$^{-1}$ diamond at a cell voltage of 15 V.
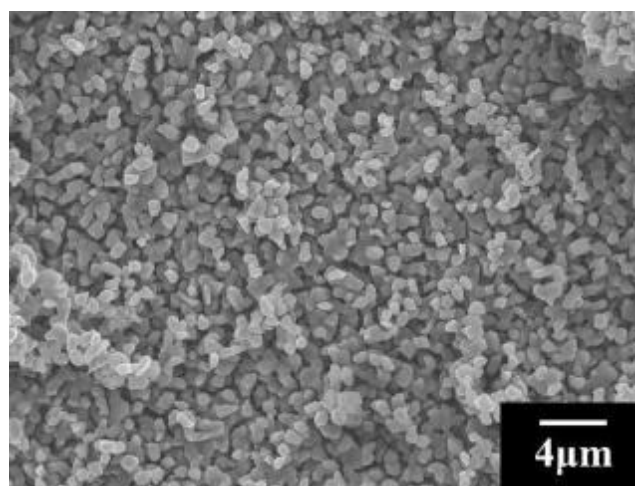


Fig. 4-13 Low magnification SEM image of a film, formed from 1 g L$^{-1}$ ChANa solutions, containing 1 g L$^{-1}$ diamond at a cell voltage of 15 V.
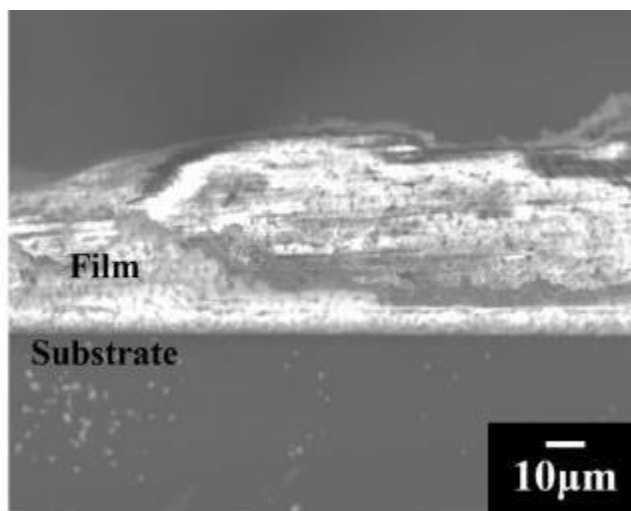
Fig. 4-14 Cross section SEM image of a film, formed from 1 g L$^{-1}$ ChANa solutions, containing 1 g L$^{-1}$ diamond at a cell voltage of 15 V.
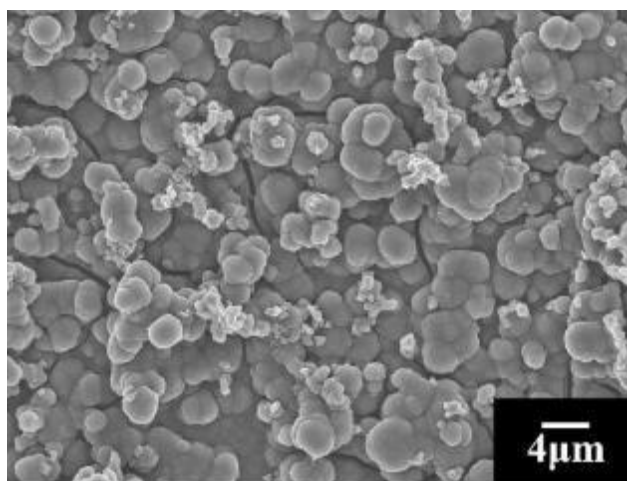


Fig. 4-15 Low magnification SEM image for PPy-diamond films, formed from 0.1 Py solution, containing 0.01 M Tiron, 1 g L$^{-1}$ diamond and 0.5 g L$^{-1}$ ChANa at a cell voltage of 7 V.
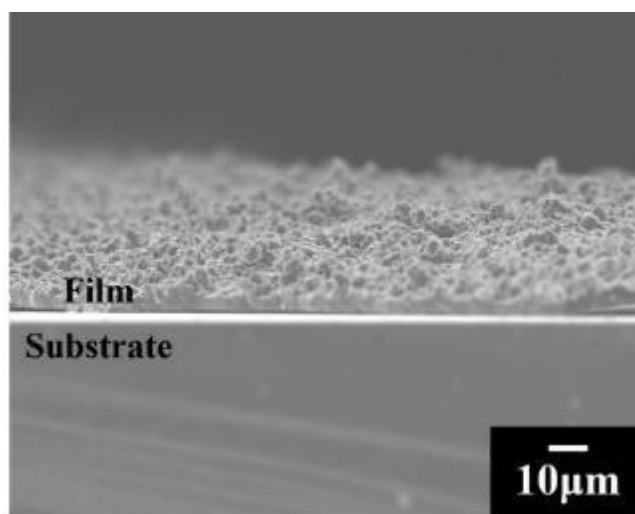
Fig. 4-16 Cross section SEM image for PPy-diamond films, formed from 0.1 Py solution, containing 0.01 M Tiron, 1 g $L^{-1}$ diamond and 0.5 g $L^{-1}$ ChANa at a cell voltage of 7 V.
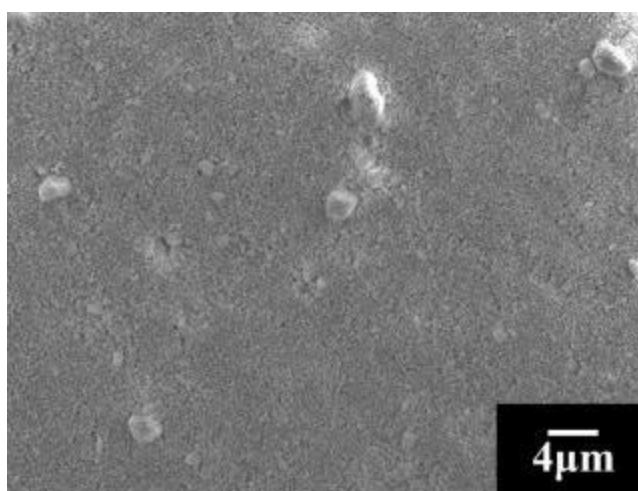


Fig. 4-17 Low magnification SEM image of a film, formed from 1 g $L^{-1}$ ChANa solution, containing 5 g $L^{-1}$ PTFE at a cell voltage of 50 V.
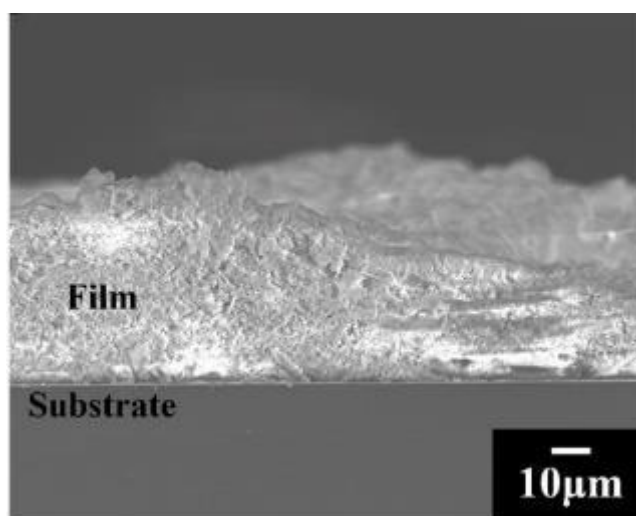
Fig. 4-18 Cross section SEM image of a film, formed from 1 g L$^{-1}$ ChANa solution, containing 5 g L$^{-1}$ PTFE at a cell voltage of 50 V.
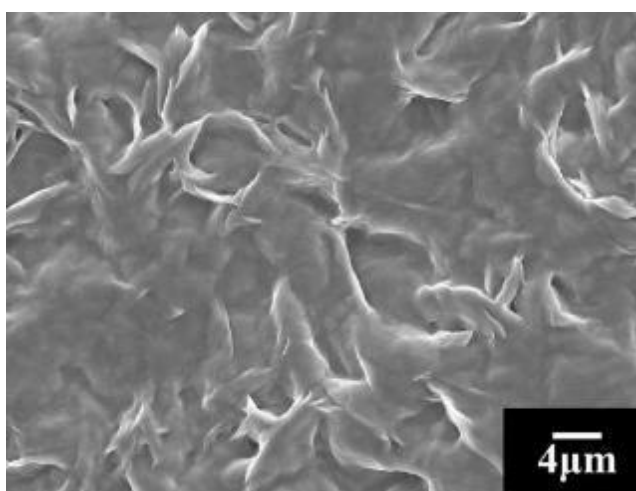


Fig. 4-19 SEM image of a film, formed from 1 g L$^{-1}$ ChANa solutions, containing 5 g L$^{-1}$ PTFE at a cell voltage of 50 V and annealed at 350º C.
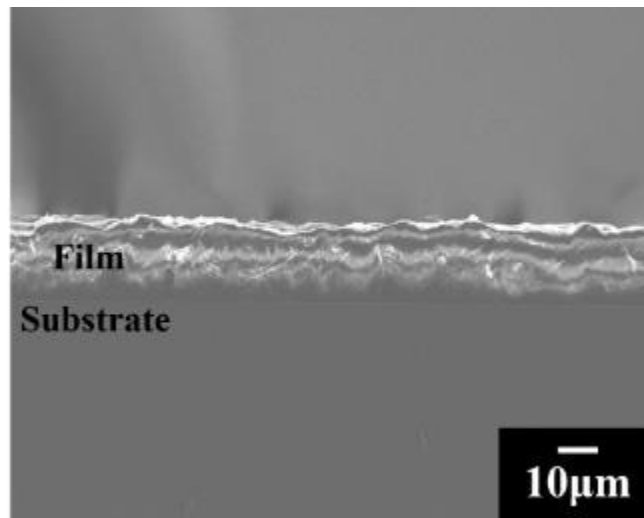
Fig. 4-20 Cross section SEM image of a film, formed from 1 g L$^{-1}$ ChANa solution, containing 5 g L$^{-1}$ PTFE at a cell voltage of 50 V and annealed at 350$^{\circ}$ C.
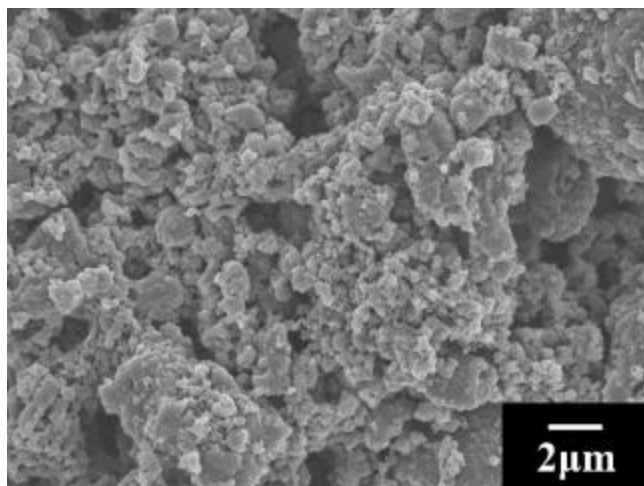


Fig. 4-21 Low magnification SEM image of a film, formed from 1 g L$^{-1}$ ChANa solution, containing 0.5 g L$^{-1}$ graphene at a cell voltage of 50 V.

## 4.6  Contribution Statement

X.Liu: Conceptualization, investigation, formal analysis; Q.Zhao: Formal analysis, methodology; S. Veldhuis: Funding acquisition, project administration; I.Zhitomirsky: Conceptualization, investigation, formal analysis, supervision, validation, writing.

71

## 4.7 References

[1] L. Galantini, M.C. di Gregorio, M. Gubitosi, L. Travaglini, J.V. Tato, A. Jover, F. Meijide, V.H.S. Tellini, N.V. Pavel, Bile salts and derivatives: Rigid unconventional amphiphiles as dispersants, carriers and superstructure building blocks, Current opinion in colloid & interface science 20(3) (2015) 170-182.

[2] W.C. Herndon, The structure of choleic acids, Journal of chemical education 44(12) (1967) 724.

[3] S. Mukhopadhyay, U. Maitra, Chemistry and biology of bile acids, Current Science 87(12) (2004) 1666-1683.

[4] Z. Sun, V. Nicolosi, D. Rickard, S.D. Bergin, D. Aherne, J.N. Coleman, Quantitative evaluation of surfactant-stabilized single-walled carbon nanotubes: dispersion quality and its correlation with zeta potential, The Journal of Physical Chemistry C 112(29) (2008) 10692-10699.

[5] M. Gubitosi, J.V. Trillo, A. Alfaro Vargas, N.V. Pavel, D. Gazzoli, S. Sennato, A. Jover, F. Meijide, L. Galantini, Characterization of carbon nanotube dispersions in solutions of bile salts and derivatives containing aromatic substituents, The Journal of Physical Chemistry B 118(4) (2014) 1012-1021.

[6] M.S. Ata, R. Poon, A.M. Syed, J. Milne, I. Zhitomirsky, New developments in non-covalent surface modification, dispersion and electrophoretic deposition of carbon nanotubes, Carbon 130 (2018) 584-598.

[7] M. Ata, I. Zhitomirsky, Colloidal methods for the fabrication of carbon nanotube–manganese dioxide and carbon nanotube–polypyrrole composites using bile acids, Journal of colloid and interface science 454 (2015) 27-34.

[8] K. Shi, X. Yang, E.D. Cranston, I. Zhitomirsky, Efficient lightweight supercapacitor with compression stability, Advanced Functional Materials 26(35) (2016) 6437-6445.

[9] W. Wenseleers, I.I. Vlasov, E. Goovaerts, E.D. Obraztsova, A.S. Lobach, A. Bouwen, Efficient isolation and solubilization of pristine single-walled nanotubes in bile salt micelles, Advanced Functional Materials 14(11) (2004) 1105-1112.

[10] A. Sayyed-Ahmad, L.M. Lichtenberger, A.A. Gorfe, Structure and dynamics of cholic acid and dodecylphosphocholine− cholic acid aggregates, Langmuir 26(16) (2010) 13407-13414.

[11] S. Lin, D. Blankschtein, Role of the bile salt surfactant sodium cholate in enhancing the aqueous dispersion stability of single-walled carbon nanotubes: a molecular dynamics simulation study, The Journal of Physical Chemistry B 114(47) (2010) 15616-15625.

[12] M. Lotya, P.J. King, U. Khan, S. De, J.N. Coleman, High-concentration, surfactant-stabilized graphene dispersions, 4(6) (2010) 3155-3162.

[13] P. Kumar, H. Bohidar, Aqueous dispersion stability of multi-carbon nanoparticles in anionic, cationic, neutral, bile salt and pulmonary surfactant solutions, Colloids and Surfaces A: Physicochemical and Engineering Aspects 361(1-3) (2010) 13-24.

[14] I. Singh, P. Bhatnagar, P. Mathur, L. Bharadwaj, Optical absorption spectrum of single-walled carbon nanotubes dispersed in sodium cholate and sodium dodecyl sulfate, Journal of Materials Research 23(3) (2008) 632-636.

[15] J. Naime Filho, F. Silvério, M. Dos Reis, J. Valim, Adsorption of cholate anions on layered double hydroxides: effects of temperature, ionic strength and pH, Journal of materials science 43(21) (2008) 6986-6991.

[16] H.M. Willemen, A.T. Marcelis, E.J. Sudhölter, W.G. Bouwman, B. Demé, P. Terech, A small-angle neutron scattering study of cholic acid-based organogel systems, Langmuir 20(6) (2004) 2075-2080.

[17] A. Chakrabarty, U. Maitra, A.D. Das, Metal cholate hydrogels: versatile supramolecular systems for nanoparticle embedded soft hybrid materials, Journal of Materials Chemistry 22(35) (2012) 18268-18274.

[18] K. Nakano, K. Sada, K. Nakagawa, K. Aburaya, N. Yoswathananont, N. Tohnai, M. Miyata, Organic Intercalation Material: Reversible Change in Interlayer Distances by Guest Release and Insertion in Sandwich-Type Inclusion Crystals of Cholic Acid, Chemistry–A European Journal 11(6) (2005) 1725-1733.

[19] S. Koutsopoulos, E. Dalas, Hydroxyapatite crystallization on sodium cholate, Journal of crystal growth 222(1-2) (2001) 279-286.

[20] D.C. Culita, L. Patron, V.S. Teodorescu, I. Balint, Synthesis and characterization of spinelic ferrites obtained from coordination compounds as precursors, Journal of alloys and compounds 432(1-2) (2007) 211-216.

[21] S. Kalepu, V. Nekkanti, Insoluble drug delivery strategies: review of recent advances and business prospects, Acta Pharmaceutica Sinica B 5(5) (2015) 442-453.

[22] M. Poša, J. Csanádi, K.E. Kövér, V. Guzsvány, G. Batta, Molecular interactions between selected sodium salts of bile acids and morphine hydrochloride, Colloids and Surfaces B: Biointerfaces 94 (2012) 317-323.

[23] S. Glanzer, S.A. Pulido, S. Tutz, G.E. Wagner, M. Kriechbaum, N. Gubensäk, J. Trifunovic, M. Dorn, W.M. Fabian, P. Novak, Structural and functional implications of the interaction between macrolide antibiotics and bile acids, Chemistry–A European Journal 21(11) (2015) 4350-4358.

[24] M.A. Rub, M.S. Sheikh, A.M. Asiri, N. Azum, A. Khan, A.A.P. Khan, S.B. Khan, Aggregation behaviour of amphiphilic drug and bile salt mixtures at different compositions and temperatures, The Journal of Chemical Thermodynamics 64 (2013) 28-39.

[25] S. Sen, B.K. Paul, N. Guchhait, Differential interaction behaviors of an alkaloid drug berberine with various bile salts, Journal of colloid and interface science 505 (2017) 266-277.

[26] T. Yadav, D. Tikariha, S. Sinha, K.K. Ghosh, Biophysical studies on the interactions between antidepressant drugs and bile salts, Journal of Molecular Liquids 233 (2017) 23-28.

[27] H. Chen, Y. Kang, F. Cai, S. Zeng, W. Li, M. Chen, Q. Li, Electrochemical conversion of Ni 2 (OH) 2 CO 3 into Ni (OH) 2 hierarchical nanostructures loaded on a carbon nanotube paper with high electrochemical energy storage performance, Journal of Materials Chemistry A 3(5) (2015) 1875-1878.

[28] J. Park, J.U. Choi, K. Kim, Y. Byun, Bile acid transporter mediated endocytosis of oral bile acid conjugated nanocomplex, Biomaterials 147 (2017) 145-154.

[29] Q. Gao, C. Huang, B. Sun, B.M. Aqeel, J. Wang, W. Chen, X. Mo, X. Wan, Fabrication and characterization of metal stent coating with drug-loaded nanofiber film for gallstone dissolution, Journal of biomaterials applications 31(5) (2016) 784-796.

[30] M. Nurunnabi, Z. Khatun, V. Revuri, M. Nafiujjaman, S. Cha, S. Cho, K.M. Huh, Y.-k. Lee, Design and strategies for bile acid mediated therapy and imaging, RSC Advances 6(78) (2016) 73986-74002.

[31] A. Clifford, I. Zhitomirsky, Aqueous electrophoretic deposition of drugs using bile acids as solubilizing, charging and film-forming agents, Materials Letters 227 (2018) 1-4.

[32] H. Hou, C.E. Banks, M. Jing, Y. Zhang, X. Ji, Carbon Quantum Dots and Their Derivative 3D Porous Carbon Frameworks for Sodium-Ion Batteries with Ultralong Cycle Life, Advanced Materials 27(47) (2015) 7861-7866.

[33] M. Cheong, I. Zhitomirsky, Electrophoretic deposition of manganese oxide films, Surface Engineering 25(5) (2009) 346-352.

[34] Y. Li, K. Wu, I. Zhitomirsky, Electrodeposition of composite zinc oxide–chitosan films, Colloids and Surfaces A: Physicochemical and Engineering Aspects 356(1) (2010) 63-70.

[35] C. Noberi, F. Kaya, C. Kaya, Synthesis, structure and characterization of hydrothermally synthesized Ag-TiO2 nano-structures onto Ni filters using electrophoretic deposition, Ceramics International 42(15) (2016) 17202-17209.

[36] A. Affoune, B. Prasad, H. Sato, T. Enoki, Electrophoretic deposition of nanosized diamond particles, Langmuir 17(2) (2001) 547-551.

[37] L. La-Torre-Riveros, K. Soto, M.A. Scibioh, C.R. Cabrera, Electrophoretically fabricated diamond nanoparticle-based electrodes, Journal of The Electrochemical Society 157(6) (2010) B831-B836.

[38] Y. Wang, I. Deen, I. Zhitomirsky, Electrophoretic deposition of polyacrylic acid and composite films containing nanotubes and oxide particles, Journal of colloid and interface science 362(2) (2011) 367-374.

[39] J. Valdes, J. Mitchel, J. Mucha, L. Seibles, H. Huggins, Selected-Area Nucleation and Patterning of Diamond Thin Films by Electrophoretic Seeding, Journal of the Electrochemical Society 138(2) (1991) 635-636.

[40] D.-G. Lee, R.K. Singh, Synthesis of (111) oriented diamond thin films by electrophoretic deposition process, Applied physics letters 70(12) (1997) 1542-1544.

[41] Y. Wang, Y. Liang, X. Cheng, H. Huang, J. Zang, J. Lu, Y. Yu, X. Xu, Preparing porous diamond composites via electrophoretic deposition of diamond particles on foam nickel substrate, Materials Letters 138 (2015) 52-55.

[42] B. Dzepina, I. Sigalas, M. Herrmann, R. Nilen, The aqueous electrophoretic deposition (EPD) of diamond–diamond laminates, International Journal of Refractory Metals and Hard Materials 36 (2013) 126-129.

[43] I. Zhitomirsky, Cathodic electrophoretic deposition of diamond particles, Materials Letters 37(1-2) (1998) 72-78.

[44] K. Kamada, K. Maehara, M. Mukai, S. Ida, Y. Matsumoto, Fabrication of metal oxide–diamond composite films by electrophoretic deposition and anodic dissolution, Journal of materials research 18(12) (2003) 2826-2831.

[45] Y. Wang, Q. Chen, J. Cho, A. Boccaccini, Electrophoretic co-deposition of diamond/borosilicate glass composite coatings, Surface and Coatings Technology 201(18) (2007) 7645-7651.

[46] S. Yu, Z. Chen, Y. Wang, R. Luo, T. Xu, Y. Pan, J. Liao, Fabrication of SiC/diamond composite coatings by electrophoretic deposition and chemical vapor deposition, International Journal of Applied Ceramic Technology 14(4) (2017) 644-651.

[47] C. Shi, I. Zhitomirsky, Electrodeposition and capacitive behavior of films for electrodes of electrochemical supercapacitors, Nanoscale research letters 5(3) (2010) 518.

[48] Y. Cheng, X. Luo, J. Betz, G.F. Payne, W.E. Bentley, G.W. Rubloff, Mechanism of anodic electrodeposition of calcium alginate, Soft Matter 7(12) (2011) 5677-5684.

[49] H.W. Starkweather Jr, R.C. Ferguson, D.B. Chase, J.M. Minor, Infrared spectra of amorphous and crystalline poly (tetrafluoroethylene), Macromolecules 18(9) (1985) 1684-1686.

[50] R. Wang, G. Xu, Y. He, Structure and properties of polytetrafluoroethylene (PTFE) fibers, e-Polymers 17(3) (2017) 215-220.

[51] A. Iveković, S. Novak, M. Lukek, M. Kalin, Aqueous electrophoretic deposition of bulk polyether ether ketone (PEEK), Journal of Materials Processing Technology 223 (2015) 58-64.

[52] D. Luo, I. Zhitomirsky, Electrophoretic deposition of polyetheretherketone composites, containing huntite and alumina platelets, Journal of The Electrochemical Society 162(11) (2015) D3057.

[53] S. Goenka, V. Sant, S. Sant, Graphene-based nanomaterials for drug delivery and tissue engineering, Journal of Controlled Release 173 (2014) 75-88.

[54] J. Dong, K. Wang, L. Sun, B. Sun, M. Yang, H. Chen, Y. Wang, J. Sun, L. Dong, Application of graphene quantum dots for simultaneous fluorescence imaging and tumor-targeted drug delivery, Sensors and Actuators B: Chemical 256 (2018) 616-623.

[55] Y. Wang, A. Hu, Carbon quantum dots: synthesis, properties and applications, Journal of Materials Chemistry C 2(34) (2014) 6921-6939.

[56] K. Shi, I. Zhitomirsky, Electrophoretic nanotechnology of graphene–carbon nanotube and graphene–polypyrrole nanofiber composites for electrochemical supercapacitors, Journal of Colloid and Interface Science 407 (2013) 474-481.

[57] I.A. Jankovic, Z.V. Saponjic, M.I. Comor, J.M. Nedeljkovic, Surface modification of colloidal TiO2 nanoparticles with bidentate benzene derivatives, The Journal of Physical Chemistry C 113(29) (2009) 12645-12652.

[58] D. Philip, A. John, C.Y. Panicker, H.T. Varghese, FT-Raman, FT-IR and surface enhanced Raman scattering spectra of sodium salicylate, Spectrochimica Acta Part A: Molecular and Biomolecular Spectroscopy 57(8) (2001) 1561-1566.

# Chapter 5  Biomimetic strategies in colloidal-electrochemical deposition of functional materials and composites using chenodeoxycholic acid

Xinqian Liu, Amanda Clifford, Qinfu Zhao, Igor Zhitomirsky

## Graphic abstract
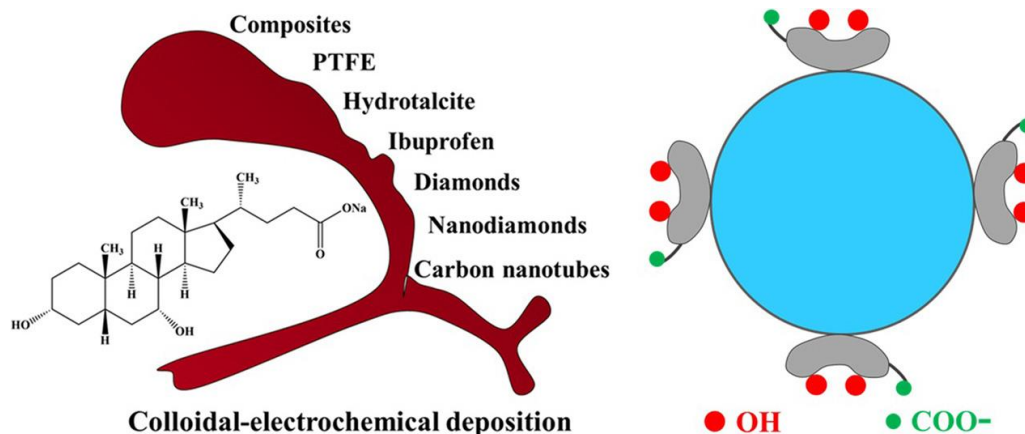


## Abstract

For the first time thin films of chenodeoxycholic acid (CDCH) were electrodeposited from

sodium chenodeoxycholate (CDCNa) solutions potentiodynamically and by constant voltage

deposition. The proposed deposition method was based on pH-dependent gel-forming

properties of CDCH. CDCNa was found to be an efficient anionic surfactant for electrophoretic

deposition (EPD) of carbon materials, such as submicrometre diamond, nanodiamond, carbon

nanotubes, as well as memory type Zr-doped hydrotalcite (MHT) and poly(tetrafluoroethylene)

(PTFE). In this approach, bifacial amphipathic CDCNa acted as a compatibilizing agent

between the hydrophobic material surface and water. This study enabled the fabrication of

composite coatings using CDCNa as a co-dispersing surfactant. An important practical

outcome of this work was the development of advanced coatings for corrosion protection. We

present a conceptually new strategy which enhances the protective properties of polymer

coatings. It is based on the memory properties of MHT, which are linked to its ability to restore

the original structure and composition after thermal dehydration. The protection mechanism involves in-situ MHT reconstruction, which limits water diffusion in pores of coatings. Another new finding was that CDCNa facilitated solubilization and EPD of ibuprofen in water. This finding paves the way for the development of drug delivery technologies and deposition of various water insoluble organic functional materials. Particularly important for future applications is the possibility of EPD of various hydrophobic polymers and composites using a biomimetic approach based on the CDCNa mediated deposition.

## 5.1 Introduction

This investigation was motivated by unique colloidal properties of sodium chenodeoxycholate (CDCNa), which are promising for new applications of this biomolecule for surface modification and colloidal processing of advanced materials. It is known that CDCNa has important functional properties in a human body. It facilitates solubilization and transportation of lipids in the intestine and accelerates colonic transit. [1, 2] The unique colloidal properties of CDCNa were used in pharmaceutical nanotechnologies for dissolving cholesterol gallstones gallstones. [2, 3] The CDCNa-mediated dissolution therapy via oral administration is an important alternative to surgery. [4] The gallstone treatment method was based on the analysis of the molecular-level dissolution of cholesterol in the presence of CDCNa. [4]

The strong solubilization power of CDCNa has been utilized for the development of new strategies for the solubilization and delivery of poorly soluble drug molecules. [5] CDCNa exhibits antimicrobial properties, which are currently under investigations for various applications in medicine [6]. Biomedical studies revealed interesting adsorption and solubilization properties, catalytic effect, charge transfer and chelating properties of CDCNa. [6-8] Other investigations revealed thermal stability [9] and pH-dependent gel forming properties [10] of this biomolecule. Such properties are promising for novel applications in nanotechnology of organic and inorganic materials.

CDCNa has been widely investigated as a co-adsorbent for the dye sensitized nanocrystalline solar cells. [11-13] The adsorbed CDCNa prevented dye aggregation on the TiO2 surface and allowed for larger electron lifetime, higher open circuit voltage and enhanced cell efficiency. [11-13] Enhanced performance was achieved not only by coadsorption, but also by incorporation of CDCNa into the electrolyte solutions. [14] Comparison of the data for electrodes prepared with and without CDCNa showed its strong impact on the photovoltaic cell performance. [15-17] CDCNa has been successfully combined with various dyes [16-20], containing different anchoring ligands. Furthermore, the use of CDCNa allowed for reduced dye loadings. [19] These studies revealed promising properties of CDCNa for surface modification of photovoltaic materials. [21] However, despite the tremendous progress achieved in the use of CDCNa for biomedical and photovoltaic applications, the potential of CDCNa for many other applications remains unexplored.

The goal of this investigation was the application of CDCNa for surface modification and electrodeposition of organic and inorganic materials. We discovered that thin films of chenodeoxycholic acid (CDCH) can be prepared from CDCNa solutions by colloidal-electrochemical deposition using potentiodynamic and constant voltage techniques. The proposed deposition mechanism was based on the gelforming properties of CDCH. The method allowed for the control of the deposition yield.

Following the goal of this investigation we used CDCNa for surface modification, charging, dispersion and electrophoretic deposition (EPD) of chemically inert and electrically neutral materials such as poly (tetrafluoroethylene) (PTFE), submicrometre diamond (SD) and nanodiamond (ND), carbon nanotubes, memory type Zr- doped hydrotalcite (MHT) and composites. We demonstrated that the bifacial amphipathic structure of CDCNa was beneficial for dispersion of PTFE, carbon nanotubes and diamonds. In our approach, CDCNa acted as a compatibilizing agent between the hydrophobic material surface and water. The chelating properties of CDCNa facilitated its adsorption on MHT. Experimental results of this investigation indicated that CDCNa can be used as a co-dispersant for various materials and deposition of composites. PTFE films have been developed for corrosion protection of stainless steel. The use of CDCNa as a co-dispersant for PTFE and MHT allowed for the development of composite coatings with enhanced corrosion protection. A conceptually new approach has been developed, which was based on the memory properties of MHT. It was found that MHT additive limited electrolyte diffusion in pores of PTFE coating. Another important finding was

the solubilization and electrodeposition of ibuprofen (IBP) in the presence of CDCNa, which

is promising for biomedical applications.

## 5.2  Experimental Procedures

### 5.2.1  Materials

Sodium chenodeoxycholate (CDCNa), submicrometre diamond (SD, size<1 μm),

nanodiamond (ND, size<10 nm), ibuprofen (IBP), poly(tetrafluoroethylene) (PTFE, size<1 μm)

(Aldrich), carbon nanotubes (multiwalled, Bayer) and Zr-doped hydrotalcite (MHT, Zr:Mg:Al

atomic ratio of 0.14:3:0.78) (MEL Chemicals) were used.

### 5.2.2  Coating Deposition

Electrodeposition process of CDCH was investigated potentiodynamically from aqueous

1 g $L^{-1}$ CDCNa solution. Cyclic voltammetry (CV) data was recorded at a sweep rate of 5 mV

$s^{-1}$ using an electrochemical cell described in Ref. [22]. In-situ studies of the deposition yield

were performed at a constant voltage mode from 0.1 g $L^{-1}$ CDCNa solution at a cell voltage of

5 V using a quartz crystal microbalance (QCM) and a cell described in Ref. [23]. Constant

voltage deposition was also performed from 1 g $L^{-1}$ CDCNa solution using a two-electrode

EPD cell, containing a stainless steel (304 type) substrate (25×45×0.1 mm) and a Pt foil

counter-electrode. The electrode separation was 17 mm and cell voltage was 10 V.

EPD of diamonds and nanodiamonds, carbon nanotubes, PTFE and MHT particles was performed in the EPD cell at a deposition voltage of 50 V, the particle concentration in the suspensions was 0.5−5 g L$^{-1}$ and dissolved CDCNa concentration was 1 g L$^{-1}$. EPD of PTFE was performed using a mixed water-ethanol solvent (40 % ethanol). The use of ethanol facilitated PTFE dispersion. Other materials were deposited from aqueous suspensions. The obtained suspensions were ultrasonicated for 10 min before the deposition. The deposition time was 5 min. The obtained coatings were dried in air for 24 h. The concentrations of suspensions and deposition voltages were optimized. The experimental data for different coatings were presented at optimized conditions, described in figure captions.

### 5.2.3 Characterization

Electrochemical studies were performed in an aqueous 30 g L$^{-1}$ NaCl aqueous solution using a PARSTAT 2273 potentiostat and a 3-electrode electrochemical cell with coated or uncoated stainless steel as a working electrode, SCE (reference saturated calomel electrode) and Pt counter-electrode. Potentiodynamic polarization studies were performed at a sweep rate of 1 mV s$^{-1}$. Electrochemical impedance spectroscopy (EIS) data at an AC signal amplitude of 5 mV was obtained in the frequency range of 0.01 Hz – 10 kHz and presented in Bode plots. A JEOL scanning electron microscope (SEM) JSM-7000 F was used for microstructure investigations. A Bruker Vertex 70 spectrometer was used for the Fourier Transform Infrared Spectroscopy (FTIR) studies. Xray diffraction (XRD) experiments were carried out using a

Nicolet I2 powder diffractometer, with monochromatized CuKα radiation. The coating

adhesion strength was measured using D3359−17 standard, ASTM.

## 5.3  Results and discussion

CDCNa has been chosen as a promising surfactant for EPD due to its bifacial amphipathic

structure (Supplementary information, Fig. 5-12) and electric charge. The CDCNa structure

has a hydrophilic side, containing OH groups and a hydrophobic side. The CDCNa dissociation

results in charged $CDC^-$ species, the negative electric charge of them is attributed to anionic

$COO^-$ groups:

$$CDCNa \rightarrow CDC^- + Na^+ \tag{1}$$

Electrodeposition of organic and inorganic materials involves their transport in an electric

field. [24-26] Film formation is based on their discharge or charge compensation [26, 27],

which facilitate coagulation at the electrode. We demonstrated here for the first time the

electrodeposition of chenodeoxycholic acid (CDCH) films from CDCNa solutions and

proposed a deposition mechanism.

Fig. 5-1(A) shows CVs for an Au electrode in $1 \text{ g L}^{-1}$ CDCNa solution. Cycling of the Au

electrodes in the $1 \text{ g L}^{-1}$ CDCNa solution resulted in the film formation. The current gradually

decreased with increasing cycle number due to the formation of an insulating film on the

electrode. The reduction of current indicated film formation. The film deposition process has

also been investigated using in-situ mass gain measurements by QCM. Fig. 5-1(B) shows a

continuous mass gain achieved during the constant voltage deposition. The decrease in the slop

of the curve resulted from the continuous increase of film resistance with increasing deposit

mass [28] and corresponding decrease of electric field in the suspension.
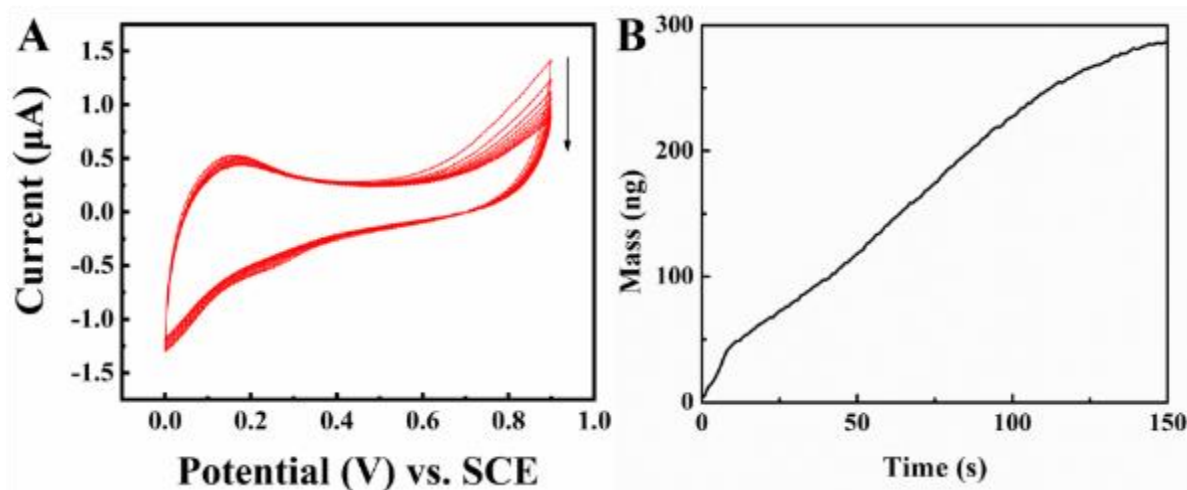


Fig. 5-1 (A) CVs for an Au electrode in aqueous 1 g L$^{-1}$ CDCNa solution at a sweep rate of 5 mV s$^{-1}$ (arrow shows increasing cycle number), (B) QCM data for in-situ deposit mass measurements at a deposition voltage of 5 V in 0.1 g L$^{-1}$ CDCNa solution for a gold coated quartz electrode with an area of 0.2 cm$^2$.

The proposed mechanism of deposition was based on the analysis of literature data on pH-

dependent water solubility and adsorption properties of CDCH. [29] The literature studies of

CDCH solubility and adsorption involved the analysis of CDCH in supernatant and precipitate

phases of gastrointestinal contents with different pH from stomach, duodenum and jejunum.

[30] It was found that pKa of CDCH is 6.2 and CDCH precipitates at pH=4 [29]. The pH

reduction promoted enhanced adsorption and gelation of CDCH. The pH increase above

pH=7.5 resulted in increasing solubility of CDCH, which allowed for solubilization of

gallstones and other biomolecules. [30] The precipitation and gelation of CDCH at low pH was

also confirmed in other studies. [10]

It was hypothesized that an acidic pH was created locally at the anode area due to the reaction:

$$H_2O \rightarrow 2H^+ + 2e^- + \tfrac{1}{2} O_2 \qquad (2)$$

The CDC$^-$ transport to the anode allowed for CDCH film deposition by an electrogenerated acid method, which involved charge neutralization, local precipitation and formation of insoluble film at the electrode surface:

$$CDC^- + H^+ \rightarrow CDCH \qquad (3)$$

Electrodeposition was also performed on stainless steel substrates. Fig. 5-2 shows SEM images of films deposited potentiodynamically at a sweep rate of 5 mV s$^{-1}$ and at a constant voltage of 10 V. The potentiodynamically deposited film was porous and consisted of submicrometre particles. The film deposited at a constant voltage showed a continuous dense layer and submicrometre particles deposited on the top of the dense layer.
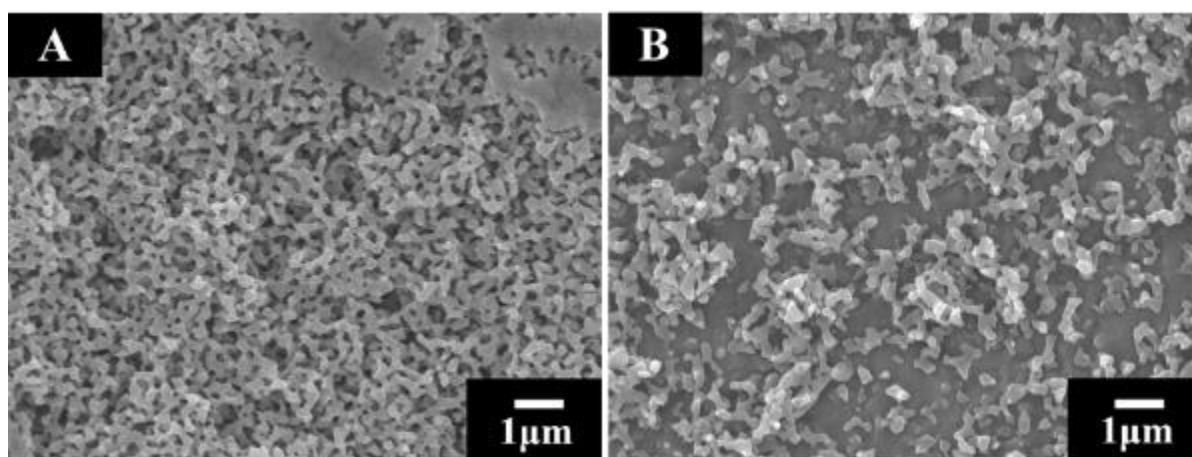


Fig. 5-2 SEM images of CDCH films on stainless steel deposited from 1 g L$^{-1}$ CDCNa solutions: (A) potentiodynamically at a sweep rate of 5 mV s$^{-1}$ and (B) at a constant voltage of 10 V.

The proposed deposition mechanism was confirmed by the analysis of the FTIR spectra

(Fig. 5-3). The spectrum of as-received CDCNa and deposited material showed absorptions at

1078 and 1077 $cm^{-1}$, respectively, attributed to C-O stretching vibration. [31] As-received

CDCNa also showed absorptions at 1406 and 1558 $cm^{-1}$ which resulted from symmetric and

asymmetric COO- vibration. [31] The peak at 1708 $cm^{-1}$ in the spectrum of the deposited

materials is related to stretching of protonated COOH. [32] This peak has not been detected in

the spectrum of CDCNa. Therefore, FTIR analysis confirmed CDCH deposition from CDCNa

solutions.
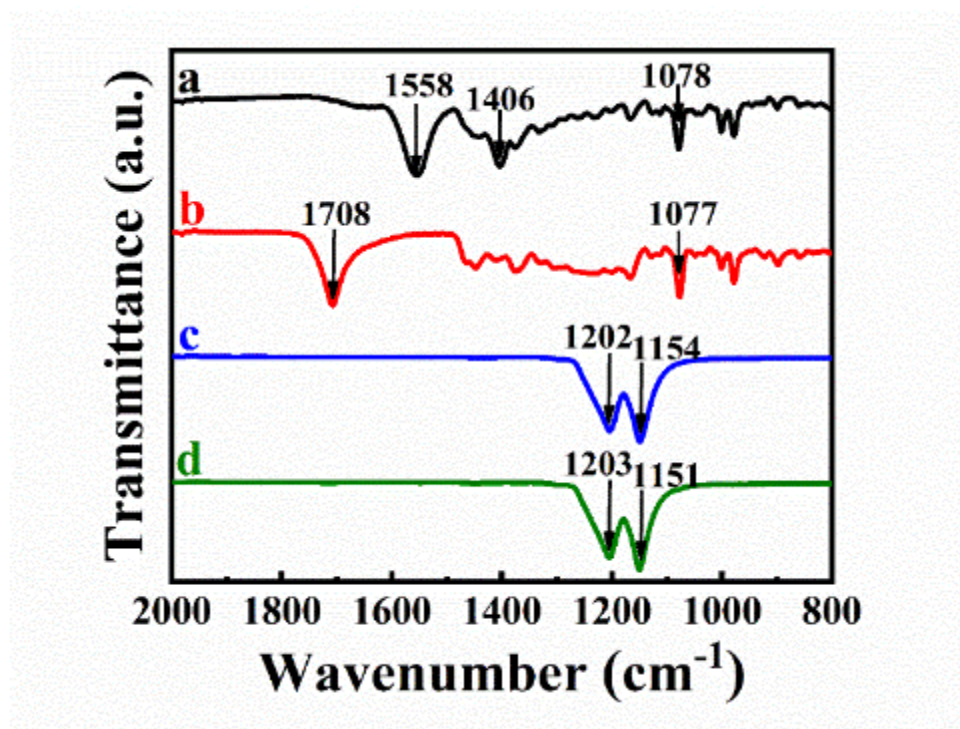


Fig. 5-3 FTIR spectra of (a) as-received CDCNa, (b) deposited CDCH, (c) as-received PTFE
and (d) deposit, obtained from 5 g $L^{-1}$ PTFE suspension, containing dissolved 1 g $L^{-1}$ CDCNa.

FTIR spectroscopy has also been used for the analysis of PTFE deposition. The FTIR

spectrum of as-received PTFE (Fig. 5-3) showed peaks at 1154 and 1202 $cm^{-1}$, which resulted

from $CF_2$ asymmetric and symmetric vibrations, respectively. [33, 34]The peaks at 1151 and

1203 $cm^{-1}$ in the spectrum of the deposited material provided evidence of the successful EPD

of PTFE (Fig. 5-3). The concentration of CDCNa was significantly lower than the

concentration of PTFE in the suspension. As a result, the FTIR spectrum (Fig. 5-3(d)) of the

deposited material showed mainly peaks of PTFE.
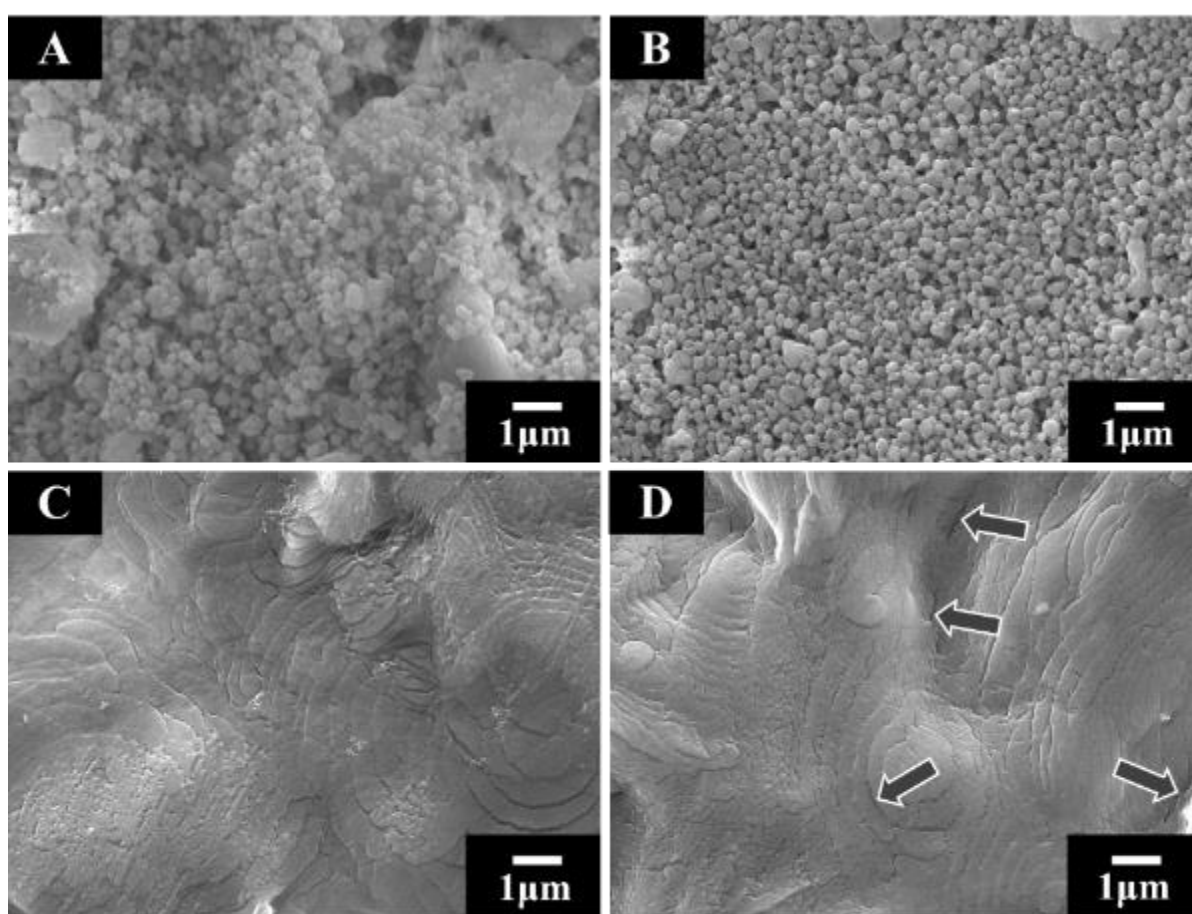


Fig. 5-4 SEM images of (A,B) as deposited films and (C,D) films, annealed at 350 ºC, prepared from (A,C) 1 g $L^{-1}$ PTFE suspensions, (B,D) 5 g $L^{-1}$ PTFE suspensions, containing dissolved 1 g $L^{-1}$ CDCNa at a deposition voltage of 50 V, arrows in (D) show nanocracks.

The SEM images of as-deposited PTFE coatings are shown in Fig. 5-4. The image of the

coating, prepared from 1 g $L^{-1}$ PTFE suspensions, containing 1 g $L^{-1}$ CDCNa, revealed

porosity and particle agglomeration. The deposit, obtained from 5 g $L^{-1}$ PTFE suspensions,

containing 1 g L$^{-1}$ CDCNa, showed significantly reduced agglomeration and lower porosity.

Annealing of the coatings resulted in increased density (Fig. 5-4). However, the coatings

showed small nanocracks. SEM investigations of the annealed coatings showed that coating

thickness increased with increasing deposition duration. The thickness of the films deposited

at the voltage of 50 V and deposition duration of 5 min was about 10 μm. The coating adhesion

strength (D3359−17 standard, ASTM) was found to correspond to 5B grade (Supplementary

information, Fig. 5-13).

SEM investigations showed that MHT can be deposited using 5 g L$^{-1}$ MHT suspensions,

containing dissolved 1 g L$^{-1}$ CDCNa at a deposition voltage of 50 V (Fig. 5-5). However, PTFE

and MHT have no charge and cannot be deposited electrochemically without charging

additives. It was hypothesized that CDCNa adsorbed on PTFE and MHT, imparting a negative

charge for electrodeposition. Therefore, CDCNa can be used as a co-dispersant for the

deposition of composite films, containing PTFE and MHT. The co-deposition of PTFE and

MHT was confirmed by the deposition yield measurements at different deposition durations. It

was found that the addition of MHT to the PTFE suspension resulted in enhanced deposition

yield due to co-deposition of both materials (Supplementary information, Fig. 5-14 and related

data analysis).
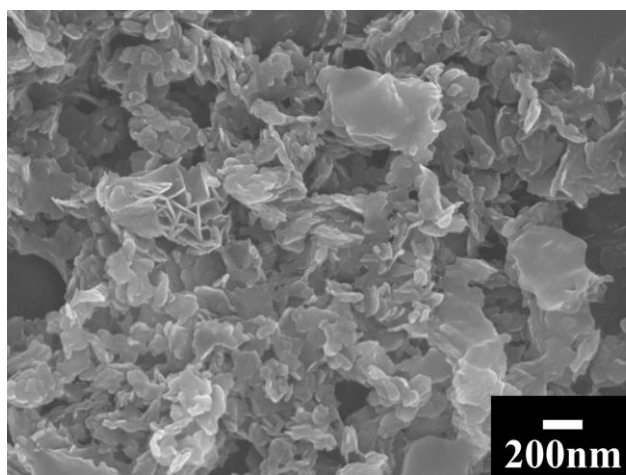
Fig. 5-5 SEM image of a film, deposited from 5 g L$^{-1}$ MHT suspensions, containing dissolved 1 g L$^{-1}$ CDCNa at a deposition voltage of 50 V.

It was suggested that annealed PTFE and composite films can provide corrosion protection of stainless steel. Potentiodynamic and impedance spectroscopy studies are important tools to investigate the corrosion protection of polymer and composite coatings. [35-38] The increase in corrosion potential and reduction of anodic current of PTFE coated stainless steel in comparison with uncoated steel are indicators of corrosion protection (Fig. 5-6(A)). The corrosion current decreased from 2.63 μA cm$^{-2}$ for uncoated sample to 0.40 μA cm$^{-2}$ for PTFE coated sample. Coated stainless steel showed significantly higher impedance |Z| (Fig. 5-6(B)), compared to uncoated stainless steel due to insulating properties and low capacitance of the coating. The impedance of uncoated stainless steel is influenced by the capacitive properties of the electrical double layer [35, 39] at the solution/electrode interface. As a result, the impedance |Z| of the uncoated steel decreased with increasing frequency (Fig. 5-6(B)). A defect-free coating provides a barrier to electrolyte diffusion and prevents corrosion. [39-41] However, small defects in coatings [42] create low resistance paths for electrolyte diffusion.

The electrochemical impedance of coated stainless steel is usually described by a general transmission line model [39, 43], which includes different parameters, such as coating capacitance C, coating resistance perpendicular to the surface $R_p$, solution resistance $R_s$, impedance at the metal/coating interface $Z_I$, coating resistance tangential to surface $R_t$, and interfacial resistance $R_i$. At low frequencies ($\omega$) the impedance of the coated electrode can be described by the equation [39, 43]:

$$Z = R_s + R_p + \frac{R_t}{2} + \sqrt{\frac{R_t^2}{4} + \frac{R_t R_i}{1 - \omega j C R_i}} \qquad (4)$$

At low frequencies the impedance is nearly independent on the frequency. [39, 43] Indeed, the impedance |Z| of the uncoated sample (Fig. 5-6(B)) showed very small variations in the range of 10 mHz-100 Hz. The decrease of |Z| and increase of phase angle at higher frequencies are attributed to reduced impedance of the capacitive component (Fig. 5-6(B,C)).
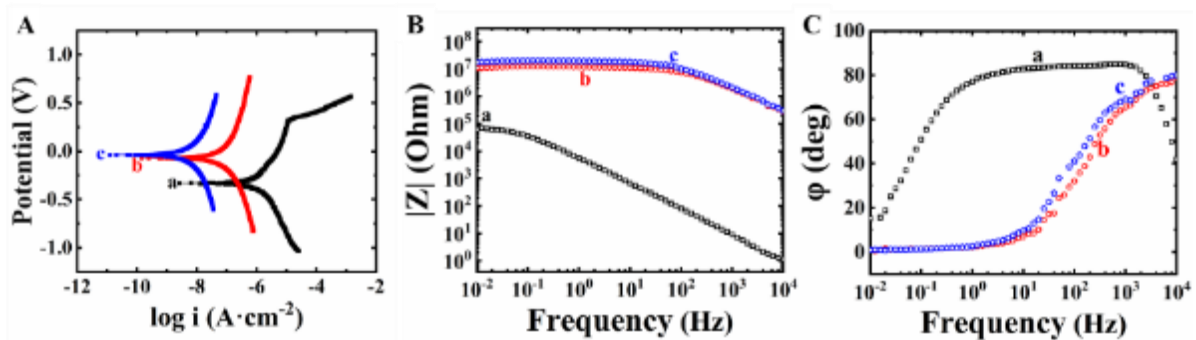


Fig. 5-6 (A) Tafel plots and (B,C) EIS data: (B) absolute values of impedance │Z│ and (C) phase angles φ versus frequency for (a) uncoated stainless steel, (b,c) coated stainless steel from (b) 5 g L$^{-1}$ PTFE and (c) 5 g L$^{-1}$ PTFE and 0.5 g L$^{-1}$ MHT suspensions, containing dissolved 1 g L$^{-1}$ CDCNa at a deposition voltage of 50 V. The coated samples were annealed at 350 ⁰C for 1 h.

Literature data [44] on the corrosion protection of metals by organic coatings in aqueous NaCl solutions indicated that water diffusion in pores must be prevented in order to improve

protective properties of coatings. Our efforts to enhance corrosion protection have resulted in

a conceptually new strategy, based on the use of memory properties of MHT. Previous

investigations showed [45] that MHT is an important flame retardant material, which exhibits

mass loss of 44 % resulting from dehydration under thermal annealing. The annealed material

can be completely reconstructed [45] by addition of water. Building on the memory properties

of MHT [45], we used this material as an additive in order to limit water diffusion in the

nanocracks and nanopores of the PTFE coating. Turning again to the SEM image shown in Fig.

5-4(D) it should be noted that such nanocracks or nanopores can provide paths for the water

transport.

Fig. 5-7 shows a schematic of the strategy used in this investigation to limit electrolyte

diffusion in pores. MHT was used as an additive and it was co-deposited with PTFE by EPD.

Taking into account the thermogravimetry data [45] for MHT, it is obvious that annealing of

the composite coatings at 350ºC resulted in the dehydration of MHT. However, previous

investigation [45] showed memory properties of annealed MHT, which can be easily

reconstructed in the presence of water to form original hydroxide material. It is suggested that

water diffusion led to the in-situ hydration and reconstruction of the dehydrated MHT particles,

which was accompanied by water uptake, increase of particle volume and blocking of porous

channels. Tafel plot showed an increase in corrosion potential and reduction of the anodic

current of the composite coating, compared to pure PTFE sample (Fig. 5-6). The composite

coating showed lower corrosion current, which was found to be 0.11 $\mu A\ cm^{-2}$. Moreover, the

composite coatings, containing MHT showed enhanced impedance, compared to pure PTFE

coating (Fig. 5-6). From the electrochemical testing results it is evident that MHT additive is

beneficial for the development of protective coatings. However, the concentration of MHT in

the coatings must be optimized.
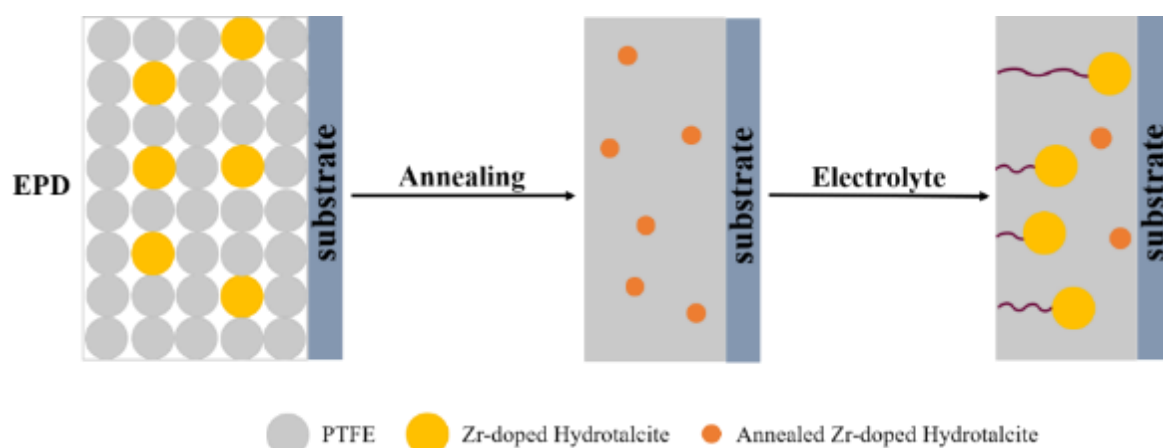


Fig. 5-7 Schematic of a coating deposited by EPD, annealed coating and annealed coating in the electrolyte solution.

The use of MHT represents a conceptually new strategy in the development of advanced

coatings for corrosion protection. It is important to note that many polymers, such as PTFE,

show good chemical stability. Such polymers are attractive materials for the development of

protective coatings. The failure of polymer coatings often results from diffusion of electrolyte

in nanopores and nanocracks of the polymer coating, which leads to corrosion of metals below

the coating-substrate interface, loss of adhesion and peeling off the chemically stable coating

material. Our strategy allowed for water consumption by dehydrated memory-type MHT in-

situ, which limited the electrolyte diffusion. In contrast to other materials from the bile salt

family [46], CDCNa allowed co-dispersion and co-deposition of PTFE and MHT. The use of

CDCNa was a key for the fabrication of composite coatings by EPD from colloidal suspensions and development of a new strategy based on the application of memory properties of MHT. CDCNa is a promising dispersing, charging and film forming agent, which can potentially be used for the co-deposition of other electrically neutral polymers with MHT or other chemically active additives for the development of advanced coatings.

This study indicates that chemical structure of bile salts is an important factor for their application in colloidal-electrochemical processing of materials. Other bile salts, such as taurocholic acid, taurodeoxycholic acid and lithocholic acid cannot be deposited by EPD due to their different structure and solubility properties. Deoxycholic acid can be used for the dispersion and deposition of limited number of organic materials. [46] In contrast, we found that CDCNa allows deposition of various organic and inorganic materials and their co-deposition.

It is hypothesized that hydrophobic surface of the steroid CDCNa skeleton allowed for adsorption of this molecule on the hydrophobic surfaces of PTFE and the bifacial amphipathic structure of CDCNa facilitated PTFE particles dispersion. CDCNa acted as a compatibilizing agent between the hydrophobic material surface and water (Supplementary information, Fig. 5-15). It was suggested that interactions of $COO^-$ groups of dissociated CDCNa with metal atoms on the MHT surface facilitated $CDC^-$ adsorption on MHT. The adsorption mechanisms of various molecules, containing chelating carboxylic groups, on inorganic particles were described in literature. [47, 48]

CDCNa was used for dispersion, charging and EPD of carbon materials, such as SD, ND

and carbon nanotubes from aqueous suspensions. Fig. 5-8 shows X-ray diffraction patterns of

deposits, obtained from SD and ND suspensions, containing CDCNa. The diffraction patterns

show peaks of diamond, corresponding to the JCPDS file 6–675. ND exhibited broad peaks

due to the small particles size. The SEM images showed diamond particles on the surface of

continuous CDCH layer, ND particles were agglomerated (Fig. 5-9).
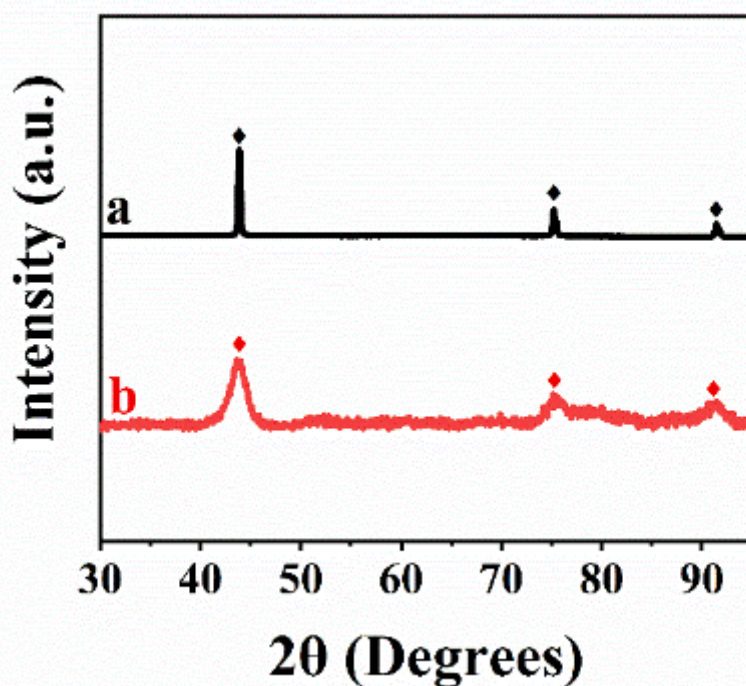


Fig. 5-8 X-ray diffraction patterns of coatings prepared using (a) 5 g L$^{-1}$ SD and (b) 5 g L$^{-1}$ ND suspensions, containing dissolved 1 g L$^{-1}$ CDCNa at a deposition voltage of 50 V ($\blacklozenge$ - JCPDS file 6-675 of diamond).
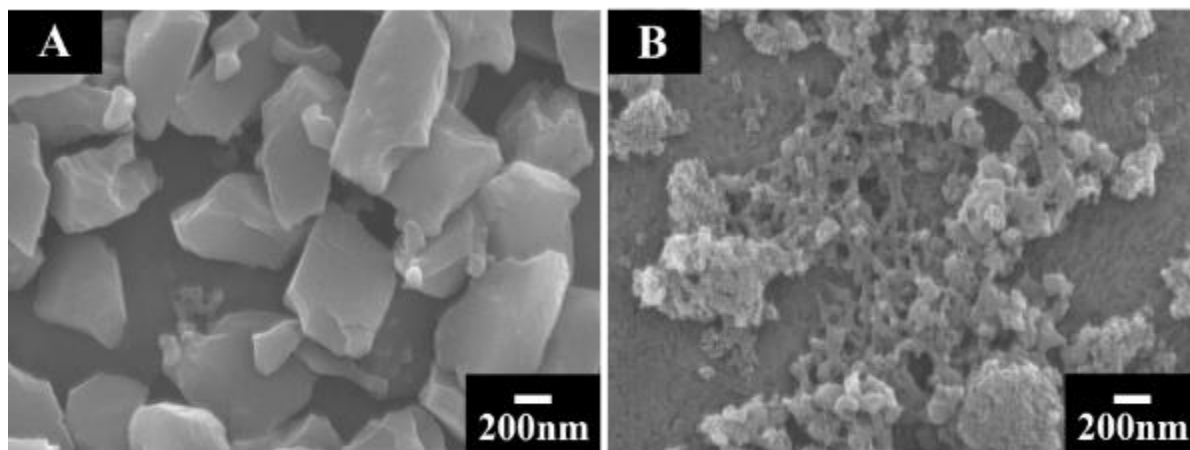
Fig. 5-9 SEM images of deposits, prepared from (A) 1 g $L^{-1}$ SD and (B) 1 g $L^{-1}$ ND suspensions, containing 1 g $L^{-1}$ CDCNa at a deposition voltage of 50 V.

EPD of ND presents difficulties, related to poor dispersant adsorption on the ND surface and poor colloidal stability of ND suspensions. Our method offers advantages, compared to another EPD strategy, described in literature [49]. According to ref. [49], ND particles were charged by adsorbed $H^+$, which were generated in chemical reaction of $I_2$ and acetone. However, this method introduces problems related to corrosion of electrodes in the highly acidic bath, poor adhesion and deposit contamination. Another difficulty involves chemical degradation of materials in the $I_2$–acetone mixture, which limits the application of this bath for the EPD of composites. In contrast, CDCNa is a versatile dispersant for the EPD of different materials and composites. Moreover, film forming and binding properties of CDCH are beneficial for the fabrication of adherent coatings.

SEM studies showed that carbon nanotubes formed a continuous network, CDCH was deposited in the spaces between the nanotubes and acted as a binder (Fig. 5-10). The experimental data presented in Figs. 5-8–5-10 show the feasibility of EPD of SD, ND and

carbon nanotubes. The suggested adsorption mechanism of CDCNa on SD, ND and carbon

nanotubes are shown in Fig. 5-15 and Fig. 5-16 (Supplementary information). For practical

applications such materials can be co-deposited with polymers, such as PTFE to form

composites.
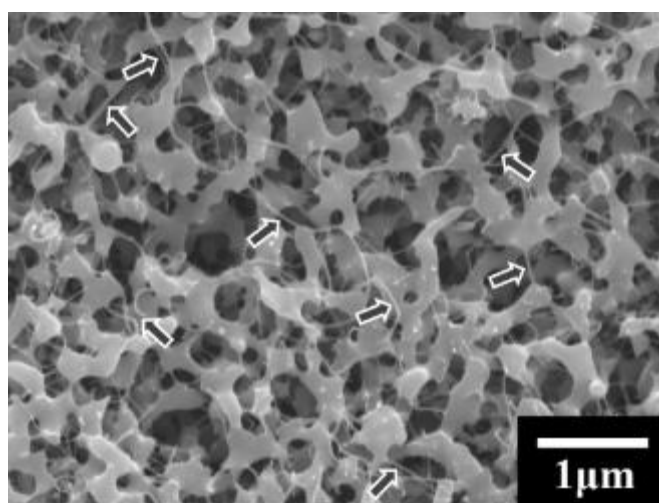


Fig. 5-10 SEM image of a deposit, obtained from 1 g $L^{-1}$ carbon nanotube suspensions, containing 1 g $L^{-1}$ CDCNa at a deposition voltage of 30 V, arrows show carbon nanotubes.

This investigation showed that CDCNa is a versatile dispersant for co-deposition of

different materials from colloidal suspensions. Moreover, CDCNa is a promising solubilizing

agent, which can be potentially used for solubilizing of different drug molecules and their EPD.

It is important to note that the delivery of insoluble drugs is an important direction in modern

biomedical research. [50] Many failures in the development and applications of new drugs are

related to their poor water solubility. [50] The deposition of composite coatings by EPD is a

promising strategy for drug delivery. As a step in this direction, we investigated EPD of IBP,

which was used as a model water insoluble drug. [51] It was found that CDCNa facilitated IBP

solubilization in water and allowed film formation by EPD. XRD analysis revealed that CDCH

was amorphous (Fig. 5-11). In contrast, the diffraction pattern of a deposit prepared from an

IBP solution, containing CDCNa, showed well defined peaks of IBP, corresponding to the

JCPDS file 32–1723. We suggested that mixed micelles of CDCNa and IBP were formed in

water and facilitated IBP transport to the anode surface, where IBP incorporated into the CDCH

film. This mechanism can potentially be used for the deposition of other drugs and various

functional molecules for biomedical, electronic, energy storage and other applications.
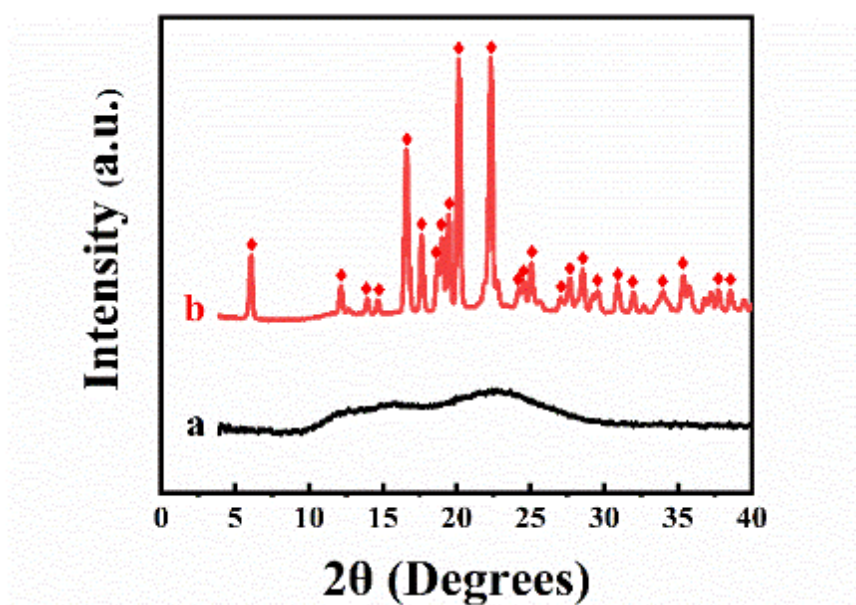


Fig. 5-11 X-ray diffraction patterns of (a) as-received CDCNa and (b) deposit, obtained from 3 g $L^{-1}$ IBP aqueous solution, containing 1 g $L^{-1}$ CDCNa at a deposition voltage of 30 V (♦ - JCPDS file 32-1723 of IBP).

## 5.4 Conclusions

For the first time we demonstrate that CDCH films can be deposited using an

electrogenerated acid method and pH-dependent gel-forming properties of CDCH. Another

major finding was that CDCNa allowed EPD of carbon materials, such as SD, ND and carbon

nanotubes, as well as PTFE and MHT. This discovery paved the way for the fabrication of composite coatings using CDCNa as a co-dispersing surfactant. This study represents an advance in the EPD of hydrophobic materials from aqueous solutions. In our approach, bifacial amphipathic CDCNa acted as a compatibilizing agent between the hydrophobic material surface and water. An important practical outcome of this study was the development of advanced coatings for enhanced corrosion protection of stainless steel.

We put forward a conceptually novel strategy to enhance protective properties of polymer coatings, which is based on the memory properties of MHT. The mechanism involves in-situ MHT reconstruction, which limits water diffusion in pores. This strategy paves the way for the fabrication of advanced polymer coatings for corrosion protection. It is expected that this strategy can be utilized for other advanced polymers and chemically active additives for corrosion protection in different environments. The feasibility of co-deposition of various materials using CDCNa as a co-dispersing surfactant opens new avenues for the fabrication of new composites with enhanced functional properties. Another important finding was that CDCNa facilitated IBP solubilization and deposition of CDCH films, containing IBP. This finding has practical significance for development of new drug delivery technologies and deposition of various water insoluble organic functional materials. Particularly important for future applications is the possibility of EPD of various hydrophobic polymers, functional materials and composites from aqueous suspensions using a biomimetic approach based on the CDCNa mediated deposition.

## 5.5 Supplementary information
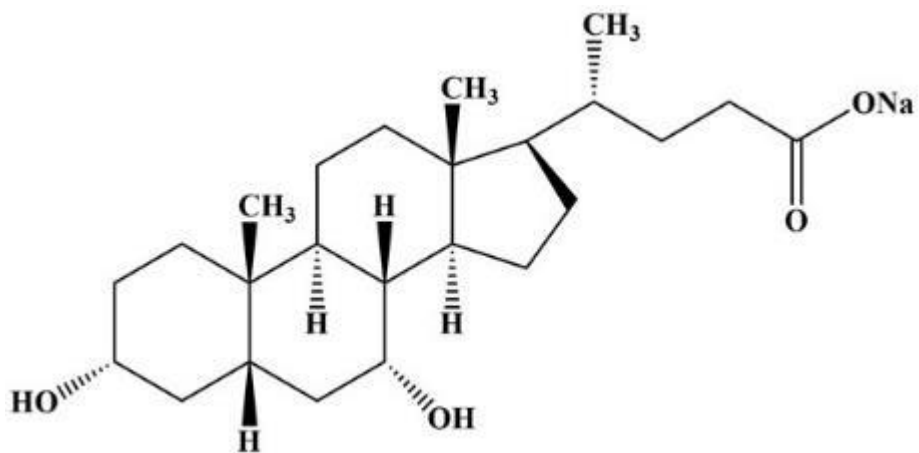


Fig. 5-12 Chemical structure of CDCNa.
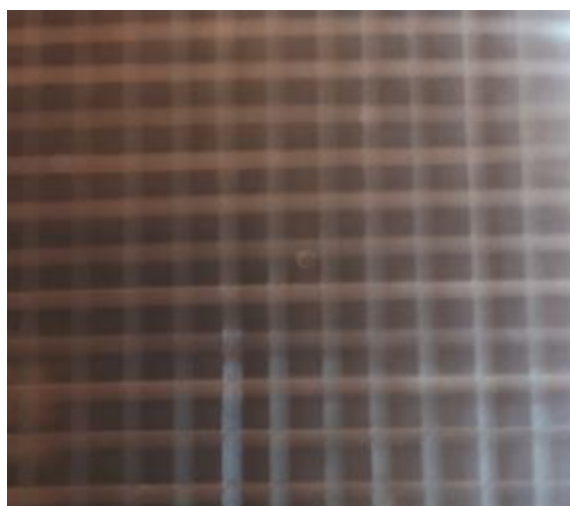


Fig. 5-13 Results of adhesion test for PTFE film.
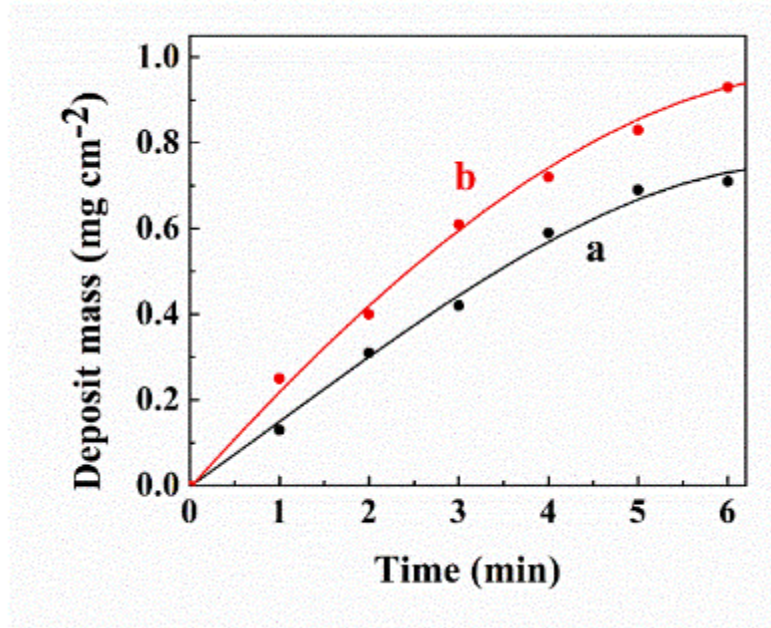
Fig. 5-14 Deposit mass versus deposition time for 5 g L$^{-1}$ PTFE suspension, containing 1g L$^{-1}$ CDCNa: (a) without MHT and (b) containing 2 g L$^{-1}$ MHT at a deposition voltage of 50 V.

According to Hamaker equation the deposition yield M per unit area  of the electrode is proportional to the concentration of particles in suspension C, deposition time, electrophoretic mobility μ, electric field E[52].

$$M= \mu EtC \qquad\qquad (S1)$$

In the case of co-deposition, the deposition yield is given by

$$M= \mu_1 EtC_1 + \mu_2 EtC_2 \qquad\qquad (S2)$$

where subscripts 1 and 2 correspond to different materials in the suspension. The addition of MHT to PTFE resulted in increased deposition yield in agreement with equation S2.

Therefore, the deposition yield measurements confirm co-deposition of PTFE and MHT.

The deviation from the linear dependence at deposition time above 4 min can result from the reduction in electric field in the bulk of the suspension due to the voltage drop in the insulating deposit. [28]
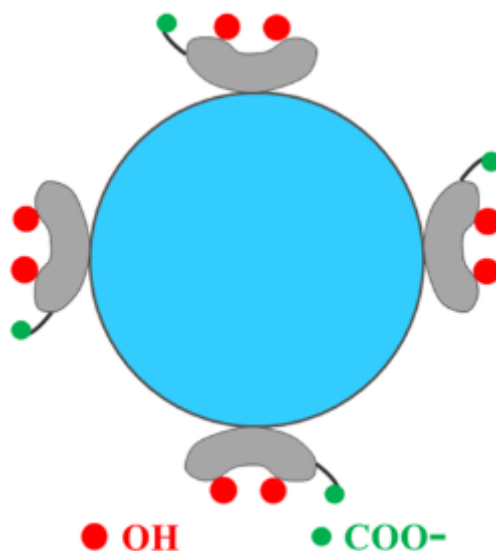


Fig. 5-15 Schematic of CDCNa adsorption on a hydrophobic particle.

## 5.6  Contribution Statement

Xinqian Liu: Methodology, Validation, Formal analysis, Investigation, Writing - original draft. Amanda Clifford: Methodology, Validation, Conceptualization. Qinfu Zhao: Investigation, Formal analysis, Methodology. Igor Zhitomirsky: Conceptualization, Investigation.

## 5.7  Reference

[1] A.S. Rao, B.S. Wong, M. Camilleri, S.T. Odunsi–Shiyanbade, S. McKinzie, M. Ryks, D. Burton, P. Carlson, J. Lamsam, R. Singh, Chenodeoxycholate in females with irritable

bowel syndrome-constipation: a pharmacodynamic and pharmacogenetic analysis, Gastroenterology 139(5) (2010) 1549-1558. e1.

[2] C. Jiang, Q. Xu, X. Wen, H. Sun, Current developments in pharmacological therapeutics for chronic constipation, Acta Pharmaceutica Sinica B 5(4) (2015) 300-309.

[3] Y.-S. Lin, K.-C. Su, R.K. Kankala, C.-H. Lee, C.-L. Liu, Y.-F. Hu, A Model Prediction for Chenodeoxycholate Aggregate Formation, Journal of pharmaceutical sciences 106(5) (2017) 1391-1395.

[4] R.S. Abendan, J.A. Swift, Cholesterol Monohydrate Dissolution in the Presence of Bile Acid Salts, Crystal growth & design 13(8) (2013) 3596-3602.

[5] T. Kauss, A. Gaubert, L. Tabaran, G. Tonelli, T. Phoeung, M.-H. Langlois, N. White, A. Cartwright, M. Gomes, K. Gaudin, Development of rectal self-emulsifying suspension of a moisture-labile water-soluble drug, International journal of pharmaceutics 536(1) (2018) 283-291.

[6] V. Urdaneta, J. Casadesús, Interactions between bacteria and bile salts in the gastrointestinal and hepatobiliary tracts, Frontiers in medicine 4 (2017) 163.

[7] L. Bogdanova, E. Ermakova, B. Idiyatullin, L.Y. Zakharova, A. Konovalov, Y.F. Zuev, Micellar catalytic effect as a factor of lipase activity regulation, Doklady. Biochemistry and biophysics, Springer Science & Business Media, 2012, p. 238.

[8] R. Ninomiya, K. Matsuoka, Y. Moroi, Micelle formation of sodium chenodeoxycholate and solubilization into the micelles: comparison with other unconjugated bile salts, Biochimica et Biophysica Acta (BBA)-Molecular and Cell Biology of Lipids 1634(3) (2003) 116-125.

[9] I. Ledeti, A.M. Pusztai, M. Murariu, S. Olariu, C. Ivan, D. Circioban, G. Vlase, A. Ledeti, T. Vlase, P. Matusz, Comparative instrumental investigations of some bile acids, Journal of Thermal Analysis and Calorimetry 134(2) (2018) 1345-1350.

[10] H. Igimi, M.C. Carey, pH-Solubility relations of chenodeoxycholic and ursodeoxycholic acids: physical-chemical basis for dissimilar solution and membrane phenomena, Journal of lipid research 21(1) (1980) 72-90.

[11] J. Yum, S. Moon, R. Humphry-Baker, P. Walter, T. Geiger, F. Nüesch, M. Grätzel, M. d K Nazeeruddin, Effect of coadsorbent on the photovoltaic performance of squaraine sensitized nanocrystalline solar cells, Nanotechnology 19(42) (2008) 424005.

[12] J. Warnan, L. Favereau, Y. Pellegrin, E. Blart, D. Jacquemin, F. Odobel, A compact diketopyrrolopyrrole dye as efficient sensitizer in titanium dioxide dye-sensitized solar cells, Journal of Photochemistry and Photobiology A: Chemistry 226(1) (2011) 9-15.

[13] C.V. Kumar, D. Raptis, E.N. Koukaras, L. Sygellou, P. Lianos, Study of an indoline–phenothiazine based organic dye for Dye-Sensitized Solar Cells. Theoretical calculations and experimental data, Organic Electronics 25 (2015) 66-73.

[14] P. Salvatori, G. Marotta, A. Cinti, C. Anselmi, E. Mosconi, F. De Angelis, Supramolecular interactions of chenodeoxycholic acid increase the efficiency of dye-sensitized solar cells based on a cobalt electrolyte, The Journal of Physical Chemistry C 117(8) (2013) 3874-3887.

[15] V. Leandri, H. Ellis, E. Gabrielsson, L. Sun, G. Boschloo, A. Hagfeldt, An organic hydrophilic dye for water-based dye-sensitized solar cells, Physical Chemistry Chemical Physics 16(37) (2014) 19964-19971.

[16] S. Jungsuttiwong, K. Sirithip, N. Prachumrak, R. Tarsang, T. Sudyoadsuk, S. Namuangruk, N. Kungwan, V. Promarak, T. Keawin, Significant enhancement in the performance of porphyrin for dye-sensitized solar cells: aggregation control using chenodeoxycholic acid, New Journal of Chemistry 41(15) (2017) 7081-7091.

[17] D. Xu, C. Shi, L. Wang, L. Qiu, F. Yan, Co-grafting of surfactants: a facile and effective method for the performance enhancement of plastic crystal based solid-state dye-sensitized solar cells, Journal of Materials Chemistry A 2(25) (2014) 9803-9811.

[18] M. García-Iglesias, J.-J. Cid, J.-H. Yum, A. Forneli, P. Vázquez, M.K. Nazeeruddin, E. Palomares, M. Grätzel, T. Torres, Increasing the efficiency of zinc-phthalocyanine based solar cells through modification of the anchoring ligand, Energy & Environmental Science 4(1) (2011) 189-194.

[19] N.R. Neale, N. Kopidakis, J. Van De Lagemaat, M. Grätzel, A.J. Frank, Effect of a coadsorbent on the performance of dye-sensitized $TiO_2$ solar cells: shielding versus band-edge movement, The Journal of Physical Chemistry B 109(49) (2005) 23183-23189.

[20] I.R. Perera, A. Gupta, W. Xiang, T. Daeneke, U. Bach, R.A. Evans, C.A. Ohlin, L. Spiccia, Introducing manganese complexes as redox mediators for dye-sensitized solar cells, Physical Chemistry Chemical Physics 16(24) (2014) 12021-12028.

[21] J. Li, W. Wu, J. Yang, J. Tang, Y. Long, J. Hua, Effect of chenodeoxycholic acid (CDCA) additive on phenothiazine dyes sensitized photovoltaic performance, Science China Chemistry 54(4) (2011) 699.

[22] A. Clifford, I. Zhitomirsky, Aqueous electrophoretic deposition of drugs using bile acids as solubilizing, charging and film-forming agents, Materials Letters 227 (2018) 1-4.

[23] G.M. Jacob, I. Zhitomirsky, Microstructure and properties of manganese dioxide films prepared by electrodeposition, Applied Surface Science 254(20) (2008) 6671-6676.

[24] C. Streich, S. Koenen, M. Lelle, K. Peneva, S. Barcikowski, Influence of ligands in metal nanoparticle electrophoresis for the fabrication of biofunctional coatings, Applied Surface Science 348 (2015) 92-99.

[25] C.B. Ustundag, F. Kaya, M. Kamitakahara, C. Kaya, K. Ioku, Production of tubular porous hydroxyapatite using electrophoretic deposition, Journal of the Ceramic Society of Japan 120(1408) (2012) 569-573.

[26] H. Yi, L.-Q. Wu, W.E. Bentley, R. Ghodssi, G.W. Rubloff, J.N. Culver, G.F. Payne, Biofabrication with chitosan, Biomacromolecules 6(6) (2005) 2881-2894.

[27] I. Zhitomirsky, A. Petric, Electrochemical deposition of yttrium oxide, Journal of Materials Chemistry 10(5) (2000) 1215-1218.

[28] I. Zhitomirsky, L. Gal-Or, Formation of hollow fibers by electrophoretic deposition, Materials Letters 38(1) (1999) 10-17.

[29] M.P.D. LEON, P. Loria, N. Carulli, G. Murphy, R.H. DOWLING, Intestinal solubilization, absorption, pharmacokinetics and bioavailability of chenodeoxycholic acid, European journal of clinical investigation 10(4) (1980) 261-271.

[30] M. Ata, I. Zhitomirsky, Colloidal methods for the fabrication of carbon nanotube–manganese dioxide and carbon nanotube–polypyrrole composites using bile acids, Journal of colloid and interface science 454 (2015) 27-34.

[31] D.C. Culita, L. Patron, V.S. Teodorescu, I. Balint, Synthesis and characterization of spinelic ferrites obtained from coordination compounds as precursors, Journal of alloys and compounds 432(1-2) (2007) 211-216.

[32] L. Yang, Y. Xu, Y. Su, J. Wu, K. Zhao, J.e. Chen, M. Wang, FT-IR spectroscopic study on the variations of molecular structures of some carboxyl acids induced by free electron laser, Spectrochimica Acta Part A: Molecular and Biomolecular Spectroscopy 62(4) (2005) 1209-1215.

[33] R. Wang, G. Xu, Y. He, Structure and properties of polytetrafluoroethylene (PTFE) fibers, e-Polymers 17(3) (2017) 215-220.

[34] H.W. Starkweather Jr, R.C. Ferguson, D.B. Chase, J.M. Minor, Infrared spectra of amorphous and crystalline poly (tetrafluoroethylene), Macromolecules 18(9) (1985) 1684-1686.

[35] F. Mansfeld, Use of electrochemical impedance spectroscopy for the study of corrosion protection by polymer coatings, Journal of Applied Electrochemistry 25(3) (1995) 187-202.

[36] V. Saraswat, M. Yadav, I. Obot, Investigations on eco-friendly corrosion inhibitors for mild steel in acid environment: Electrochemical, DFT and Monte Carlo Simulation approach, Colloids Surfaces A: Physicochemical Engineering Aspects 599 (2020) 124881.

[37] Z. Yu, C. Zhou, R. Liu, Q. Zhang, J. Gong, D. Tao, Z. Ji, Fabrication of superhydrophobic surface with enhanced corrosion resistance on H62 brass substrate, Colloids Surfaces A: Physicochemical Engineering Aspects 589 (2020) 124475.

[38] F. Zhang, W. Liu, L. Liang, C. Liu, S. Wang, H. Shi, Y. Xie, M. Yang, K. Pi, Applications of hydrophobic α, ω-bis (amino)-terminated polydimethylsiloxane-graphene oxide in enhancement of anti-corrosion ability of waterborne polyurethane, Colloids Surfaces A: Physicochemical Engineering Aspects 600 (2020) 124981.

[39] J.R. Scully, Electrochemical impedance of organic-coated steel: correlation of impedance parameters with long-term coating deterioration, Journal of the Electrochemical Society 136(4) (1989) 979-989.

[40] F. Gao, A. Du, R. Ma, C. Lv, H. Yang, Y. Fan, X. Zhao, J. Wu, X. Cao, Improved corrosion resistance of acrylic coatings prepared with modified MoS2 nanosheets, Colloids Surfaces A: Physicochemical Engineering Aspects 587 (2020) 124318.

[41] Y. Xie, C. Liu, W. Liu, L. Liang, S. Wang, F. Zhang, H. Shi, M. Yang, A novel approach to fabricate polyacrylate modified graphene oxide for improving the corrosion resistance of epoxy coatings, Colloids Surfaces A: Physicochemical Engineering Aspects 593 (2020) 124627.

[42] A. Amirudin, D. Thieny, Application of electrochemical impedance spectroscopy to study the degradation of polymer-coated metals, Progress in organic coatings 26(1) (1995) 1-28.

[43] M. Kendig, F. Mansfeld, S. Tsai, Determination of the long term corrosion behavior of coated steel with AC impedance measurements, Corrosion Science 23(4) (1983) 317-329.

[44] J. Zhang, J. Hu, J. Zhang, C. Cao, Studies of impedance models and water transport behaviors of polypropylene coated metals in NaCl solution, Progress in Organic Coatings 49(4) (2004) 293-301.

[45] P. Wojtal, S. Chen, K. Shi, R. Mathews, I. Zhitomirsky, Electrophoretic deposition of a memory-type flame retardant material, Materials Letters 153 (2015) 106-109.

[46] Q. Zhao, X. Liu, S. Veldhuis, I. Zhitomirsky, Sodium deoxycholate as a versatile dispersing and coating-forming agent: A new facet of electrophoretic deposition technology, Colloids Surfaces A: Physicochemical Engineering Aspects 588 (2020) 124382.

[47] K.D. Dobson, A.J. McQuillan, In situ infrared spectroscopic analysis of the adsorption of aromatic carboxylic acids to TiO2, ZrO2, Al2O3, and Ta2O5 from aqueous solutions, Spectrochimica Acta Part A: Molecular Biomolecular Spectroscopy 56(3) (2000) 557-565.

[48] S. Tunesi, M.A. Anderson, Surface effects in photochemistry: an in situ cylindrical internal reflection-Fourier transform infrared investigation of the effect of ring substituents on chemisorption onto titania ceramic membranes, Langmuir 8(2) (1992) 487-495.

[49] A. Affoune, B. Prasad, H. Sato, T. Enoki, Electrophoretic deposition of nanosized diamond particles, Langmuir 17(2) (2001) 547-551.

[50] S. Kalepu, V. Nekkanti, Insoluble drug delivery strategies: review of recent advances and business prospects, Acta Pharmaceutica Sinica B 5(5) (2015) 442-453.

[51] R.K. Janjikhel, C.M. Adeyeye, Dissolution of ibuprofen enantiomers from coprecipitates and suspensions containing chiral excipients, Pharmaceutical development and technology 4(1) (1999) 9-17.

[52] X. Pang, T. Casagrande, I. Zhitomirsky, Electrophoretic deposition of hydroxyapatite–CaSiO3–chitosan composite coatings, Journal of colloid and interface science 330(2) (2009) 323-329.

# Chapter 6  Carbenoxolone as a multifunctional vehicle for electrodeposition and surface modification of materials

Xinqian Liu, Stephen Veldhuis, Ritch Mathews and Igor Zhitomirsky

Applied sciences

Volume 11, pp. 9110

27 Sep 2021

## Abstract

This investigation describes for the first time the application of carbenoxolone for electrophoretic deposition (EPD) of different carbon materials, polytetrafluoroethylene (PTFE) and their composite films. Carbenoxolone is a versatile biosurfactant, which adsorbs on materials due to its amphiphilic structure and allows their charging and dispersion. Moreover, carbenoxolone exhibits film-forming properties, which are investigated in experiments on EPD of films using water and ethanol-water solvents. The new deposition process is monitored in situ and the deposition yield and film microstructure are analyzed at different conditions. The EPD mechanism of materials involves electrode reactions of the carbenoxolone surfactant. The data of potentiodynamic studies coupled with the results of impedance spectroscopy show that PTFE films can be applied to protect metals from corrosion. Electron microscopy, electrochemical techniques and modeling are used for analysis of the microstructure and porosity of films prepared at different conditions. Carbenoxolone is applied as a co-surfactant for the EPD of composites.

## 6.1  Introduction

EPD and other electrochemical strategies are widely applied to modify the surfaces of materials and to form coatings and thin films [1-6]. The EPD technique involves electrophoresis of charged particles and their deposition on the electrode surface [7-10]. Many investigations have been conducted to develop surface engineering strategies to charge

particles and to develop deposition mechanisms and optimize the deposition conditions [11-14]. Advanced techniques, novel additives and bath compositions have been applied for EPD [15-17]. There has been significant progress in the EPD of composite and multilayer films [18-21]. EPD was combined with electrosynthesis for the manufacturing of nanocomposite organic–inorganic films [22, 23]. A new approach involved the use of film-forming charged dispersants for EPD of materials [24, 25]. It was found that small organic molecules such as bile salts adsorbed on carbon nanotubes and the negative charge of the adsorbed molecules facilitated carbon nanotube dispersion [24]. Moreover, bile salts exhibited both a pH-dependent charge and gel properties, which facilitated the fabrication of thin films of bile acids [24]. The film-forming and binding properties of bile salts facilitated EPD of materials. Therefore, further development of film-forming charged dispersants is a promising approach to surface modification and EPD of materials.

EPD is an eco-friendly technology which facilitates the deposition of thin films of different functional materials, avoiding the use of toxic precursors and solvents [26]. It is widely used for high quality film deposition for various electronic and biomedical applications due to the high purity of the deposited materials [26, 27]. One of the challenges in designing EPD processes is the development of eco-friendly charged surfactants for various materials. Therefore, the use of natural and biocompatible surfactants for charging and dispersion of materials is of particular interest for the development of EPD technology.

Carbenoxolone sodium salt (CBXNa$_2$) is a promising biocompatible molecule which can potentially be used for surface modification and EPD of materials [28]. This molecule was used as an anionic dopant for electropolymerization of polypyrrole [28]. CBXNa$_2$ is currently used in medicine for the treatment of gastric and duodenal ulcers. This drug molecule exhibits important antiviral and gel-forming properties. CBXNa$_2$ is a derivative of glycyrrhetinic acid (Fig. 6-1) with a steroid-like chemical structure. It is a bipolar amphiphilic molecule, containing carboxylic and succinyl groups bonded to opposite sides of the steroid-like core. Dissociated CBXNa$_2$ exhibits anionic properties in aqueous solutions due to its two COO$^-$ groups. The COO$^-$ groups are protonated in acidic solutions to form insoluble CBXH$_2$. Compared to bile salts, CBXNa$_2$ offers the benefit of a higher charge to mass ratio, which is important for electrostatic dispersion of materials. Another advantage of CBXNa$_2$ is that the succinyl group of CBXNa$_2$ facilitates its bonding to various materials [29].

The goal of this study was the development of a new and versatile approach for EPD of different materials, such as carbon materials, PTFE and composites. It involved the application of CBXNa$_2$ as a versatile surface modification, dispersion, charging and film-forming agent. We analyzed the deposition mechanisms, film microstructures and properties.
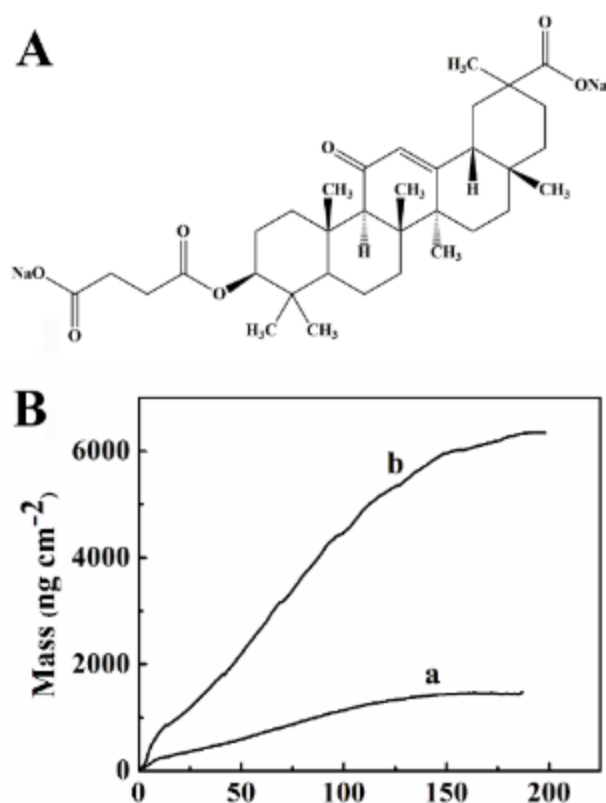
Fig. 6-1 (A) CBXNa$_2$ structure, (B) film mass as a function of time analyzed in situ using QCM for 0.1 gL$^{-1}$ CBXNa$_2$ solutions in water at deposition voltages of (a) 3 and (b) 5V.

## 6.2 Materials and Methods

CBXNa$_2$, diamond (size < 1 μm), nanodiamond (size < 10 nm), graphene nanoplatelets (BET area 750 m$^2$g$^{-1}$, size < 2 μm) and PTFE (~1 μm) (Aldrich) were used. Carbon dots were prepared as described in [30]. CBXNa$_2$ solutions in water or water-ethanol solvents with dispersed particles of the carbon materials and PTFE were prepared for EPD. The particle concentration was 0.1–10 gL$^{-1}$, deposition voltages were 3–70V, deposition times were 3–5 min. The distance between stainless steel (type 304) and counterelectrodes (Pt foil) in the EPD cell was 15 mm. The electrode dimensions were 25 × 30 × 0.1 mm. PTFE coated samples were

annealed at 350 °C for 1 h. The yield of EPD has been analyzed in situ using a microbalance

(AMETEK, QCM 922) and Au coated quartz crystals. The area of the electrode was 0.18 cm$^2$.

Corrosion protection of the electrophoretically deposited films was studied in 3% (mass

per volume) sodium chloride solutions using a potentiostat (AMETEK 2273) and a three-

electrode cell with uncoated or coated substrate, Pt auxiliary electrode and an SCE reference.

The working electrode area was 1 cm$^2$. Potentiodynamic testing was carried out at a 60

mVmin$^{-1}$ scan rate in the potential range of $-1.1$–$+0.8$ V versus SCE. EIS data was acquired at

a 5 mV voltage amplitude in the frequency range of 10 mHz–10 kHz. Microstructure studies

were carried out using a JSM-7000F microscope (JEOL, SEM) at voltages 5–10 kV. XRD

testing was carried out with a Nicolet I2 diffractometer and CuKα radiation. A Bruker FTIR

spectrometer (Vertex 70) was applied for spectroscopy analysis using the attenuated total

reflection (ATR) technique.

## 6.3  Results

A typical requirement for EPD is the colloidal stability of charged species in the

deposition bath. The charging agent selection plays an essential role in the control of bath

stability and the rate of electrophoresis. However, strong repulsion of charged particles inhibits

film formation. Therefore, when selecting charging surface agents for EPD it is important to

consider not only bulk suspension stability but also the ability of the agents to facilitate particle

discharge and coagulation at the substrate surface. Our strategy is based on the charging of

particles by $CBX^{2-}$ species in $CBXNa_2$ solutions and their discharge in electrode reactions.

The ability to form films from pure $CBXNa_2$ solutions is a favorable factor for EPD of

materials. The deposition mechanism involved electrolysis of water in an anodic reaction [24,

25, 31, 32]:

$$2H_2O \rightarrow O_2 + 2H^+ + 2e^- \tag{1}$$

The electromigration of $CBX^{2-}$ species led to their discharge at the anode and formation

of $CBXH_2$ films:

$$CBX^{2-} + 2H^+ \rightarrow CBXH_2 \tag{2}$$

Reaction (2) is critical for the deposition process, because it results in the discharge of

$CBX^{2-}$ and deposition of insoluble $CBXH_2$. The deposition mechanism described in Reactions

(1) and (2) is similar to that used for anodic deposition of other small organic molecules and

macromolecules [24, 25, 33, 34].

Water is an important component of an electrodeposition bath because it is necessary for the

$H^+$ generation in Reaction (1). However, organic solvents offer several benefits for EPD of

materials. The EPD yield is proportional to the electric field in the suspension [35]. The

generation of high electric fields in aqueous suspensions by the application of high voltages

presents difficulties due to the high conductivity of aqueous suspensions, which results in high

currents, significant $O_2$ gas evolution and enhanced $H^+$ generation in Reaction (1). The high

rate of $H^+$ generation can result in expansion of a low pH region away from the anode. This can potentially lead to the precipitation of $CBXH_2$ at some distance from the electrode surface. Moreover, significant $O_2$ evolution results in porous films. The use of ethanol-water mixture as a solvent is beneficial for EPD at relatively high voltages and a reduced rate of Reaction (1). The dispersion of hydrophobic PTFE in water presented difficulties. However, PTFE suspensions were formed in an ethanol-water mixture.

The deposition of pure $CBXH_2$ films was studied using water and ethanol-water (5% water) solvents. The deposition yield was analyzed by in situ method, based on continuous QCM monitoring of deposit mass during the deposition. This technique has limitations, because it can be used for relatively low deposition yields. Therefore, QCM analysis was performed at relatively low voltages and low solution concentrations. The deposition yield data presented in Figure 1B showed continuous mass increase with time due to film growth. The increase in the applied voltage led to a higher rate of deposition. The rate of mass gain reduced with EPD time due to the continuous rise of the voltage drop in the deposit and reduction of electric field strength in the solution [35].

EPD from aqueous $CBXNa_2$ solutions at voltages below 15V led to the formation of continuous films which were crack-free (Figure 2A,B). However, the deposition at higher voltages resulted in the formation of pinholes, due to the $O_2$ evolution. In contrast, significantly higher voltages can be applied for the EPD of films from the solutions of $CBXNa_2$ in the ethanol-water mixture. The EPD process resulted in the formation of continuous films at voltages of 20–80 V. The

microstructure of the films formed at 20 V showed a large number of fibers with a typical

length of 5–10 μm and diameters of about 0.5 μm. Fiber formation can result from self-

assembly of water-insoluble hydrophobic $CBXH_2$ molecules. The formation of fibrous

particles by electrochemical self-assembly was observed in other experiments on anodic

electrodeposition of other small organic molecules [36, 37]. Such fibers were not observed at

higher voltages. The increase of voltage above 80V in the water-ethanol solvent resulted in

pinholes. Therefore, the EPD from aqueous suspensions was limited to voltages not higher than

15 V, whereas the deposition from ethanol-water suspensions was performed at voltages below

80 V. It is important to note that the selection of a solvent is important for the fabrication of

stable suspensions for EPD. Therefore, in this investigation EPD of different materials was

performed in aqueous or ethanol-water suspensions in order to achieve good suspension

stability for each material.
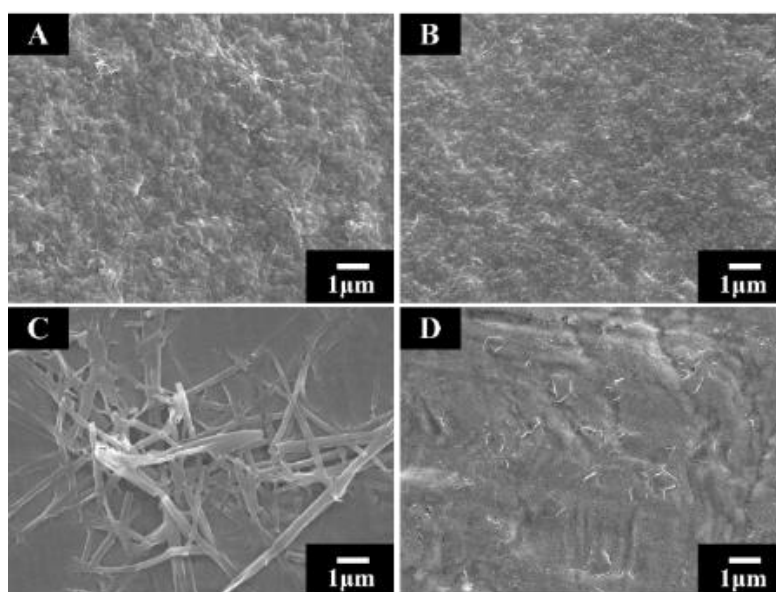


Fig. 6-2 SEM images of films, deposited from 1 g L$^{-1}$ $CBXNa_2$ solutions in water at (A) 5 V, (B) 15 V and in ethanol-water solvent (5% water) at (C) 20 V and (D) 80 V.

The deposition mechanism of carbon materials and PTFE involved $CBX^{2-}$ adsorption; the adsorbed $CBX^{2-}$ makes the materials negatively charged and facilitates EPD from stable suspensions. Fig. 6-3 shows microstructures of films containing diamond and nanodiamond, as well as the XRD patterns of the films. Electron microscopy showed the formation of continuous films, which were crack-free and contained diamonds (Fig.6-3(A)). Nanodiamond particles showed poor dispersion in water. However, relatively stable suspensions were obtained in ethanol-water solvent, which facilitated nanodiamond dispersion in the presence of $CBXNa_2$. Electron microscopy studies showed some agglomerates on the film surface (Fig. 6-3(B)). The size of the primary particles in such agglomerates was significantly larger than the size of the nanodiamond particles. The agglomeration of the nanodiamond particles can result from their lower zeta-potential (Supplementary material, Table 6-1). The incorporation of diamond and nanodiamond in the films was confirmed by XRD (Fig. 6-3(C)), which showed peaks (111), (220) and (113) of diamond. The peak broadening for nanodiamond resulted from its small size (Fig. 6-3(C)).
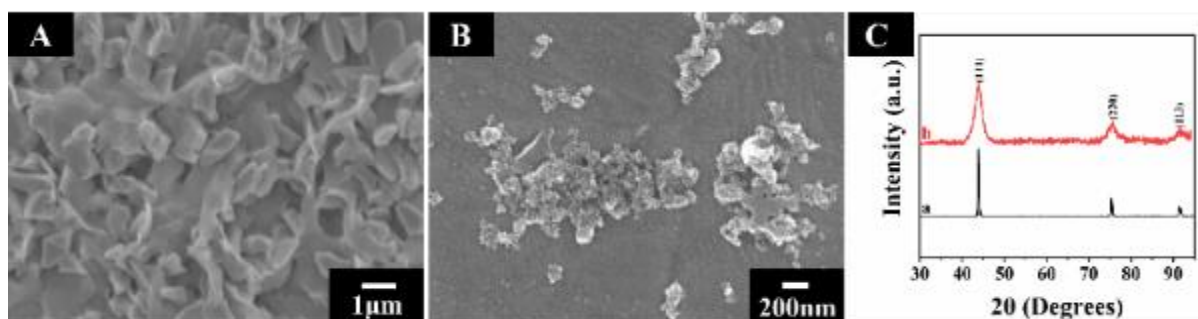


Fig. 6-3 (A,B) SEM and (C) XRD data for films prepared from 1 $gL^{-1}$ $CBXNa_2$ solutions with (A,C(a)) 1 $gL^{-1}$ diamond at 7 V in water and (B,C(b)) 1 $gL^{-1}$ nanodiamond at 70 V in ethanol-water (5% water) solvent.

The feasibility of diamond deposition by EPD from their dispersion in CBXNa$_2$ solutions indicated that CBX$^{2-}$ adsorbed on chemically inert diamond surfaces. It was hypothesized that the hydrophobic interactions allowed for adsorption of amphiphilic CBX$^{2-}$ on the diamond particles. It was found that other carbon materials, such as carbon dots and graphene, can also be deposited from their dispersions in the CBXNa$_2$ solutions. Fig. 6-4 shows that continuous and crack-free films were deposited. The SEM image shows relatively large graphene particles. The incorporation of carbon dots into the CBXH$_2$ films was verified by FTIR.
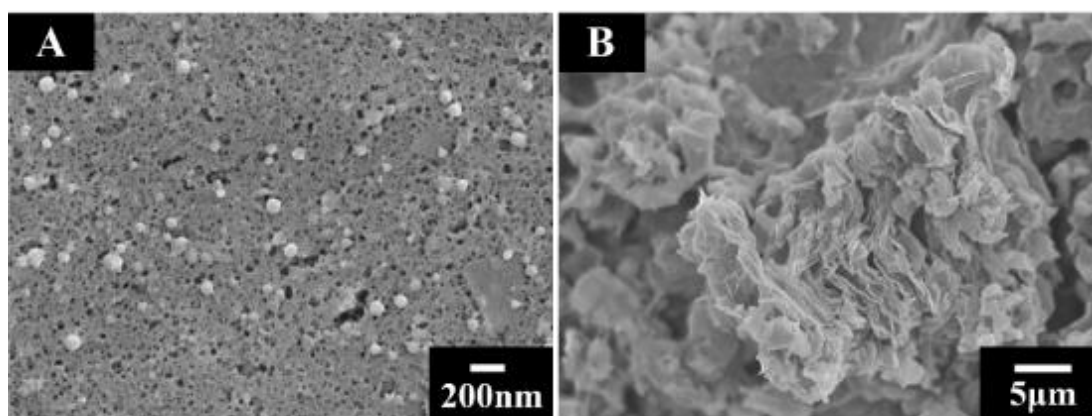


Fig. 6-4 SEM images of films, prepared from (A) 0.5 gL$^{-1}$ CBXNa$_2$ with 0.5 gL$^{-1}$ carbon dots in water at 15 V and (B) 1 gL$^{-1}$ CBXNa$_2$ with 1 gL$^{-1}$ graphene in water at 10 V.

The FTIR spectrum of CBXNa$_2$ (Fig. 6-5(A(a))) presents peaks at 1397 and 1564 cm$^{-1}$, owing to symmetric and asymmetric vibrating of salified carboxylic groups, respectively [38]. Such absorptions were not observed for the deposited CBXH$_2$ (Fig. 6-5(A(b))) which exhibited enhanced absorption at 1716 cm$^{-1}$ due to stretching of the protonated COOH ligand [38]. The peaks at 1647 cm$^{-1}$ (Fig. 6-5(A(a))) and 1650 cm$^{-1}$ (Fig. 6-5(A(b))) resulted from C=C stretching [39]. Carbon dots (Fig. 6-5(A(c))) showed absorptions at 1457 cm$^{-1}$, attributed to

stretching of a C-C type. The minimum, at 1368 cm$^{-1}$, was observed due to bending of surface

C-OH groups [39]. Similar peaks were recorded for the films formed from carbon dot

suspensions (Fig. 6-5(A(d))).

EPD of PTFE was performed from suspension of PTFE particles, which were dispersed

and charged using CBX$^{2-}$. (Fig. 6-5(B(a))) shows FTIR data for PTFE, which exhibits

absorptions at 1149 and 1203 cm$^{-1}$. According to the literature, C─C and C─F$_2$ asymmetric

vibrating contribute to absorption at 1149 cm$^{-1}$, whereas the minimum at 1203 cm$^{-1}$ was due

to symmetric vibrating of C─F$_2$ [40]. The FTIR spectra of deposits prepared from CBXNa$_2$

solutions (Fig. 6-5(B(b,c))) containing PTFE showed similar peaks, and confirm the deposition

of PTFE.
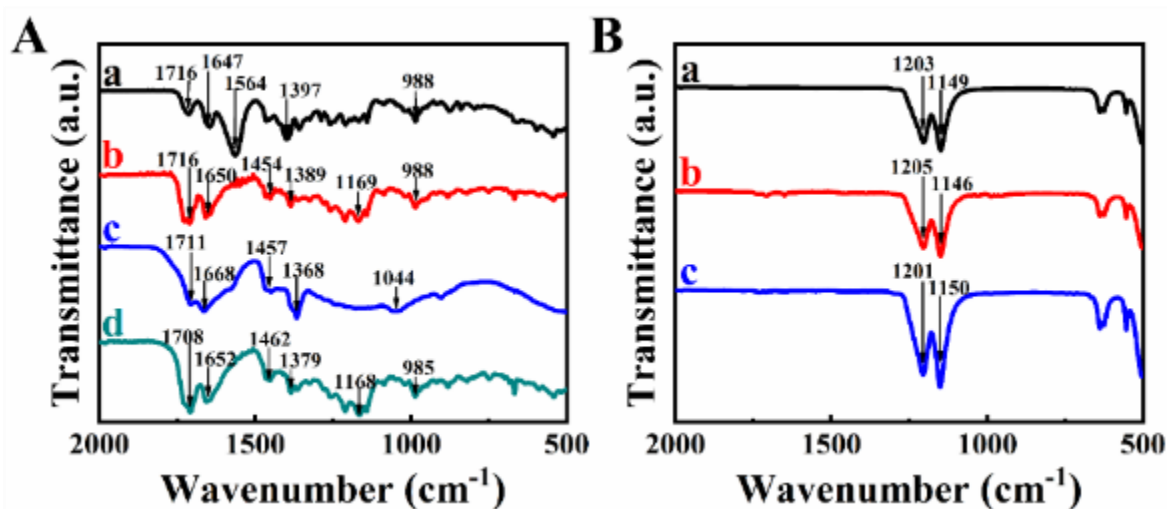


Fig. 6-5 FTIR testing data for (A) (a) original CBXNa$_2$, (b) film material, formed from 1gL$^{-1}$ CBXNa$_2$ in water at 15 V, (c) carbon dots, (d) deposit formed from 0.5 gL$^{-1}$ CBXNa$_2$ with 0.5 gL$^{-1}$ carbon dots in water at 15 V; (B) (a) PTFE (b,c) deposits, obtained from 1 gL$^{-1}$ CBXNa$_2$ with (b) 0.5 gL$^{-1}$ and (c) 1 gL$^{-1}$ PTFE in ethanol-water solvent at 50 V.

The higher polymer content in the suspension led to the enlarged polymer content in the film. The electron microscopy imaging data (Fig. 6-6) for the composite deposit formed by EPD from 10 $gL^{-1}$ PTFE suspension contained larger number of the PTFE particles, compared to the film formed from the 5 $gL^{-1}$ PTFE bath. The SEM analysis revealed the formation of continuous deposits. The SEM images for the films prepared from 10 $gL^{-1}$ PTFE suspension showed reduced porosity and relatively dense packing of the submicrometre PTFE particles. Annealing led to the burning out of the $CBXH_2$ phase and melting of the PTFE particles, which resulted in reduced porosity. The films prepared from 5 $gL^{-1}$ PTFE suspension were porous (Fig. 6-6) due to low PTFE content. The increase in the PTFE content in the films resulted in reduced porosity, as indicated by the electron microscopy images of films formed from 10 $gL^{-1}$ PTFE suspensions (Fig. 6-6). Such films were analyzed by potentiodynamic and EIS studies in the 3% NaCl solutions.
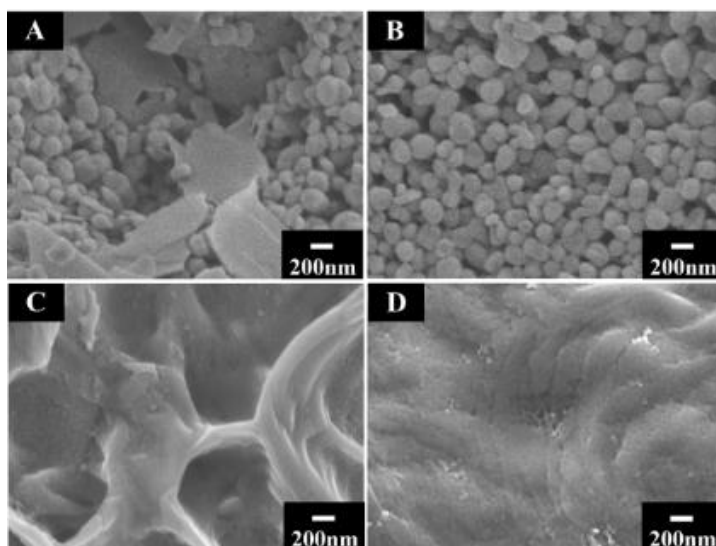


Fig. 6-6 SEM data for films (A,B) before and (C,D) after annealing (1 h at 350 °C), for films prepared using 1 $gL^{-1}$ $CBXNa_2$ with (A,C) 5 $gL^{-1}$ PTFE and (B,D) 10 $gL^{-1}$ PTFE in ethanol-water solvent at 50 V.

The data from electrochemical testing presented in Fig. 6-7 demonstrate that films of the

PTFE polymer allowed for corrosion protection. The Tafel graphs show that coating deposition

resulted in a lower current for the anodic part of the graph, with an enlarged corrosion potential.

The analysis of the Tafel plots showed corrosion currents of 0.01 and 2.6 $\mu Acm^{-2}$ for coated

and uncoated substrates, respectively. The EIS data presented in the Nyquist plot were analyzed

using an equivalent circuit (Fig. 6-7), similar to that described in **[41]**, where $R_s$, $R_{pore}$ and $R_{ct}$

are solution resistance, resistance of electrolyte in pores and charge transfer resistance,

respectively. $C_1$ represents capacitance of the film and $C_2$ is a double layer capacitance at the

substrate surface in pores. The modeling results correlated with the experimental data.
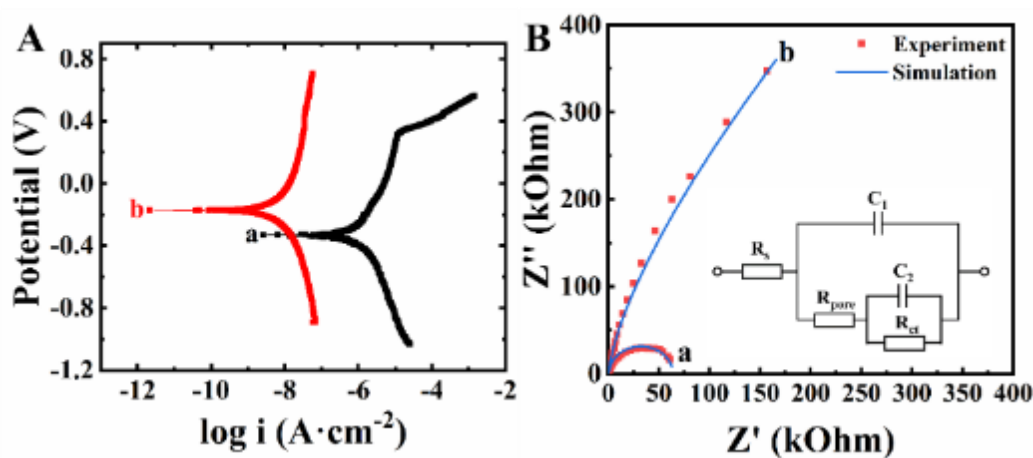


Fig. 6-7 (A) Tafel plot, (B) Nyquist plot for substrate (a) without and (b) with coating; inset
shows equivalent circuit. The working electrode area was 1 cm$^2$. The coating was deposited
from 1 gL$^{-1}$ CBXNa$_2$ with 10 gL$^{-1}$ PTFE in a mixed ethanol-water solvent at 50 V and annealed
(1 h at 350 °C).

The porosity (P) of the films was tested according to Ref. [41] by the equation

$$P=\frac{R_{pm}}{R_p}\times 10^{-\left| \Delta E/\beta \right|}$$

(3)

where $\Delta E$ is the difference of corrosion potentials for the substrates with and without films, $\beta$ and $R_{pm}$ are the slope of the anodic part of the Tafel graph and the substrate polarization resistance, respectively, $R_p$ is the polarization resistance of the coated substrate, and $R_p = R_{pore} + R_{ct}$. The EIS data was analyzed with the aid of a circuit (Figure 7) [41], which allowed for measurement of $R_{pm}$ and $R_p$. The film porosity was found to be 0.28%.

In this investigation the possibility of EPD of PTFE composites has been studied using CBXNa$_2$ as a co-dispersant. Figure 8 presents electron microscopy data for the composite coatings prepared from mixed PTFE and diamond suspensions. The SEM images show relatively dense packing of the PTFE and diamond particles. The electron microscopy images showed that the higher concentration of diamond in the suspension led to a larger diamond content in the films. The films deposited from 1 gL$^{-1}$ CBXNa$_2$ solutions with 5 gL$^{-1}$ PTFE and 0.5 gL$^{-1}$ diamond show individual diamond particles incorporated in the relatively dense PTFE layer. The higher diamond concentration in the EPD bath resulted in films which mainly contained diamond, with PTFE acting as a binder for the diamond particles (Fig. 6-8). The results of the microscopy indicated that the composition of the films can be controlled and varied.
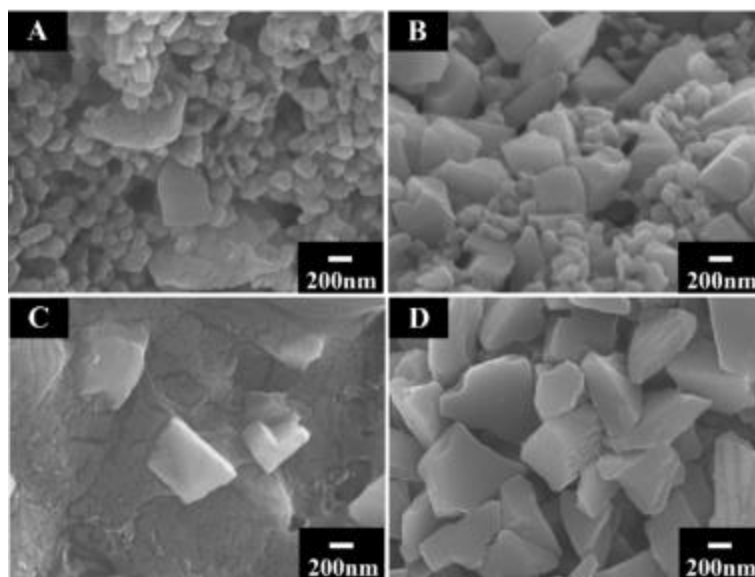
Fig. 6-8 SEM data for films (A,B) before and (C,D) after annealing (1 h at 350 °C), for films prepared from 1 $gL^{-1}$ CBXNa$_2$ solutions with 5 $gL^{-1}$ PTFE with (A,C) 0.5 $gL^{-1}$ and (B,D) 1 $gL^{-1}$ diamond at 50 V.

The fabrication of continuous CBXH$_2$ films provided evidence of the film-forming properties of CBXNa$_2$. It can also be used as a charging and dispersing agent for particles with functional properties. The combination of film-forming, charging and dispersing properties makes CBXNa$_2$ a promising additive for EPD of materials. The results of this investigation also indicated that CBXNa$_2$ is a versatile dispersing, charging and film forming agent for co-EPD of different materials. However, due to the difference in the surface chemistry and properties of different materials, deposition parameters such as CBXNa$_2$ concentration, voltage and solvent must be optimized for each material. CBXNa$_2$ can be used for EPD of other materials, such as carbon nanotubes. The deposition yield (Supplementary information, Fig. 6-9) was comparable with that obtained using a bile salt such as cholic acid sodium salt as a dispersant and film forming agent [24].

## 6.4 Conclusions

The deposition mechanism of pure $CBXH_2$ involved protonation of $CBX^{2-}$ in the anodic reactions and the forming of insoluble $CBXH_2$ films. The EPD mechanism of carbon materials, PTFE and composites involved adsorption of $CBX^{2-}$ on particles, electrophoretic transport and discharge of adsorbed $CBX^{2-}$, which facilitated film formation. The deposition rate, film morphology and composition can be varied and controlled. $CBXNa_2$ is a versatile surfactant and co-surfactant for EPD of various materials and composites. The EPD method can be applied for protection of metals from corrosion in industry. $CBXNa_2$ is a promising surface modification agent for future applications in EPD of functional inorganic materials due to the chelating properties of its carboxylic groups. Therefore, further progress in $CBXNa_2$ applications can result in the manufacturing of advanced functional composites by EPD.

## 6.5 Supplementary Information
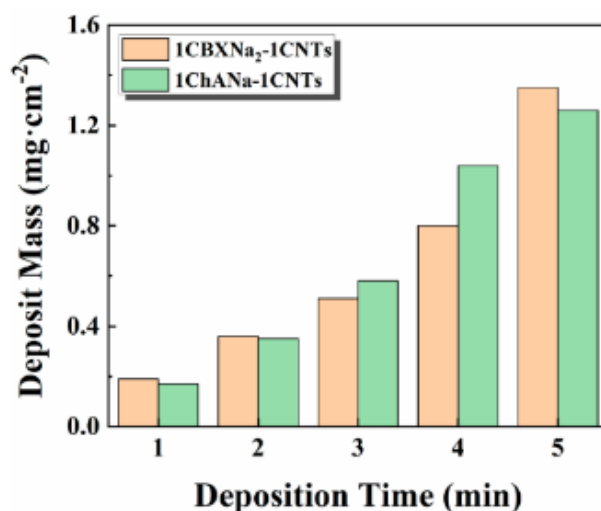


Fig. 6-9 Deposition yields at different deposition times obtained from aqueous 1 $gL^{-1}$ suspensions of multiwalled carbon nanotubes (Bayer, Germany) containing 1 $gL^{-1}$

carbenoxolone (1CBXNa$_2$-1CNTs) and aqueous 1 gL$^{-1}$ suspensions of multiwalled carbon nanotubes, containing 1 gL$^{-1}$ cholic acid sodium salt (1ChANa-1CNTs) at a deposition voltage of 5 V.

| Material | Zeta-potential, mV |
|----------|--------------------|
| Graphene | 6.93 |
| Diamond | 37.22 |
| Nanodiamond | 0.3 |
| PTFE | 4.38 |

Table 6-1 Zeta potentials of materials, dispersed by CBXNa$_2$, measured by the method, described in Hashita,M; Okamoto, H.; Nurishi, Y.; Hiramatsu, K. The zeta-potential measurements for concentrated aqueous suspension by improved electrophoretic mass transport apparatus-application to Al$_2$O$_3$, ZrO$_2$ and SiC suspensions, Journal of Materials Science 1968, 23, 2893-2896.

## 6.6  Contribution Statement

 Conceptualization, X.L., S.V. and I.Z.; methodology, X.L., S.V. and R.M.; validation, X.L.; Formal analysis, X.L. and R.M.; investigation, X.L.; writing—original draft preparation, X.L.; writing—review and editing, X.L. and I.Z.; supervision, I.Z.; project administration, I.Z.; funding acquisition, I.Z. All authors have read and agreed to the published version of the manuscript.

## 6.7  References

[1] M. Cheong, I. Zhitomirsky, Electrophoretic deposition of manganese oxide films, Surface Engineering 25(5) (2009) 346-352.

[2] J.A. Argüello, A. Cerpa, R. Moreno, Reinforcing effect of graphene nanoplatelets in the electrochemical behaviour of manganese oxide-based supercapacitors produced by EPD, Ceramics International 45(11) (2019) 14316-14321.

[3] J. Yus, Y. Bravo, A.J. Sanchez-Herencia, B. Ferrari, Z. Gonzalez, Electrophoretic deposition of RGO-NiO core-shell nanostructures driven by heterocoagulation method with high electrochemical performance, Electrochimica Acta 308 (2019) 363-372.

[4] C. Jin, Y. Wang, Z. Yang, D. Wang, C/C composite surface modified by electrophoretic depositing SiC nanowires and its brazing to Nb, Ceramics International 46(1) (2020) 204-211.

[5] R. Boudaira, O. Meglali, A. Bouraiou, N. Attaf, C. Sedrati, M. Aida, Optimization of sulphurization temperature for the production of single-phase CZTS kesterite layers synthesized by electrodeposition, Surface Engineering 36(9) (2020) 1000-1011.

[6] P. Mandal, S.C. Mondal, Enhancement of electro-thermal and mechanical properties for Cu-SWCNT coated 6061Al, Surface Engineering 36(2) (2020) 135-143.

[7] L. Yang, X. Pang, G. Fox-Rabinovich, S. Veldhuis, I. Zhitomirsky, Electrophoretic deposition of polymer and composite films, Surface engineering 28(8) (2012) 585-589.

[8] Y. Sun, M. Ata, I. Zhitomirsky, Electrophoretic deposition of linear polyethylenimine and composite films, Surface engineering 29(7) (2013) 495-499.

[9] Z. Jabbari, B. Nassernejad, N. Fallah, M. Javanbakht, N. Afsham, Fabrication of novel binderless anode via electrophoretic deposition for HT-PEMFC, Surface Engineering 35(12) (2019) 1013-1020.

[10] S.M. Emarati, M. Mozammel, Fabrication of superhydrophobic titanium dioxide coating on AISI 316L stainless steel by electrophoretic deposition and using trimethoxy (propyl) silane modification, Surface Engineering 35(5) (2019) 456-465.

[11] A. Rousta, D. Dorranian, M. Elahi, Electrophoretic deposition of cobalt oxide nanoparticles on aluminium substrate, Surface Engineering 36(9) (2020) 919-928.

[12] A. Saadati, H. Hesarikia, M.R. Nourani, R.A. Taheri, Electrophoretic deposition of hydroxyapatite coating on biodegradable Mg–4Zn–4Sn–0.6 Ca–0.5 Mn alloy, Surface Engineering 36(9) (2020) 908-918.

[13] M. Gorji, S. Sanjabi, C. Edtmaier, Combination of electrophoretic and electroless depositions to fabricate Ni/TiC cladding, Surface Engineering 36(9) (2020) 929-935.

[14] P. Tiwari, N.D. Ferson, J.S. Andrew, Elucidating the role of electrophoretic mobility for increasing yield in the electrophoretic deposition of nanomaterials, Journal of colloid and interface science 570 (2020) 109-115.

[15] J.A. Arguello, J.M. Rojo, R. Moreno, Electrophoretic deposition of manganese oxide and graphene nanoplatelets on graphite paper for the manufacture of supercapacitor electrodes, Electrochimica Acta 294 (2019) 102-109.

[16] B. Choudhary, S. Anwar, L. Besra, S. Anwar, Electrophoretic deposition studies of Ba (Zr-Ce-Y) O3 ceramic coating, International Journal of Applied Ceramic Technology 16(3) (2019) 1022-1031.

[17] M. Jafarpour, H. Aghajani, A.G. Ajabshir, Stability and electrophoretic deposition of nano-SiC assisted by PEI, Journal of Dispersion Science and Technology 40(12) (2019) 1715-1724.

[18] E. Avcu, F.E. Baştan, H.Z. Abdullah, M.A.U. Rehman, Y.Y. Avcu, A.R. Boccaccini, Electrophoretic deposition of chitosan-based composite coatings for biomedical applications: A review, Progress in Materials Science 103 (2019) 69-108.

[19] R. Sikkema, K. Baker, I. Zhitomirsky, Electrophoretic deposition of polymers and proteins for biomedical applications, Advances in Colloid and Interface Science 284 (2020) 102272.

[20] I. Deen, X. Pang, I. Zhitomirsky, Electrophoretic deposition of composite chitosan–halloysite nanotube–hydroxyapatite films, Colloids and Surfaces A: Physicochemical and Engineering Aspects 410 (2012) 38-44.

[21] S. Amiri, R.E. Hayes, P. Sarkar, Evolution of electronic conductivity in a Ni/YSZ electrode fabricated by electrophoretic deposition, The Canadian Journal of Chemical Engineering 97(5) (2019) 1114-1120.

[22] X. Pang, I. Zhitomirsky, M. Niewczas, Cathodic electrolytic deposition of zirconia films, Surface and Coatings Technology 195(2) (2005) 138-146.

[23] I. Zhitomirsky, A. Petric, Electrochemical deposition of yttrium oxide, Journal of Materials Chemistry 10(5) (2000) 1215-1218.

[24] M. Ata, I. Zhitomirsky, Colloidal methods for the fabrication of carbon nanotube–manganese dioxide and carbon nanotube–polypyrrole composites using bile acids, Journal of colloid and interface science 454 (2015) 27-34.

[25] M. Ata, Y. Sun, X. Li, I. Zhitomirsky, Electrophoretic deposition of graphene, carbon nanotubes and composites using aluminon as charging and film forming agent, Colloids and Surfaces A: Physicochemical and Engineering Aspects 398 (2012) 9-16.

[26] O.O. Van der Biest, L.J. Vandeperre, Electrophoretic deposition of materials, Annual Review of Materials Science 29(1) (1999) 327-352.

[27] B. Ferrari, R. Moreno, EPD kinetics: a review, Journal of the European Ceramic Society 30(5) (2010) 1069-1078.

[28] J. Li, P. Wojtal, C. Wallar, I. Zhitomirsky, Electrochemical deposition of polypyrrole–carbon nanotube films using steroid dispersants, Materials and Manufacturing Processes 33(10) (2018) 1062-1066.

[29] W. Duax, D. Ghosh, V. Pletnev, J. Griffin, Three-dimensional structures of steroids and their protein targets, Pure and applied chemistry 68(6) (1996) 1297-1302.

[30] H. Hou, C.E. Banks, M. Jing, Y. Zhang, X. Ji, Carbon Quantum Dots and Their Derivative 3D Porous Carbon Frameworks for Sodium-Ion Batteries with Ultralong Cycle Life, Advanced Materials 27(47) (2015) 7861-7866.

[31] M. Ammam, Electrophoretic deposition under modulated electric fields: a review, RSC advances 2(20) (2012) 7633-7646.

[32] S. Hu, W. Li, W. Li, N. Zhang, H. Qi, H. Finklea, X. Liu, Aqueous electrophoretic deposition of gadolinium doped ceria, Colloids Surfaces A: Physicochemical Engineering Aspects 579 (2019) 123717.

[33] R. Sikkema, B. Keohan, I.J.M. Zhitomirsky, Hyaluronic-Acid-Based Organic-Inorganic Composites for Biomedical Applications, Materials 14(17) (2021) 4982.

[34] R. Sikkema, B. Keohan, I. Zhitomirsky, Alginic Acid Polymer-Hydroxyapatite Composites for Bone Tissue Engineering, Polymers 13(18) (2021) 3070.

[35] I. Zhitomirsky, L. Gal-Or, Formation of hollow fibers by electrophoretic deposition, Materials Letters 38(1) (1999) 10-17.

[36] P. Wojtal, I. Zhitomirsky, Surface modification and electrophoretic deposition of materials using 2, 2′-biquinoline-4, 4′-dicarboxylic acid, Materials Letters 174 (2016) 44-47.

[37] Y. Su, I. Zhitomirsky, Electrophoretic assembly of organic molecules and composites for electrochemical supercapacitors, Journal of colloid and interface science 392 (2013) 247-255.

[38] M. Cheong, I. Zhitomirsky, Electrodeposition of alginic acid and composite films, Colloids and Surfaces A: Physicochemical and Engineering Aspects 328(1-3) (2008) 73-78.

[39] M.S. Ata, R. Poon, A.M. Syed, J. Milne, I. Zhitomirsky, New developments in non-covalent surface modification, dispersion and electrophoretic deposition of carbon nanotubes, Carbon 130 (2018) 584-598.

[40] R. Wang, G. Xu, Y. He, Structure and properties of polytetrafluoroethylene (PTFE) fibers, e-Polymers 17(3) (2017) 215-220.

[41] S. Ahn, J. Lee, H. Kim, J. Kim, A study on the quantitative determination of through-coating porosity in PVD-grown coatings, Applied Surface Science 233(1-4) (2004) 105-114.

# Chapter 7    Versatile    natural    dispersants    for electrophoretic deposition of materials

Xinqian Liu, Qinfu Zhao and Igor Zhitomirsky

Materials Letters

Volume 313, pp 131828

26 Jan 2022

# Abstract

Natural anionic molecules, such as glycyrrhizic acid and 18β-Glycyrrhetinic acid are used as dispersants for electrophoretic deposition (EPD) of polyvinylidene fluoride, polytetrafluoroethylene, diamond and composites. The superior behavior of the dispersants is linked to the beneficial effects of their chemical structure, pH-dependent charge, pH-dependent solubility, and film-forming properties. The analysis of the deposition yield provides an insight into the influence of the chemical structure of the dispersants on EPD efficiency of different materials. Obtained films provide corrosion protection of steel and can be used for various applications based on advanced functional properties of the deposited materials.

## 7.1  Introduction

Electrophoretic deposition (EPD) has generated significant interest for the fabrication of coatings and thin films for biomedical, electronic, energy storage, photovoltaic and other applications. [1-4] Major challenges in the EPD are related to the development of efficient and nontoxic charging dispersants and versatile co-dispersants for deposition of composite materials. The dispersant adsorption on particles is critically important for particle charging and formation of stable suspensions.

Natural anionic molecules, such as glycyrrhizic acid (GRZA) and its principal metabolite 18β-Glycyrrhetinic acid (GRTA) [5] have attracted our attention for application as dispersants for the EPD method. GRZA is derived from the licorice root. GRZA and GRTA are advanced

functional materials for various biomedical applications [6, 7], such as anti-tumor, anti-inflammatory, antioxidant, antimicrobial, antiulcer and other applications. GRZA is currently under investigation as a drug for Covid-19 treatment and other antiviral applications. [6] GRZA and GRTA showed a remarkable ability to bind different organic molecules and to adsorb on different surfaces, which are important factors for their potential application for EPD of organic materials. [6] Of particular importance for possible application in EPD are pH dependent charge, pH-dependent solubility and gel-forming properties of GRZA and GRTA. [8]

The goal of this investigation was the application of GRZA and GRTA for EPD of polymers, carbon materials and composites. The results presented below indicated that GRZA and GRTA efficiently adsorbed on the surfaces of chemically inert materials and can be used as efficient dispersing and charging agents for deposition and co-deposition of different materials. We proposed deposition mechanisms and analyzed the influence of chemical structures of the dispersants on the deposition efficiency. The microstructure and properties of the deposited films were analyzed.

## 7.2  Experimental procedures

18β-Glycyrrhetinic acid (GRTA), glycyrrhizic acid ammonium salt (GRZA), NaOH, submicrometre powders of polyvinylidene fluoride (PVDF), polytetrafluoroethylene (PTFE), and diamond were used.

EPD was performed in an ethanol-water medium (95 % ethanol) containing particles of

the deposited material dispersed in 1 g·L$^{-1}$ GRTA or GRZA solutions. A few drops of 0.1 M

NaOH was added to facilitate dissolution of GRTA. The particle concentrations of PVDF,

PTFE, and diamond in the suspension were 10, 1 and 1 g·L$^{-1}$, respectively (Supplementary

information). Constant voltage EPD was carried out in a two-electrode cell, containing a low

cost 304 stainless steel substrate (25×30×0.1 mm) and a Pt counter cathode (20×30×0.1 mm)

using a 237 Keithley Sourcemeter. The electrode separation was 1.5 cm. EPD was performed

at selected deposition parameters (Supplementary information), such as deposition voltages

10–50 V for 5 mins. The PVDF and PTFE films were annealed at 200 and 350 $^{\circ}$C, respectively,

for 1 h.

A JEOL JSM-7000F microscope was used for microstructure investigations.

Electrochemical studies were performed in an aqueous 30 g·L$^{-1}$ NaCl solution using a

potentiostat (PARSTAT 2273, Ametek) and a 3-electrode electrochemical cell with coated or

uncoated stainless steel as a working electrode, SCE (reference saturated calomel electrode)

and Pt counter-electrode. Potentiodynamic studies were performed at a scan rate of 1 mV s$^{-1}$,

and obtained data were presented in Tafel plots. Electrochemical impedance spectroscopy (EIS)

data at an AC signal amplitude of 5 mV was obtained in the frequency range of 0.01 Hz – 10

kHz at an open circuit potential and presented in Bode plots.

## 7.3  Results and discussion

Fig. 7-1 shows chemical structures of the GRTA and GRZA molecules. GRTA is a pentacyclic triterpenoid hydrophobic molecule, containing an anionic COOH group. In contrast to GRTA, the GRZA molecule has an amphipathic character due to a hydrophilic diglucuronic unit. GRZA has three carboxylic groups, which can impart a higher charge to this molecule in solutions, compared to that of GRTA.
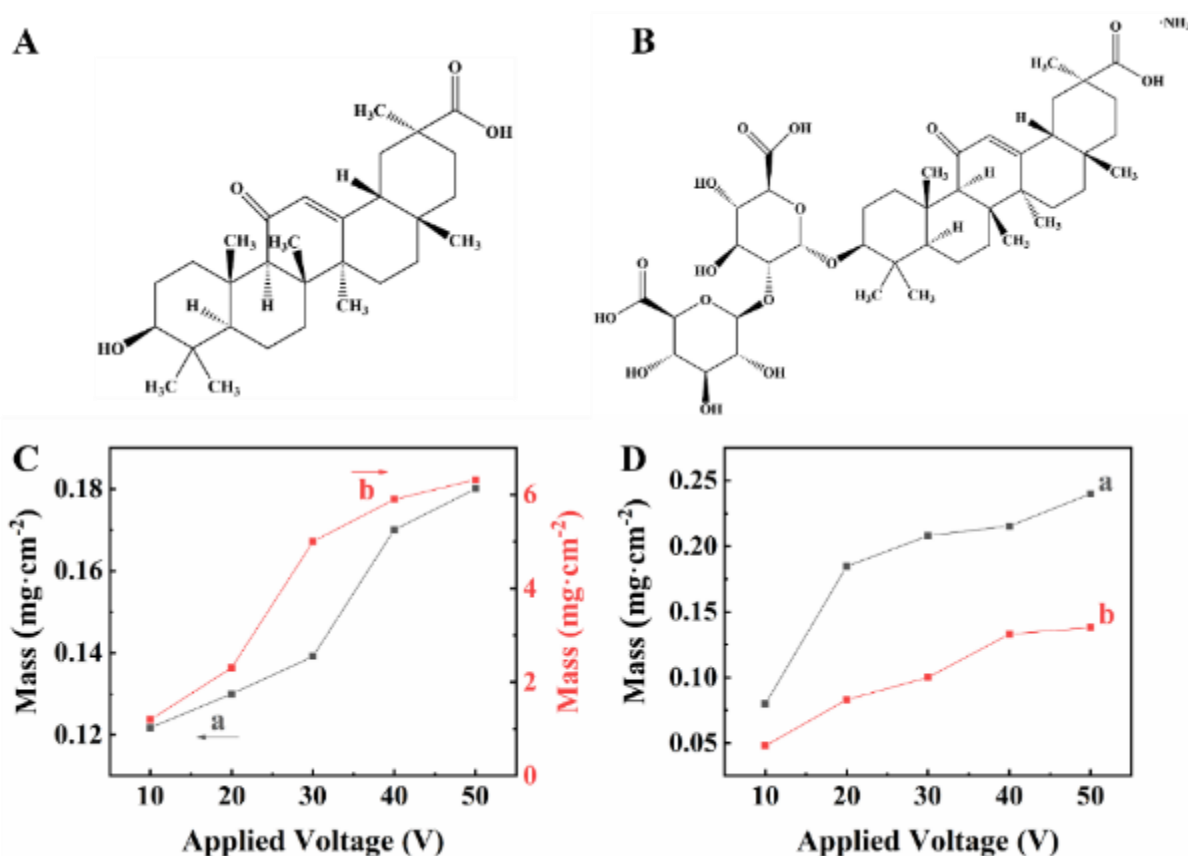


Fig. 7-1 Chemical structure of (A) GRTA and (B) GRZA. Deposit mass of (C) PVDF films, prepared from (a) GRTA and (b) GRZA solutions containing PVDF, and (D) PTFE films, prepared from (a) GRTA and (b) GRZA solutions containing PTFE at different voltages.

Anodic films were prepared from pure GRZA and GRTA solutions. The films were continuous and crack-free (Supplementary information Fig. 7-5). It is suggested that the

deposition mechanism was similar to that, proposed for other organic molecules, containing carboxylic groups. [9, 10] It involved electrophoresis of the dissociated anionic molecules, protonation of the COO– groups and charge neutralization in the low pH region at the anode surface, which facilitated film formation. The film-forming properties of GRZA and GRTA is an important factor for their application for EPD of materials.

It is challenging to disperse and deposit chemically inert materials such as PVDF, PTFE and diamonds. However, such materials were successfully deposited using GRZA and GRTA as dispersants. Zeta-potential measurements confirmed negative charges of the particles in the suspensions (Supplementary information, Table 7-1). Fig. 7-1(C,D) compares deposition yields obtained at different voltages. The deposit mass increased with increasing voltage. Significantly higher deposition yield of PVDF was achieved using GRZA, compared to that for GRTA. This can be attributed to higher charge of the GRZA molecules. However, the use of GRTA allowed higher deposition yield of PTFE, which can result from better adsorption of hydrophobic GRTA on hydrophobic PTFE particles, which facilitated their dispersion, charging and EPD. The deposition current decreased during constant voltage EPD due to the voltage drop in the formed film and corresponding voltage drop reduction in the bulk of the suspension (Supplementary information, Fig. 7-6 and 7-7).
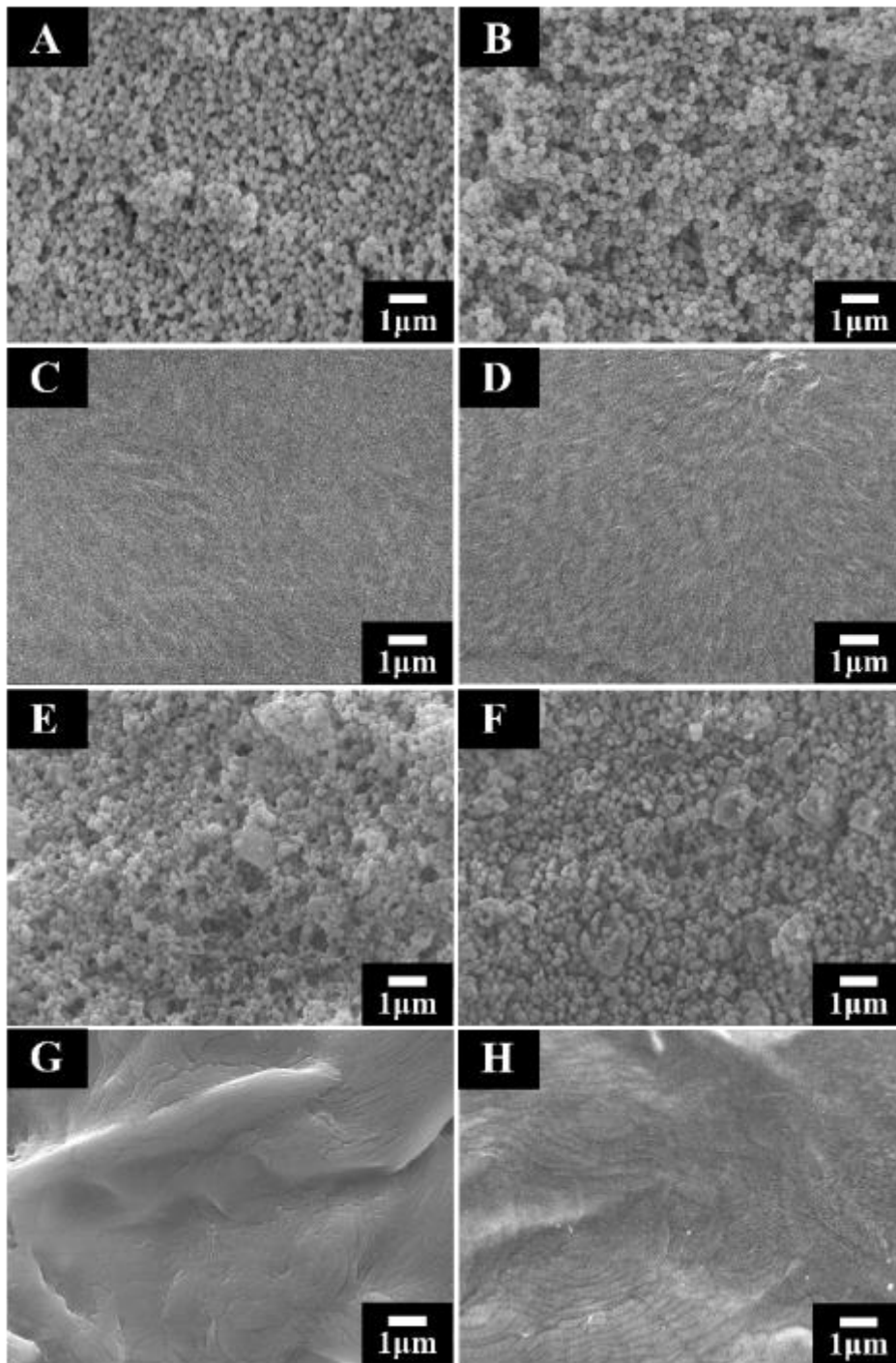
Fig. 7-2 SEM images of (A,B) as-deposited and (C,D) annealed PVDF films, prepared from (A,C) GRTA and (B,D) GRZA solutions containing PVDF, and (E,F) asdeposited and (G,H) annealed PTFE films, prepared from (E,G) GRTA and (F,H) GRZA solutions containing PTFE.

The deposition of PVDF and PTFE was confirmed by the FTIR analysis of the deposited

films (Fig. 7-8 and 7-9). The SEM images of the asdeposited films (Fig. 7-2) showed relatively

dense packing of the PVDF and PTFE particles, which facilitated the fabrication of dense films

after annealing. The films were crack-free (Fig. 7-2) and provided corrosion protection of the

substrates.
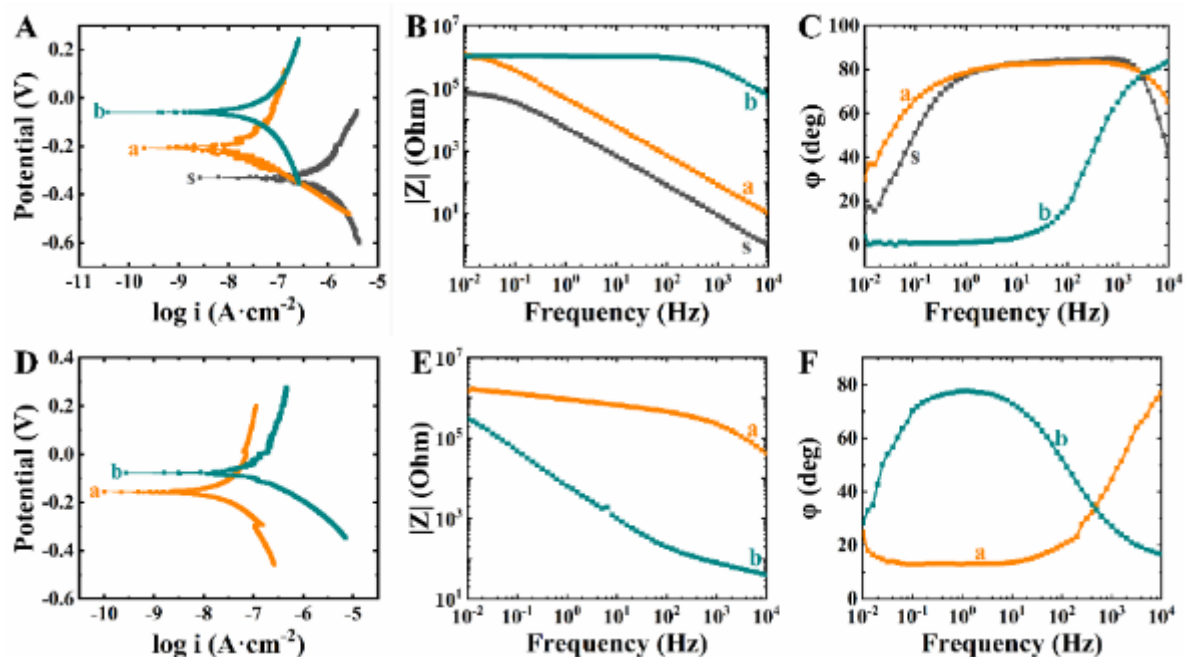


Fig. 7-3 Tafel plots and EIS data for (s) uncoated and (a, b) coated stainless steel, (A-C) PVDF and (D-F) PTFE films, prepared using (a) GRTA and (b) GRZA dispersants.

Fig.7-3 shows testing results for PVDF and PTFE films prepared using GRTA and GRZA

dispersants at a deposition voltage of 50 V and deposition time of 5 min. The films provided

corrosion protection of stainless steel, as it was indicated by the higher corrosion potential,

lower anodic current and higher impedance of the coated samples, compared to the uncoated

substrates.

Testing results correlated with the deposition yield measurements and indicated that

coatings with higher film mass provided better corrosion protection. PVDF coatings prepared

using GRZA (Fig. 7-3A–C) showed higher corrosion potential and significantly higher

impedance, especially at high frequencies. In contrast, the PTFE coatings prepared using

GRZA (Fig. 7-3D–F) showed higher anodic current and significantly lower impedance,

especially at high frequencies, compared to the PTFE coating formed using GRTA.
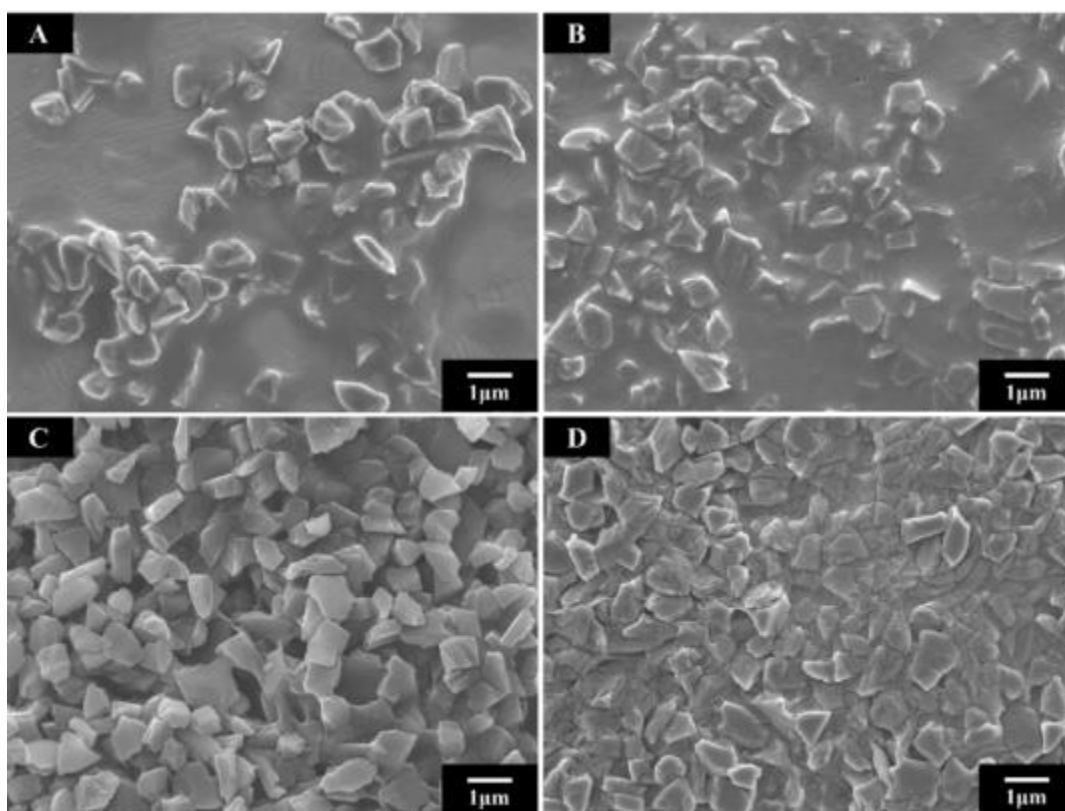


Fig. 7-4 SEM images of annealed (A,B) PVDF-diamond films, prepared from (A) GRTA and
(B) GRZA solutions containing PVDF and diamond, and (C,D) PTFE-diamond films, prepared
from (C) GRTA or (D) GRZA solutions containing PTFE and diamond.

GRTA and GRZA were also used as co-dispersants for diamond, PVDF and PTFE for

EPD of composite PVDF-diamond and PTFE-diamond films. Fig. 7-4 shows SEM images of

the composite films, containing diamond particles in the PTFE or PVDF matrix.

GRTA allowed good dispersion and EPD of carbon nanotube films (Fig. 7-10). However, no deposition of carbon nanotubes was achieved using amphipathic GRZA molecules. These results coupled with EPD data for PVDF and PTFE indicated that the efficiency of such dispersants is influenced by their chemical structure. The EPD of diamond, PVDF, PTFE and composites is promising for various applications, based on advanced functional properties of such materials. Despite the tremendous previous research efforts, the progress in this area was limited due to the lack of efficient dispersants. The method developed in this investigation allowed efficient EPD of such materials and composites using natural molecules as dispersants and co-dispersants for different materials. The unique pharmacological and biological properties of GRTA and GRZA as well as film-forming and gel-forming properties of such molecules make them promising multifunctional dispersants for various applications in thin film EPD technology.

## 7.4  Conclusions

GRTA or GRZA are new versatile film-forming dispersants, which allowed controlled EPD of chemically inert PVDF and PTFE polymers and diamonds. The results presented stressed the importance of the chemical structure of GRTA and GRZA for the deposition of different materials. GRZA allowed for higher deposition yield of PVDF, whereas the use of GRTA resulted in higher deposition yield of PTFE. GRTA and GRZA can be used as co-dispersants for the fabrication of PVDF-diamond and PTFE-diamond composites. Obtained

films can be used for corrosion protection of metals and offer benefits for other applications based on the advanced functionality of the deposited materials.

## 7.5 Supplementary data

### Selection of the deposition voltage and time.

The selection of the deposition voltages was based on the following considerations[11, 12]:

High voltages offer the advantage of smaller deposition times and higher deposition rates. However, higher voltages usually result in significant gas evolution and increased film porosity. High voltages can promote agglomeration of small particles and sedimentation. A certain voltage (electric field) is necessary in order to overcome interparticle interactions and allow particles to bond to the substrate. High voltage can result in non-uniform deposits.

### Selection of the bath composition.

The dispersants showed different efficiencies in dispersion, charging and EPD of PVDF, PTFE and diamonds. Therefore, for comparison, the concentrations of the dispersants were selected at 1 g $L^{-1}$ and at this dispersant concentration the materials (PVDF, PTFE and diamonds) content was selected in order to achieve sufficiently high deposition rates for deposition of individual materials and comparable deposition rates of the individual materials for the deposition of composites.

## Cost of dispersants and estimated cost of protection of 1 m² of stainless steel

Cost of GRTA $13/g

Cost of GRZA $5/g

Estimated cost of protecting 1 m² of stainless steel

PVDF coating $ 4.5

PTFE coating $ 8.2

Table 7-1 Zeta potentials of materials measured using the mass transport method [13]

| Material | Dispersant | Zeta-potential, mV |
|----------|------------|--------------------|
| PTFE | GRTA | -12.3 |
| PVDF | GRTA | -6.3 |
| Diamond | GRTA | -20.1 |
| PTFE | GRZA | -7.2 |
| PVDF | GRZA | -32.4 |
| Diamond | GRZA | -24.1 |
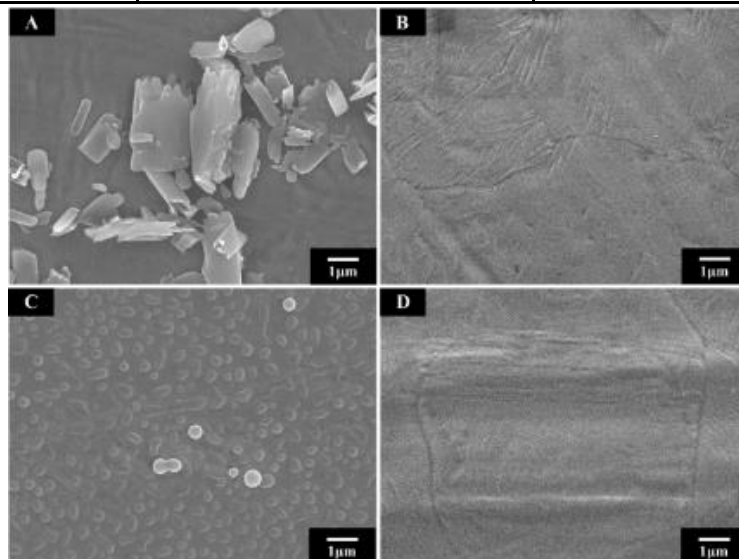


Fig. 7-5 SEM images of as-deposited (A,C) GRTA and (B,D) GRZA films, prepared from 1 g·L⁻¹ GRTA and 1 g·L⁻¹ GRZA solutions in (A,B) water or in (C,D) the mixture of 95% ethanol and 5% water at a deposition voltage of 20 V for 5mins.
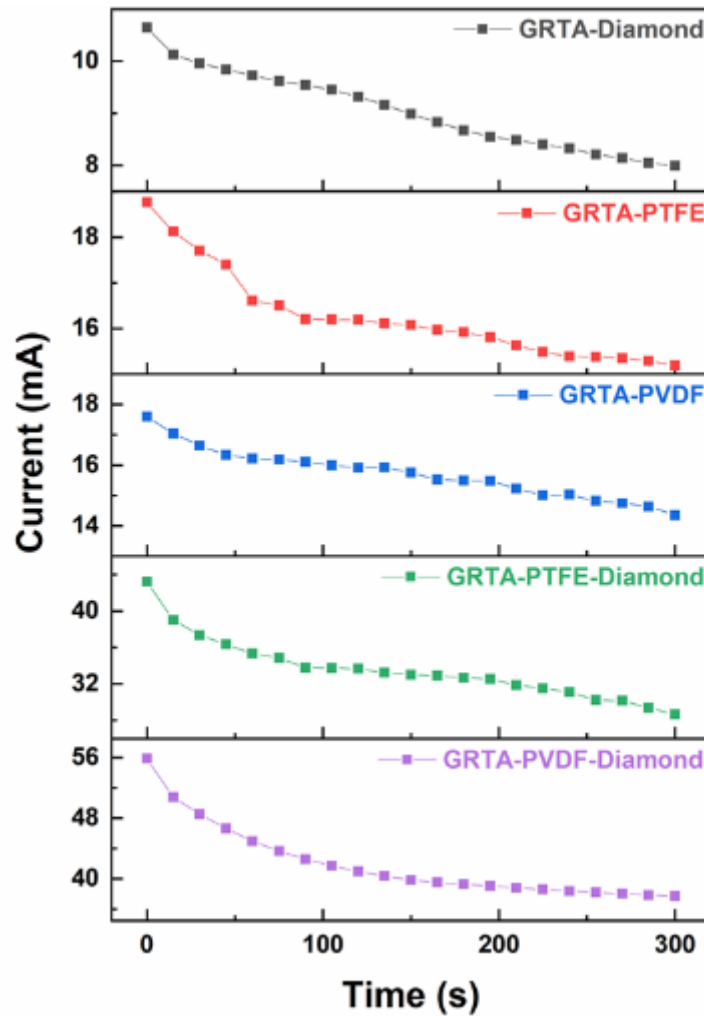
Fig. 7-6 Current-time dependencies for EPD of different materials using GRTA as a dispersant at a deposition voltage of 50V and a substrate area of 10 cm$^2$. The concentrations of GRTA, PVDF, PTFE, and diamond in the suspension were 1, 10, 1 and 1 g·L$^{-1}$, respectively.
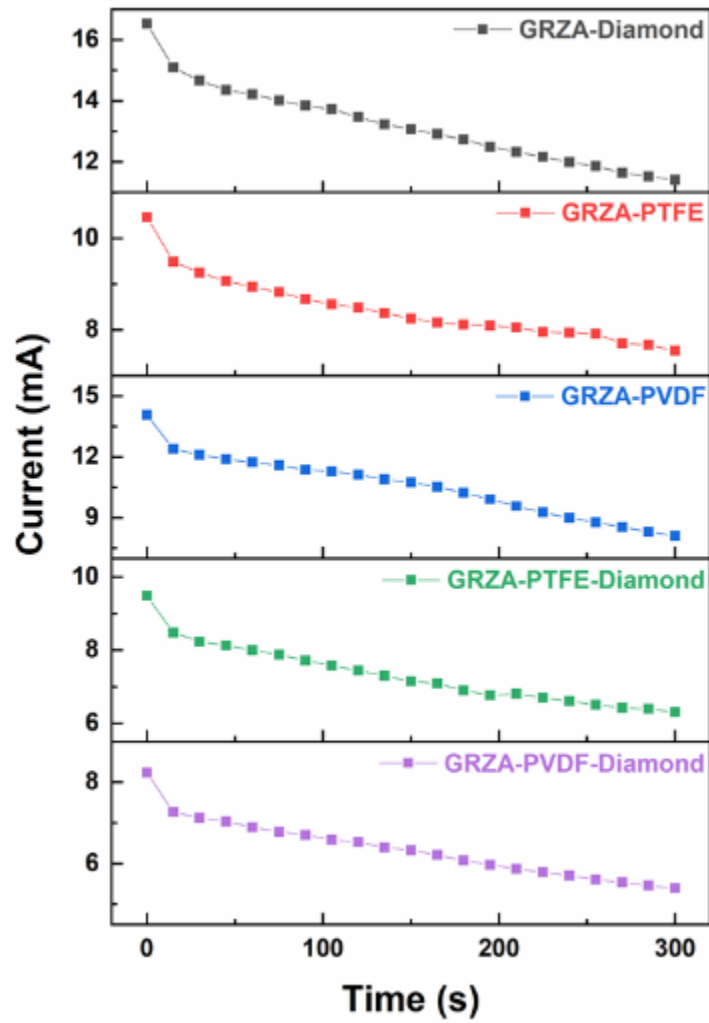
Fig. 7-7 Current-time dependencies for EPD of different materials using GRZA as a dispersant at a deposition voltage of 50V and a substrate area of 10 cm$^2$. The concentrations of GRZA, PVDF, PTFE, and diamond in the suspension were 1, 10, 1 and 1 g·L$^{-1}$, respectively.
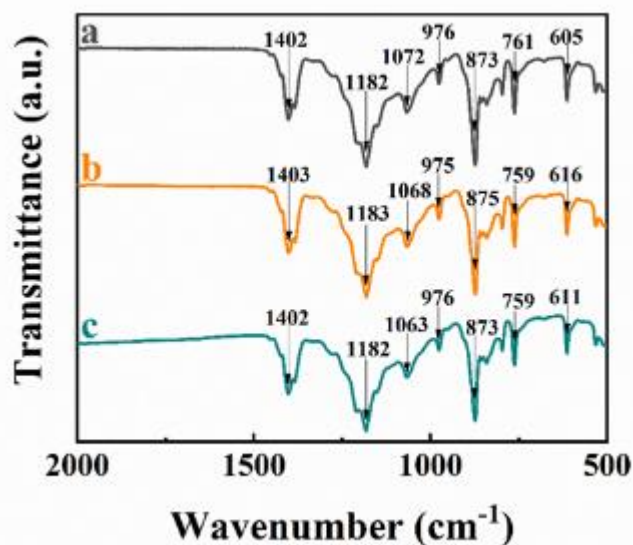
Fig. 7-8 FTIR spectra of (a) as-received PVDF and deposited PVDF films, prepared from (b) GRTA and (c) GRZA solutions containing PVDF. (A Bruker Vertex 70 spectrometer was used for the FTIR studies.). The FTIR spectra of the deposited materials show characteristic peaks of PVDF[14, 15] and confirm PVDF deposition.
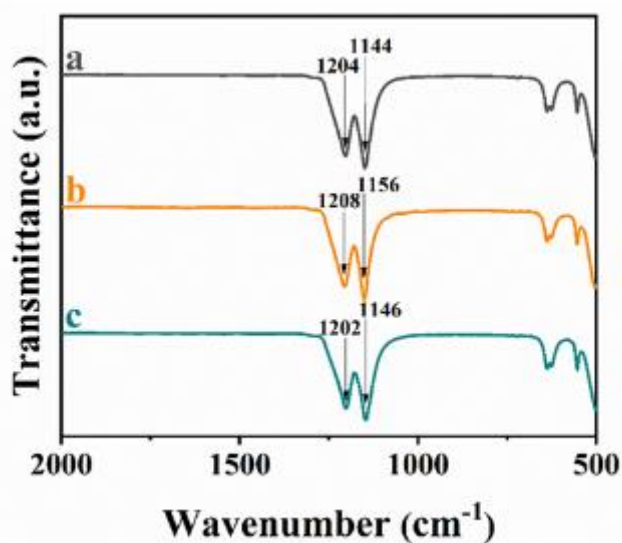


Fig. 7-9 FTIR spectra of (a) as-received PTFE and as-deposited PTFE films, prepared from (b) GRTA and (c) GRZA solutions containing PTFE. The FTIR spectra of the deposited materials show characteristic peaks of PTFE[16, 17] and confirm PTFE deposition.
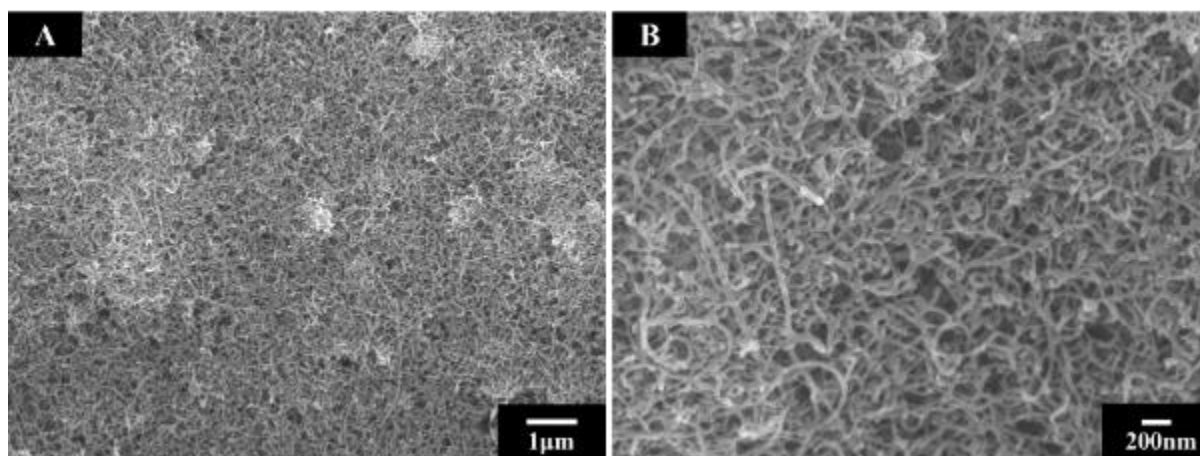
Fig. 7-10 SEM images at different magnifications of films, prepared from 1 g·L$^{-1}$ GRTA solutions containing 1 g·L$^{-1}$ multiwalled CNT at a deposition voltage of 30 V for 5 mins.

## 7.6  Contribution Statement

Xinqian Liu: Methodology, Validation, formal analysis, Investigation, Writing – original draft; Stephen Veldhuis: Methodology, Conceptualization. Ritch Mathews: Formal analysis, Methodology. Igor Zhitomirsky: Conceptualization, Writing, Project Administration.

## 7.7  References

[1] I. Corni, M.P. Ryan, A.R. Boccaccini, Electrophoretic deposition: From traditional ceramics to nanotechnology, Journal of the European Ceramic Society 28(7) (2008) 1353-1367.

[2] K. Ishii, C. Matsunaga, K. Kobayashi, A.J. Stevenson, C. Tardivat, T. Uchikoshi, Fabrication of BSCF-based mixed oxide ionic-electronic conducting multi-layered membrane by sequential electrophoretic deposition process, Journal of the European Ceramic Society 41(4) (2021) 2709-2715.

[3] S.B.A. Boraei, J. Nourmohammadi, F.S. Mahdavi, J. Yus, A. Ferrandez-Montero, A.J. Sanchez-Herencia, Z. Gonzalez, B. Ferrari, Effect of SrR delivery in the biomarkers of bone regeneration during the in vitro degradation of HNT/GN coatings prepared by EPD, Colloids and Surfaces B: Biointerfaces 190 (2020) 110944.

[4] I. Zhitomirsky, L. Gal-Or, Formation of hollow fibers by electrophoretic deposition, Materials Letters 38(1) (1999) 10-17.

[5] L.A. Baltina, R.M. Kondratenko, L.A. Baltina, O.A. Plyasunova, A.G. Pokrovskii, G.A. Tolstikov, Prospects for the creation of new antiviral drugs based on glycyrrhizic acid and its derivatives (a review), Pharmaceutical Chemistry Journal 43(10) (2009) 539-548.

[6] C. Bailly, G. Vergoten, Glycyrrhizin: An alternative drug for the treatment of COVID-19 infection and the associated respiratory syndrome?, Pharmacology & therapeutics 214 (2020) 107618.

[7] A. Kowalska, U. Kalinowska-Lis, 18β-Glycyrrhetinic acid: its core biological properties and dermatological applications, International journal of cosmetic science 41(4) (2019) 325-331.

[8] M. Malík, J. Velechovský, P. Tlustoš, Natural pentacyclic triterpenoid acids potentially useful as biocompatible nanocarriers, fitoterapia 151 (2021) 104845.

[9] K. Baker, R. Sikkema, W. Liang, I. Zhitomirsky, Multifunctional Properties of Commercial Bile Salts for Advanced Materials Engineering, Advanced Engineering Materials 23 (2021) 2001261.

[10] R. Sikkema, K. Baker, I. Zhitomirsky, Electrophoretic deposition of polymers and proteins for biomedical applications, Advances in Colloid and Interface Science 284 (2020) 102272.

[11] O.O. Van der Biest, L.J. Vandeperre, Electrophoretic deposition of materials, Annual Review of Materials Science 29(1) (1999) 327-352.

[12] I. Zhitomirsky, L. Gal-Or, Electrophoretic deposition of hydroxyapatite, Journal of Materials Science: Materials in Medicine 8(4) (1997) 213-219.

[13] M. Hashiba, H. Okamoto, Y. Nurishi, K. Hiramatsu, The zeta-potential measurement for concentrated aqueous suspension by improved electrophoretic mass transport apparatus— application to Al 2 O 3, ZrO 3 and SiC suspensions, Journal of materials science 23(8) (1988) 2893-2896.

[14] I.Y. Abdullah, M. Yahaya, M.H.H. Jumali, H.M. Shanshool, Effect of annealing process on the phase formation in poly (vinylidene fluoride) thin films, AIP conference proceedings, American Institute of Physics, 2014, pp. 147-151.

[15] N. Daems, S. Milis, R. Verbeke, A. Szymczyk, P.P. Pescarmona, I.F. Vankelecom, High-performance membranes with full pH-stability, RSC advances 8(16) (2018) 8813-8827.

[16] H.W. Starkweather, R.C. Ferguson, D.B. Chase, J.M. Minor, Infrared spectra of amorphous and crystalline poly(tetrafluoroethylene), Macromolecules 18(9) (1985) 1684-1686.

[17] R. Wang, G. Xu, Y. He, Structure and properties of polytetrafluoroethylene (PTFE) fibers, e-Polymers 17(3) (2017) 215-220.

# Chapter 8   Dip coating of poly(ethyl methacrylate) and composites from solutions in isopropanol-water co-solvent

Xinqian Liu, Stephen Veldhuis, Ritch Mathews, Igor Zhitomirsky

## Graphical abstract
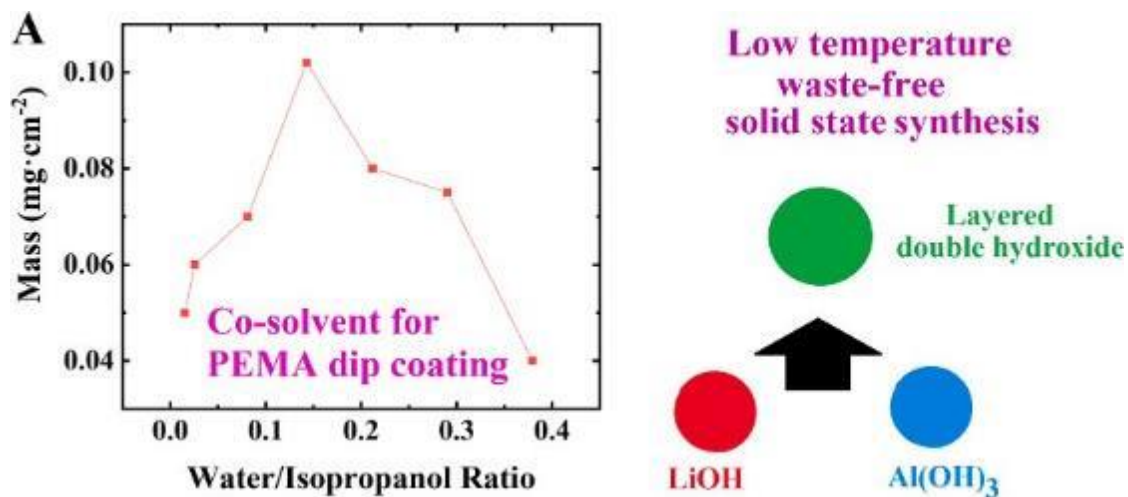


## Abstract

This paper reports the feasibility of fabrication of poly(ethyl methacrylate) (PEMA) and composite films by a dip coating method. We demonstrate that PEMA can be dissolved in a mixed isopropanol-water co-solvent avoiding the use of traditional toxic solvents. The feasibility of fabricating concentrated solutions of high molecular weight PEMA is a key factor the fabrication of monolayer or multilayer coatings by a dip coating method. The solubilization range is established and 10 g L$^{-1}$ PEMA solutions are prepared with water/isopropanol volume ratio ($R_S$) of 0.015–0.380. PEMA precipitation is observed at $R_S > 0.4$. It is found that PEMA solutions with concentration as high as 50 g L$^{-1}$ can be obtained at $R_S = 0.176$. The deposit mass is influenced by $R_S$, PEMA concentration and number of the deposited layers. PEMA coatings provide corrosion protection of stainless steel in 3% NaCl solutions. The dip coating method is used for the fabrication of composite coating, containing layered double hydroxide

$LiAl_2(OH)_7.2H_2O$ (LiAlDH) and PEMA. LiAlDH is prepared by novel solid state synthesis method, which is simple, waste-free and facilitates the control of stoichiometry. The synthesis time decreases with increasing synthesis temperature from 20∘ to 70 ℃. The relatively short synthesis time makes this low-temperature method suitable for the large scale production of LiAlDH. This waste-free method is promising for the fabrication of other advanced DHs. LiAlDH shows advanced properties for its applications as flame retardant additive (FR) for polymer coatings. LiAlDH outperforms traditional inorganic FR materials of hydroxide type. Another finding is that PEMA-LiAlDH interactions facilitated the fabrication of stable suspensions for dip coating of composites. Corrosion protection of PEMA-LiAlDH coatings with different LiAlDH content is investigated. The advantages of bi-layer coatings containing individual layers with different compositions are demonstrated. The proposed method is promising for the fabrication of other composites, containing various functional materials in the PEMA matrix, which can be deposited as monolayers, multilayers or coatings of graded composition.

## 8.1  Introduction

Poly(ethyl methacrylate) (PEMA) is an advanced polymer, which exhibits important properties, such as mechanical strength and thermal stability [1], biocompatibility and chemical stability [2]. PEMA has generated significant interest for various applications, such as bone and cartilage repair [2], polymer electrolytes and membranes for energy generation and storage

devices [3, 4], biodegradable antimicrobial packaging materials [5], optical and electronic components [6], and coatings for corrosion protection [7]. PEMA offers great promise for the development of shape memory materials [8]. Significant interest has been generated in the development of functional PEMA composites with graphene [9, 10], carbon nanotubes and cellulose [11]. PEMA composites, containing fatty acids were developed as phase change materials for thermal energy storage [12]. High-performance PEMA composites, containing inorganic oxide and hydroxide particles possess a set of properties that make them desirable materials for optical and electrochemical devices. [13-15] PEMA-hydroxyapatite composites are known to have potential for the fabrication of bone cements [16].

It has previously been shown [17] that polymer materials, containing inorganic double hydroxides (DH) exhibit advanced optical, electrical, mechanical, magnetic, thermal and fire retardant (FR) properties. Moreover, high-performance polymer-DH composites possess a set of properties that make them desirable materials for drug delivery, corrosion protection and catalysis. [18-20] Many investigations focused on the development of polymer-DH composites for biomedical implants, sensors, and energy storage applications. [18, 20, 21] DH have been gaining ground as FR additives for various polymer products. [22, 23] The FR properties of DH are related to water release resulting from their thermal dehydration and related endothermic effect. [23, 24] Moreover, some complex hydroxides exhibit promising memory properties [25], which make them especially attractive for FR applications. $LiAl_2(OH)_7.2H_2O$ (LiAlDH) is a promising DH for the application as an FR additive for polymer composites, due

to its high water release. [26] The theoretical mass loss related to LiAlDH dehydration is 46%

of the initial mass. It is higher than the 35% mass loss of Al(OH)$_3$, which is used as an advanced

FR for many applications. [27, 28] Moreover LiAlDH is a promising material for corrosion

protection of metals and alloys. [29, 30]

The goal of this investigation was the fabrication of PEMA and PEMA-LiAlDH

composite coatings by a dip coating method. PEMA is soluble in toxic solvents, such as

tetrahydrofuran, chloroform, dimethyl formamide, benzene and toluene, which were used in

the literature for the coating formation by casting and spin coating methods. [31-37] The use

of such solvents and methods required relatively long solution preparation and film deposition

procedures. Moreover, in many cases the fabrication procedures required long-time heating to

remove a toxic solvent. [6, 33-36, 38] Motivated by the need to find a non-toxic solvent for dip

coating, we found a possibility of PEMA dissolution in a mixed water-isopropanol co-solvent

despite the PEMA insolubility in water and isopropanol. We established a range of co-solvent

compositions, which allowed for PEMA solubilization and proposed a solubilization

mechanism. The key factor for the PEMA deposition by the dip coating method was the

discovered ability to dissolve high molecular weight PEMA and achieve high concentrations

of the solutions. We found that PEMA coatings can be deposited as monolayers or multilayers

and analyzed the deposition yield at different PEMA concentrations, solvent compositions and

number of the deposited layers. This approach paves a way for the deposition of other polymers

using non-toxic co-solvents. Another key finding was corrosion protection properties of the

PEMA coatings, prepared by simple dip coating method. The composite PEMA-LiAlDH films were prepared. Avoiding the multiple disadvantages of wet chemical methods for the fabrication of complex hydroxides, we developed a solid-state synthesis method and demonstrated that this method can be used for mass production of LiAlDH. We investigated the influence of temperature and time on the LiAlDH synthesis. The method is simple, fast, and chemical waste-free. It allows excellent stoichiometry control. This method represents an unexplored route for the fabrication of stoichiometric complex hydroxides and complex oxides. We proposed the LiAlDH synthesis mechanism and obtained PEMA-LiAlDH composites. Such composites combine advanced properties of PEMA polymer and functional properties of LiAlDH, such as FR properties and corrosion inhibition. We complemented these findings with analysis of FR properties of LiAlDH, which showed advantages, compared to other hydroxide type FR additives. Results from this work represent the feasibility step towards the fabrication of multilayer and functionally graded composites based on PEMA and LiAlDH. Evidence was presented that demonstrates a chemical interaction of PEMA and LiAlDH, which is a key factor for the fabrication of stable LiAlDH dispersions in PEMA solutions and variation of LiAlDH content in the composite films. The results of electrochemical studies showed that pure PEMA coatings, PEMA-LiAlDH composite coatings and coatings of graded composition can be used for corrosion protection of metals. Thermal analysis showed that LiAlDH can be used as an FR additive for PEMA coatings.

## 8.2  Experimental procedures

Poly(ethyl methacrylate) (PEMA, $M_W$=515,000), LiOH.$H_2$O, Al(OH)$_3$, isopropanol,

NaCl (Aldrich) were used. The synthesis of LiAlDH was performed by a solid state synthesis

method from mixtures of LiOH.$H_2$O and Al(OH)$_3$ in a humid air (96% humidity). The synthesis

temperature was varied in the range of 20–70 °C. PEMA was dissolved in a mixed isopropanol-

water solvent at 60 °C and cooled down to room temperature. Stainless steel foils (304 type,

thickness 0.1 mm) were used as substrates for coating deposition. Dip coating was performed

from pure PEMA solutions with concentration of 1–50 g $L^{-1}$ or 10 g $L^{-1}$ PEMA solutions,

containing 5–10 g $L^{-1}$ LiAlDH. A JEOL SEM (scanning electron microscope, JSM-7000F) was

used for the analysis of coating microstructure. A Bruker Smart 6000 X-ray diffractometer

(XRD, CuKα radiation) was utilized for the analysis of coating composition. Electrochemical

characterization was performed using a PARSTAT 2273 (Ametek) potentiostat-impedance

analyzer. Testing was carried out in 30 g $L^{-1}$ NaCl solution in water using a corrosion cell,

containing a working electrode (coated or uncoated stainless steel), counter-electrode (Pt mesh)

and a reference electrode (SCE, saturated calomel electrode). The results of potentiodynamic

studies (1 mV $s^{-1}$ rate) were presented in Tafel plots. Electrochemical impedance spectroscopy

(EIS) data was obtained using alternating current (AC) in the frequency range of 0.01 Hz–10

kHz and voltage amplitude of 5 mV. Thermogravimetric analysis (TGA, thermoanalyzer

Netzsch STA-409) was performed at 5 °C min-1 heating rate in air. The deposits were removed

from the substrates for the TGA studies. Fourier Transform Infrared Spectroscopy (FTIR) studies were performed using a Bruker Vertex 70 spectrometer.

## 8.3  Results and discussion

This investigation showed that PEMA can be dissolved in a water-isopropanol co-solvent despite the insolubility of PEMA in pure water or pure isopropanol. This finding offers benefits of using a non-toxic solvent for the fabrication of PEMA coatings. The ability to dissolve PEMA with high $M_W$ of 515 kDa and to form PEMA solutions of relatively high concentrations in the range of 10–50 g $L^{-1}$ was a vital factor for the development of the dip coating method. It should be noted that polymers with low $M_W$ show weak film-forming and binding properties. However, the solubility of various polymers usually decreases [39, 40] with increasing $M_W$ due to enhanced interactions of the polymer chains. Moreover, it is difficult to achieve good substrate coverage using dilute polymer solutions. In this investigation, 10 g $L^{-1}$ PEMA solutions were prepared from water-isopropanol mixtures with water/isopropanol ratio ($R_S$) of 0.015–0.380. PEMA precipitation was observed at $R_S > 0.4$. The ability to use water-isopropanol solvent for dip coating eliminates the need in toxic solvents [31-37] and long-time heating procedures for their removal [6, 33-36, 38], which were used for other film deposition techniques.
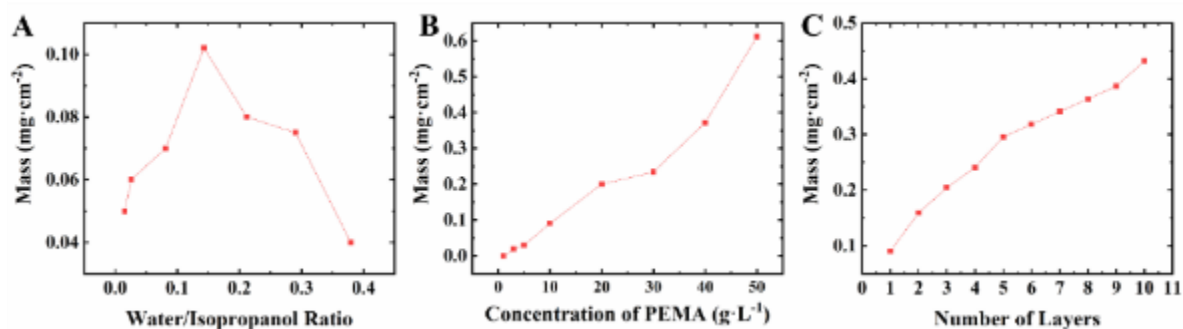
Fig. 8-1 Coating mass for (A) monolayer coatings prepared from 10 g L$^{-1}$ PEMA solutions versus $R_S$, (B) monolayer coatings versus PEMA concentration for $R_S$ = 0.176, (C) multilayer coatings versus number of individual layers, prepared from 10 g L$^{-1}$ PEMA solutions with $R_S$ = 0.176.

It is suggested that at a low water content in the mixture, the water molecules are separated in isopropanol and such molecules can solvate carbonyl groups of PEMA and facilitate PEMA dissolution. [41] The increase in the water content resulted in enhanced solvation and solubilization of PEMA. The solvation shell around the carbonyl groups acted as compatibilizing layers [41] between isopropanol and PEMA. It was found that 50 g L$^{-1}$ PEMA solutions can be obtained at $R_S$ = 0.176. Further increase in water content resulted in the formation of water clusters and the creation of H-bonds between water molecules. [41] This led to the reduced polymer solvation and precipitation of PEMA at higher water content. CH$_2$ groups of the polymer can potentially exert influence on polymer solvation by water molecules. In order to analyze the possible effect of the CH$_2$ groups we investigated the solubilization of polymethylmethacrylate (PMMA) and polybuthylmethacrylate (PBMA) of similar molecular mass in the mixed water-isopropanol solvent. PEMA showed enhanced solubility in a wider range of concentrations, compared to PMMA. PMMA solubility was limited to 20 g L$^{-1}$, whereas PEMA solutions with concentration above 50 g L$^{-1}$ were obtained. PBMA was

insoluble in water-isopropanol mixtures as well as in the individual solvents. Therefore, the difference in the length of the $C_nH_{2n+1}$ chain cannot explain the difference in polymer solubilities. Fig. 8-1(A) shows the deposition yield of the dip coating method for water-isopropanol mixtures with different $R_S$ at PEMA concentration of $10 \text{ g L}^{-1}$. The deposition yield increased with increasing $R_S$, showed a maximum and then decreased. It was hypothesized that enhanced PEMA solvation with increasing $R_S$ at low $R_S$ values facilitated PEMA-substrate interactions and coating formation. On the other hand, further RS increase resulted in reduced PEMA solvation and lower deposition yield. The deposition yield increased with increasing PEMA concentration from 1 to $50 \text{ g L}^{-1}$ at $R_S = 0.176$ (Fig. 1(B)). The coatings can be deposited as monolayers or laminates. The deposition yield increased with increasing number of the individual layers (Fig. 8-1(C)). It will be shown below that the ability to deposit multilayer coatings is important for the fabrication of not only pure PEMA but also composite coatings, containing different layers. The results of this study indicated that the use of toxic solvents for the fabrication of PEMA films can be avoided. This new approach is especially important for biomedical applications of PEMA coatings. Moreover, this approach can potentially be used for the fabrication of PEMA coatings and bulk composite materials by other colloidal methods. It can be expected that further development of this method will result in advances in colloidal processing of other polymers using non-toxic solvents.
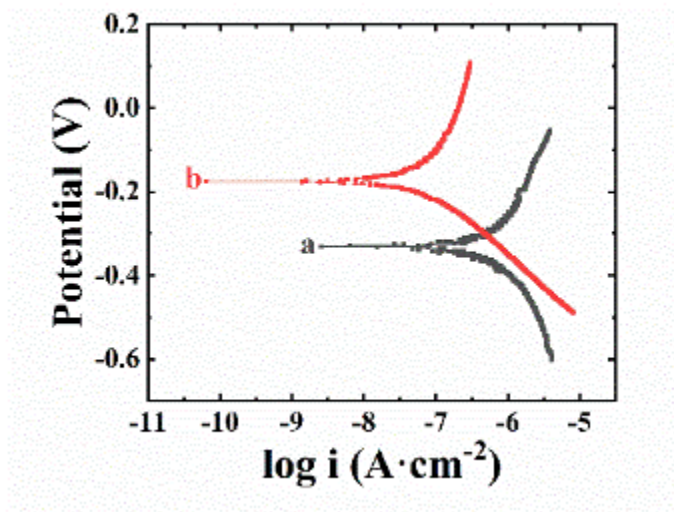
Fig. 8-2 Tafel plots for (a) uncoated substrate and (b) coated from 10 g L$^{-1}$ PEMA solutions with $R_S = 0.176$.
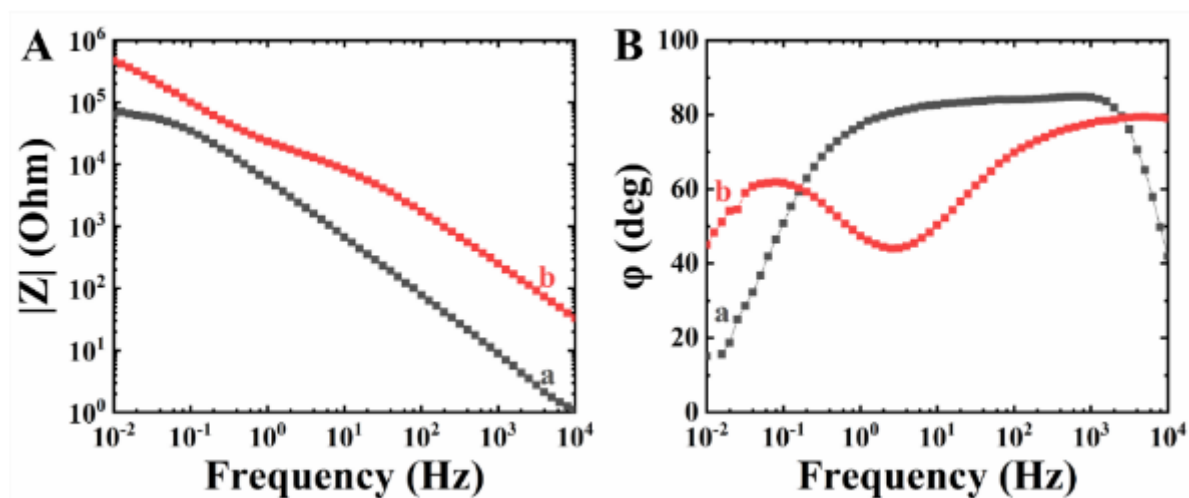


Fig. 8-3 EIS Bode plots for (a) uncoated substrate and (b) coated from 10 g L$^{-1}$ PEMA solutions with $R_S = 0.176$.

Another key finding of this work was that PEMA coatings provided corrosion protection

of stainless steel substrates. Fig. 8-2 shows Tafel plots for uncoated and coated stainless steel.

The coated substrates showed reduced anodic current and increased corrosion potential. The

analysis of EIS data (Fig. 8-3) showed higher impedance of the coated samples in a wide

frequency range. The EIS data showed that the deposited layer acted as a barrier, which

prevented electrolyte access to the substrate surface.
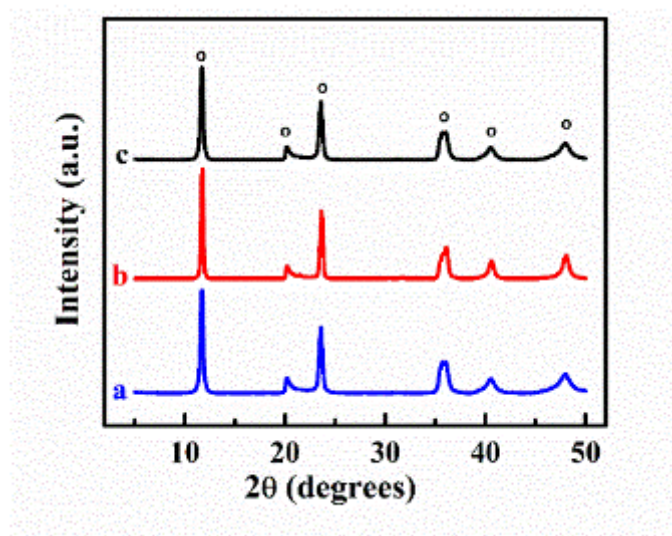


Fig. 8-4 X-ray diffraction patterns of LiAlDH synthesized at (a) 20 °C for 10 days, (a) 50 °C for 3 days, and (a) 70 °C for 1 day (o – peaks corresponding to PDF 031–0704).

Dip coating method was used for the fabrication of composite coatings, containing

LiAlDH. Avoiding multiple problems of wet chemical synthesis methods, such as

stoichiometry control, time consuming washing and drying steps and chemical waste removal,

we prepared LiAlDH by a simple solid state synthesis method. Fig. 8-4 shows XRD patterns

of the LiAlDH powders prepared by a solid state synthesis method. The synthesis was

performed at different temperatures in the range of 20–70 °C in order to analyze the influence

of temperature on the synthesis process. Pure LiAlDH phase was obtained at 20 °C after

synthesis for 10 days. The X-ray diffraction pattern presented in Fig. 8-4 shows diffraction

peaks, corresponding to PDF 031-0704. The increase in temperature allowed for reduced

synthesis time. Pure LiAlDH phase was obtained at 50 and 70 °C for synthesis times of 3 days

and 1 day, respectively (Fig. 8-4). DHs are usually produced by different methods, such as coprecipitation from mixed solutions of metal salts, reconstruction, ion exchange and hydrothermal methods. [17] The solid-state synthesis method is simple and offers processing advantages. The ability to reduce the synthesis time is important for scaling-up the synthesis method. It is expected that other DHs can potentially be produced by a solid state synthesis method. The solid state method facilitates the stoichiometry control. It is in this regard that the fabrication of double hydroxides by traditional co-precipitation methods requires a selection of pH suitable for the controlled co-precipitation. In many cases the selection of such pH presents difficulties. However, the mechanism of solid-state synthesis is not well understood. It is suggested that condensation of water molecules from humid air resulted in release of $Li^+$ ions to the aqueous phase. It is known that $Li^+$ ions are strongly adsorbed by $Al(OH)_3$ and such adsorption was used for commercial $Li^+$ extraction. [42] It has been reported [43] that the adsorption of $Li^+$ by $Al(OH)_3$ results in the formation of LiAlDH phase at the surface of the $Al(OH)_3$ particles. Therefore, it is hypothesized that the release of $Li^+$ ions from the LiOH phase and their adsorption on the $Al(OH)_3$ particles in the mixture of LiOH and $Al(OH)_3$ particles used for the synthesis, resulted in the formation of the LiAlDH phase at the particle interface. Further release of $Li^+$ ions resulted in the gradual transformation of the mixture of two hydroxides into the pure LiAlDH phase. This process was accelerated with a temperature increase and allowed for the reduced synthesis time. Fig. 8-5 shows morphology of the LiAlDH particles, prepared by the solid-state synthesis method. The SEM image shows platelet shape

LiAlDH particles, some particles showed agglomerates, containing submicron primary particles. The small particle size is beneficial for the fabrication of composites, containing LiAlDH as an FR additive.
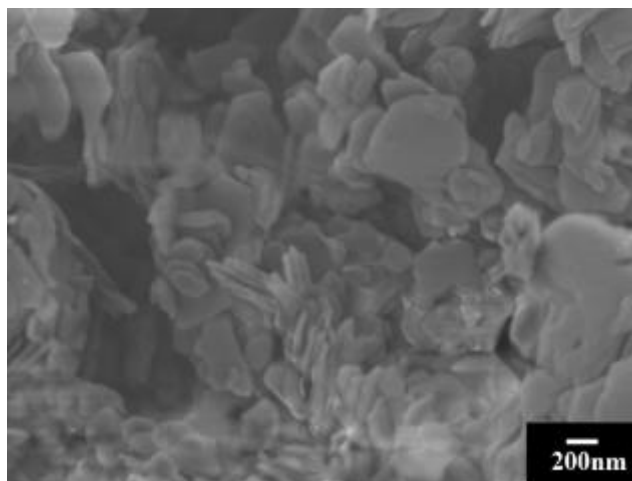


Fig. 8-5 SEM image of LiAlDH particles, prepared at 70 $^{\circ}$C.

Fig. 8-6(a) shows TGA data for LiAlDH. The observed mass loss was attributed to dehydration. The total mass loss at 1000 $^{\circ}$C was found to be 45.9%, which is close to the theoretical value for this material.

As pointed out above, LiAlDH offers advantages of higher mass loss related to dehydration (45.9%), compared to that (35%) of $Al(OH)_3$, which is widely used for many commercial applications. An important finding of this investigation was the ability to form stable suspensions of LiAlDH particles in the PEMA solutions, which facilitated the fabrication of composite films and variation of LiAlDH concentration in the films. It was hypothesized that particle-polymer interactions allowed the fabrication of stable suspensions. Such interactions can involve H-bonding of the surface OH groups of the LiAlDH particles and

carbonyl groups of PEMA. It is thus possible that PEMA acted not only as a film-forming agent

but also as a dispersant.
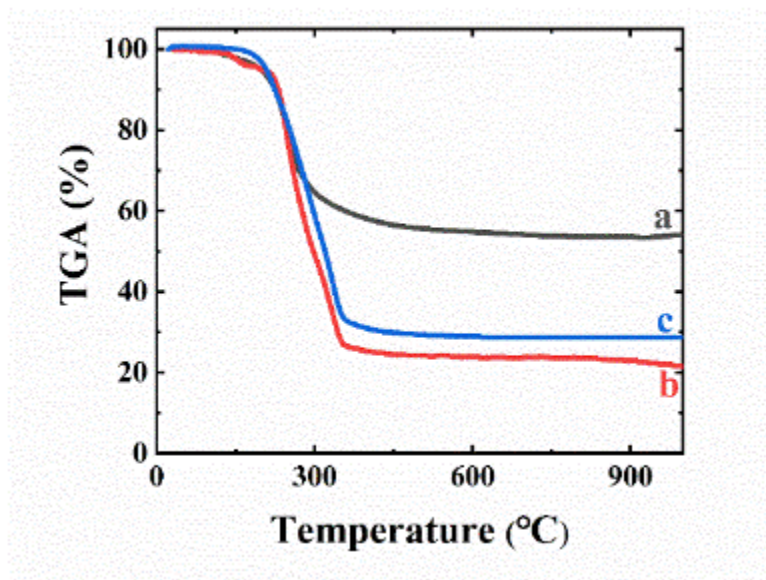


Fig. 8-6 TGA data for (a) LiAlDH prepared by solid state synthesis at 70 °C during 24 h and (b,c) PEMA-LiAlDH composites obtained from 10 g L$^{-1}$ PEMA solutions with (b) 5 and (c) 10 g L$^{-1}$ LiAlDH.

TGA studies were also performed using deposited materials, prepared by dip coatings

from PEMA solutions, containing LiAlDH (Fig. 8-6(b,c)). The deposits, prepared from

LiAlDH suspensions in the 10 g L$^{-1}$ PEMA solutions, with 5 and 10 g L$^{-1}$ LiAlDH showed total

mass loss of 78.6% and 71.2%, respectively.
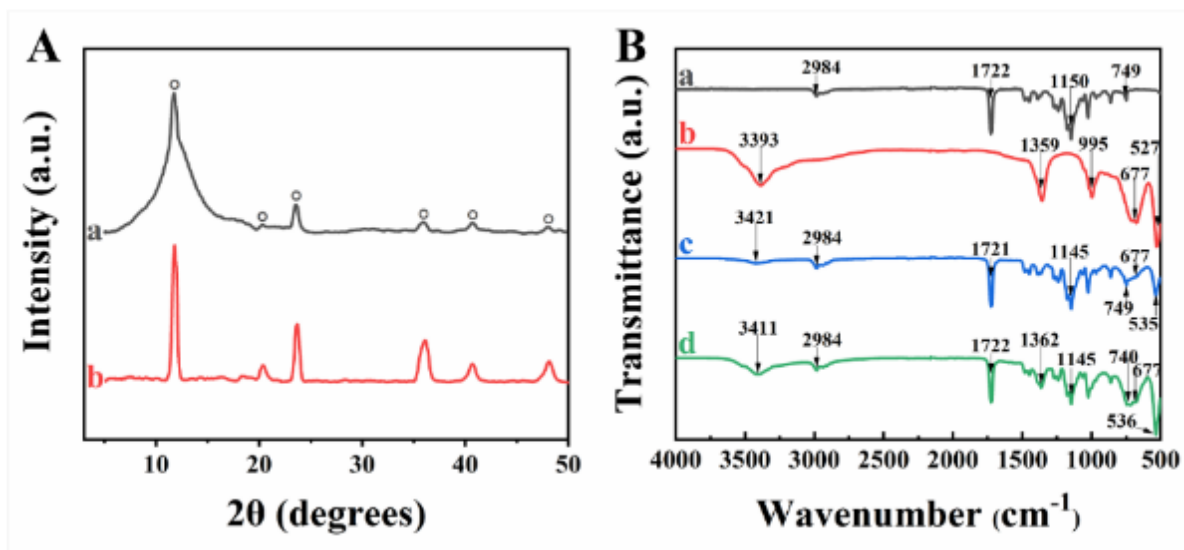
Fig. 8-7 (A) XRD patterns for PEMA-LiAlDH composite prepared from 10 g L$^{-1}$ PEMA solutions, with (a) 5 and (b) 10 g L$^{-1}$ LiAlDH (o – peaks corresponding to PDF 031–0704), (B) FTIR spectra for (a) as-received PEMA, (b) as-prepared LiAlDH and composites, prepared from 10 g L$^{-1}$ PEMA solutions, with (a) 5 and (b) 10 g L$^{-1}$ LiAlDH.
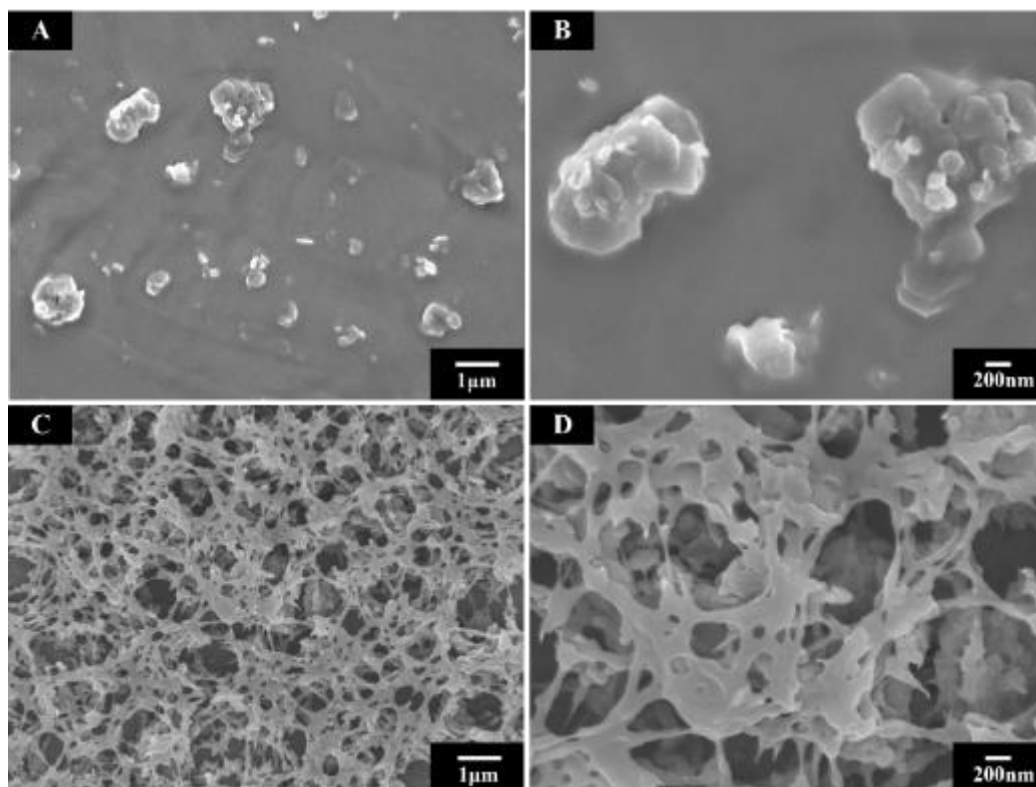


Fig. 8-8 SEM images at different magnifications for deposits prepared from 10 g L$^{-1}$ PEMA solutions, containing (A,B) 5 and (C,D) 10 g L$^{-1}$ LiAlDH.

The total mass loss of the deposited materials included mass loss related to burning out of

PEMA and dehydration of LiAlDH. Therefore, the results of TGA studies indicated the

formation of composite coatings containing FR LiAlDH additive in the PEMA matrix. The

lower mass loss for the coatings prepared from 10 g L$^{-1}$ LiAlDH resulted from higher LiAlDH

content in the deposited layer. The incorporation of LiAlDH into the PEMA coating was also

confirmed by the results of XRD and SEM studies. The X-ray diffraction pattern of the coating

showed peaks of LiAlDH (Fig. 8-7(A)). The peak broadening at low angles for the sample with

lower LiAlDH content resulted from the contribution of the PEMA phase, which shows a very

broad diffraction peak. [36, 44] The FTIR spectra of PEMA (Fig. 8-7B(a)) showed vibrational

peaks at 2984 cm$^{-1}$, which resulted from the asymmetric C-H stretching of the methylene group

of PEMA. [44] The peak at 1722 cm$^{-1}$ was assigned to the C–O carbonyl group. The vibrational

peaks corresponding to -CH$_2$ rocking was observed at 749 cm$^{-1}$. The peak at 1150 cm$^{-1}$ was

attributed to carboxylic acid ester groups. [44] The FTIR spectra of as-synthesized LiAlDH

(Fig. 8-7B(b)) showed a broad absorption band at about 3393 cm$^{-1}$ which was assigned to the

O-H stretching of hydroxy groups. [45] Sharp peaks at 677 and 527 cm$^{-1}$ were characteristics

of AlO$_6$ octahedra. [45] The FTIR spectra of composite coatings showed (Fig. 8-7B(c,d))

characteristic peaks of both PEMA and LiAlDH and provided evidence of their successful co-

deposition. SEM images showed LiAlDH particles in the dense PEMA layer (Fig. 8-8 (A,B))

for the coating prepared from 10 g L$^{-1}$ PEMA solutions with 5 g L$^{-1}$ LiAlDH. However, the

increase in the LiAlDH concentration resulted in porous coatings (Fig. 8-8 (C,D)), containing

LiAlDH particles in the porous fibrous PEMA network.
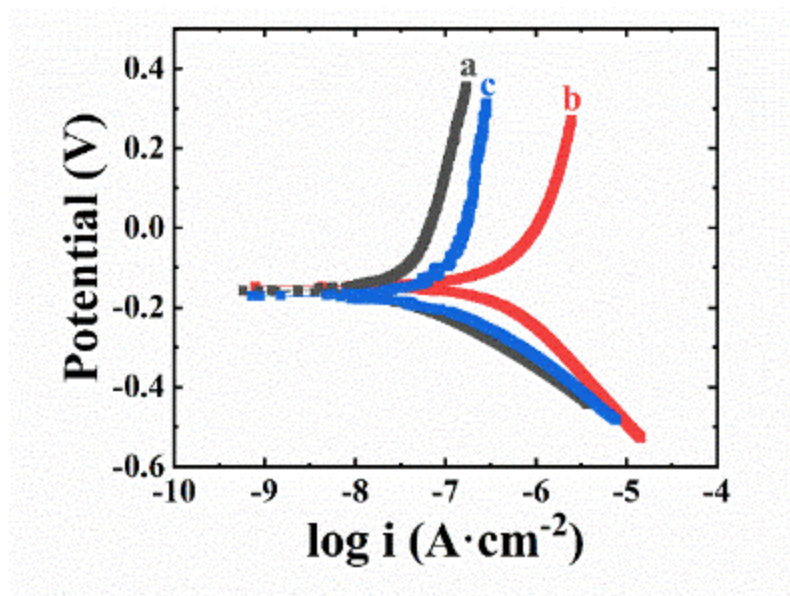


Fig. 8-9 Tafel plots for stainless steel substrates coated from (a) 10 g L$^{-1}$ PEMA solution, containing 5 g L$^{-1}$ LiAlDH, (b) 10 g L$^{-1}$ PEMA solution, containing 10 g L$^{-1}$ LiAlDH, (c) 10 g L$^{-1}$ PEMA solution (first layer) and 10 g L$^{-1}$ PEMA solution, containing 10 g L$^{-1}$ LiAlDH (second layer).

The results of potentiodynamic studies showed that the coating prepared from 10 g L$^{-1}$

PEMA solution, containing 5 g L$^{-1}$ LiAlDH provided corrosion protection of stainless steel.

The comparison with the data for the coated substrate (Fig. 8-9(a)) and uncoated (Fig. 8-2(a))

indicated that the coating deposition resulted in the increased corrosion potential and

significant reduction of the anodic current. The corrosion current for the coated sample (Fig.

8-9(a)) was 0.05 μA cm$^{-2}$.
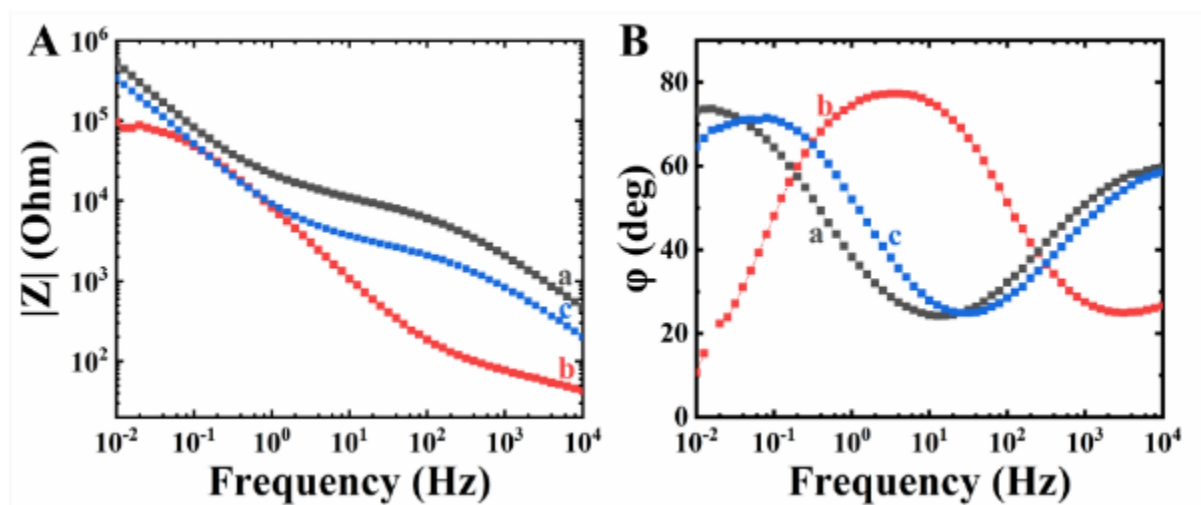
Fig. 8-10 Bode plots for stainless steel substrates coated from (a) 10 g L$^{-1}$ PEMA solution, containing 5 g L$^{-1}$ LiAlDH, (b) 10 g L$^{-1}$ PEMA solution, containing 10 g L$^{-1}$ LiAlDH, (c) 10 g L$^{-1}$ PEMA solution (first layer) and 10 g L$^{-1}$ PEMA solution, containing 10 g L$^{-1}$ LiAlDH (second layer).

The coating, prepared from 10 g L$^{-1}$ PEMA solution, containing 10 g L$^{-1}$ LiAlDH showed a higher corrosion current (Fig. 8-9(b)) of 0.76 µA cm$^{-2}$, which resulted from higher coating porosity. Fig. 8-9(c) presents testing results for a bi-layer coating, containing a pure polymer bottom layer, prepared from 10 g L$^{-1}$ PEMA solution and a top composite layer, prepared from 10 g L$^{-1}$ PEMA solution, containing 10 g L$^{-1}$ LiAlDH. The corrosion current for this coating was 0.15 µA cm$^{-2}$. In this approach the bottom layer provided enhanced corrosion protection, whereas the top layer contained relatively large amount of FR LiAlDH additive. Therefore, the dip coating method can potentially be used for the fabrication of multilayer coatings and coatings of graded composition, containing individual layers with different functionality. The EIS data presented in Fig. 10 indicate that coated substrates with composite PEMA-LiAlDH coating showed higher impedance, compared to uncoated samples (Fig. 8-3A(a)). The coating prepared from the suspension, containing 10 g L$^{-1}$ LiAlDH showed lower impedance,

compared to the suspension, containing 5 g L$^{-1}$ LiAlDH. This can be attributed to higher porosity of the coating prepared from the 10 g L$^{-1}$ LiAlDH suspension. However, the bi-layer coating showed significantly higher impedance compared to the monolayer coatings and indicated better corrosion protection.

## 8.4 Conclusions

We demonstrated that PEMA can be dissolved in a mixed isopropanol-water co-solvent. In this approach the use of traditional toxic solvents can be avoided. The ability to dissolve high molecular mass PEMA and achieve high PEMA concentration are the key factors for the development of the dip coating method. The method offers advantages compared to other coating techniques, which are based on the use of toxic solvents and require long deposition time and long-time heating procedures for solvent removal. Room temperature processing of the proposed method is critically important for the fabrication of composites, containing FR additives of DH type. This approach is especially important for biomedical applications of PEMA coatings. The solubilization range was established and 10 g L$^{-1}$ PEMA solutions were prepared from water-isopropanol mixtures with R$_S$ of 0.015–0.380. PEMA precipitation was observed at R$_S$> 0.4. It was found that 50 g L$^{-1}$ PEMA solutions can be obtained at R$_S$=0.176. The proposed PEMA solubilization mechanism was based on the co-solvation effect of water and isopropanol, it involves hydrogen bonding of PEMA and water molecules. The deposition yield of the dip coating method was influenced by R$_S$ and PEMA concentration. The coatings

can be deposited as monolayers or multilayers. It can be expected that further development of this method will result in advances in colloidal processing of other polymers using non-toxic solvents.

PEMA coatings prepared by the dip coating method can be used for corrosion protection of metals. LiAlDH was prepared by a novel solid state synthesis method, which offers many advantages, compared to traditional techniques, such as waste-free processing, excellent stoichiometry control and ability to avoid waste removal, washing and drying procedures. The synthesis time decreased with increasing temperature in the range of 20–70 °C. The relatively short synthesis time at 70 °C makes this waste-free technique very promising for the mass production of other DHs for FR and other applications. LiAlDH is a promising material for FR applications due to its relatively high water release on dehydration. LiAlDH was used as FR material for polymer coatings. LiAlDH outperforms traditional FR materials of hydroxide type due to its high water content. It was found that PEMA-LiAlDH interactions facilitated the fabrication of stable suspensions for dip coating of composites. Dip coating method allowed for the fabrication of composite PEMA-LiAlDH coatings with different LiAlDH content. Bi-layer coatings, containing different layers offer benefits for the development of coatings with improved corrosion protection and FR properties. The approach developed in this study can potentially be used for the fabrication of monolayer, multilayer coatings as well as coatings of graded composition, containing other functional materials. The results of this investigation open an avenue for a variety of future investigations of both a technological and fundamental

nature, focused on the synthesis of complex hydroxides and oxides by low temperature synthesis methods, colloidal processing of polymers using non-toxic solvents and fabrication of organic-inorganic composites by different colloidal methods.

## 8.5  Contribution Statement

Xinqian Liu: Methodology, Validation, formal analysis, Investigation, Writing – original draft; Stephen Veldhuis: Methodology, Conceptualization. Ritch Mathews: Formal analysis, Methodology. Igor Zhitomirsky: Conceptualization, Writing, Project Administration.

## 8.6  References

[1] S. Ramesh, O. Uma, R. Shanti, L.J. Yi, K. Ramesh, Preparation and characterization of poly (ethyl methacrylate) based polymer electrolytes doped with 1-butyl-3-methylimidazolium trifluoromethanesulfonate, Measurement 48 (2014) 263-273.

[2] G. Hutcheon, C. Messiou, R. Wyre, M. Davies, S. Downes, Water absorption and surface properties of novel poly (ethylmethacrylate) polymer systems for use in bone and cartilage repair, Biomaterials 22(7) (2001) 667-676.

[3] K.S. Ngai, S. Ramesh, K. Ramesh, J.C. Juan, A review of polymer electrolytes: fundamental, approaches and applications, Ionics 22(8) (2016) 1259-1279.

[4] C.M. Mathew, B. Karthika, M. Ulaganathan, S. Rajendran, Electrochemical analysis on poly (ethyl methacrylate)-based electrolyte membranes, Bulletin of Materials Science 38(1) (2015) 151-156.

[5] F. Mohanty, S.K. Swain, Nano silver embedded starch hybrid graphene oxide sandwiched poly (ethylmethacrylate) for packaging application, Nano-Structures & Nano-Objects 18 (2019) 100300.

[6] E. Abdelrazek, Influence of FeCl3 filler on the structure and physical properties of polyethyl-methacrylate films, Physica B: Condensed Matter 400(1-2) (2007) 26-32.

[7] R. Armstrong, J. Wright, Impedance studies of poly ethylmethacrylate coatings formed upon tin-free steel, Corrosion science 33(10) (1992) 1529-1539.

[8] J. Lai, X. Li, R. Wu, J. Deng, Y. Pan, Z. Zheng, X. Ding, A rapidly recoverable shape memory polymer with a topologically well-controlled poly (ethyl methacrylate) structure, Soft Matter 14(36) (2018) 7302-7309.

[9] F. Mohanty, S.K. Swain, Silver Nanoparticles Decorated Polyethylmethacrylate/Graphene Oxide Composite: As Packaging Material, Polymer Composites 40(S2) (2019) E1199-E1207.

[10] S.M. Oh, H.-i. Lee, H.M. Jeong, B.K. Kim, The properties of functionalized graphene sheet/poly (ethyl methacrylate) nanocomposites: The effects of preparation method, Macromolecular Research 19(4) (2011) 379.

[11] M. Imai, K. Akiyama, T. Tanaka, E. Sano, Highly strong and conductive carbon nanotube/cellulose composite paper, Composites Science and Technology 70(10) (2010) 1564-1570.

[12] A. Sari, A. Karlı, C. Alkan, A. Karaipekli, Polyethyl methacrylate (PEMA)/fatty acids blends as novel phase change materials for thermal energy storage, Energy Sources, Part A: Recovery, Utilization, and Environmental Effects 35(19) (2013) 1813-1819.

[13] M. Agrawal, N.E. Zafeiropoulos, S. Gupta, E. Svetushkina, J. Pionteck, A. Pich, M. Stamm, A novel approach for mixing ZnO nanoparticles into poly (ethyl methacrylate), Macromolecular rapid communications 31(4) (2010) 405-410.

[14] P. Pradeepa, S. Edwinraj, M.R. Prabhu, Effects of ceramic filler in poly (vinyl chloride)/poly (ethyl methacrylate) based polymer blend electrolytes, Chinese Chemical Letters 26(9) (2015) 1191-1196.

[15] K. Prusty, S.K. Swain, Nano ZrO2 reinforced cellulose incorporated polyethylmethacrylate/polyvinyl alcohol composite films as semiconducting packaging materials, Journal of Applied Polymer Science 137(42) (2020) 49284.

[16] J.C. Arnold, N.P. Venditti, Prediction of the long-term creep behaviour of hydroxyapatite-filled polyethylmethacrylate bone cements, Journal of Materials Science: Materials in Medicine 18(9) (2007) 1849-58.

[17] S. Mallakpour, M. Hatami, Condensation polymer/layered double hydroxide NCs: Preparation, characterization, and utilizations, European Polymer Journal 90 (2017) 273-300.

[18] I. Deen, X. Pang, I. Zhitomirsky, Electrophoretic deposition of composite chitosan–halloysite nanotube–hydroxyapatite films, Colloids and Surfaces A: Physicochemical and Engineering Aspects 410 (2012) 38-44.

[19] Y. Wang, I. Deen, I. Zhitomirsky, Electrophoretic deposition of polyacrylic acid and composite films containing nanotubes and oxide particles, Journal of Colloid and Interface Science 362(2) (2011) 367-374.

[20] I. Deen, I. Zhitomirsky, Electrophoretic deposition of composite halloysite nanotube–hydroxyapatite–hyaluronic acid films, Journal of Alloys and Compounds 586 (2014) S531-S534.

[21] A. Chatterjee, P. Bharadiya, D. Hansora, Layered double hydroxide based bionanocomposites, Applied Clay Science 177 (2019) 19-36.

[22] Y. Gao, J. Wu, Q. Wang, C.A. Wilkie, D. O'Hare, Flame retardant polymer/layered double hydroxide nanocomposites, Journal of Materials Chemistry A 2(29) (2014) 10996-11016.

[23] Z. Matusinovic, C.A. Wilkie, Fire retardancy and morphology of layered double hydroxide nanocomposites: a review, Journal of Materials Chemistry 22(36) (2012) 18701-4.

[24] Y. Liu, Y. Gao, Q. Wang, W. Lin, The synergistic effect of layered double hydroxides with other flame retardant additives for polymer nanocomposites: a critical review, Dalton Transactions 47(42) (2018) 14827-14840.

[25] P. Wojtal, S. Chen, K. Shi, R. Mathews, I. Zhitomirsky, Electrophoretic deposition of a memory-type flame retardant material, Materials Letters 153 (2015) 106-109.

[26] J. Thiel, C. Chiang, K.R. Poeppelmeier, Structure of lithium aluminum hydroxide dihydrate (LiAl2 (OH) 7.2 H2O), Chemistry of Materials 5(3) (1993) 297-304.

[27] S. Elbasuney, Novel multi-component flame retardant system based on nanoscopic aluminium-trihydroxide (ATH), Powder Technology 305 (2017) 538-545.

[28] J. Liang, Y. Zhang, A study of the flame-retardant properties of polypropylene/Al (OH) 3/Mg (OH) 2 composites, Polymer international 59(4) (2010) 539-542.

[29] L. Anicǎi, A. Manea, T. Visan, Lithium-aluminium hydroxide hydrate thin layers on Al based substrates-new ecological process for corrosion resistance increase, Molecular Crystals and Liquid Crystals 418(1) (2004) 41-53.

[30] C. Drewien, M. Eatough, D. Tallant, C. Hills, R. Buchheit, Lithium-aluminum-carbonate-hydroxide hydrate coatings on aluminum alloys: Composition, structure, and processing bath chemistry, Journal of materials research 11(6) (1996) 1507-1513.

[31] Y. Kamiya, K. Mizoguchi, Y. Naito, A dielectric relaxation study of plasticization of poly (ethyl methacrylate) by carbon dioxide, Journal of Polymer Science Part B: Polymer Physics 28(11) (1990) 1955-1964.

[32] G. Gery, H. Masuhara, Laser-induced molecular mixing of electron donor and acceptor in poly (ethyl methacrylate), Chemical Communications (7) (1998) 811-812.

[33] M. Sanopoulou, D. Stamatialis, Study of the transition from Fickian to Case II sorption kinetics in the system poly (ethyl methacrylate)–liquid methyl alcohol, Polymer 42(4) (2001) 1429-1439.

[34] C. Chen, M.L. Clarke, J. Wang, Z. Chen, Comparison of surface structures of poly (ethyl methacrylate) and poly (ethyl acrylate) in different chemical environments, Physical Chemistry Chemical Physics 7(11) (2005) 2357-2363.

[35] S. Rajendran, M.R. Prabhu, M.U. Rani, Ionic conduction in poly (vinyl chloride)/poly (ethyl methacrylate)-based polymer blend electrolytes complexed with different lithium salts, Journal of power sources 180(2) (2008) 880-883.

[36] A. Tiwari, A. Gupta, R. Bajpai, J. Keller, Structural and mechanical studies of in-situ generated poly (vinylidene fluoride) particle comprising poly (ethylmethacrylate) and poly (methylmethacrylate) ternary films, Polymer-Plastics Technology Engineering 49(6) (2010) 573-580.

[37] J.A. Gómez-Tejedor, N. Van Overberghe, P. Rico, J.L.G. Ribelles, Assessment of the parameters influencing the fiber characteristics of electrospun poly (ethyl methacrylate) membranes, European Polymer Journal 47(2) (2011) 119-129.

[38] J. Chiou, D. Paul, Gas sorption and permeation in poly (ethyl methacrylate), Journal of membrane science 45(1-2) (1989) 167-189.

[39] B.A. Miller-Chou, J.L. Koenig, A review of polymer dissolution, Progress in Polymer Science 28(8) (2003) 1223-1270.

[40] R. Hoogenboom, C.R. Becer, C. Guerrero-Sanchez, S. Hoeppener, U.S. Schubert, Solubility and thermoresponsiveness of PMMA in alcohol-water solvent mixtures, Australian journal of chemistry 63(8) (2010) 1173-1178.

[41] Q. Zhang, R. Hoogenboom, Polymers with upper critical solution temperature behavior in alcohol/water solvent mixtures, Progress in Polymer Science 48 (2015) 122-142.

[42] I. Pelly, Recovery of lithium from Dead Sea brines, Journal of Applied Chemistry Biotechnology 28(7) (1978) 469-474.

[43] H. Van Straten, M. Schoonen, P. De Bruyn, Precipitation from supersaturated aluminate solutions. III. Influence of alkali ions with special reference to Li+, Journal of colloid and interface science 103(2) (1985) 493-507.

[44] M. Ulaganathan, C.M. Mathew, S. Rajendran, Highly porous lithium-ion conducting solvent-free poly (vinylidene fluoride-co-hexafluoropropylene)/poly (ethyl methacrylate) based polymer blend electrolytes for Li battery applications, Electrochimica Acta 93 (2013) 230-235.

[45] M. Nayak, T. Kutty, V. Jayaraman, G. Periaswamy, Preparation of the layered double hydroxide (LDH) LiAl2 (OH) 7· 2H2O, by gel to crystallite conversion and a hydrothermal method, and its conversion to lithium aluminates, Journal of Materials Chemistry 7(10) (1997) 2131-2137.

# Chapter 9 Poly(ethyl methacrylate) composite coatings with halogen-free inorganic flame-retardant additives

Xinqian Liu, Stephen Veldhuis, Ritch Mathews, Igor Zhitomirsky

## Abstract

This investigation is motivated by the need for the development of polymer coatings, containing inorganic flame retardant materials (FRM) and replacement of toxic halogenated FRM. A green strategy is reported for the fabrication of poly(ethyl methacrylate) (PEMA)-FRM composite coatings by a dip coating method. The use of water-isopropanol co-solvent allows the replacement of regular toxic solvents for PEMA. The ability to form concentrated solutions of high molecular mass PEMA and disperse FRM particles in such solutions are the main factors for the fabrication of coatings by a dip coating technique. Huntite, halloysite and hydrotalcite are used as advanced FRM for the fabrication of PEMA-FRM coatings. FTIR, XRD, SEM and TGA data are used for the analysis of microstructure and composition of PEMA-FRM coatings. PEMA and PEMA-FRM coatings provide corrosion protection of stainless steel. The ability to form laminates of different layers by a dip coating method facilitates the fabrication of composite coatings with enhanced properties.

## 9.1 Introduction

Flame retardant materials (FRM) are vital for the development of composites for various industrial applications[1, 2]. FRM additives have many applications in various composite products, such as insulation of black boxes for flight data recorders and aircraft coatings[3], communication and electrical cables[4], furniture and coatings for various wood products[3], electrical cables[4], mining and transportation equipment[4], polymer coatings for corrosion

protection of metals[4], wind turbines[5], asphalt binders[6], papers[7], thermoplastics, thermosets, and flame resistant fabrics[4]. FRM are gaining increasing attention for the development of composites for advanced energy generation devices[8, 9]. FRM are mandatory components of various building product composites, such as wall and ceiling linings, fabrics for office and residential buildings[4], fire blankets[4], theatre curtains and a large variety of consumer products, including window blinds, electrical appliances, furniture and children's toys[10].

There is a large demand for novel composites with FRM additives for cars, aircrafts and ships due to the increasing use of flammable plastics and polymer materials[4, 11]. FRM are used in car seats, car upholstery, electronic devices and paints[12, 13]. FRM additives for polymers are increasingly important due to the replacement of metals with polymer based composites[10, 14]. FRM are of special importance for equipment of communication and computing centres[15, 16]. The use of FRM is of critical importance for polymer industry in order to meet nonflammability standards for a large variety of polymer products[17]. However, the benefits of FRM must be weighed against the potential risks associated with human or environmental impacts. Various materials and flame retardant mechanisms were investigated for applications in commercial products[1, 2, 18].

Many polymer products contained halogen based FRM[16]. The heating of such materials results in the formation of volatile metal halides, acting as flame inhibitors. The halogen based

FRM are usually introduced into the polymer chain by copolymerization. However, the halogenated FRM are toxic and bioaccumulative[19-26].

Investigations showed[19, 27, 28] that the use of toxic halogen based FRM resulted in widespread contamination of the environment. A high level of toxic FRM contaminations was found in soil[27], rivers[21], atmosphere, soft drinks, food [22-25], and home dust [20]. Such investigations showed the need in replacement of toxic halogenated FRM with more environmentally friendly inorganic FRM materials. Significant interest has been generated in the development of polymer composites containing advanced inorganic FRM additives of hydroxide and carbonate type [14, 29, 30]. The flame retardant properties of such FRM materials result from the release of water or $CO_2$, which limit oxygen access to the polymer materials and from related endothermic effect.

This investigation was inspired by increasing interest in the development of composite polymer coatings, containing inorganic FRM additives of hydroxide and carbonate type and the need for avoiding halogenated FRM. Poly(ethyl methacrylate) (PEMA) was selected as a model functional polymer for the development of composite coatings. The selection of this polymer was based on its advanced functional properties for various applications, such as corrosion protection of metals [31], thermal [32] and electrical [33, 34] energy storage, materials for packaging [35, 36], biomedical composites [37] and other applications. In this investigation, huntite ($Mg_3Ca(CO_3)_4$ platelets, halloysite ($Al_2Si_2O_5(OH)_4 \cdot 2H_2O$ nanotubes, and submicrometre hydrotalcite ($Mg_6Al_2(CO_3)(OH)_{16} \cdot 4H_2O$, particles were used as inorganic FRM

materials of hydroxide or carbonate type. The results presented below indicated that composite

coatings can be prepared, containing FRM additives in the PEMA matrix. The thermal and

corrosion protection properties of the composite coatings were analyzed. Moreover, in the

proposed approach the use of regular toxic solvents for the processing of PEMA and its

composites was avoided.

## 9.2  Materials and Methods

Poly(ethyl        methacrylate)        (PEMA,        $M_W$=515,000),        hydrotalcite

($Mg_6Al_2(CO_3)(OH)_{16} \cdot 4H_2O$, size ~ 0.5 μm), halloysite ($Al_2Si_2O_5(OH)_4 . 2H_2O$ nanotubes, length

1–2 μm, diameter 100–150 nm), isopropanol (MilliporeSigma) and huntite ($Mg_3Ca(CO_3)_4$

platelets, Sibelco, size ~ 0.5–3 μm) were used. PEMA was dissolved in a mixed solvent of 85%

isopropanol and 15% water at 60 °C and subsequently cooled to room temperature. A 0.1 mm

thick stainless-steel foil (304 types) was used as a substrate for coating deposition. The

substrates were polished with sandpaper, washed with water and isopropanol. 10-20 g $L^{-1}$

PEMA solutions were used for dip coating of pure PEMA coatings. The substrates were

immersed into the solutions during 1 min and then were withdrawn from the solutions at a

constant speed of 1 cm $min^{-1}$. Coatings were obtained after solvent evaporation by drying in

air. Pure PEMA coatings were annealed at 200 °C for 1 h. The monolayer composite coatings

were prepared by a similar dip coating procedure using 10 g $L^{-1}$ PEMA solutions, containing

different FRM additives, such as huntite, halloysite and hydrotalcite. The FRM concentration

in the suspensions was 10 g L$^{-1}$. The bi-layer composite coatings were prepared by deposition of first layer from 10 g L$^{-1}$ PEMA solutions followed by annealing procedure at 200 °C for 1 h and then formation of as-deposited second layer from 10 g L$^{-1}$ PEMA solutions, containing 10 g L$^{-1}$ FRM. The suspensions were ultrasonicated for 5 min before film deposition using Fisher Scientific FB-505 sonic dismembrator.

The microstructure of coatings was studied using a JEOL SEM (scanning electron microscope, JSM-7000 F). A Bruker Vertex 70 spectrometer was used for FTIR spectroscopy. Coating composition was analyzed using a Bruker Smart 6000 X-ray diffractometer (XRD, CuKα radiation). A potentiostat-impedance analyzer PARSTAT 2273 (Ametek) was utilized to perform the electrochemical characterization in 3% NaCl aqueous solution with a 3-electrode corrosion cell, which included uncoated or coated stainless steel as the working electrode, Pt mesh as counter electrode and saturated calomel electrode (SCE) as the reference electrode. Electrochemical impedance spectroscopy (EIS) was performed using alternating current (AC) in the frequency range from 10 mHz to 10kHz and voltage amplitudes of 5 mV. The results of potentiodynamic studies (1 mV s$^{-1}$ rate) and EIS were presented in Tafel and Bode plots. Thermogravimetric analysis (TGA) was conducted in air at a heating rate of 5 °C min$^{-1}$ utilizing a thermal analyzer (Netzsch STA-409). The samples for TGA analysis contained as-deposited coating materials, which were removed from the substrates.

## 9.3  Results and Discussion

The approach developed in this investigation offers environmental benefits by avoiding the use of regular toxic solvents for PEMA and halogenated FRM. PEMA is soluble only in relatively toxic and carcinogenic individual solvents, such as methyl ethyl ketone, toluene and benzene. PEMA is insoluble in alcohols and water. In our approach, PEMA was dissolved in a mixed co-solvent, containing isopropanol and water, avoiding the use of traditional toxic and carcinogenic solvents. The main factor to achieving coating deposition by a dip-coating method was solubilization of high molecular mass PEMA at formation of concentrated solutions. This investigation addressed the need to replace the toxic halogenated FRM with more environmentally friendly materials. Our approach was based on the use of environmentally friendly inorganic FRM such as hydrotalcite, halloysite and huntite. The mass losses for hydrotalcite, halloysite and huntite related to release of water and $CO_2$ are 43.1, 24.5 and 49.9 %, respectively. Hydrotalcite offers benefits of relatively high mass loss, which is mainly due to the release of water. Despite lower mass loss, halloysite offers many benefits for the development of composite coatings. The tubular shape of natural halloysite particles is beneficial for the mechanical reinforcement of a polymer matrix. The hollow space of the halloysite nanotubes can be loaded with corrosion inhibitors and other functional materials, which can impart advanced functional properties to the composites. Huntite offers benefits of relatively high decomposition temperature, which makes it a material of choice for the polymer coatings, requiring post-deposition thermal treatment. Huntite belongs to the carbonate type-

materials, which are currently under intensive investigations for the development of polymer

composites with enhanced mechanical properties[38].  It will be shown below that corrosion

protection properties of PEMA can be improved by annealing at 200°C. The thermal stability

of huntite at this temperature is beneficial for the fabrication of PEMA-huntite composites. The

results presented below also showed that the dip coating procedure allowed for the fabrication

of coatings of graded composition and microstructure, with an annealed bottom PEMA layer

and a composite top layer, containing inorganic FRM.
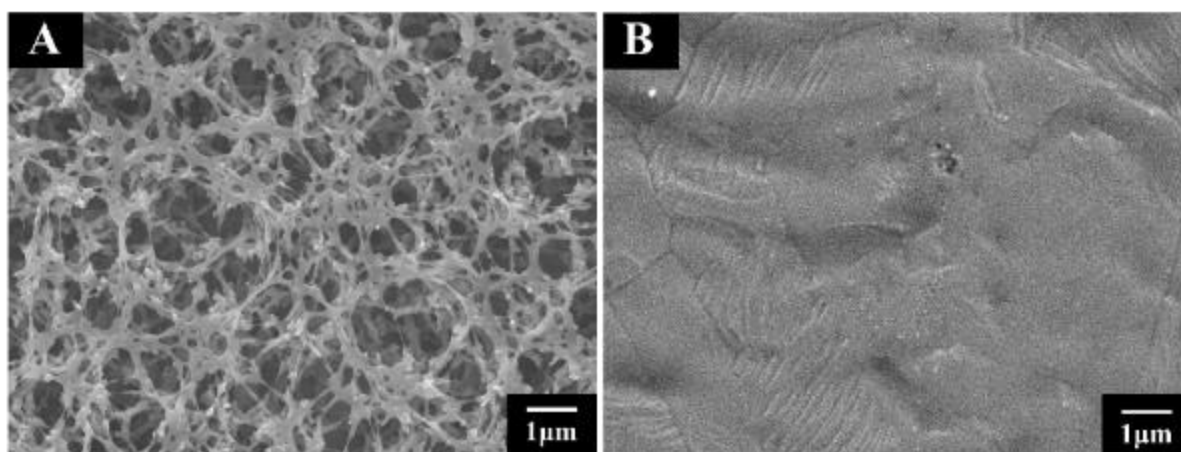


Figure 9-1 **.** SEM images of (A) as-deposited coatings and (B) coatings annealed at 200 °C for
1h, prepared from 20 g L$^{-1}$ PEMA solutions.

Fig. 9-1 shows SEM images of PEMA coatings, prepared from 20 g L$^{-1}$ PEMA solutions.

The as-deposited coatings showed a relatively porous surface (Fig. 9-1 A). Annealing at 200°C

resulted in the formation of dense coatings (Fig. 9-1 B). The thickness of the annealed coatings

was about 2 μm. The as-deposited and annealed PEMA coatings prepared from 10 g L$^{-1}$ PEMA

solutions showed a similar morphology (Supplementary information, Fig. 9-9) with a thickness

of the annealed coating of about 1 μm.

The annealed PEMA coatings showed corrosion protection of the substrates. Fig. 9-2 shows Tafel and Bode plots for the coated and uncoated substrates. Compared with the uncovered stainless steel, both as-deposited and annealed PEMA coatings showed lower anodic currents and higher corrosion potentials. Accordingly, the Bode plot showed much higher absolute impedances |Z| of the coated samples in a wide frequency range from 10 mHz to 10 kHz. Therefore, PEMA coatings acted as a barrier layer, which limited the electrolyte penetration to the substrate.
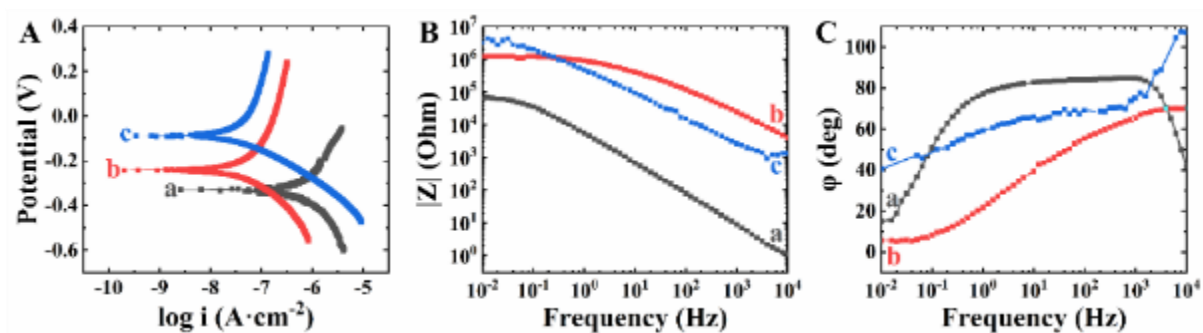


Figure 9-2 (A) Tafel and (B,C) EIS data for (a) uncoated and (b,c) coated substrate, for coatings: (b) as-deposited and (c) annealed at 200 °C for 1h, prepared from 20 g L$^{-1}$ PEMA solutions.
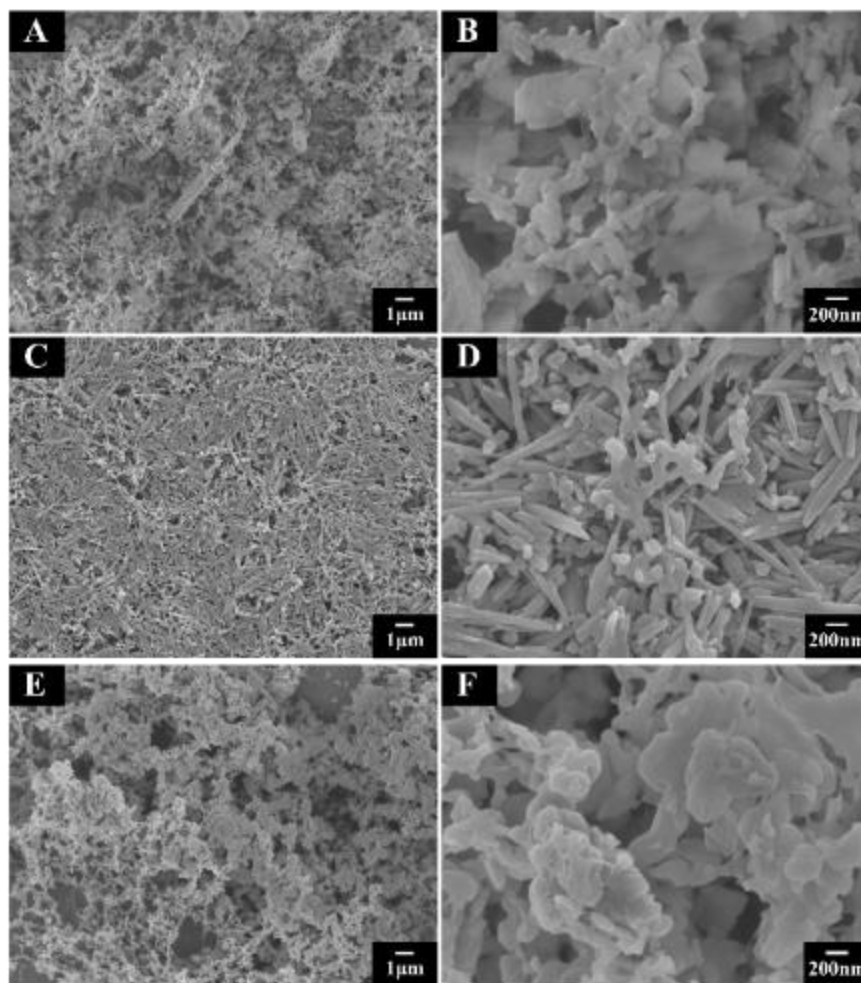
Figure 9-3 SEM images at different magnifications of as-deposited monolayer composite coatings: (A,B) PEMA-huntite, (C,D) PEMA-halloysite and (E,F) PEMA-hydrotalcite.

PEMA-based composite coatings were deposited with three types of FRM. The SEM images (Fig. 9-3) at low magnification showed continuous porous composite coating formed by the dip coating technique. The images at high magnification revealed the presence of FRM particles. Fig. 9-3B shows the platelet morphology of huntite in the PEMA matrix. Halloysite nanotubes were densely packed, as shown in Fig. 9-3D. Fig. 9-3F shows submicrometric hydrotalcite particles embedding in PEMA matrix. Voids were inevitable in the composite layers due to the packing of FRM particles. The thickness of the coatings was about 2-2.5 μm.
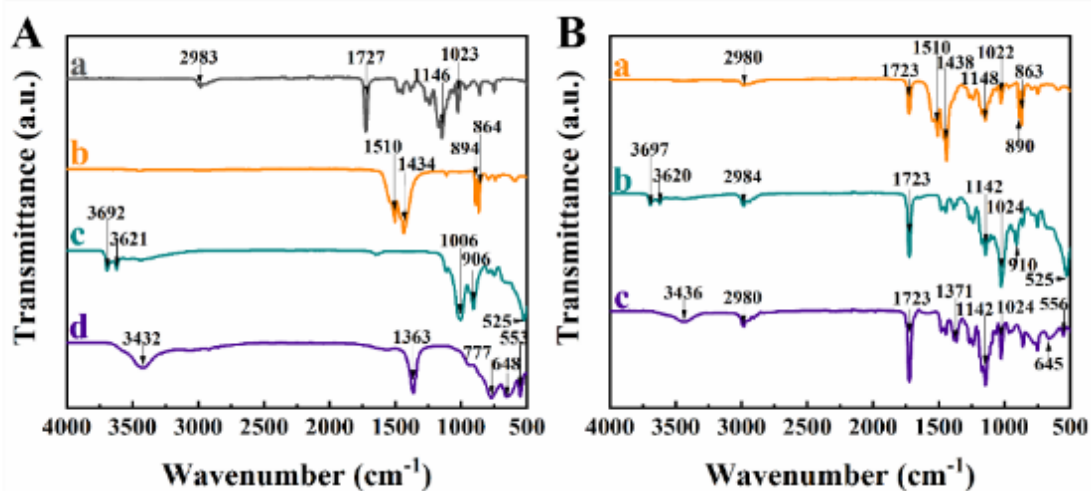
Figure 9-4 FTIR spectra of (A) as-received materials: (a) PEMA, (b) huntite, (c) halloysite and (d) hydrotalcite, and (B) as-deposited composite coatings: (a) PEMA-huntite, (b) PEMA-halloysite, and (c) PEMA-hydrotalcite.

FTIR and XRD results confirmed the successful fabrication of PEMA-FRM composite coatings. The spectrum of as-received PEMA in Fig. 9-4A(a) showed absorptions at 2983, 1727, 1146 and 1023 cm$^{-1}$ due to the asymmetric C–H stretching, C=O stretching, C-O-C symmetric stretching and C-H bending, respectively[39, 40]. These four characteristic peaks were also observed in FTIR spectra of composite coatings, as shown in Fig. 9-4B(a-c). The FTIR spectrum of as-received huntite (Fig. 9-4A(b) showed characteristic absorptions at 1510, 1434, 894, and 864 cm$^{-1}$, attributed to carbonate ligands[41-44].

The as-received halloysite showed peaks at 3692 and 3621 cm$^{-1}$ due to the presence of the surface hydroxyl group (Fig. 9-4A(c))[45]. The peaks at 1006, 906, and 525 cm$^{-1}$ were ascribed to the stretching mode of Si-O-Si, bending vibrations of Al-OH, and bending and stretching vibrations of Si-O-Al, respectively[46, 47]. The as-received hydrotalcite (Fig. 9-4A(d)) showed a peak at 3432 cm$^{-1}$ due to stretching mode of the hydroxy groups, the asymmetric stretching

of the carbonate contributed to the peak at 1363 cm$^{-1}$, the bands at 777, 648, and 553 cm$^{-1}$ were assigned to oxygen–metal-oxygen stretching[48, 49]. The spectra of the composite coatings showed absorptions of huntite (Fig. 9-4B(a)), halloysite (Fig. 9-4B(b)) and hydrotalcite (Fig.9-4B(c)) in addition to the PEMA absorptions and confirmed FRM incorporation into the PEMA coatings.

Fig. 9-5 shows XRD data for the composite coatings. The peaks of huntite, halloysite and hydrotalcite were found in XRD patterns of composite coatings.
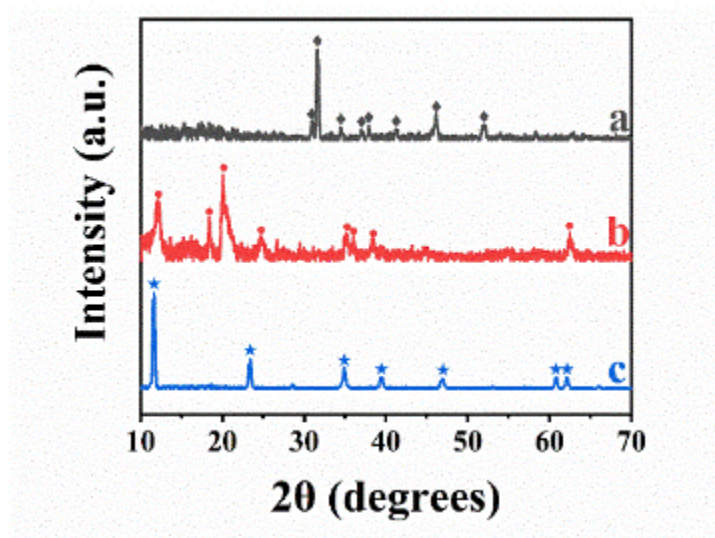


Figure 9-5 XRD patterns of as-deposited composite coatings: (a) PEMA-huntite, (b) PEMA-halloysite, and (c) PEMA-hydrotalcite (♦- JCPDS file 14-0409, ● - JCPDS file 09-0453, ★- JCPDS file 50-1684.

The composite coatings were studied by TGA. The TGA analysis of pure PEMA was reported in several investigations[50-54]. It was found that PEMA decomposition starts at 230°C and complete burning-out of PEMA was observed at 400°C. Fig. 9-6 shows several steps in mass loss of composite coatings related to decomposition of FRM and burning out of

PEMA. The total mass loss of PEMA-huntite at 900°C was 76.5%. From the TGA data the huntite content in the coating was found to be 46.9%. The total loss in mass of PEMA-halloysite was 62.6%, and the halloysite content in the composite was 49.5%. The mass loss for PEMA-hydrotalcite was 76.6% and the hydrotalcite content in the composite coating was found to be 41.1%. The calculations of the FRM content in the composite coatings were based on the theoretical mass loss of 49.9, 24.5 and 43.1% for huntite, halloysite and hydrotalcite, respectively. The experimental mass loss for such materials was very close to the theoretical mass loss[41, 55, 56].

Composite coatings are promising due to the possibility of combining corrosion protection and FRM properties. The experimental results presented above showed enhanced corrosion protection of annealed PEMA. However, annealing at 200°C can result in partial decomposition of halloysite and hydrotalcite. Therefore, in this investigation bi-layer coatings were prepared, containing annealed bottom layer of pure PEMA and as-deposited composite PEMA-FRM layer. The microstructure of PEMA-FRM layers deposited on annealed PEMA layers (Supplementary information, Fig. 9-10), was similar to the microstructure of PEMA-FRM layers deposited directly on stainless steel (Fig.9-3). Dip coating is a versatile method[57] for the fabrication of composite and multilayer coatings. It is known that multilayer and functionally graded materials offer advantages for the fabrication of composites with enhanced functional properties[58, 59]. In contrast to other techniques, such as electrophoretic deposition[60, 61], dip coatings can be obtained on conductive and insulating substrates.
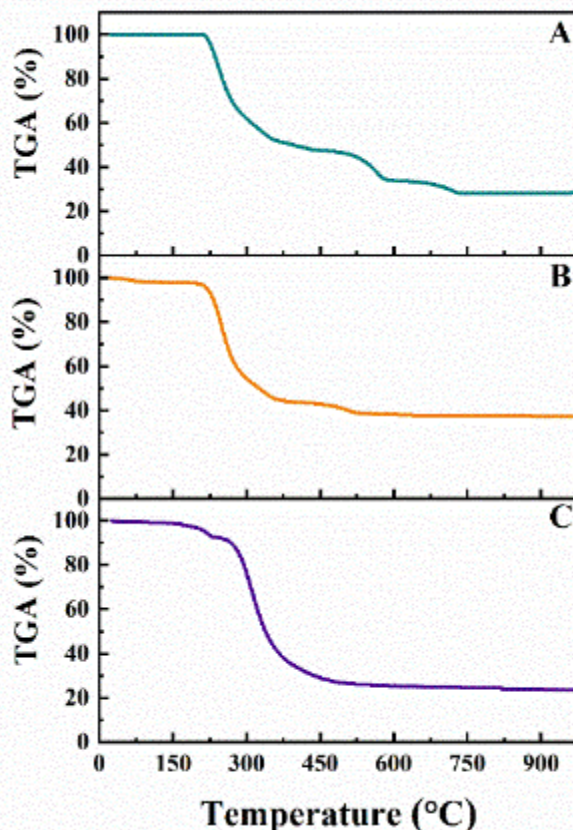
Figure 9-6 TGA data for as-deposited composite coatings: (A) PEMA-huntite, (B) PEMA-halloysite, and (C) PEMA-hydrotalcite.

Fig. 9-7 compares results of potentiodynamic testing of monolayer PEMA-FRM coatings and bi-layer coatings, containing annealed bottom PEMA layer and top PEMA-FRM layer. The comparison of Tafel plots for PEMA-FRM coated substrates (Fig. 9-7A(a), B(a) and C(a)) with corresponding data for uncoated samples (Fig. 9-2A(a)) indicated that PEMA-FRM coatings provided corrosion protection of the substrates. The coated samples showed lower anodic currents, compared to uncoated samples and higher corrosion potentials. As it was hypothesized, the bi-layer coatings provided improved corrosion protection, compared to the monolayer coatings. The Tafel plots showed further reduction of the anodic current, compared

to the monolayer coatings (Fig. 9-7A(b), B(b) and C(b). The corresponding Bode plots were

presented in Fig. 9-8.
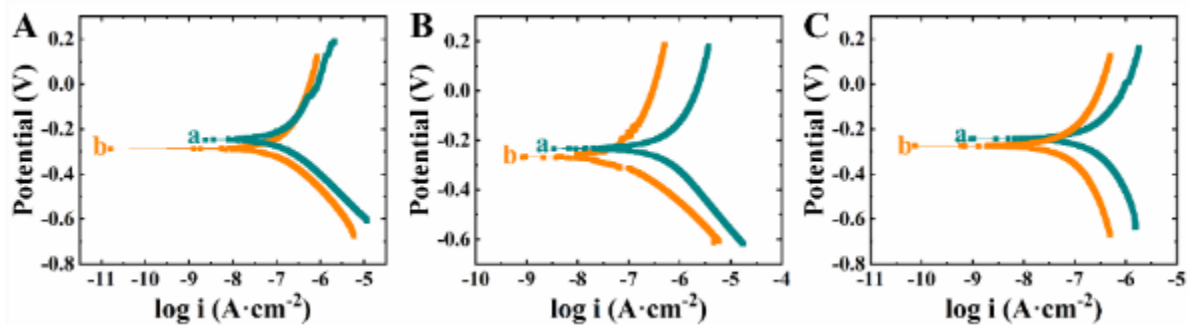


Figure 9-7 (A-C) Tafel plots for as-deposited (a) monolayer PEMA-FRM coatings and (b) bi-layer composite coatings, containing annealed PEMA bottom layer and PEMA-FRM top layer with (A) huntite, (B) halloysite, and (C) hydrotalcite.

The Bode plots for the monolayer PEMA-FRM coatings showed enhanced impedance |Z|

(Fig. 9-8A(a), C(a) and E(a)), compared to uncoated stainless steel (Fig. 9-2B(a)). The bi-layer

coating showed higher |Z| (Fig. 9-8A(b), C(b) and E(b)), compared to the monolayer coatings.

Therefore, bi-layer coatings represented an enhanced barrier for electrolyte
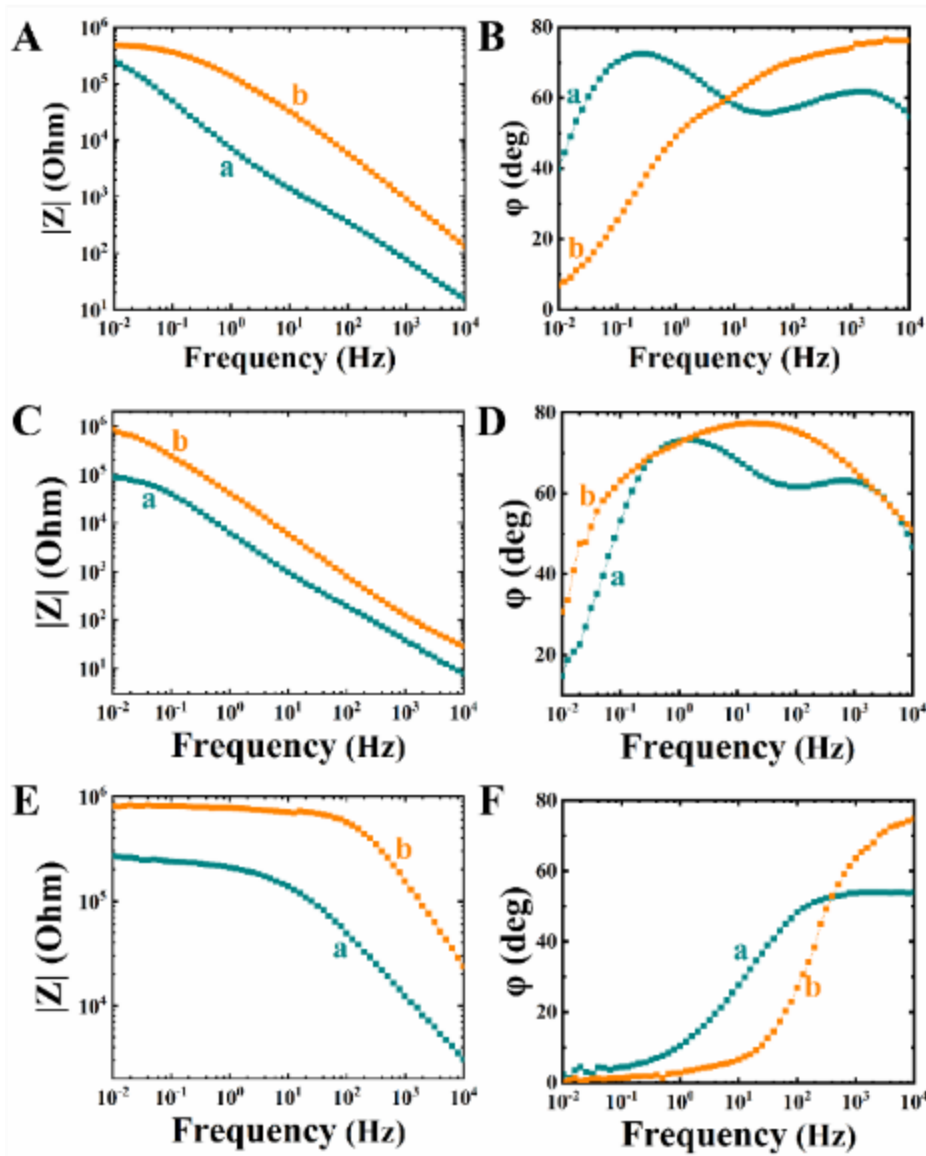
Figure 9-8 (A-F) EIS data for as-deposited (a) monolayer PEMA-FRM coatings and (b) bi-layer composite coatings, containing annealed PEMA bottom layer and PEMA-FRM top layer with (A,B) huntite, (C,D) halloysite, and (E,F) hydrotalcite.

## 9.4 Conclusions

The approach developed in this investigation offers benefits of using a non-toxic co-solvent and replacement of regular toxic solvents for PEMA. The use of advanced inorganic FRM materials, such as huntite, halloysite and hydrotalcite instead of toxic halogenated FRM

offers additional environmental benefits. The ability to obtain concentrated solutions of high molecular mass PEMA and disperse FRM particles in such solutions plays a vital role in the fabrication of coatings by a dip coating method. SEM, TGA, XRD and FTIR studied confirmed the fabrication of composite coatings with a large FRM content. Pure PEMA and PEMA-FRM coatings provide corrosion protection of stainless steel. Annealed PEMA coatings provide enhanced corrosion protection due to lower porosity. The ability to form composite laminates, containing different layers by a dip coating method is a promising strategy for the fabrication of composite coatings with enhanced functionality.

## 9.5 Supplementary data
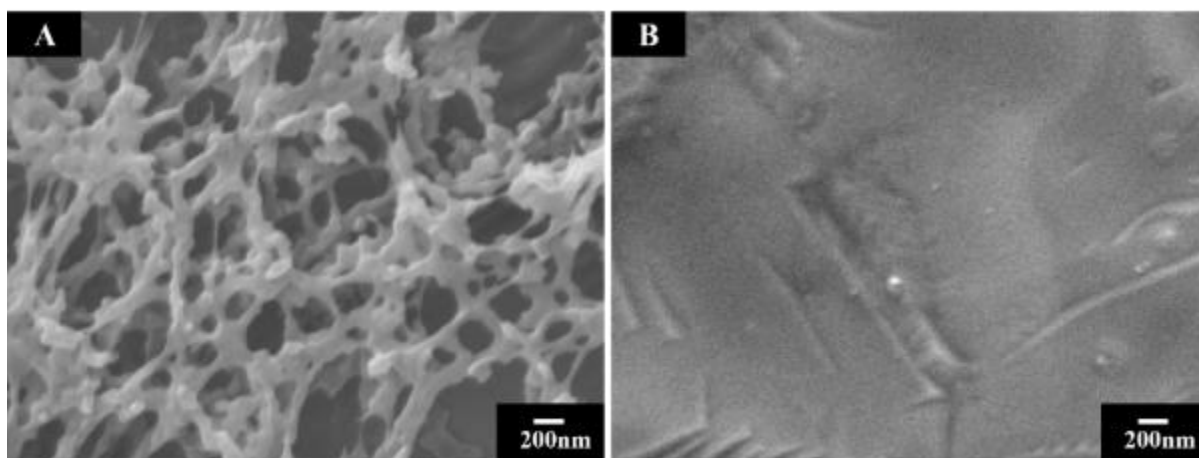


Figure 9-9 SEM images of (A) as-deposited coatings and (B) coatings annealed at 200 °C for 1h, prepared from 10 g L$^{-1}$ PEMA solutions.
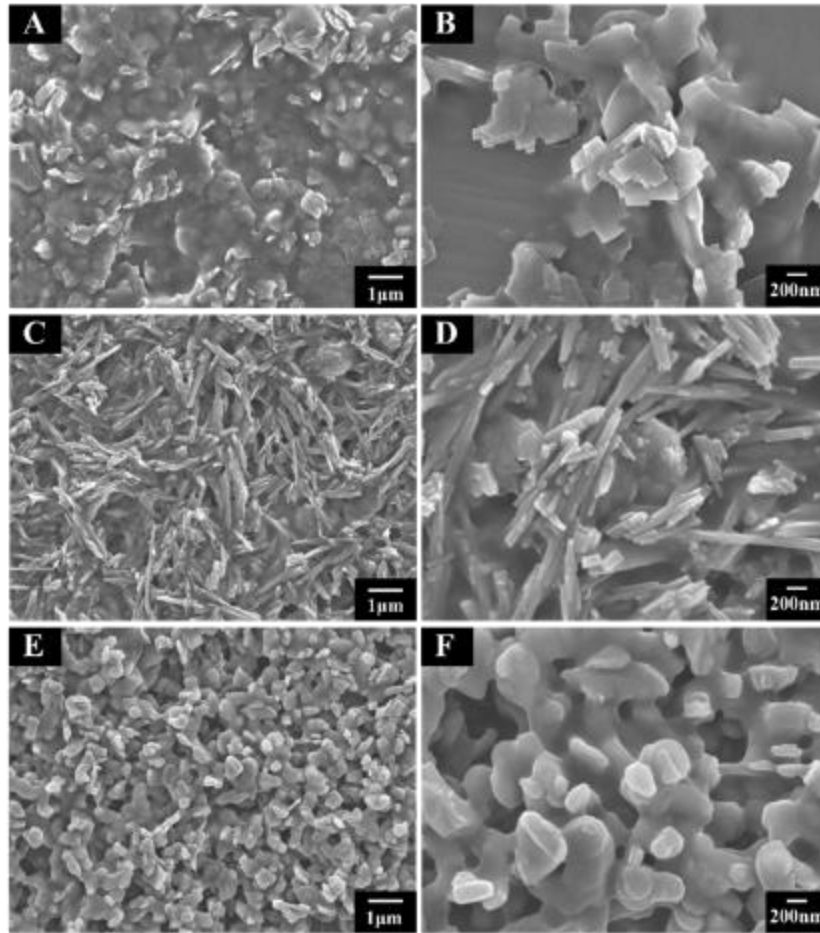
Figure 9-10 SEM images at different magnifications of as-deposited bi-layer composite coatings, containing annealed PEMA bottom layer and PEMA-FRM top layer with (A,B) huntite, (C,D) halloysite, and (E,F) hydrotalcite.

## 9.6 Contribution Statement

Conceptualisation, X.L., I.Z., and S.V.; methodology, X.L.; software, X.L.; validation, X.L., R.M., and I.Z.; formal analysis, X.L.; investigation, X.L.; resources, S.V. and R.M.; data curation, X.L.; writing—original draft preparation, X.L. and I.Z.; writing—review and editing, X.L. and I.Z.; visualisation, X.L.; supervision, S.V. and I.Z.; project administration, I.Z.; funding ac-quisition, S.V., R.M., and I.Z. All authors have read and agreed to the published version of the man-uscript.

## 9.7  Reference

[1] L. Chen, Y.Z. Wang, A review on flame retardant technology in China. Part I: development of flame retardants, Polymers for Advanced Technologies 21(1) (2010) 1-26.

[2] H. Lu, L. Song, Y. Hu, A review on flame retardant technology in China. Part II: flame retardant polymeric nanocomposites and coatings, Polymers for Advanced Technologies 22(4) (2011) 379-394.

[3] K.L. Gordon, C.M. Thompson, R.E. Lyon, Flame retardant epoxy resins containing aromatic poly(phosphonamides), High Performance Polymers 22(8) (2010) 945-958.

[4] E.D. Weil, Fire-Protective and Flame-Retardant Coatings-A State-of-the-Art Review, Journal of Fire Sciences 29(3) (2011) 259-296.

[5] Z.T. Wang, Y.K. Luo, X. Ding, G.F. Xi, The Research on Flame Retardant Wind Turbines Nacelle Made through VARTM Process, Advanced Materials Research 450 (2012) 508-512.

[6] T. Xu, X. Huang, Combustion properties of asphalt binder containing flame retardant, Fire and Materials 36(2) (2012) 97-106.

[7] S. Wang, J. Huang, F. Chen, STUDY ON MG-AL HYDROTALCITES IN FLAME RETARDANT PAPER PREPARATION, BioResources 7(1) (2012) 0997-1007.

[8] N.D. Nam, I.J. Park, J.G. Kim, H.S. Kim, Effect of flame-retarding additives on surface chemistry in Li-ion batteries, Materials Research Bulletin 47 (2012) 2811-2814.

[9] S. Chen, Z. Wang, H. Zhao, H. Qiao, H. Luan, L. Chen, A novel flame retardant and film-forming electrolyte additive for lithium ion batteries, Journal of Power Sources 187(1) (2009) 229-232.

[10] S. Hamdani, C. Longuet, D. Perrin, J.-M. Lopez-cuesta, F.o. Ganachaud, Flame retardancy of silicone-based materials, Polymer Degradation and Stability 94(4) (2009) 465-495.

[11] A.P. Mouritz, Review of smoke toxicity of fiber-polymer composites used in aircraft, Journal of Aircraft 46(3) (2009) 735-745.

[12] J. Holbery, D. Houston, Natural-fiber-reinforced polymer composites in automotive applications, JOM 58(11) (2006) 80-86.

[13] P. Ding, S. Tang, H. Yang, L. Shi, PP/LDH nanocomposites via melt-intercalation: Synergistic flame retardant effects, properties, and applications in automobile industries, Advanced Materials Research 87-88 (2010) 427-432.

[14] F. Laoutid, L.l. Bonnaud, M.l. Alexandre, J.-M. Lopez-Cuesta, P. Dubois, New prospects in flame retardant polymer materials: From fundamentals to nanocomposites, Materials Science and Engineering: R: Reports 63(3) (2009) 100-125.

[15] G. Camino, L. Costa, G. Martinasso, Intumescent fire-retardant systems, Polymer Degradation and Stability 23(4) (1989) 359-376.

[16] G. Camino, L. Costa, M. Luda di Cortemiglia, Overview of fire retardant mechanisms, Polymer Degradation and Stability 33(2) (1991) 131-154.

[17] B.H. Wilford, M. Shoeib, T. Harner, J. Zhu, K.C. Jones, Polybrominated diphenyl ethers in indoor dust in Ottawa, Canada: Implications for sources and exposure, Environmental Science and Technology 39(18) (2005) 7027-7035.

[18] D. Porter, E. Metcalfe, M. Thomas, Nanocomposite fire retardants-a review, Fire and Materials 24(1) (2000) 45-52.

[19] R.E. Clement, E.J. Reiner, S.P. Bhavsar, Organohalogen contaminants of emerging concern in Great Lakes fish: A review, Analytical and Bioanalytical Chemistry 404(9) (2012) 2639-2658.

[20] M. Shoeib, T. Harner, G.M. Webster, E. Sverko, Y. Cheng, Legacy and current-use flame retardants in house dust from Vancouver, Canada, Environmental Pollution 169(0) (2012) 175-182.

[21] M.-L. Gentes, R.J. Letcher, E. Caron-Beaudoin, J. Verreault, Novel flame retardants in urban-feeding ring-billed gulls from the St. Lawrence River, Canada, Environmental Science and Technology 46(17) (2012) 9735-9744.

[22] D. Chen, R.J. Letcher, N.M. Burgess, L. Champoux, J.E. Elliott, C.E. Hebert, P. Martin, M. Wayland, D.V. Chip Weseloh, L. Wilson, Flame retardants in eggs of four gull species (Laridae) from breeding sites spanning Atlantic to Pacific Canada, Environmental Pollution 168 (2012) 1-9.

[23] J.J. Alava, D. Lambourn, P. Olesiuk, M. Lance, S.J. Jeffries, F.A.P.C. Gobas, P.S. Ross, PBDE flame retardants and PCBs in migrating Steller sea lions (Eumetopias jubatus) in the Strait of Georgia, British Columbia, Canada, Chemosphere 88(7) (2012) 855-864.

[24] F. Wong, P. Kurt-Karakus, T.F. Bidleman, Fate of brominated flame retardants and organochlorine pesticides in urban soil: Volatility and degradation, Environmental Science and Technology 46(5) (2012) 2668-2674.

[25] H. Xiao, L. Shen, Y. Su, E. Barresi, M. Dejong, H. Hung, Y.-D. Lei, F. Wania, E.J. Reiner, E. Sverko, S.-C. Kang, Atmospheric concentrations of halogenated flame retardants at two remote locations: The Canadian High Arctic and the Tibetan Plateau, Environmental Pollution 161 (2012) 154-161.

[26] F. Ivol, M. Porcher, A. Ghosh, J. Jacquemin, F. Ghamouss, Phenylacetonitrile (C6H5CH2CN) Ionic Liquid Blends as Alternative Electrolytes for Safe and High-Performance Supercapacitors, Molecules 25(11) (2020) 2697.

[27] C.A. McDonough, G. Puggioni, P.A. Helm, D. Muir, R. Lohmann, Spatial Distribution and Air–Water Exchange of Organic Flame Retardants in the Lower Great Lakes, Environmental Science & Technology 50(17) (2016) 9133-9141.

[28] M. Venier, A. Dove, K. Romanak, S. Backus, R. Hites, Flame retardants and legacy chemicals in Great Lakes' water, Environmental Science & Technology 48(16) (2014) 9563-9572.

[29] J. Yang, J.Z. Liang, C.Y. Tang, Studies on melt flow properties during capillary extrusion of PP/Al(OH)3/Mg(OH)2 flame retardant composites, Polymer Testing 28(8) (2009) 907-11.

[30] L. Jizhao, Z. Yingjie, A study of the flame-retardant properties of polypropylene/Al(OH)3/Mg(OH)2 composites, Polymer International 59(4) (2010) 539-42.

[31] R. Armstrong, J. Wright, Impedance studies of poly ethylmethacrylate coatings formed upon tin-free steel, Corrosion science 33(10) (1992) 1529-1539.

[32] A. Sari, A. Karlı, C. Alkan, A. Karaipekli, Polyethyl methacrylate (PEMA)/fatty acids blends as novel phase change materials for thermal energy storage, Energy Sources, Part A: Recovery, Utilization, and Environmental Effects 35(19) (2013) 1813-1819.

[33] M. Ulaganathan, C.M. Mathew, S. Rajendran, Highly porous lithium-ion conducting solvent-free poly (vinylidene fluoride-co-hexafluoropropylene)/poly (ethyl methacrylate) based polymer blend electrolytes for Li battery applications, Electrochimica Acta 93 (2013) 230-235.

[34] S. Ramesh, O. Uma, R. Shanti, L.J. Yi, K. Ramesh, Preparation and characterization of poly (ethyl methacrylate) based polymer electrolytes doped with 1-butyl-3-methylimidazolium trifluoromethanesulfonate, Measurement 48 (2014) 263-273.

[35] F. Mohanty, S.K. Swain, Silver Nanoparticles Decorated Polyethylmethacrylate/Graphene Oxide Composite: As Packaging Material, Polymer Composites 40(S2) (2019) E1199-E1207.

[36] F. Mohanty, S.K. Swain, Nano silver embedded starch hybrid graphene oxide sandwiched poly (ethylmethacrylate) for packaging application, Nano-Structures & Nano-Objects 18 (2019) 100300.

[37] J.C. Arnold, N.P. Venditti, Prediction of the long-term creep behaviour of hydroxyapatite-filled polyethylmethacrylate bone cements, Journal of Materials Science: Materials in Medicine 18(9) (2007) 1849-58.

[38] Y. Peng, M. Musah, B. Via, X. Wang, Calcium Carbonate Particles Filled Homopolymer Polypropylene at Different Loading Levels: Mechanical Properties Characterization and Materials Failure Analysis, Journal of Composites Science 5(11) (2021) 302.

[39] X. Li, I. Zhitomirsky, Deposition of poly (methyl methacrylate) and composites containing bioceramics and bioglass by dip coating using isopropanol-water co-solvent, Progress in Organic Coatings 148 (2020) 105883.

[40] I.A. Jankovic, Z.V. Saponjic, M.I. Comor, J.M. Nedeljkovic, Surface modification of colloidal TiO2 nanoparticles with bidentate benzene derivatives, The Journal of Physical Chemistry C 113(29) (2009) 12645-12652.

[41] T. Zhang, D. Luo, P. Wojtal, I. Zhitomirsky, Electrophoretic deposition of flame retardant polymer–huntite coatings, Materials Letters 159 (2015) 106-109.

[42] F. Şen, S. Madakbaş, M.V. Kahraman, Preparation and characterization of polyaniline/Turkish Huntite-hydromagnesite composites, Polymer composites 35(3) (2014) 456-460.

[43] S. Madakbaş, Z. Celik, F. Dumludağ, M.V. Kahraman, Preparation, characterization and electrical properties of polyacrylonitrile/huntite composites, Polymer bulletin 71(6) (2014) 1471-1481.

[44] Y. Seki, K. Sever, M. Sarikanat, A. Sakarya, E. Elik, Effect of huntite mineral on mechanical, thermal and morphological properties of polyester matrix, Composites Part B: Engineering 45(1) (2013) 1534-1540.

[45] S. Zainuddin, A. Fahim, S. Shoieb, F. Syed, M.V. Hosur, D. Li, C. Hicks, S. Jeelani, Morphological and mechanical behavior of chemically treated jute-PHBV bio-nanocomposites reinforced with silane grafted halloysite nanotubes, Journal of Applied Polymer Science 133(39) (2016).

[46] C. Li, Y. Zhao, T. Zhu, J. Ruan, G. Li, Effective solvent-free oxidation of cyclohexene to allylic products with oxygen by mesoporous etched halloysite nanotube supported Co 2+, RSC advances 8(27) (2018) 14870-14878.

[47] X. Li, Z. Wang, S. Sakib, R. Mathews, I. Zhitomirsky, Poly (Methyl Methacrylate) Coatings Containing Flame Retardant Additives from Suspensions in Water-2-Propanol, Molecules 26(7) (2021) 1974.

[48] M.A. González, R. Trócoli, I. Pavlovic, C. Barriga, F. La Mantia, Capturing Cd (II) and Pb (II) from contaminated water sources by electro-deposition on hydrotalcite-like compounds, Physical Chemistry Chemical Physics 18(3) (2016) 1838-1845.

[49] X. Tian, J. Wang, H. Zhang, Z. Cao, M. Zhao, Y. Guan, Y. Zhang, Establishment of transport channels with carriers for water in reverse osmosis membrane by incorporating hydrotalcite into the polyamide layer, RSC advances 8(22) (2018) 12439-12448.

[50] E. Abdelrazek, I. Elashmawi, Characterization and physical properties of CoCl2 filled polyethyl-methacrylate films, Polymer composites 29(9) (2008) 1036-1043.

[51] M. Gradwell, D. Hourston, T. Pabunruang, F.U. Schafer, M. Reading, High-resolution thermogravimetric analysis of polyurethane/poly (ethyl methacrylate) interpenetrating polymer networks, Journal of applied polymer science 70(2) (1998) 287-295.

[52] M. Agrawal, N.E. Zafeiropoulos, S. Gupta, E. Svetushkina, J. Pionteck, A. Pich, M. Stamm, A novel approach for mixing ZnO nanoparticles into poly (ethyl methacrylate), Macromolecular rapid communications 31(4) (2010) 405-410.

[53] S. Rajendran, M.R. Prabhu, M.U. Rani, Characterization of PVC/PEMA based polymer blend electrolytes, International journal of electrochemical science 3(3) (2008) 282-290.

[54] L. Sim, S. Majid, A. Arof, Effects of 1–butyl–3–methyl imidazolium trifluoromethanesulfonate ionic liquid in poly (ethyl methacrylate)/poly (vinylidenefluoride–co–hexafluoropropylene) blend based polymer electrolyte system, Electrochimica Acta 123 (2014) 190-197.

[55] Y. Sun, M. Ata, I. Zhitomirsky, Electrophoretic deposition of linear polyethylenimine and composite films, Surface engineering 29(7) (2013) 495-499.

[56] K.P. Nicolini, C.R.B. Fukamachi, F. Wypych, A.S. Mangrich, Dehydrated halloysite intercalated mechanochemically with urea: Thermal behavior and structural aspects, Journal of Colloid and Interface Science 338(2) (2009) 474-479.

[57] Y. Peng, R. Burtovyy, R. Bordia, I. Luzinov, Fabrication of Porous Carbon Films and Their Impact on Carbon/Polypropylene Interfacial Bonding, Journal of Composites Science 5(4) (2021) 108.

[58] F.C. Garcia Filho, F.S. Luz, M.S. Oliveira, W.B.A. Bezerra, J.D.V. Barbosa, S.N. Monteiro, Influence of Rigid Brazilian Natural Fiber Arrangements in Polymer Composites: Energy Absorption and Ballistic Efficiency, Journal of Composites Science 5(8) (2021) 201.

[59] H. Tsukamoto, Tribological Characterization of Carbon Nanotube/Aluminum Functionally Graded Materials Fabricated by Centrifugal Slurry Methods, Journal of Composites Science 5(10) (2021) 254.

[60] Y. Su, I. Zhitomirsky, Electrophoretic deposition of graphene, carbon nanotubes and composite films using methyl violet dye as a dispersing agent, Colloids and Surfaces A: Physicochemical and Engineering Aspects 436 (2013) 97-103.

[61] K. Wu, Y. Wang, I. Zhitomirsky, Electrophoretic deposition of TiO2 and composite TiO2–MnO2 films using benzoic acid and phenolic molecules as charging additives, Journal of colloid and interface science 352(2) (2010) 371-378.

# Chapter 10  Conclusion and Future Works

## 10.1 Summary of conclusions

In summary, the primary objective of this work was to develop novel colloidal strategies for the fabrication of polymer and composite coatings with advanced functionality. The overarching objective was accomplished. Conceptually new strategies have been developed for the deposition of advanced polymers and other functional particles. New technologies offer processing advantages and can be used for the manufacturing of coatings with advanced functionality. The major achievements of this dissertation can be summarized as follows:

1.  The bile salt ChANa can adsorb on the surface of different materials, such as diamonds, CDs, graphene and PTFE, and facilitate their efficient dispersion and charging. The gel-forming properties, pH-dependent solubility and charge of ChANa allowed for the use of this natural organic molecule as a coating-forming agent. ChANa can be utilized as a versatile co-dispersant for co-EPD of composite coatings. EPD of diamonds was combined with PPy electropolymerization for the deposition of diamond-PPy composites. It was shown that annealed PTFE films provide corrosion protection of stainless steel. It is expected that ChANa-mediated EPD will allow the deposition of other functional materials of different types.

2.  For the first time it was demonstrated that CDCH films can be deposited using an electrogenerated acid method and pH-dependent gel-forming properties of CDCH.

194

Another major finding was that CDCNa allowed EPD of carbon materials, such as SD, ND and carbon nanotubes, as well as PTFE and MHT. A conceptually novel strategy to enhance protective properties of polymer coatings was put forward, which was based on the memory properties of MHT. This strategy will pave the way for the fabrication of advanced polymer coatings for corrosion protection in the future.

3. The deposition mechanism of pure $CBXH_2$ involved protonation of $CBX^{2-}$ in the anodic reactions and the forming of insoluble $CBXH_2$ films. The EPD mechanism of carbon materials, PTFE and composites involved adsorption of $CBX^{2-}$ on particles, electrophoretic transport and discharge of adsorbed $CBX^{2-}$, which facilitated film formation. The deposition rate, film morphology and composition can be varied and controlled. $CBXNa_2$ is a versatile surfactant and co-surfactant for EPD of various materials and composites. The EPD method can be applied for protection of metals from corrosion in industry. $CBXNa_2$ is a promising surface modification agent for future applications in EPD of functional inorganic materials due to the chelating properties of its carboxylic groups. Therefore, further progress in $CBXNa_2$ applications can result in the manufacturing of advanced functional composites by EPD.

4. GRTA or GRZA are new versatile film-forming dispersants, which allowed controlled EPD of chemically inert PVDF and PTFE polymers and diamonds. The results presented stressed the importance of the chemical structure of GRTA and

GRZA for the deposition of different materials. GRZA allowed for higher deposition yield of PVDF, whereas the use of GRTA resulted in higher deposition yield of PTFE. GRTA and GRZA can be used as co-dispersants for the fabrication of PVDF-diamond and PTFE-diamond composites. Obtained films can be used for corrosion protection of metals and offer benefits for other applications based on the advanced functionality of the deposited materials.

5. This research demonstrated that PEMA can be dissolved in a mixed isopropanol-water co-solvent which avoided the use of toxic solvents. The ability to dissolve high molecular mass PEMA and achieve high PEMA concentration were the key factors considered for the development of the dip coating method. PEMA coatings prepared by the dip coating method can be used for corrosion protection of metals. LiAlDH was prepared by a novel solid state synthesis method, which offers many advantages, compared to traditional techniques. LiAlDH was used as FR material for polymer coatings due to its relatively high water release on dehydration. It was found that dip coating method allowed for the fabrication of composite PEMA-LiAlDH coatings with different LiAlDH content. Bi-layer coatings, containing different layers offer benefits for the development of coatings with improved corrosion protection and FR properties. The approach can potentially be used for the fabrication of monolayer, multilayer coatings as well as coatings of graded composition, containing other functional materials.

196

6. The FRM materials can be well dispersed in PEMA solution which allows the fabrication of PEMA-FRM composite coatings. The use of advanced inorganic FRM materials, such as huntite, halloysite and hydrotalcite instead of toxic halogenated FRM offers additional environmental benefits. The ability to obtain concentrated solutions of high molecular weight PEMA and disperse FRM particles in such solutions plays a vital role in the fabrication of coatings by a dip coating method. Pure PEMA and PEMA-FRM coatings provide corrosion protection of stainless steel. Annealed PEMA coatings provide enhanced corrosion protection due to lower porosity. The ability to form composite laminates containing different layers by a dip coating method was demonstrated to be a promising strategy for the fabrication of composite coatings with enhanced functionality.

## 10.2 Future Work

Although several novel strategies have been developed to fabricate polymer and polymer composite coatings through EPD and dip coating technique, there is still much work that could be done, as explained below.

In this work, two types of bile salts, ChANa and CDCNa, and three types of biosurfactants, CBXNa$_2$, GRTA, and GRZA, were proposed as charging dispersants for various materials. All the molecules are efficient in dispersing PTFE and imparting the charge onto the particle surface of PTFE for EPD. The GRTA-mediated and GRZA-mediated EPD were compared and

it was found that GRTA resulted in a higher deposition yield of PTFE. However, the efficiencies of each of the five dispersants have not yet been compared, nor have the structural differences among these molecules, which influence their efficiency, been discussed. For future work, further investigation into the relationship between the structure and the efficiency of adsorbing, dispersing and charging through these methods should be compared. More bio-surfactants and functional materials can be added to this research if necessary. Only through this method can a complete selection system be constructed to assist in matching the most efficient bio-surfactant with a specific type of material. This selection system has not previously been explored.

Furthermore, previous studies have shown that PEMA coatings were commonly fabricated in a toxic solvent, using various techniques, including casting, spin coating, and electrospinning. The toxic solvents also need a long-time heating procedure for removal. This research proposed using a mixture of water-isopropanol as a co-solvent to dissolve high $M_w$ PEMA at high concentrations for dip coating. Previous problems have been solved with this method. However, if PEMA can be charged and well-dispersed in a non-toxic solvent, then the EPD method is also a good choice for fabricating the PEMA coating. Therefore, based on the high efficiency of bile salts for the EPD of different materials, it is recommended to select a suitable bile salt as dispersing, charging and film-forming agent for the EPD of PEMA. Its composite coatings are expected to be fabricated through this method as well.